

Doctoral Dissertation

博士論文

**A Study on Structural Analysis Method with Uncertainty by Stochastic
Finite Element Method**

不確定性を考慮した確率有限要素法による
構造解析手法の研究

By

Xi Chen

**Graduate School of Engineering
Yokohama National University**

September 15, 2017

TABLE OF CONTENTS

Abstract	1
Acknowledgement	3
List of Figures	5
1. Introduction	11
1.1 Research Background	11
1.1.1 Concepts of Uncertainty Analysis	12
1.1.2 The Uncertainty Analysis Method	13
(1) Non-Intrusive Method	14
(2) Intrusive Method	15
1.1.3 Literature Review	16
(1) Stochastic 2D Elastostatic Problem	16
(2) Stochastic Eigenvalue Problem	17
1.1.4 Importance of Uncertainty Analysis	17
1.2 Research Purposes	19
1.1.1 2D Elastostatic Problem	19
1.1.2 Eigenvalue Problem	19
2. Theoretical Background	21
2.1 Probabilistic Domain	21
2.1.1 Polynomial Chaos Expansion (PCE)	21
2.1.2 Applications of Polynomial Chaos	25
2.1.3 Numerical Example	28
2.2 Structural Domain-2D Structural Static Problem	33

2.3 Structural Domain- Eigenvalue Problem	37
2.3.1 In the Vibrations Analysis	37
2.3.2 In Linear Buckling Analysis	39
2.3.3 A Numerical Algorithm	39
(1) The Inverse Power Method	40
(2) The Wielandt Deflation Method	42
3. Stochastic 2D Elastostatic Problem	49
3.1 The Formularization of Stochastic Finite Element Method for Uncertainty in Shape Following normal Distribution	50
3.1.1 Introduction of Input Random Variable	50
3.1.2 Stochastic Finite Element Formulation	52
(1) Stochastic Element Stiffness Matrix	52
(2) Stochastic Force Vector	59
(3) The Stiffness Equation of SFEM	61
3.1.3 Numerical Example	74
(1) A Plate with a Circular Hole with Uncertainty	63
(2) A Cruciform Weld Joint with Uncertainty in the Magnitude of Misalignment	68
3.1.4 Accuracy Consideration	72
3.2 The Formularization of Stochastic Finite Element Method for Uncertainty in Shape Following Non-normal Distribution	75
3.2.1 An Approximate Method for Non-normal Distribution	75
3.2.2 Example for Approximation of Non-normal Distribution	77

3.2.3 Stochastic Finite Element Formulation	79
(1) Stochastic Element Stiffness Matrix	79
(2) Stochastic Force Vector	83
(3) Assembly of Global Stiffness Matrix	83
(4) The Stiffness Equation of SFEM	84
3.2.4 Algorithm of SFEM with Uncertainty in Shape	85
(1) Overview of Analysis Procedure	85
(2) Algorithm of SFEM	87
3.2.5 Numerical Example	92
(1) A Plate with a Circular Hole with Uncertainty	92
(2) A Cruciform Weld Joint with Uncertainty in the Weld Toe Radius	96
3.2.6 Conclusions	101
3.3 Evaluation of Accuracy of the Analysis Method	103
4. Stochastic eigenvalue Problem	109
4.1 Statement of the Stochastic Eigenvalue Problem	110
4.2 The Formularization of I-SIPM for Solution of the Stochastic Eigenvalue Problem	114
4.3 The Formularization of the Stochastic Wielandt Deflation Method	122
4.4 Numerical Examples	129
4.4.1 Two Degrees of Freedom Undamped System	129
(1) Case (1): The Three Springs Stiffness is Considered as Obeying Some Variable θ_1	129

(2) Case (2): The Three Springs Stiffness is Considered as Obeying Different Variable θ_1, θ_1	138
4.4.2 A Continuous Beam with Uncertainty in Section Dimension	154
(1) Case (1): The Depth H is Assumed as Including A Small Deviation	155
(2) Case (2): The Depth H is Assumed as Including A Large Deviation	159
4.4.3 A Beam with Uncertainty in Young's Modulus	162
4.4.4 The Dynamic Damper Problem	168
(1) Concepts of Dynamic Damper	168
(2) Selection Methods for the Mass and Stiffness of A Dynamic Damper	170
(3) Modelling and Condition	174
(4) The Spring Stiffness of Dynamic Damper with Uncertainty	177
(5) The Spring Stiffness and Mass of Dynamic Damper with Uncertainty	181
4.5 Conclusions	186
5. Conclusions and Future Recommendations	189
5.1 Conclusions	189
5.1.1 Conclusions: Linear Static Analysis	189
5.1.2 Stochastic Finite Element Formulation	190
5.2 Future Work	192
Bibliography	193

ABSTRACT

In structural mechanics in the field of naval architecture and ocean engineering, currently, the structural analysis is very important such as linear static analysis and the eigenvalue analysis. In practical cases, the physical characteristics are not deterministic. There are a lot of uncertainties in load, material property, geometrical shape, corrosion and other characteristics in the structures. Such uncertainties may cause serious problems as reduction of strength or increase of stress which may reduce fatigue strength of the structure or reduction of buckling load because the influence of the uncertainties is usually unknown. So it can't be ignored in practice. Structural analysis when uncertainty exists in the structure is very important for safety risk assessment of ships and offshore structures.

This method which consider some uncertain input parameters to compute these uncertain results are usually referred to as uncertainty analysis. In the conventional uncertainty analysis, Monte Carlo Simulation methods (MCS) combined with finite element methods (FEM) is usually used when uncertainty is considered. However, MCS needs heavy and a large number of calculations, so that application of MCS to practical problems is sometimes very difficult to get reasonable results. Thus, it is very necessary that propose a new method of structural analysis to solve problems of response uncertainty when the case involves inherent uncertainty. In this study, we will discuss uncertainty problem from two aspects: linear static analysis (about studying of uncertainty in shape) and eigenvalue analysis.

In linear static analysis problem, in order to achieve effectively evaluate uncertainly of response (displacement, strain and stress), the Stochastic Finite Element Method (SFEM) based on response surface methodology is proposed for the solution of problems of response uncertainty for the case that involves uncertainty in shape following the normal distribution or non-normal distribution. The proposed method makes use of an Hermite polynomial chaos expansion (PCE) (response surface method) to represent the uncertainty of shapes and the response surface extending the deterministic finite element. And the proposed method ultimately achieved that the uncertainty of response of a displacement, strain and stress can be estimated by this method that solves the main stiffness equation only once. Some example problems are investigated by the method. The validity of the

proposed method of structural analysis is discussed by comparing the results of the method with the MCS solution of the deterministic problems.

In eigenvalue analysis problem, in order to achieve effectively evaluate uncertainty of response (a natural frequency and natural mode in vibrations analysis or a buckling load and buckling mode in buckling analysis), we have been studied about solution of stochastic eigenvalue problems to discuss inherent uncertainty influences on the stochastic response eigenvalues and stochastic response eigenvectors. As solution of stochastic eigenvalue problem, in this study, we have proposed two methods. Firstly, the improved stochastic inverse power method (I-SIPM) based on response surface methodology is proposed by which minimum eigenvalue and eigenvector of stochastic eigenvalue problems can be effectively evaluated. Secondly, the stochastic Wielandt deflation method (SWDM) is proposed which can realize to evaluate $i^{th}(i>1)$ eigenvalues and eigenvectors of stochastic eigenvalue problems by using response surface method to extend the Widlandt deflation method. Finally, example problems are investigated to discuss the validity of the proposed new methods compared with a Monte-Carlo simulation, i.e. the vibration problem and the buckling problem when consider uncertainty exists in the model.

ACKNOWLEDGEMENTS

First and foremost I would like to thank my academic supervisor Prof. Yasumi Kawamura for his unequivocal patience and support throughout my doctoral five years studies. And in five years studies, his backing and thorough encouragement has integral to the progress in every ways. I have been very grateful to be under his mentorship and learnt the virtues of hard work, meticulous understanding and gaining confidence to face the difficulties and challenges from his guidance. I would like that this is greatest gain of all for me in these five years. Invaluable suggestions from Prof. Tetsuo Okada have helped me immensely in about my research problem. I am highly indebted to him. I would like to convey sincere gratitude to my senior colleague, Mr. Riddhideep Mandal, Mrs. Myo Myo Htun and Mr. KuiLin Yuan for helping me with some the technical discussions. I greatly appreciate the support provided by Mr. Shunichi Michiyama with all the computer hardware and software that involved a lot of troubleshooting. Your time and patience helped me immensely for a smooth and conducive environment in our laboratory. And I would like to thank reviewers of submitted paper for his valuable comments. Special acknowledgement is due for my family whose support and sacrifice has enabled me to be where I am today. I will be forever indebted to them. Last but not the least; I would like to thank all of my friends, and I will cherish memories forever in Yokohama since the last five years.

LIST OF FIGURES

Fig.1.1 (a): Example of Uncertainty in Randomness in Manufacturing

Fig.1.1 (b): Example of Uncertainty in Corrosion

Fig.1.2: General Concept of Uncertainty Analysis

Fig.1.3: Intrusive and Non-Intrusive Formulation

Fig.1.4: Conventional Monte Carlo Simulation

Fig.1.5: A PDF of the Difference Between σ_y and $\sigma(r)$

Fig.2.1: The Spectral Approach Concept

Fig.2.2: A Spring Problem

Fig.2.3: The probability density distributions of the buckling load

Fig.2.4: The Distributed Load along the Side of Element

Fig.2.5: Flowchart of the Wielandt Deflation Method

Fig.3.1: Model of Linear Deformation.

Fig.3.2: The Distributed Load along the Side of Element

Fig.3.3: The Geometrical Deformation of the Hole

Fig.3.4: The Response Surface of Stress (Standard Deviation is 0.5mm)

Fig.3.5: Stochastic Responses to Shape Uncertainty

Fig.3.6: Error of the Stress Concentration Factor

Fig.3.7: Response Surface of $1/|J'(\xi, \eta; \theta)|$ (Standard Deviation is 1mm)

Fig.3.8: The Cruciform Weld Joint

Fig.3.9: Model of Linear Deformation

Fig.3.10: The Response Surface of Stress

Fig.3.11: Stochastic Responses to Shape Uncertainty

Fig.3.12: Probability Density Estimate of l

Fig.3.13: An Overall Flowchart

Fig.3.14: Flowchart of the SFEM

Fig.3.15: The Geometrical Deformation of the Hole

Fig.3.16: The Response Surface of Stress (Logarithmic Distribution)

Fig.3.17: Stochastic Responses to Shape Uncertainty

Fig.3.18 (a): The Cruciform Weld Joint: Model

Fig.3.18 (b): The Cruciform Weld Joint: Mesh

Fig.3.19: Approximation of Probability Distribution

Fig.3.20: The Response Surface of Stress for Different Degree

Fig.3.21: Stochastic Responses to Shape Uncertainty

Fig.3.22: Mesh for Case1

Fig.3.23: Mesh for Case2

Fig.3.24: Mesh near Circular Hole for Case1

Fig.3.25: Mesh near Circular Hole for Case2

Fig.4.1: A Discrete 2-DOF Undamped System

Fig.4.2: The Response Surface of Eigenvalues

Fig.4.3: The Probability Density Distributions of Eigenvalue $\lambda'_{(1)}(\boldsymbol{\theta})$.

Fig.4.4: The Probability Density Distributions of Eigenvalue $\lambda'_{(2)}(\boldsymbol{\theta})$

Fig.4.5: The Response Surface of Eigenvector Components: $\mathbf{u}'_{(1)}(\theta)$.

Fig.4.6: The Response Surface of Eigenvector Components: $\mathbf{u}'_{(2)}(\theta)$.

Fig.4.7: The Probability Density Distributions of Eigenvector $\mathbf{u}'_{(1)}(\theta)$.

Fig.4.8: The Probability Density Distributions of Eigenvector $\mathbf{u}'_{(2)}(\theta)$.

Fig.4.9: A Discrete 2-DOF Undamped System

Fig.4.10 (a): The Response Surface of Eigenvalues $\lambda'_{(1)}(\boldsymbol{\theta})$: I-SIPM

Fig.4.10 (b): The Response Surface of Eigenvalues $\lambda'_{(1)}(\boldsymbol{\theta})$: The reference values (deterministic cases)

Fig.4.11 (a): The Response Surface of Eigenvalues $\lambda'_{(2)}(\boldsymbol{\theta})$: SWDM

Fig.4.11 (b): The Response Surface of Eigenvalues $\lambda'_{(2)}(\boldsymbol{\theta})$: The reference values (deterministic cases)

Fig.4.12: The Probability Density Distributions of Eigenvalue $\lambda'_{(1)}(\boldsymbol{\theta})$

Fig.4.13: The Probability Density Distributions of Eigenvalue $\lambda'_{(2)}(\boldsymbol{\theta})$

Fig.4.14 (a): The Response Surface of Eigenvector Components: $\mathbf{u}'_{(1),1}(\theta)$:I-SIPM

Fig.4.14 (b): The Response Surface of Eigenvector Components: $\mathbf{u}'_{(1),1}(\theta)$: The reference values (deterministic cases)

Fig.4.15 (a): The Response Surface of Eigenvector Components: $\mathbf{u}'_{(1),2}(\theta)$:I-SIPM

Fig.4.15 (b): The Response Surface of Eigenvector Components: $\mathbf{u}'_{(1),2}(\theta)$: The reference values (deterministic cases)

Fig.4.16 (a): The Response Surface of Eigenvector Components: $\mathbf{u}'_{(2),1}(\theta)$:SWDM

Fig.4.16 (b): The Response Surface of Eigenvector Components: $\mathbf{u}'_{(2),1}(\theta)$: The reference values (deterministic cases)

Fig.4.17 (a): The Response Surface of Eigenvector Components: $\mathbf{u}'_{(2),2}(\theta)$:SWDM

Fig.4.17 (b): The Response Surface of Eigenvector Components: $\mathbf{u}'_{(2),2}(\theta)$: The reference values (deterministic cases)

Fig.4.18 (a): The Probability Density Distributions of Eigenvector $\mathbf{u}'_{(1)}(\theta)$: Components $\mathbf{u}'_{(1),1}(\theta)$

Fig.4.18 (b): The Probability Density Distributions of Eigenvector $\mathbf{u}'_{(1)}(\theta)$: Components $\mathbf{u}'_{(1),2}(\theta)$

Fig.4.19 (a): The Probability Density Distributions of Eigenvector $\mathbf{u}'_{(2)}(\theta)$: Components $\mathbf{u}'_{(2),1}(\theta)$

Fig.4.19 (b): The Probability Density Distributions of Eigenvector $\mathbf{u}'_{(2)}(\theta)$: Components $\mathbf{u}'_{(2),2}(\theta)$

Fig.4.20: Free-Standing Beam

Fig.4.21: The Response Surface of the Buckling Load for Case 1.

Fig.4.22: The Probability Density Distributions of the Buckling Load for Case 1.

Fig.4.23: The Response Surface of the Buckling Load for Case 2.

Fig.4.24: The Probability Density Distributions of the Buckling Load for Case 2.

Fig.4.25: Free-Standing Beam

Fig.4.26: The Response Surface of the Buckling Load

Fig.4.27: The Probability Density Distributions of the Buckling Load

Fig.4.28: The Buckling Mode 1 by using I-SIPM

Fig.4.29: The Buckling Mode 1 by usual theoretical formula

Fig.4.30 (a): The 2DOF System (Without the Dynamic Damper Attached): 2DOF system

Fig.4.30 (b): The 2DOF System (Without the Dynamic Damper Attached): Resonance curve for 2DOF system

Fig.4.31 (a): 3DOF System (The Dynamic Damper Attached): 3DOF system

Fig.4.31 (b): 3DOF System (The Dynamic Damper Attached): Resonance curve for 3DOF system

Fig.4.32: Superstructure

Fig.4.33: Superstructure (Simple Model)

Fig.4.34: The Image for Ranges of the Third Order and the Fourth Order Exciting Frequency of the Main Engine

Fig.4.35: The Probability Density Distributions of First Order Frequency. (The Spring Stiffness with Uncertainty)

Fig.4.36: The Response Surface by I-SIPM (Case(2)).

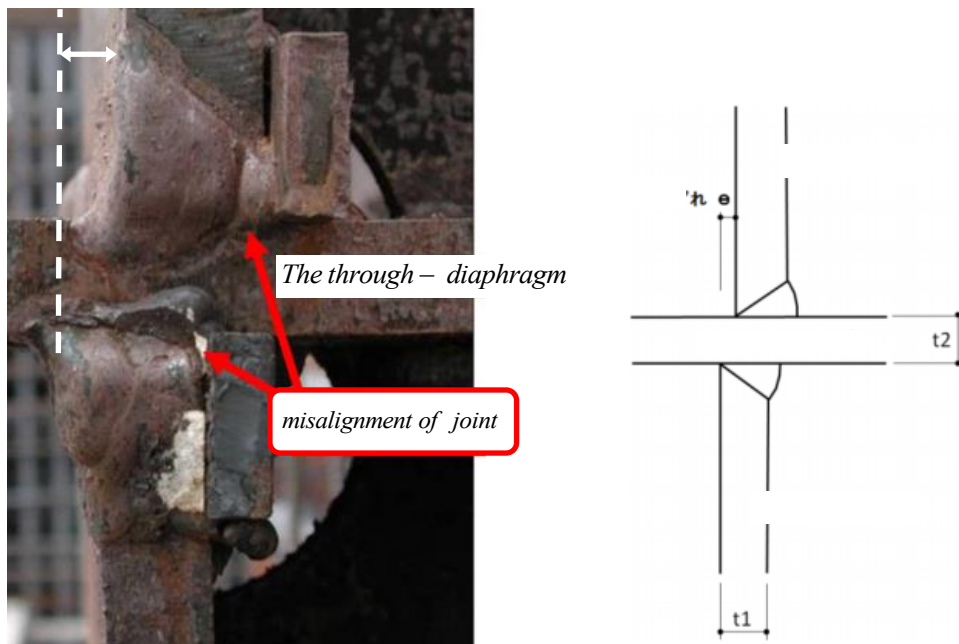
Fig.4.37: The Response Surface by Deterministic Values (Case(2)).

Fig.4.38: The Probability Density Distributions of First Order Frequency (Both the Spring Stiffness and the Mass with Uncertainty)

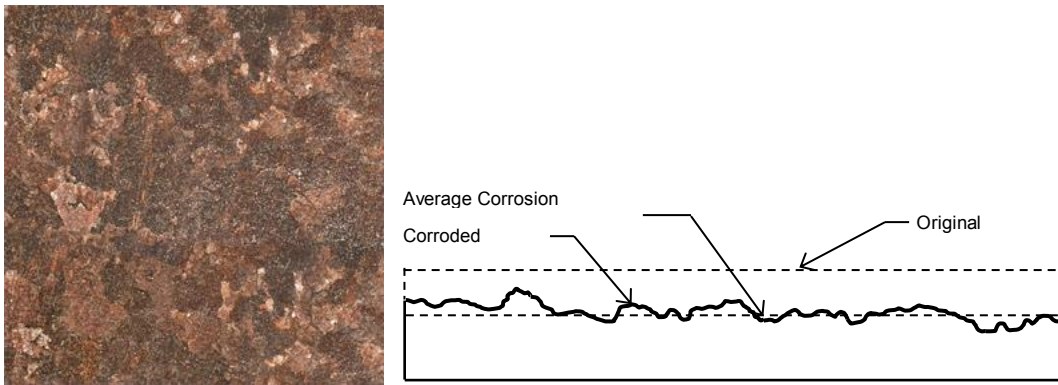
1. Introduction

1.1 Research Background

In structural mechanics in the field of naval architecture and ocean engineering, currently, the structural analysis is very important such as linear static analysis and the eigenvalue analysis. In practical cases, the physical characteristics are not deterministic. There are a lot of uncertainties in load, material property, geometrical shape, corrosion and other characteristics in the structures (Fig 1.1). Such uncertainties may cause serious problems as reduction of strength or increase of stress which may reduce fatigue strength of the structure or reduction of buckling load because the influence of the uncertainties is usually unknown. Such as Fig 1.1(a), we show the example of a cruciform weld joint. We can find that the structure has misalignment in the joint. When external force is applied to the structure, the local stress is increased because the structure occurs additional bending due to the eccentricity. So it can't be ignored in practice. Structural analysis when uncertainty exists in the structure is very important for safety risk assessment of ships and offshore structures.



(a) Geometrical shape (Randomness in Manufacturing)[1]



(b) Corrosion (Wastage after Years of Exposure in the Operation)[2]

Fig 1.1: Example of Uncertainty

In order to deal with the uncertainty problems, the uncertainty analysis has been developed. Firstly, we will explain the concepts of uncertainty analysis in section 1.1.1. Secondly, the typical uncertainty analysis method will be introduced in section 1.1.2. Thirdly, the literature will be reviewed in section 1.1.3. Finally, the importance of the uncertainty analysis will be explained in section 1.1.4.

1.1.1 Concepts of Uncertainty Analysis

In Fig.1.2 we show the concept of uncertainty analysis. Here, the inherent randomness such as material property, geometrical shape is considered as the input parameter that has a probability density function. Then it is applied to 'Analysis Method' (finite element method, etc.), we can obtain a response $u(\theta_1, \theta_2)$ (e.g. stress/displacement/ eigenvalue/ eigenvector, etc.) of the system that will be a function of input random variables. In simple terms, this means when the input parameters of a physical problem are considered as uncertain, the derived output will be also uncertain. Like this methods to compute these uncertain results are usually referred to as uncertainty analysis, which focuses on the computation of the statistical characterization (mean, standard deviation, etc.) of the uncertain output. About uncertainty analysis method, we will introduce and review in following section.

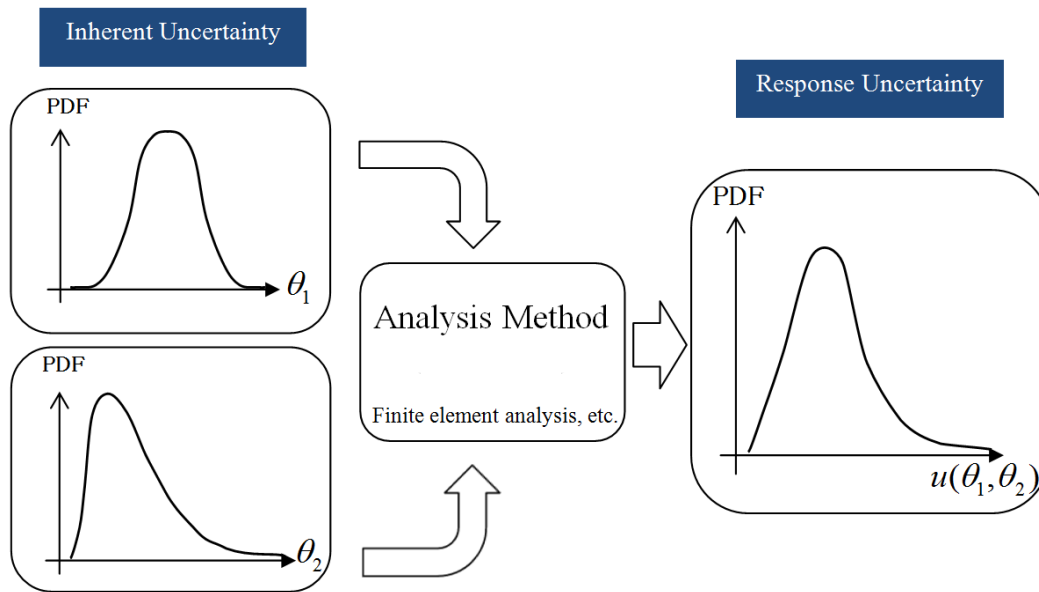


Fig.1.2: General Concept of Uncertainty Analysis

1.1.2 The Uncertainty Analysis Method

The uncertainty analysis method has been developed in recent years. The efficiency of this method is proved by many studies in engineering problems and summarised in a general review with regards to its development in the past, present and future of SFEM [3] and practical application of SFEM [4]. We can categorize the uncertainty analysis method into two major types, “non-intrusive method” and “intrusive method”, as shown in Fig.1.3.

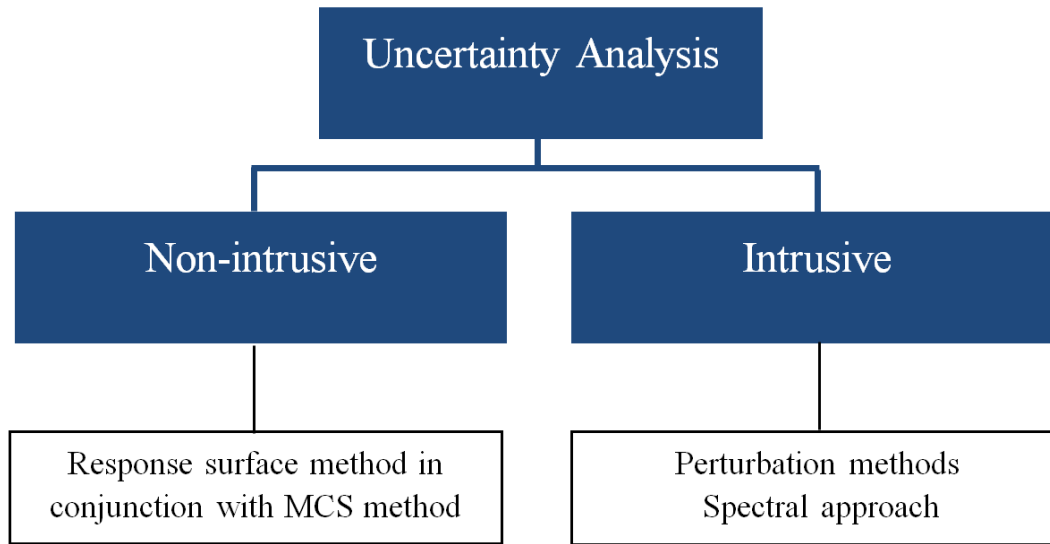


Fig.1.3: Intrusive and Non-Intrusive Formulation

(1) Non-Intrusive Method

As typical representative of the non-intrusive method, Monte Carlo Simulation Method (MCS) is most widely used technique which is used to evaluate response uncertainty [5-10]. In Fig. 1.4, we show the MCS procedure. The inherent randomness is considered as uncertain, and we have information about the input parameters, θ_1, θ_2 (such as the input parameters θ_1 is following normal distribution and the input parameters θ_2 is following Non-normal distribution), then we can get the response $(u(\theta_1^i, \theta_2^i) i = 1, \dots, m)$ through m realization of set of input random variables $((\theta_1^i, \theta_2^i) i = 1, \dots, m)$ in the analysis method. We can understand that the statistics of the response needs to be evaluated by the large number of responses which is obtained by using different samples of the input parameters into the 'Analysis Method' because the MCS is a non-intrusive method which without any interferes with the 'Analysis Method'. Hence it is considered that application of MCS to practical problems is sometimes very difficult to get reasonable results.

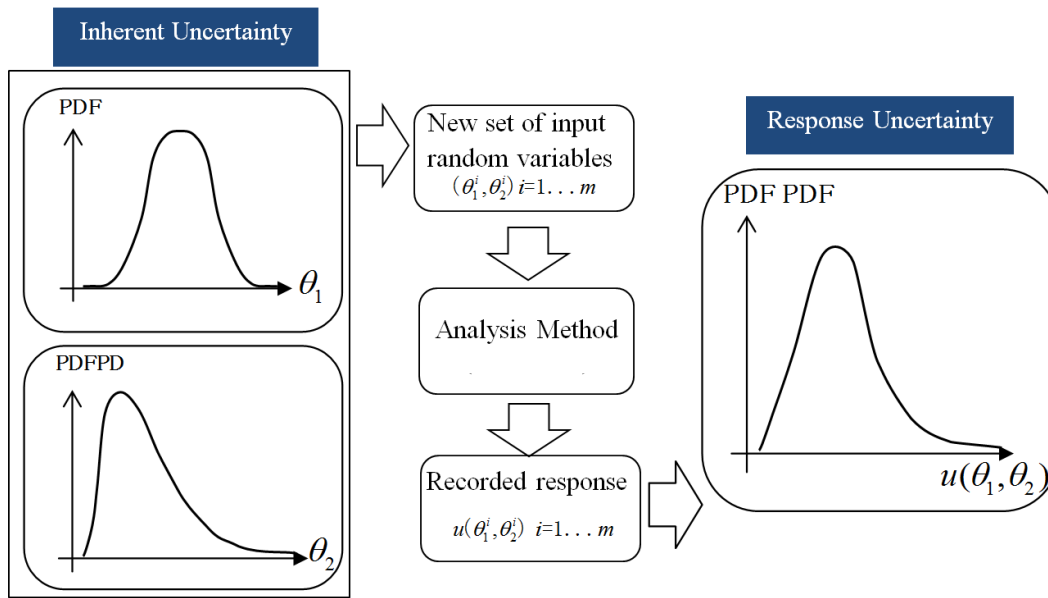


Fig.1.4: Conventional Monte Carlo Simulation

(2) Intrusive Method

To avoid a large number of calculations, the intrusive method has been developed as uncertainty analysis method. The intrusive method is constructing the stochastic response surface which does not require multiple simulations of the “Analysis Method” like the MCS. Here the two important intrusive method will be introduced, i.e., the typical representative are “Perturbation Methods” [11-18] and “Response Surface Method and Spectral Approach” [19-25].

1) Perturbation Method

SFEM based on perturbation is summarised by Kleiber et al. [18]. The perturbation method uses Taylor series expansions to introduce randomness into the finite element equation. Ultimately, the influence of the mean and standard deviation and covariance of responses variables can be estimated. The perturbation method can reduce computing costs compared with the MCS method, but it only can deal with the small variability problem.

2) Response Surface Method and Spectral Approach

And in response surface method and spectral approach, the input parameter and the response is expanded in a series of orthogonal polynomials, and introduce the expanded input parameter and response into the finite element equation. This method has been introduced by Ghanem and Spanos [19] as an extension of the deterministic finite element method. Ultimately, the response surface can be estimated, and the mean, the standard deviation and the probability density distribution can be also obtained by the obtained response surface. The response surface method can reduce computing costs compared with the MCS method, and it can deal with the large variability problem.

1.1.3 Literature Review

Based on the research of uncertainty analysis by using these methods, we find that they are mainly concerned with only the random material properties of a structure. Uncertainty in shape is less developed in recent years in linear static analysis, and uncertainty analysis for the eigenvalue problems has not been developed.

(1) Literature Review : Stochastic 2D Elastostatic Problem

Nakagiri et al. [26] reported works on uncertainty in shape, material uncertainty and boundary uncertainty, in which the mean value and the variance of stress are obtained by SFEM based on perturbation method. However, it only can deal with the small deformation problem because perturbation method has limitations. Recently, Honda [27] proposed stochastic boundary element method by using the PCE and a Karhunen-Loeve expansion method in which uncertainty of shape of boundary following normal distribution is assumed. However, it is less developed that SFEM consider uncertainty in shape of structures, and because Karhunen-Loeve expansion method is based on the normal distribution, the uncertainty in Shape in the proposed method [27] can only deal with normal distribution in general. However, in many practical cases, the uncertainties are not following normal distribution. Thus, the research for the structural model involves uncertainty in shape to follow the non-normal distribution is important.

(2) Literature Review : Stochastic Eigenvalue Problem

In structural mechanics in the field of naval architecture and ocean engineering, eigenvalue problems commonly appear in the context of, e.g. vibrations and buckling. The stochastic natural frequency in vibrations analysis and the stochastic buckling load in buckling analysis can be obtained when the stochastic eigenvalue is evaluated. Thus eigenvalue analysis when uncertainty exists in the structure is very important for safety assessment of ships and offshore structures.

It is also noted that from the above we can find that SFEM are well developed for linear structured systems, but are less developed for the eigenvalue problem. However, in uncertainty analysis, eigenvalue analysis is also an important problem in a variety of fields.

About discussion of stochastic eigenvalue problems, the mathematical base of the iterative inverse power method as an algorithm for solution of the stochastic eigenvalue problem has been discussed in Verhoosel et al. [28]. Sepahvand et al. also discussed the efficiency of the developed method by applying it to two examples [29]. However, the authors found that the method sometimes cannot give satisfactory results. Based on these studies, we find that improving the stochastic inverse power method is necessary.

1.1.4 Importance of Uncertainty Analysis

With the development of risk-based rules and the development of structural design methods in recent years, reliability evaluation and risk evaluation are valued. Hence it is considered necessary that the uncertainty analysis apply to reliability evaluation and risk evaluation. Here, we show the simple example to explain the reliability index and failure probability. In Fig.1.5, a probability density function of the difference, M , between the yield stress σ_y and the maximum stress response $\sigma(r)$ is shown. We can find that M has a probability because the maximum stress response has a probability nature and obtained through the uncertainty analysis. When the PDF of M is obtained, the failure probability can be calculated by $M < 0$, and the reliability index can be also calculated by $\beta = \sigma / \mu$ in which σ and μ are mean and standard deviation respectively.

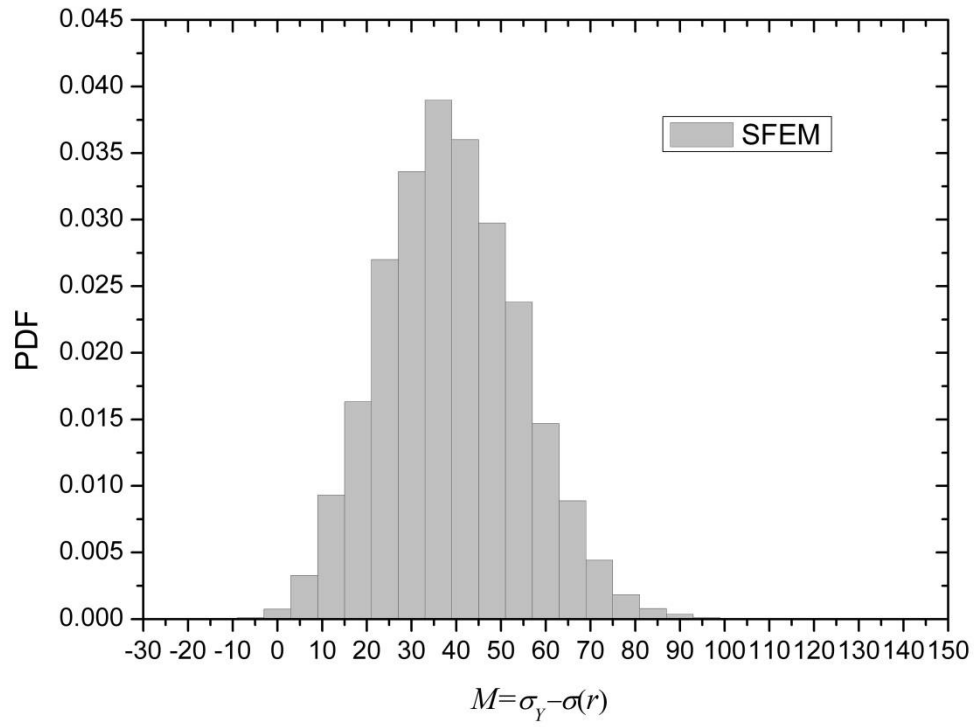


Fig.1.5: A PDF of the Difference Between σ_y and $\sigma(r)$

1.2 Research Purposes

Based on the above studies, in this paper, the following tasks have been studied.

1.2.1 2D Elastostatic Problem

The Stochastic Finite Element Method (SFEM) based on response surface methodology is formulated for the 2D elastostatic problem with uncertainty in shape to follow the normal distribution and non-normal distribution. The uncertainty of response of a displacement, strain and stress can be estimated by this method that solves the main stiffness equation only once. The proposed method makes use of an Hermite polynomial chaos expansion (PCE) to represent the uncertainty of shapes and the response surface, and involves a mathematical formulation which is a natural extension of the deterministic finite element concept to the space of random variables.

1.2.2 Eigenvalue Problem

In order to solve the stochastic eigenvalue problem, as the second objective, we have proposed two methods. Firstly, the improved stochastic inverse power method (I-SIPM) based on response surface methodology is proposed. The method is different with previous stochastic inverse power method [28]. The minimum eigenvalue and eigenvector of stochastic eigenvalue problems can be effectively evaluated by using the proposed method. Secondly, the stochastic Wielandt deflation method (SWDM) is proposed which can realize to evaluate $i^{\text{th}}(i>1)$ eigenvalues and eigenvectors of stochastic eigenvalue problems.

In Chapter 2, we have detailed on the general theories required for the stochastic model formulation. And theories used in the probabilistic domain have been illustrated in detail. In Chapter 3 we show the formulation of stochastic 2D structural static problem which consists of three parts: the stochastic finite element method for uncertainty in shape following normal distribution, the stochastic finite element method for uncertainty in shape following non-normal distribution and evaluation of accuracy of the proposed analysis

method. In Chapter 4 we show the formulation of stochastic eigenvalue problems which consists of four parts: statement of the stochastic eigenvalue problem, the formularization of the improved stochastic inverse power method, the formularization of the stochastic Wielandt deflation method and numerical examples. Finally in Chapter 5 the study have been summarized and future works have also been illustrated.

2. Theoretical Background

In order to realize the uncertainty assessment of the response of structures, in this chapter, we require to investigate two different domains. One is the probabilistic domain in which the uncertainty of the structures response is depending on the uncertainty of an input parameter that may have significant effect on the response. So, we require use an appropriate techniques to approximate the response of structure and to represent the input parameters. In section 2.1, the appropriate techniques will be illustrated. The other one is the structural domain which involves some mathematical techniques, i.e., the finite element method-2D elastostatic problems, and the technique about eigenvalue problems in vibration analysis and buckling analysis which involves two numerical methods to evaluate the eigenvalue and the eigenvector. In this chapter, we introduce both the probabilistic problem and the structural problem in detail. It is very important to understand how both the domains can be integrated which will be presented in chapter 3 and chapter 4.

2.1 Probabilistic Domain

2.1.1 Polynomial Chaos Expansion (PCE)

In this section, we will introduce polynomial chaos expansion techniques because it will be used to expand the deterministic finite element method to stochastic finite element method.

The polynomial chaos is an expansion of orthogonal polynomials in terms of random variables to approximate the uncertainty distribution of the input/output by using orthogonal basis functions, $\Psi_i(\boldsymbol{\theta})$. This concept was originally developed by Weiner et al. [30]. The general random response surface $X(\boldsymbol{\theta})$, viewed as a function of the input random variables can be represented by the following equation.

$$X(\boldsymbol{\theta}) = \sum_{i=0}^{\infty} x_i \Psi_i(\boldsymbol{\theta}), \quad (2.1)$$

where $\boldsymbol{\theta} = \{\theta_1, \dots, \theta_n\}$ is a set of n -dimensional input random variables. $\Psi_i(\boldsymbol{\theta})$ denotes the i^{th} basis function represented by Hermite polynomials of the variables $(\boldsymbol{\theta})$. And, x_i are the unknown coefficients and the response surface can be obtained when the coefficients are determined. i represents the items of expansion polynomials and the items can be an infinite ($i = 0, 1, 2, \dots, \infty$) because theoretically, the larger items is more similar to real result. However, this is difficult to achieve. Thus, we will consider a finite terms of expansion, P , and assume that it can adequately represent the stochastic response. So we have the following finite expression:

$$X(\boldsymbol{\theta}) = \sum_{i=0}^P x_i \Psi_i(\boldsymbol{\theta}), \quad (2.2)$$

where, $P+1$ can be defined by the dimension of the random variables n and the order of polynomials [31].

$$P+1 = \frac{(m+n)!}{m!n!}. \quad (2.3)$$

When the input random variables, $\boldsymbol{\theta}$, are considered as standard normal, the basis functions, $\Psi_i(\boldsymbol{\theta})$, will be represented by Hermite polynomials[31]. So that the orthogonal properties of the Hermite polynomials with respect to a weight function $W(\boldsymbol{\theta})$ as shown following.

$$\int_D \Psi_i(\boldsymbol{\theta}) \Psi_j(\boldsymbol{\theta}) W(\boldsymbol{\theta}) d\boldsymbol{\theta} = \langle \Psi_i^2(\boldsymbol{\theta}) \rangle \delta_{ij}, \quad (2.4)$$

where δ_{ij} represents the Kronecker-Delta property. When Hermite polynomials are used as basis functions, the weight function $W(\boldsymbol{\theta})$ is the probability density function of the standard normal distribution [32] as follows:

$$W(\boldsymbol{\theta}) = \frac{1}{\sqrt{(2\pi)^n}} e^{-\frac{1}{2}\boldsymbol{\theta}^T \boldsymbol{\theta}}. \quad (2.5)$$

As an example, orthogonal basis functions and the values of $\langle \Psi_i^2(\boldsymbol{\theta}) \rangle$ for 1-D and 2-D by Hermite polynomials are shown in Table 2.1 and Table 2.2 respectively.

Table 2.1 One-Dimensional Hermite polynomial chaoses[33]

(Basis functions)

i	Order of the Basis function	i^{th} Basis function Ψ_i	$\langle \Psi_i^2 \rangle$
0	0	1	1
1	1	θ	1
2	2	$\theta^2 - 1$	2
3	3	$\theta^3 - 3\theta$	6
4	4	$\theta^4 - 6\theta^2 + 3$	24

Table 2.2 Two-Dimensional Hermite polynomial chaoses[33]

(Basis functions)

i	Order of the Basis function	i^{th} Basis function Ψ_i	$\langle \Psi_i^2 \rangle$
0	0	1	1
1	1	θ_1	1
2		θ_2	1
3	2	$\theta_1\theta_2$	1
4		$\theta_1^2 - 1$	2
5		$\theta_2^2 - 1$	2
6	3	$\theta_1^2\theta_2 - \theta_2$	2
7		$\theta_1\theta_2^2 - \theta_1$	2
8		$\theta_1^3 - 3\theta_1$	6
9		$\theta_2^3 - 3\theta_2$	6

Apart from the orthogonal properties, these basis functions also satisfy the following equation.

$$\begin{aligned}\langle \Psi_0(\boldsymbol{\theta}) \rangle &= \int_D \Psi_0(\boldsymbol{\theta}) W(\boldsymbol{\theta}) d\boldsymbol{\theta} = 1, \\ \langle \Psi_m(\boldsymbol{\theta}) \rangle &= \int_D \Psi_m(\boldsymbol{\theta}) W(\boldsymbol{\theta}) d\boldsymbol{\theta} = 0 \quad \text{for } m = 1, 2, \dots, p,\end{aligned}\tag{2.6}$$

where, D is the support domain of the random variable. The mean and standard deviation of the stochastic response (Eq.2.2) can be simply calculated as follows.

$$\mu_X = E[X] = \langle X \rangle = x_0,\tag{2.7}$$

$$\begin{aligned}\sigma_X &= \sqrt{\text{Var}[X]} = \sqrt{\langle (X - E[X])^2 \rangle} \\ &= \sqrt{\langle \left(\sum_{j=0}^P x_j \Psi_j(\boldsymbol{\theta}) - x_0 \right)^2 \rangle} = \sqrt{\langle \left(\sum_{i=1}^P x_i \Psi_i(\boldsymbol{\theta}) \right)^2 \rangle} \\ &= \sqrt{\sum_{i=1}^P x_i^2 \langle \Psi_i(\boldsymbol{\theta})^2 \rangle}.\end{aligned}\tag{2.8}$$

Once the response, $X(\boldsymbol{\theta})$, is determined, we can approximate the mean and standard deviation of the response by using Eq. 2.7 and Eq. 2.8. Moreover, we can obtain the probability density function of the response by using large number of realizations of standard normal random variables ($\boldsymbol{\theta}$) and plugging them into Eq. 2.2.

Above, we explained that the input random variables, $\boldsymbol{\theta}$, are standard normal distribution. When the random variables follow different probability distribution, the corresponding orthogonal polynomials have been proposed by Xiu and Karniadakis [32]. Here we show the type of independent variables in the polynomials according to the type of random distributions in Table 2.3, in which contains two parts for continuous and discrete by the Weiner-Askey scheme[32].

Table 2.3 Weiner-Askey Scheme [32]

	<i>Random variables θ</i>	<i>Polynomial</i>	<i>Support</i>
<i>Continuous</i>	<i>Gaussian</i>	<i>Hermite</i>	$(-\infty, \infty)$
	<i>Gamma</i>	<i>Laguerre</i>	$[0, \infty)$
	<i>Beta</i>	<i>Jacobi</i>	$[a, b]$
	<i>Uniform</i>	<i>Legendre</i>	$[a, b]$
<i>Discrete</i>	<i>Poisson</i>	<i>Charlier</i>	$\{0, 1, 2, \dots\}$
	<i>Binomial</i>	<i>Krawtchouk</i>	$\{0, 1, \dots, N\}$
	<i>Negative Binomial</i>	<i>Meixner</i>	$\{0, 1, 2, \dots\}$
	<i>Hypergeometric</i>	<i>Hahn</i>	$\{0, 1, \dots, N\}$

2.1.2 Application of Polynomial Chaos[32]

In this section, Applications of polynomial chaos is described. First, let us consider the stochastic differential equation with input random variables (θ).

$$\mathcal{L}(X(\mathbf{x}, \theta); u(\mathbf{x}, \theta)) = f(\mathbf{x}, \theta), \quad (2.9)$$

where, \mathcal{L} is a general differential equation and can represent linear or non-linear. $X(\mathbf{x}, \theta)$ represents the input parameters which is a function about random variables θ , and $u(\mathbf{x}, \theta)$ is the response term. $f(\mathbf{x}, \theta)$ represents the source (such as loading) term which can also contain random variables θ or do not contain random variables θ . Here, the input random variables are introduced into the system through geometrical shapes, initial conditions, material properties, etc. when the system contain random variables, the response u can be represented as random term by Polynomial Chaos Expansion (PCE) as follows:

$$u(\mathbf{x}, \theta) = \sum_{i=0}^P u_i(\mathbf{x}) \Psi_i(\theta). \quad (2.10)$$

In this equation, where $u_i(\mathbf{x})$ are the unknown coefficients of the PCE approximation and P is the number of terms which is obtained by Eq.(2.3) and $\Psi_i(\boldsymbol{\theta})$ are the polynomial basis functions (Table 2.1 and Table 2.2). Substituting Eq. (2.10) into Eq. (2.9), the equation becomes as follows:

$$\mathcal{L}\left(\mathbf{X}(\mathbf{x}, \boldsymbol{\theta}); \sum_{i=0}^P u_i(\mathbf{x}) \Psi_i(\boldsymbol{\theta})\right) = f(\mathbf{x}, \boldsymbol{\theta}), \quad (2.11)$$

where, the polynomial basis functions $\Psi_i(\boldsymbol{\theta})$ are orthogonal. Thus when the orthogonal property of polynomial is considered, we can obtain the following equation by multiplying both sides of Eq. (2.11) by $\Psi_i(\boldsymbol{\theta})W(\boldsymbol{\theta})$, and integrating the equation over the stochastic domain, we have:

$$\left\langle \mathcal{L}\left(\mathbf{x}(\boldsymbol{\theta}); \sum_{i=0}^P u_i(\mathbf{x}) \Psi_i(\boldsymbol{\theta})\right), \Psi_i(\boldsymbol{\theta}) \right\rangle = \langle f(\mathbf{x}(\boldsymbol{\theta})), \Psi_i(\boldsymbol{\theta}) \rangle. \quad (2.12)$$

When the $i = 0, 1, \dots, P$, we can obtain a set of $(P + 1)$ simultaneous equations for each unknown coefficients $u_i(\mathbf{x})$. The unknown coefficients $u_i(\mathbf{x})$ is obtained by solving these simultaneous equations, and the response can be obtained by Eq. (2.10).

In order to make the application of PCE easier to understand, we show the image of the application of PCE in Fig.2.1. The input parameters, $R(\boldsymbol{\theta})$ is expressed as a polynomial form when the inherent of model has uncertainty and obeying the different random variable (θ_1, θ_2) , then the stochastic response, $u(\boldsymbol{\theta})$ is approximated as a polynomial function (Polynomial Chaos Expansion) of the input random variables, $\boldsymbol{\theta} = \{\theta_1, \theta_2\}$ as output parameter because the input include uncertainty. When the expressed input parameters and the approximated output parameters (response) is applied to the governing equations (such as finite element equation), the governing equations will be redefined as a new equations about the deterministic coefficients, u_i , of the PCE. Thus we can understand these

unknown coefficients become the response of the governing equations. When the coefficients u_i is determined by solving the redefined governing equations, the response surface $u(\boldsymbol{\theta})$ can be obtained. And we can obtain the probability density distribution by using 10000 realization of the standard random variable $\boldsymbol{\theta}$ in the obtained response surface $u(\boldsymbol{\theta})$.

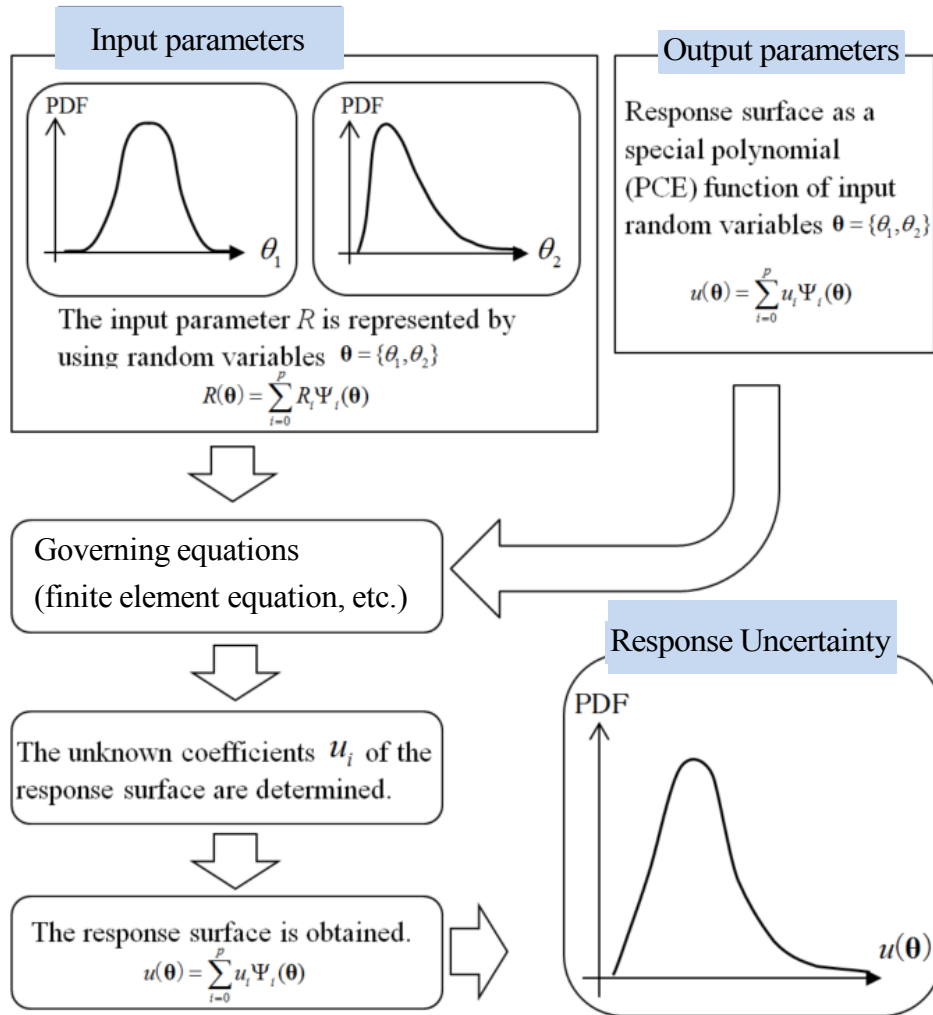


Fig.2.1: The Spectral Approach Concept

2.1.3 Numerical Example

In this section, In order to explain the application of polynomial chaos, we show a simple numerical example of a spring problem (see Fig.2.2). The displacement of the spring problem is discussed considering stiffness with uncertainty. The governing differential equation of this problem (Eq. (2.13)) and its analytical solution is well known hence it has been chosen as an example to illustrate the method.

$$ku = P , \quad (2.13)$$

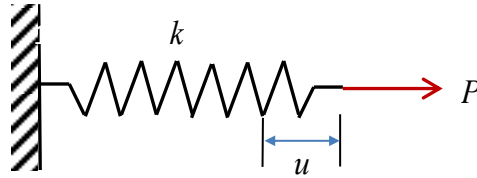


Fig.2.2: A Spring Problem

where P is the concentrated load as 1N/mm^2 , the u is displacement and is unknown, The k is spring stiffness and assumed following Gaussian distribution with mean 10N/mm^2 and standard deviation of 2N/mm^2 . So the k can be expressed as follows.

$$k = k_{\mu} + k_{\sigma}\theta , \quad (2.14)$$

where, $k_{\mu}=10\text{N/mm}^2$, $k_{\sigma}=2\text{N/mm}^2$ and θ is a standard normal random variable. In other words, the spring stiffness can be represented as follows by Hermite polynomial of 1st order.

$$\begin{aligned} k &= k_{\mu}\Psi_0(\theta) + k_{\sigma}\Psi_1(\theta) \\ &= \sum_{i=0}^1 k_i\Psi_i(\theta). \end{aligned} \quad (2.15)$$

In this problem, the displacement is considered as response of the system which has an uncertainty because the spring stiffness has an uncertainty, thus the response can be approximate by using n^{th} dimensional PCE of the random variable θ as follows.

$$u(\theta) = \sum_{i=0}^n u_i \Psi_i(\theta), \quad (2.16)$$

where $\Psi_i(\theta)$ are the orthogonal basis function by Hermite polynomials of the variables (θ) , and u_i are the unknown coefficients of PCE, θ is a Gaussian random variable. The main idea is to approximate the response $u(\theta)$ by using orthogonal polynomials with unknown coefficients u_i . At this point, it is fairly clear that we need to estimate u_i , which will enable us to generate statistics of the response completely. This can be achieved as described following.

First we substitute Eq. (2.15) and Eq. (2.16) into Eq. (2.13) as follows.

$$\sum_{i=0}^1 k_i \Psi_i(\theta) \sum_{i=0}^n u_i \Psi_i(\theta) = P. \quad (2.17)$$

Utilizing the orthogonality condition, we Multiply both sides of Eq. (2.17) by $\Psi_i(\theta)w(\theta)$, and integrating the equation, the following equations is obtained.

$$\sum_{i=0}^1 \sum_{j=0}^n k_i u_j \langle \Psi_i(\theta) \Psi_j(\theta) \Psi_i(\theta) \rangle = P \langle \Psi_i(\theta) \rangle. \quad (2.18)$$

For convenience of calculations, the order (n) of PCE approximation of Eq. (2.16) is assumed as 2.

Thus the simultaneous equations can be derived as follows.

$$\begin{bmatrix} \sum_{i=0}^1 \sum_{j=0}^2 k_i u_j \langle \Psi_i(\theta) \Psi_j(\theta) \Psi_0(\theta) \rangle \\ \sum_{i=0}^1 \sum_{j=0}^2 k_i u_j \langle \Psi_i(\theta) \Psi_j(\theta) \Psi_1(\theta) \rangle \\ \sum_{i=0}^1 \sum_{j=0}^2 k_i u_j \langle \Psi_i(\theta) \Psi_j(\theta) \Psi_2(\theta) \rangle \end{bmatrix} = \begin{bmatrix} P \langle \Psi_0(\theta) \rangle \\ P \langle \Psi_1(\theta) \rangle \\ P \langle \Psi_2(\theta) \rangle \end{bmatrix}. \quad (2.19)$$

We can see that there are three equations with three unknowns u_0, u_1, u_2 . Thus we need to solve only three deterministic equations to generate the polynomial chaos approximation of response (response surface) $u(\theta)$. We can approximate the mean and standard deviation of the response by using Eq. (2.7) and Eq. (2.8). Moreover, we can obtain the probability density function of the response by using large number of realizations of standard normal random variable (θ) and plugging them into Eq. (2.16). Thus we can clearly understand that the MCS has been avoided when this method is used.

And for clarity we show second order PCE ($n=2$). The inner product values used for $i, k=0,1,2$ are shown in the following tables.

Table 2.4 Inner Products

$$\langle \Psi_i(\theta) \Psi_k(\theta) \Psi_0(\theta) \rangle$$

$k \backslash i$	0	1	2
0	1	0	0
1	0	1	0
2	0	0	2

$$\langle \Psi_i(\theta) \Psi_k(\theta) \Psi_1(\theta) \rangle$$

$k \backslash i$	0	1	2
0	0	1	0
1	1	0	2
2	0	2	0

$$\langle \Psi_i(\theta) \Psi_k(\theta) \Psi_2(\theta) \rangle$$

$k \backslash i$	0	1	2
0	0	0	2
1	0	2	2
2	2	0	8

The following Table 2.5 shows the PCE approximated mean and standard deviation of the response $u(\theta)$ obtained from the present stochastic method. Also 10000 simulations of the deterministic problem have been carried out with variable spring stiffness to verify the accuracy.

Table 2.5 Comparative Statistics of Response $u(\theta)$ through PCE and MCS

Statistics of $u(\theta)$	MCS (10000 samples)	PCE (10000 samples)	PCE (By Eq.)
<i>Mean (mm)</i>	0.10301	0.10307	0.10309
<i>Standard dev. (mm)</i>	0.01039	0.01038	0.01039

In Fig.2.3, the polynomial chaos approximation of response is shown, and the probability density distribution is obtained by using the response surface which is shown to prove that the results are well consistent with MCS results. Also, as shown in Table 2.5, we find that the statistics are reasonably well estimated by the PCE (10000 samples) when compared with those obtained from MCS. Note that the mean and the standard deviation of “PCE” in the Table 2.5 are calculated by Eq. (2.7) and Eq. (2.8), which also takes almost same value.

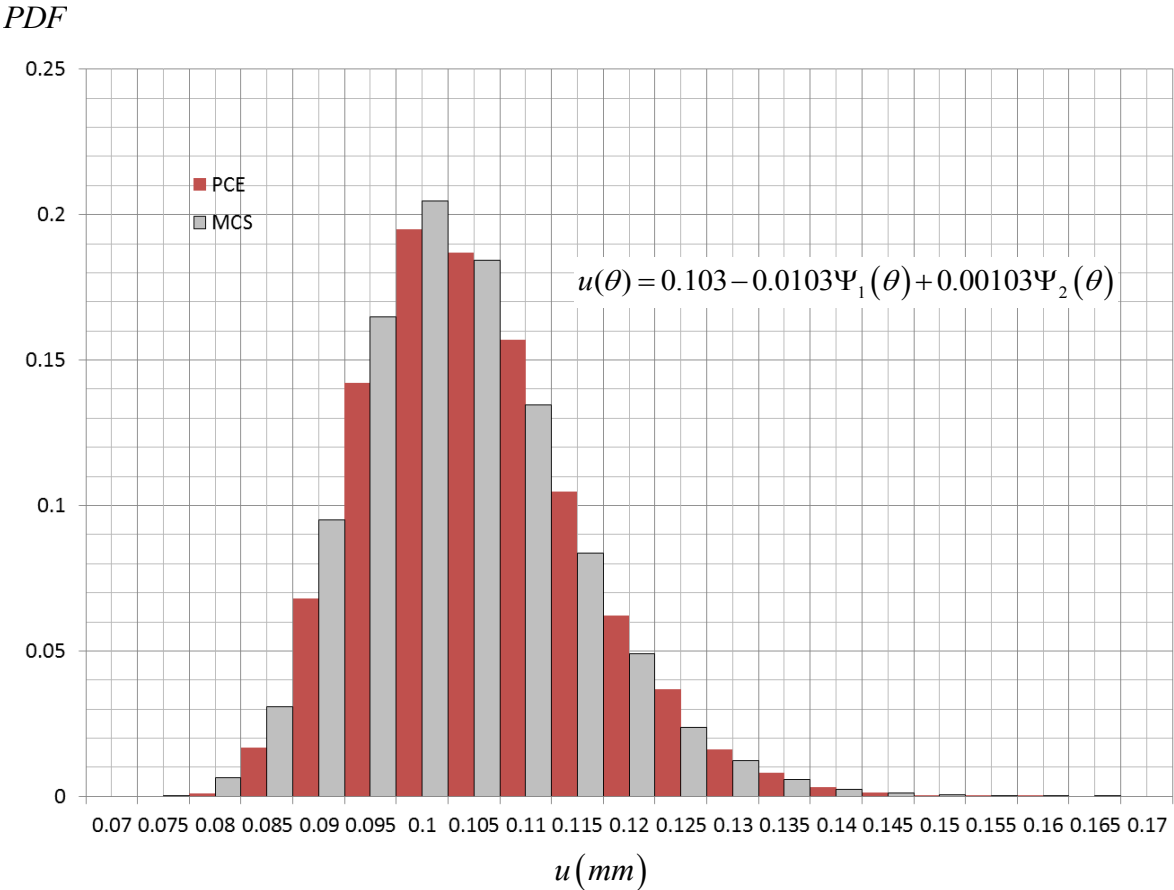


Fig. 2.3: The Probability Density Distributions of the Buckling Load

2.2 Structural Domain-2D Structural Static Problem

The goal of this section is to introduce some theories as preliminary knowledge. In this section, the basic theory about the 2D structural static problem will be briefly expounded in the linear static analysis [35]. These theories are importantly for to understand formularization in the section 3 easily.

Here, we will expound this problem from the element finite equation as follows.

$$\mathbf{k}\mathbf{u}=\mathbf{f} , \quad (2.20)$$

where, the \mathbf{k} is the global stiffness matrix which obtained from the element stiffness matrix \mathbf{k}^e , the \mathbf{u} is the displacement, the \mathbf{f} is the global force vector which obtained from the element force vector \mathbf{f}^e . And the element stiffness matrix of finite element method is construed by the integration of element coordinates (ξ, η) as shown in Eq. (2.21).

$$\mathbf{k}^e = \int_{-1}^{+1} \int_{-1}^{+1} \mathbf{B}^T(\xi, \eta) \mathbf{D} \mathbf{B}(\xi, \eta) |\mathbf{J}(\xi, \eta)| d\xi d\eta , \quad (2.21)$$

where \mathbf{B} is a strain matrix, \mathbf{D} is a matrix of material property and \mathbf{J} is a Jacobian matrix. \mathbf{B} and \mathbf{J} are related to nodal coordinates. They are shown as follows.

$$\mathbf{B} = \begin{bmatrix} \frac{\partial N_1}{\partial x} & 0 & \frac{\partial N_2}{\partial x} & 0 & \frac{\partial N_3}{\partial x} & 0 & \frac{\partial N_4}{\partial x} & 0 \\ 0 & \frac{\partial N_1}{\partial y} & 0 & \frac{\partial N_2}{\partial y} & 0 & \frac{\partial N_3}{\partial y} & 0 & \frac{\partial N_4}{\partial y} \\ \frac{\partial N_1}{\partial y} & \frac{\partial N_1}{\partial x} & \frac{\partial N_2}{\partial y} & \frac{\partial N_2}{\partial x} & \frac{\partial N_3}{\partial y} & \frac{\partial N_3}{\partial x} & \frac{\partial N_4}{\partial y} & \frac{\partial N_4}{\partial x} \end{bmatrix} , \quad (2.22)$$

where N_i is the shape functions when the Isoparametric four note element (Iso4) is considered as follows.

$$\begin{aligned}
N_1(\xi, \eta) &= \frac{1}{4}(1-\xi)(1-\eta), \\
N_2(\xi, \eta) &= \frac{1}{4}(1+\xi)(1-\eta), \\
N_3(\xi, \eta) &= \frac{1}{4}(1+\xi)(1+\eta), \\
N_4(\xi, \eta) &= \frac{1}{4}(1-\xi)(1+\eta).
\end{aligned} \tag{2.23}$$

The \mathbf{D} is the constitutive matrix in plane stress.

$$\mathbf{D} = \frac{E}{1-\nu^2} \begin{bmatrix} 1 & \nu & 0 \\ \nu & 1 & 0 \\ 0 & 0 & \frac{1-\nu}{2} \end{bmatrix}. \tag{2.24}$$

The matrix \mathbf{J} can be derived and is shown as follows.

$$\mathbf{J} = \begin{bmatrix} \frac{\partial x}{\partial \xi} & \frac{\partial y}{\partial \xi} \\ \frac{\partial x}{\partial \eta} & \frac{\partial y}{\partial \eta} \end{bmatrix} = \begin{bmatrix} \sum_{i=1}^4 \frac{\partial N_i}{\partial \xi}(x_i) & \sum_{i=1}^4 \frac{\partial N_i}{\partial \xi}(y_i) \\ \sum_{i=1}^4 \frac{\partial N_i}{\partial \eta}(x_i) & \sum_{i=1}^4 \frac{\partial N_i}{\partial \eta}(y_i) \end{bmatrix}. \tag{2.25}$$

Generally in the finite element formulation, the component, $\frac{\partial N_i}{\partial x}$ and $\frac{\partial N_i}{\partial y}$, in the \mathbf{B} matrix is depicted as follows.

$$\begin{bmatrix} \frac{\partial N_i}{\partial x} \\ \frac{\partial N_i}{\partial y} \end{bmatrix} = [\mathbf{J}]^{-1} \begin{bmatrix} \frac{\partial N_i}{\partial \xi} \\ \frac{\partial N_i}{\partial \eta} \end{bmatrix}, \tag{2.26}$$

where, $[\mathbf{J}]^{-1}$ is inverse of \mathbf{J} , and can be found by Eq. (2.27).

$$[\mathbf{J}]^{-1} = \frac{1}{\det \mathbf{J}} \begin{bmatrix} J_{22} & -J_{12} \\ -J_{21} & J_{11} \end{bmatrix}. \quad (2.27)$$

The determinant of \mathbf{J} can be given as follows.

$$\det \mathbf{J} = J_{11}J_{22} - J_{21}J_{12}. \quad (2.28)$$

The global stiffness matrix can be assembled when the element stiffness matrix is obtained. And then the element force vector is derived where only the distributed load \mathbf{h} is applied to the element edge (see edge 1-2 in Fig.2.4).

When constant surface force vector in one element edge is considered, the force vector in node A (A=1 or 2) is represented as follows.

$$\mathbf{f}_A^e(\theta) = \int_{-1}^{+1} N_A \left(N_1^0 \mathbf{h} + N_2^0 \mathbf{h} \right) j^e(\xi; \theta) d\xi, \quad (2.29)$$

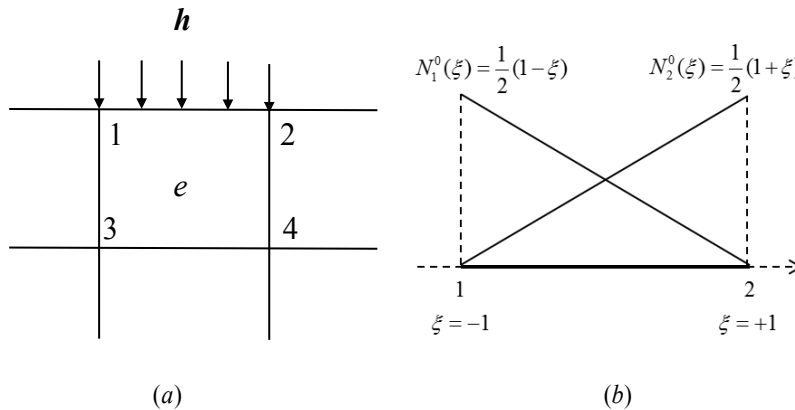


Fig.2.4: The Distributed Load along the Side of Element

where N_1^0, N_2^0 are the shape functions for the surface force applied to the edge(1-2)(see Fig.2.4(b)), and j^e is the line Jacobian (as show below).

$$j^e = \sqrt{\left(\frac{\partial x}{\partial \xi}\right)^2 + \left(\frac{\partial y}{\partial \eta}\right)^2} . \quad (2.30)$$

We use the shape functions to interpolate the coordinates between the nodes.

$$\begin{aligned} x &= \sum_{i=1}^2 N_i^0 x_i , \\ y &= \sum_{i=1}^2 N_i^0 y_i . \end{aligned} \quad (2.31)$$

The line Jacobian is obtained by substitute Eq. (2.31) into Eq. (2.30).

$$j^e = \frac{1}{2}(x_1 - x_2) . \quad (2.32)$$

Thus, the force vector is represented as follows.

$$\mathbf{f}^e = \int_{-1}^{+1} \frac{1}{2} N_A (N_1^0 \mathbf{h}_1 + N_2^0 \mathbf{h}_2) \times (x_1 - x_2) d\xi . \quad (2.33)$$

The force vector can be derived by assembly of element force vector.

When the global system stiffness system is computed, the displacement can be evaluated by solve Eq. (2.20). And the stress can be assessed by matrix of material property \mathbf{D} and strain matrix \mathbf{B} and displacement \mathbf{u} .

$$\boldsymbol{\sigma} = \mathbf{DBu} . \quad (2.34)$$

2.3 Structural Domain- Eigenvalue Problem

Eigenvalue analysis is an important problem in a variety of fields. In structural mechanics in the field of naval architecture and ocean engineering, eigenvalue problems commonly appear in the context of, e.g. vibrations and buckling. In the vibrations analysis, the eigenvalue analysis is used to evaluate the natural frequencies (or Eigen frequencies) of vibration, and the eigenvectors determine the shapes of these vibrational modes. And in the buckling analysis, eigenvalue analysis can be used to evaluate the buckling load (eigenvalue buckling analysis) and buckling mode. In section 2.3, the basic theory about eigenvalue problem is expounded in eigenvalue analysis, and solution of eigenvalue problem is also introduced because the stochastic eigenvalue problem will be proposed in section 4. These theories are importantly for to understand formularization of stochastic eigenvalue problem easily.

2.3.1 In the Vibrations Analysis[36]

Here, we consider a dynamic system. The equations of motion in matrix can be expressed as follows.

$$\mathbf{M}\ddot{\mathbf{u}} + \mathbf{B}\dot{\mathbf{u}} + \mathbf{K}\mathbf{u} = \mathbf{P}, \quad (2.35)$$

where, \mathbf{u} is displacement, and the \mathbf{M} is a mass matrix, \mathbf{B} is a damping matrix, \mathbf{K} is a stiffness matrix, and \mathbf{P} is a load vector.

When we consider this system that there is no damping and no applied loading, the equations of motion can be written as follows. We find it becomes as free vibration equation.

$$\mathbf{M}\ddot{\mathbf{u}} + \mathbf{K}\mathbf{u} = 0. \quad (2.36)$$

In order to solve Eq.(2.36), we assume the displacement can be described by a sinusoidal vibration.

$$\mathbf{u} = \Phi e^{i\omega t}, \quad (2.37)$$

where, Φ is eigenvector, ω is the circular natural frequency. And the acceleration is the second derivative of the displacement, it is shown as follows.

$$\ddot{\mathbf{u}} = -\omega^2 \Phi e^{i\omega t}. \quad (2.38)$$

Substituted into the equation of motion (Eq.(2.36)), the following is obtained.

$$-\omega^2 \mathbf{M} \Phi e^{i\omega t} + \mathbf{K} \Phi e^{i\omega t} = 0. \quad (2.39)$$

Because $e^{i\omega t}$ cannot zero, the equation will be rewritten as the form of a general eigenvalue problem.

$$(\mathbf{K} - \lambda \mathbf{M}) \Phi = 0, \quad (2.40)$$

where, \mathbf{K} is a linear stiffness matrix, \mathbf{M} is a mass matrix, λ is the eigenvalue which $\lambda = \omega^2$ that related to the natural frequency, Φ is the corresponding eigenvector that represents the vibrational mode.

As traditional eigenvalue solution, we can find that there are two possible solutions for Eq. (2.40):

1. If determinant $(\mathbf{K} - \lambda \mathbf{M}) \neq 0$, the only possible solution is shown.

$$\Phi = 0. \quad (2.41)$$

This is the trivial solution, and we can understand that it represents the case of no motion. And it is consider that this solution is totally meaningless. Thus we consider following solution.

2. If determinant $(\mathbf{K} - \lambda \mathbf{M}) = 0$, that is $\Phi \neq 0$. So the solution is obtained.

$$\text{determinant}(\mathbf{K} - \lambda\mathbf{M}) = 0. \quad (2.42)$$

By solving the equation, we can obtain the eigenvalues λ_i , and corresponding eigenvectors Φ_i . In solving the above eigenvalue problem, we can see that many eigenvalues and corresponding eigenvectors will be obtained for multi degrees of freedom problem. However, from practical problem often only some smaller natural frequency is concerned. So the frequency of first mode is always considered as important. In section 2.3.3, we will introduce a numerical method (The inverse power method) for solving the first mode, and introduce other numerical method (The Wielandt deflation method) based on the inverse power method for solving other some smaller mode.

2.3.2 In Linear Buckling Analysis

In this section, we will introduce theory of linear buckling analysis. In linear buckling analysis, the critical buckling load of structure is generally concerned. In order to estimate the critical buckling load of structures, the eigenvalue of system will be evaluated because the critical buckling load is the product of the eigenvalue and the static load. Thus eigenvalue problem is solved as follows.

$$(\mathbf{K} - \lambda\mathbf{K}_\sigma)\mathbf{U} = 0, \quad (2.43)$$

where, \mathbf{K} is the stiffness matrix, λ is the eigenvalues, \mathbf{K}_σ is the initial stress stiffness matrix which is a matrix about the static load F , and \mathbf{U} is the eigenvectors. We can understand that the solution of Eq. (2.43) has n eigenvalues in which n is the number of degrees of freedom. However, not all eigenvalues are required, only the lowest eigenvalues are required for to calculate buckling load and buckling modes. Here, the critical buckling load is shown when minimum eigenvalue is calculated.

$$F_{crit} = \lambda_{minimum} F. \quad (2.44)$$

2.3.3 A Numerical Algorithm

In this section, we will introduce a numerical algorithm to solve eigenvalue problems in order to understand the proposed methods easily in section 4. Firstly, the Inverse Power Method (IPM) is developed to compute minimum eigenvalue and eigenvector, secondly, the Wielandt Deflation Method (WDM) is developed to compute the rest of eigenvalues and eigenvectors based on the inverse power method.

(1) The Inverse Power Method

Algorithm 2.1 The Inverse Power Method [28,37]

Initialize: $\mathbf{u}^{(0)}$

While $\varepsilon > \varepsilon^*$

Step 1: $\lambda^{(q+1)} = (\mathbf{u}^{(q)})^T \mathbf{A} \mathbf{u}^{(q)}$

Step 2: $\mathbf{A} \mathbf{u}^{(q+1)} = \lambda^{(q+1)} \mathbf{u}^{(q)}$

Step 3: $\mathbf{u}^{(q+1)} \rightarrow \frac{\mathbf{u}^{(q+1)}}{\|\mathbf{u}^{(q+1)}\|_{L^2}}$

Step 4: $\varepsilon = \|\mathbf{A} - \lambda^{(q+1)} \mathbf{I}\| \mathbf{u}^{(q+1)}\|_{L^2}$

End While

Result: λ^*, \mathbf{u}^*

As shown front, we show the algorithm for the inverse power method [28, 36]. An approximate eigenvalue and the corresponding eigenvector are evaluated by using the method to solve $(\mathbf{A} - \lambda)\mathbf{u} = 0$ equation where \mathbf{A} is $\mathbf{R}^{-1}\mathbf{K}$, Note that \mathbf{R} is regular (non-singular) matrix in general vibration and buckling problems.

The inverse power method is an iterative method for computing minimum eigenvalue (Algorithm 1), where q is iterations, $\mathbf{u}^{(0)}$ is initial normalized eigenvector, \mathbf{A} is a matrix by $(\mathbf{A} - \lambda)\mathbf{u} = 0$.

step1:

The Rayleigh quotient is used to update the eigenvalue based on the normalized eigenvector $\mathbf{u}^{(q)}$ of the previous iteration using Eq. (2.45). We can see that an eigenvalue $\lambda^{(1)}$ can be found when an initial eigenvector ($q=0$) is known.

$$\lambda^{(q+1)} = (\mathbf{u}^{(q)})^T \mathbf{A} \mathbf{u}^{(q)}. \quad (2.45)$$

step2:

An updated eigenvector $\mathbf{u}^{(1)}$ is found when initial eigenvector $\mathbf{u}^{(0)}$ and eigenvalue $\lambda^{(1)}$ is known, and this equation can be rewritten as

$$\mathbf{u}^{(q+1)} = \lambda^{(q+1)} \mathbf{A}^{-1} \mathbf{u}^{(q)}. \quad (2.46)$$

step3:

In step3, we need to normalize the updated eigenvector $\mathbf{u}^{(1)}$ (this is, the length of eigenvector is 1) because the updated eigenvector is not normalized. This step is necessary, so that it can prevent the magnitude of the eigenvector increase unboundedly from increasing with each iteration step.

$$\mathbf{u}^{(q+1)} \rightarrow \frac{\mathbf{u}^{(q+1)}}{\|\mathbf{u}^{(q+1)}\|_{L^2}}. \quad (2.47)$$

step4:

Finally, the convergence of the iterative method is checked. When the condition $\varepsilon \leq \varepsilon^*$ is satisfied, the iteration will be terminated, and we can obtain an approximate eigenvalue and the corresponding eigenvector.

(2) The Wielandt Deflation Method

In order to solve the all the eigenvalues and eigenvectors, the Wielandt deflation method [38] based on the inverse power method is introduced in this section. The method can to realize computation of concerned the eigenvalues and the eigenvectors. For example, eigenvalues and eigenvectors of 1st and 2nd are only computed when we need 2nd eigenvalues and eigenvectors.

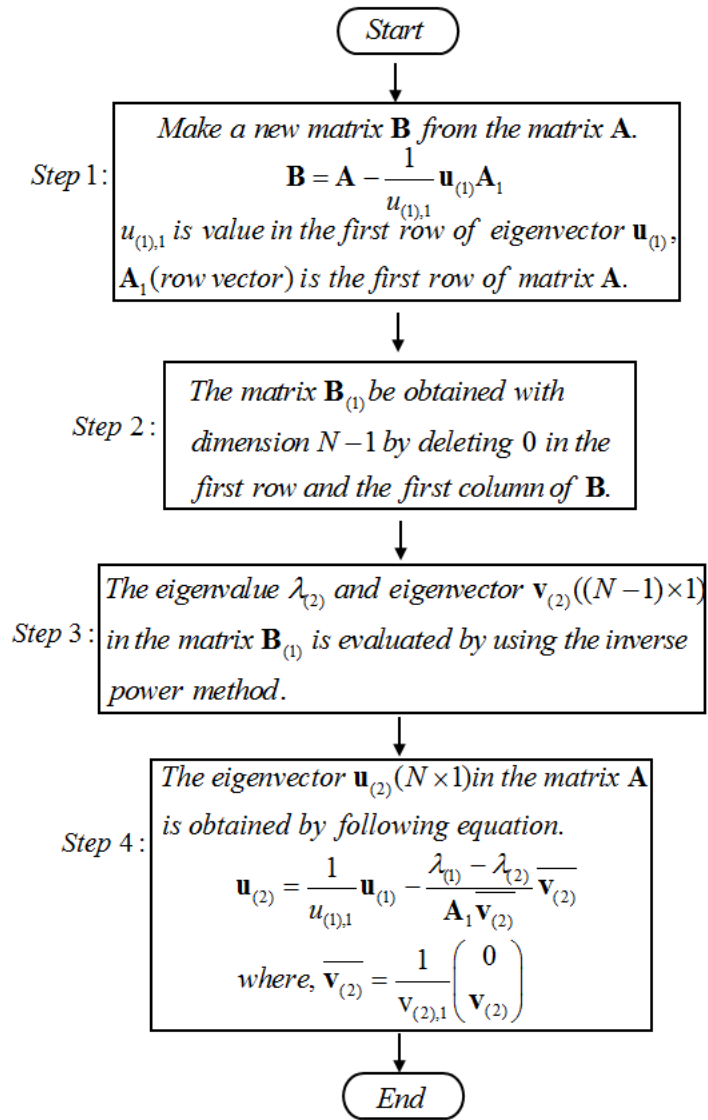


Fig.2.5: Flowchart of the Wielandt Deflation Method

In Fig.2.5, we show the flowchart of the Wielandt deflation method. Generally, if we have the minimum eigenvalue $\lambda_{(1)}$ of \mathbf{A} and corresponding normalized eigenvector $\mathbf{u}_{(1)}$ from the inverse power method, we can make a new matrix \mathbf{B} from the matrix \mathbf{A} , where the eigenvalues of \mathbf{B} are identical to all eigenvalues of \mathbf{A} except the minimum eigenvalue in \mathbf{A} .

Firstly, we will prove the new matrix \mathbf{B} identical to all eigenvalues of \mathbf{A} except the minimum eigenvalue $\lambda_{(1)}$ [38].

Here we assume that the minimum eigenvalue $\lambda_{(1)}$ and corresponding normalized eigenvector $\mathbf{u}_{(1)}$ of \mathbf{A} have been calculated by using the inverse power method. Then in order to prove the new matrix \mathbf{B} identical to all eigenvalues of \mathbf{A} except the minimum eigenvalue $\lambda_{(1)}$, we consider the deflated matrix \mathbf{B} , and it is shown as follows.

$$\mathbf{B} = \mathbf{A} - \mathbf{u}_{(1)}\mathbf{x}_1^T, \quad (2.48)$$

where \mathbf{x}_1 is any vector such that it can defined as follows.

$$\mathbf{x}_1^T \mathbf{u}_{(1)} = \lambda_1. \quad (2.49)$$

Post multiplying Eq.(2.48) by $\mathbf{u}_{(1)}$, we can obtain as follows.

$$\mathbf{B}\mathbf{u}_{(1)} = \mathbf{A}\mathbf{u}_{(1)} - \lambda_{(1)}\mathbf{u}_{(1)}\mathbf{u}_{(1)}^T \mathbf{u}_{(1)}. \quad (2.50)$$

When we consider $\mathbf{u}_{(1)}^T \mathbf{u}_{(1)} = 1$, the Eq.(2.50) can write as follows.

$$\mathbf{B}\mathbf{u}_{(1)} = \lambda_1\mathbf{u}_{(1)} - \lambda_1\mathbf{u}_{(1)} = \mathbf{0}. \quad (2.51)$$

We can see that $\mathbf{u}_{(1)}$ is an eigenvector of the matrix \mathbf{B} belonging to the null eigenvalue. So here, let us consider any vector $\mathbf{u}_{(i)} - \gamma_i \mathbf{u}_{(1)}$, and multiply Eq.(2.48) by $\mathbf{u}_{(i)} - \gamma_i \mathbf{u}_{(1)}$. ($\mathbf{u}_{(1)}^T \mathbf{u}_{(i)} = 0$)

$$\begin{aligned} \mathbf{B}(\mathbf{u}_{(i)} - \gamma_i \mathbf{u}_{(1)}) &= \mathbf{A}(\mathbf{u}_{(i)} - \gamma_i \mathbf{u}_{(1)}) - \mathbf{u}_{(1)}\mathbf{x}_{(1)}^T (\mathbf{u}_{(i)} - \gamma_i \mathbf{u}_{(1)}) \\ &= \lambda_{(i)}\mathbf{u}_{(i)} - \mathbf{u}_{(1)}\mathbf{x}_{(1)}^T \mathbf{u}_{(i)} \\ &= \lambda_{(i)} \left(\mathbf{u}_{(i)} - \left(\frac{1}{\lambda_{(i)}} \mathbf{x}_{(1)}^T \mathbf{u}_{(i)} \right) \mathbf{u}_{(1)} \right). \end{aligned} \quad (2.52)$$

By Eq.(2.52), $\gamma_i = \frac{1}{\lambda_{(i)}} \mathbf{x}_{(1)}^T \mathbf{u}_{(i)}$ and introducing the notation,

$$\mathbf{v}_{(i)} = \mathbf{u}_{(i)} - \left(\frac{1}{\lambda_{(i)}} \mathbf{x}_{(1)}^T \mathbf{u}_{(i)} \right) \mathbf{u}_{(1)}. \quad (2.53)$$

We can write Eq.(2.53) in the form.

$$\mathbf{B}\mathbf{v}_{(i)} = \lambda_{(i)} \mathbf{v}_{(i)}. \quad (2.54)$$

From which we conclude that the nonzero eigenvalues of the matrix \mathbf{B} are $\lambda_{(2)}, \lambda_{(3)}, \dots, \lambda_{(N)}$ and hence the same as the subdominant eigenvalues of the matrix \mathbf{A} . on the other hand, the corresponding eigenvectors of the matrix \mathbf{B} are $\mathbf{v}_{(2)}, \mathbf{v}_{(3)}, \dots, \mathbf{v}_{(N)}$. In order to obtain the eigenvectors of the matrix \mathbf{A} , we need to do computation by Eq.(2.53).

When we understand the above concept, the step of Wielandt deflation method will be illustrated for to evaluate all the eigenvalues and eigenvectors.

step1:

As shown in Fig.2.5, a new the matrix \mathbf{B} with dimension N can be obtained by following equation.

$$\mathbf{B} = \mathbf{A} - \frac{1}{u_{(1),1}} \mathbf{u}_{(1)} \mathbf{A}_1, \quad (2.55)$$

where $u_{(1),1}$ is value in the first row of eigenvector $\mathbf{u}_{(1)}$, and \mathbf{A}_1 (row vector) is the first row of matrix \mathbf{A} . The first row of the matrix \mathbf{B} is 0 by calculating Eq. (2.55).

step2:

In *step2*, the first row and the first column of matrix \mathbf{B} are deleted to obtain a new matrix $\mathbf{B}_{(1)}$ with dimension $N-1$. Then the matrix $\mathbf{B}_{(1)}$ has eigenvalues $\lambda_{(2)}, \lambda_{(3)}, \dots, \lambda_{(N)}$.

Step3:

Next, the defined new matrix $\mathbf{B}_{(1)}$ is used to the inverse power method to evaluate a new minimum eigenvalue (this is, the 2nd eigenvalue $\lambda_{(2)}$ in \mathbf{A}). But we need to obtain an eigenvector with dimension N , because obtained eigenvector is vector with dimension $N-1$. Therefore by *step4*, the 2nd eigenvector $\mathbf{u}_{(2)}$ can be derived.

step4:

In *step4*, Eq. (2.56) can be used to obtain the eigenvector \mathbf{u} of the matrix \mathbf{A} .

$$\mathbf{u}_{(2)} = \frac{1}{u_{(1),1}} \mathbf{u}_{(1)} - \frac{\lambda_{(1)} - \lambda_{(2)}}{\mathbf{A}_1 \mathbf{v}_{(2)}} \overline{\mathbf{v}_{(2)}}, \quad (2.56)$$

where $\lambda_{(1)}$ is minimum eigenvalue and $\mathbf{u}_{(1)}$ is corresponding eigenvector in the matrix \mathbf{A} obtained by the inverse power method. $\overline{\mathbf{v}_{(2)}}$ is defined as follows.

$$\overline{\mathbf{v}_{(2)}} = \frac{1}{v_{(2),1}} \begin{pmatrix} 0 \\ \mathbf{v}_{(2)} \end{pmatrix}, \quad (2.57)$$

where $v_{(2),1}$ is value in the first row of eigenvector $\mathbf{v}_{(2)}$.

Consequently, the 2nd eigenvalue and eigenvector in \mathbf{A} can be obtained by the above proposed method. It is noted that by using the procedure to reduce dimensionality of the

matrix ($\mathbf{A} \rightarrow \mathbf{B}_{(1)}, \mathbf{B}_{(1)} \rightarrow \mathbf{B}_{(2)}, \dots (\mathbf{B}_{(2)}$ is the matrix with dimension $N-2$)), it is possible to achieve solving m^{th} eigenvalue, $\lambda_{(m)}$, and corresponding eigenvector, $\mathbf{u}_{(m)}$, of the matrix \mathbf{A} .

3. Stochastic 2D Structural Static Problem

In the design and the construction of ships and offshore structures, there are a lot of uncertainties in the shape of the structures (welding deformation, effect of misalignment, corrosion wastage). In the conventional uncertainty analysis, Monte Carlo Simulation methods (MCS) combined with finite element methods (FEM) is usually used when uncertainty in shape is considered. However, MCS needs heavy and a large number of calculations, so that application of MCS to practical problems is sometimes very difficult to get reasonable results. In this study, a new method of structural analysis is proposed for the solution of problems of response uncertainty for the case that involves uncertainty in shape. The method makes use of an Hermite polynomial chaos expansion (PCE) to represent the uncertainty of shapes and the response surface. The proposed method involves a mathematical formulation which is a natural extension of the deterministic finite element concept to the space of random variables. In section 3.1, the stochastic finite element method for uncertainty in shape following normal distribution is formularized and the validity of the proposed method is discussed by two cases. In section 3.2, the stochastic finite element method for uncertainty in shape following non-normal distribution is formularized and an algorithm is developed that can deal with arbitrary approximate order to represent uncertainty of shape following non-normal distribution problem. In section 3.3, the evaluation of accuracy of the analysis method is discussed.

3.1 The Formularization of Stochastic Finite Element Method for Uncertainty in Shape Following normal Distribution

In this study, a new method of structural analysis is proposed for the solution of problems of response uncertainty for the case that involves uncertainty in shape following normal distribution.

3.1.1 Introduction of Input Random Variable:

In this section, the method to represent uncertainty of structural shape is considered. We first introduce a random input variable to nodal coordinate of mesh, where shape of the analysis object is changed by changing the input variable.

We assume that shape change (node coordinate change) can be expressed by liner function of the random variable, θ . Consequently, nodal coordinate can be stated as follows:

$$\begin{aligned}x'_i &= x_i + \alpha_i l, \\y'_i &= y_i + \beta_i l,\end{aligned}\tag{3.1}$$

where x_i, y_i is i -th nodal coordinate before shape change, and x'_i, y'_i is i -th nodal coordinate after shape change. Moreover α_i, β_i are coefficients of the degree of shape change at each node. l is the deviation length at the representative node. In the study, we assume that uncertainty in shape is defined as normal distribution, so that the movement of all the nodes can be expressed by linear function of the deviation length, l , as shown in Eq. (3.2):

$$l = l_0 + l_1 \theta ,\tag{3.2}$$

where l_0 is mean of l . l_1 is standard deviation of l . Fig.3.1 shows a specific example of a 1/4 model plate with a circular hole at the center, which is divided into 36 elements. It is assumed that size of a central hole has uncertainty, so that the change of the radius of the hole is considered.

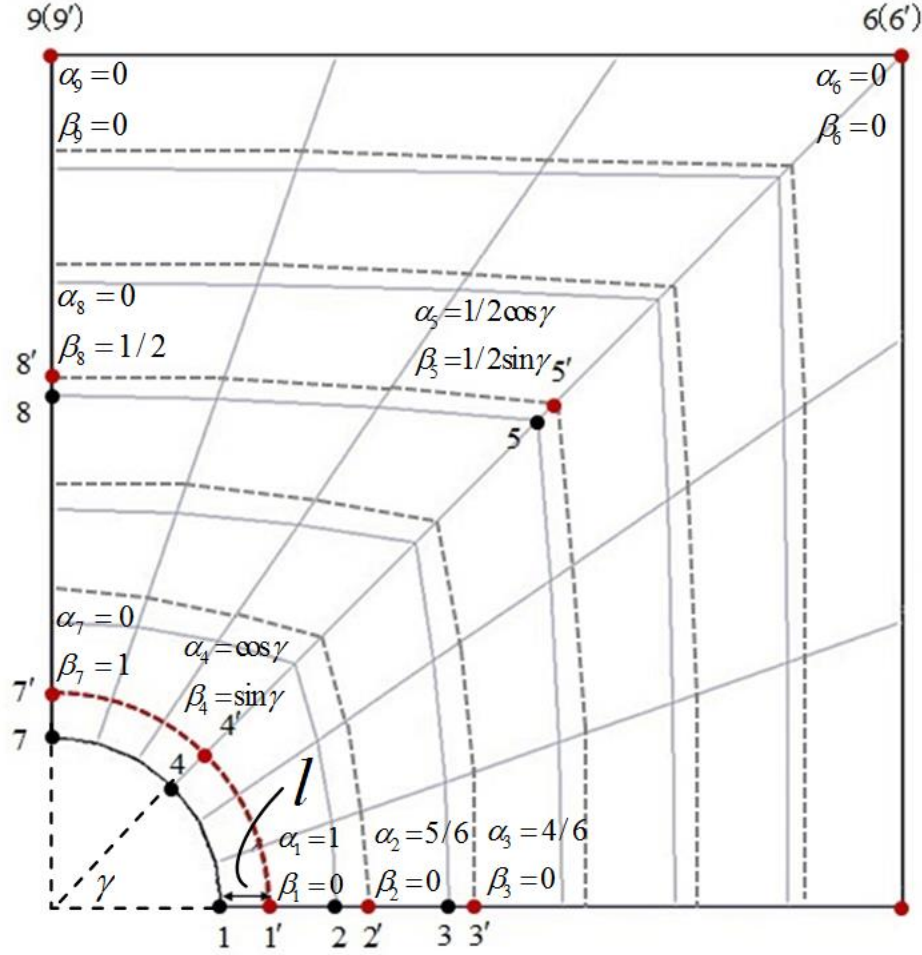


Fig 3.1: Model of Linear Deformation.

It is also assumed that the change of each nodal coordinate, as shown by a dotted line in the Fig 3.1, is represented by the deviation length (l) of the nodal point 1 (representative node). And, for example, the nodal point 2 is moved with length $5l/6$, and the nodal point 3 is moved with length $4l/6$. Fig.3.1 shows the coefficient (α_i, β_i) of all nodes when size of a central hole is changed with length l . It is noted that the change of the coordinate is assumed not only at the nodes on the hole (nodes 1, 4, 7 in Fig.3.1), but also at the other nodes in the mesh, in order to avoid the distortion of the elements by moving the nodes.

In the following section, we derive SFEM formulation involving random variable (θ) by

using the above assumption of uncertainty in shape (mesh change).

3.1.2 Stochastic Finite Element Formulation

(1) Stochastic Element Stiffness Matrix

The theory of deterministic finite element method is introduced in the section 2.2. Based on the theory of finite element method, we can construct the element stiffness matrix considering the uncertainty in shape, the following integration in terms of element coordinates (ξ, η) should be evaluated.

$$\mathbf{k}^{e}(\theta) = \int_{-1}^{+1} \int_{-1}^{+1} \mathbf{B}'^T(\xi, \eta; \theta) \mathbf{D} \mathbf{B}'(\xi, \eta; \theta) |\mathbf{J}'(\xi, \eta; \theta)| d\xi d\eta, \quad (3.3)$$

where $\mathbf{B}'(\xi, \eta; \theta)$ is a strain matrix involving random variable (θ) , $\mathbf{J}'(\xi, \eta; \theta)$ is a Jacobian matrix also involving random variable (θ) . In this study, $|\mathbf{J}'|$ and \mathbf{B}' involving uncertainty in shape (θ) is treated as follows.

1) Representation of $|\mathbf{J}'(\xi, \eta; \theta)|$

Generally, in the 4-noded plane element, mapping from element coordinate (ξ, η) to global coordinate (x', y') is expressed as follows by using shape functions (N_i) .

$$\begin{aligned} x' &= \sum_{i=1}^4 N_i(\xi, \eta) x'_i, \\ y' &= \sum_{i=1}^4 N_i(\xi, \eta) y'_i. \end{aligned} \quad (3.4)$$

The Jacobian matrix $\mathbf{J}'(\xi, \eta; \theta)$ with the uncertainty parameter (θ) is derived by substituting Eq. (3.1) into Eq. (3.4).

$$\mathbf{J}'(\xi, \eta; \theta) = \begin{bmatrix} \frac{\partial x'}{\partial \xi} & \frac{\partial y'}{\partial \xi} \\ \frac{\partial x'}{\partial \eta} & \frac{\partial y'}{\partial \eta} \end{bmatrix} = \begin{bmatrix} \sum_{i=1}^4 \frac{\partial N_i}{\partial \xi} (x_i + \alpha_i l) & \sum_{i=1}^4 \frac{\partial N_i}{\partial \xi} (y_i + \beta_i l) \\ \sum_{i=1}^4 \frac{\partial N_i}{\partial \eta} (x_i + \alpha_i l) & \sum_{i=1}^4 \frac{\partial N_i}{\partial \eta} (y_i + \beta_i l) \end{bmatrix}. \quad (3.5)$$

The determinant of the Jacobian matrix is derived by Eq. (3.5) and Eq. (3.2), and can be written in the form of the polynomial of random variable (θ) as follows.

$$|\mathbf{J}'(\xi, \eta; \theta)| = |\mathbf{J}'_0(\xi, \eta)| + |\mathbf{J}'_1(\xi, \eta)|\theta + |\mathbf{J}'_2(\xi, \eta)|\theta^2, \quad (3.6)$$

where

$$\begin{aligned} |\mathbf{J}'_0(\xi, \eta)| &= \sum_{i=1}^4 \frac{\partial N_i}{\partial \xi} x_i \times \sum_{i=1}^4 \frac{\partial N_i}{\partial \eta} y_i - \sum_{i=1}^4 \frac{\partial N_i}{\partial \eta} x_i \times \sum_{i=1}^4 \frac{\partial N_i}{\partial \xi} y_i \\ &+ \sum_{i=1}^4 \frac{\partial N_i}{\partial \xi} x_i \times \sum_{i=1}^4 \frac{\partial N_i}{\partial \eta} \beta_i l_0 - \sum_{i=1}^4 \frac{\partial N_i}{\partial \eta} x_i \times \sum_{i=1}^4 \frac{\partial N_i}{\partial \xi} \beta_i l_0 \\ &+ \sum_{i=1}^4 \frac{\partial N_i}{\partial \eta} y_i \times \sum_{i=1}^4 \frac{\partial N_i}{\partial \xi} \alpha_i l_0 - \sum_{i=1}^4 \frac{\partial N_i}{\partial \xi} y_i \times \sum_{i=1}^4 \frac{\partial N_i}{\partial \eta} \alpha_i l_0 \\ &+ \sum_{i=1}^4 \frac{\partial N_i}{\partial \xi} \alpha_i l_0 \times \sum_{i=1}^4 \frac{\partial N_i}{\partial \eta} \beta_i l_0 - \sum_{i=1}^4 \frac{\partial N_i}{\partial \eta} \alpha_i l_0 \times \sum_{i=1}^4 \frac{\partial N_i}{\partial \xi} \beta_i l_0, \end{aligned} \quad (3.7-1)$$

$$\begin{aligned} |\mathbf{J}'_1(\xi, \eta)| &= \sum_{i=1}^4 \frac{\partial N_i}{\partial \xi} x_i \times \sum_{i=1}^4 \frac{\partial N_i}{\partial \eta} \beta_i l_1 - \sum_{i=1}^4 \frac{\partial N_i}{\partial \eta} x_i \times \sum_{i=1}^4 \frac{\partial N_i}{\partial \xi} \beta_i l_1 \\ &+ \sum_{i=1}^4 \frac{\partial N_i}{\partial \eta} y_i \times \sum_{i=1}^4 \frac{\partial N_i}{\partial \xi} \alpha_i l_1 - \sum_{i=1}^4 \frac{\partial N_i}{\partial \xi} y_i \times \sum_{i=1}^4 \frac{\partial N_i}{\partial \eta} \alpha_i l_1, \end{aligned} \quad (3.7-2)$$

$$|\mathbf{J}'_2(\xi, \eta)| = \sum_{i=1}^4 \frac{\partial N_i}{\partial \xi} \alpha_i l_1 \times \sum_{i=1}^4 \frac{\partial N_i}{\partial \eta} \beta_i l_1 - \sum_{i=1}^4 \frac{\partial N_i}{\partial \eta} \alpha_i l_1 \times \sum_{i=1}^4 \frac{\partial N_i}{\partial \xi} \beta_i l_1. \quad (3.7-3)$$

2) Representation of \mathbf{B}'

Generally in the finite element formulation, the component, $\partial N_A / \partial x'$ and $\partial N_A / \partial y'$, in the \mathbf{B}' matrix is depicted as follows.

$$\begin{bmatrix} \frac{\partial N_A}{\partial x'} \\ \frac{\partial N_A}{\partial y'} \end{bmatrix} = [\mathbf{J}'(\xi, \eta; \theta)]^{-1} \begin{bmatrix} \frac{\partial N_A}{\partial \xi} \\ \frac{\partial N_A}{\partial \eta} \end{bmatrix}. \quad (3.8)$$

Using Eq. (3.5), we can arrange Eq. (3.8) as follows.

$$\begin{aligned} \frac{\partial N_A}{\partial x'} &= \frac{1}{|\mathbf{J}'_0| + |\mathbf{J}'_1|\theta + |\mathbf{J}'_2|\theta^2} \times (H_{AX1} + H_{AX1} \times \theta), \\ \frac{\partial N_A}{\partial y'} &= \frac{1}{|\mathbf{J}'_0| + |\mathbf{J}'_1|\theta + |\mathbf{J}'_2|\theta^2} \times (H_{AY0} + H_{AY1} \times \theta), \end{aligned} \quad (3.9)$$

where the coefficients, $H_{AX0}, H_{AX1}, H_{AY0}, H_{AY1}$, is expressed by differentials of shape functions in terms of (ξ, η) as follows.

$$\begin{aligned} H_{AX0} &= \left(\frac{\partial N_A}{\partial \xi} \times \sum_{i=1}^4 \frac{\partial N_i}{\partial \eta} y_i - \frac{\partial N_A}{\partial \eta} \times \sum_{i=1}^4 \frac{\partial N_i}{\partial \eta} x_i \right) \\ &+ \left(\frac{\partial N_A}{\partial \xi} \times \sum_{i=1}^4 \frac{\partial N_i}{\partial \eta} \beta_i - \frac{\partial N_A}{\partial \eta} \times \sum_{i=1}^4 \frac{\partial N_i}{\partial \eta} \alpha_i \right) \times l_0, \end{aligned} \quad (3.10-1)$$

$$H_{AX1} = \frac{\partial N_A}{\partial \xi} \times \sum_{i=1}^4 \frac{\partial N_i}{\partial \eta} \beta_i l_1 - \frac{\partial N_A}{\partial \eta} \times \sum_{i=1}^4 \frac{\partial N_i}{\partial \eta} \alpha_i l_1, \quad (3.10-2)$$

$$\begin{aligned} H_{AY0} &= \left(-\frac{\partial N_A}{\partial \xi} \times \sum_{i=1}^4 \frac{\partial N_i}{\partial \xi} y_i + \frac{\partial N_A}{\partial \eta} \times \sum_{i=1}^4 \frac{\partial N_i}{\partial \xi} x_i \right) \\ &+ \left(-\frac{\partial N_A}{\partial \xi} \times \sum_{i=1}^4 \frac{\partial N_i}{\partial \xi} \beta_i + \frac{\partial N_A}{\partial \eta} \times \sum_{i=1}^4 \frac{\partial N_i}{\partial \xi} \alpha_i \right) \times l_0, \end{aligned} \quad (3.10-3)$$

$$H_{AY1} = -\frac{\partial N_A}{\partial \xi} \times \sum_{i=1}^4 \frac{\partial N_i}{\partial \xi} \beta_i l_1 + \frac{\partial N_A}{\partial \eta} \times \sum_{i=1}^4 \frac{\partial N_i}{\partial \xi} \alpha_i l_1, \quad (3.10-4)$$

Therefore, $\mathbf{B}'(\xi, \eta; \theta)$ can be written as shown below.

$$\mathbf{B}'(\xi, \eta; \theta) = \frac{1}{|\mathbf{J}'(\xi, \eta; \theta)|} \times \mathbf{B}'_0(\xi, \eta) + \frac{1}{|\mathbf{J}'(\xi, \eta; \theta)|} \times \mathbf{B}'_1(\xi, \eta) \times \theta. \quad (3.11)$$

3) Approximation of $\frac{1}{|\mathbf{J}'(\xi, \eta; \theta)|}$

It can be seen that the item, $1/|\mathbf{J}'(\xi, \eta; \theta)|$, is remained in the integral of the element stiffness matrix after substituting Eq. (3.11) into Eq. (3.3). Generally, in the formulation of SFEM, the orthogonality is used when the stiffness matrix or the force vector is evaluated. However when denominator of $1/|\mathbf{J}'(\xi, \eta; \theta)|$ involves random variable (θ), the orthogonality is not available. In this study, to overcome this problem, it is assumed that $1/|\mathbf{J}'(\xi, \eta; \theta)|$ can be approximated by Hermite PCE as follows.

$$\frac{1}{|\mathbf{J}'(\xi, \eta; \theta)|} = \sum_{u=0}^p A_u \psi_u(\theta), \quad (3.12)$$

where, A_u are unknown coefficients of approximated polynomial, $\psi_u(\theta)$ are the basis functions, represented by Hermite polynomial.

The unknown coefficients, A_u , can be decided as follows.

Firstly, Eq. (3.12) is rewritten as follows by using Eq. (3.6) and Hermite polynomial.

$$\sum_{i=0}^2 |\mathbf{J}_i''| \psi_i(\theta) \times \sum_{u=0}^p A_u \psi_u(\theta) = 1, \quad (3.13)$$

where $|\mathbf{J}_0''| = |\mathbf{J}'_1(\xi, \eta)| + |\mathbf{J}'_2(\xi, \eta)|$, $|\mathbf{J}_1''| = |\mathbf{J}'_1(\xi, \eta)|$, $|\mathbf{J}_2''| = |\mathbf{J}'_2(\xi, \eta)|$, and we assume that $p=6$.

Multiplying $\psi_i(\theta)w(\theta)$ to both sides of Eq. (3.13), and integrating the equation, we have:

$$\int_{-\infty}^{\infty} \sum_{i=0}^2 |\mathbf{J}_i''| \psi_i(\theta) \times \sum_{u=0}^6 A_u \psi_u(\theta) \psi_i(\theta) w(\theta) d\theta = \int_{-\infty}^{\infty} 1 \times \psi_i(\theta) w(\theta) d\theta. \quad (3.14)$$

This equation can be depicted as follows.

$$\sum_{i=0}^2 |J_i^n| \sum_{u=0}^6 A_u \langle \psi_i(\theta) \psi_u(\theta) \psi_t(\theta) \rangle = \langle \psi_t(\theta) \rangle. \quad (3.15)$$

This means that the following simultaneous equations about the coefficients, A_i , are obtained.

$$\begin{bmatrix} J_{00}^{ne} & J_{01}^{ne} & \cdots & J_{06}^{ne} \\ J_{10}^{ne} & J_{11}^{ne} & \cdots & J_{16}^{ne} \\ \vdots & \vdots & \vdots & \vdots \\ J_{60}^{ne} & J_{61}^{ne} & \cdots & J_{66}^{ne} \end{bmatrix} \begin{bmatrix} A_0 \\ A_1 \\ \vdots \\ A_6 \end{bmatrix} = \begin{bmatrix} 1 \\ 0 \\ \vdots \\ 0 \end{bmatrix}, \quad (3.16)$$

where J_{ut}^{ne} is $\sum_{i=0}^2 |J_i^n| \langle \psi_i(\theta) \psi_u(\theta) \psi_t(\theta) \rangle$. It is noted that $\langle \psi_i(\theta) \psi_u(\theta) \psi_t(\theta) \rangle$ can be evaluated by numerical integration (Eq.(3.17a)) or by using Eq.(3.17b)[39]. And we can reference table 2.4 about the inner product values.

$$\langle \psi_i(\theta) \psi_u(\theta) \psi_t(\theta) \rangle = \int_D \psi_i(\theta) \psi_u(\theta) \psi_t(\theta) w(\theta) d\theta, \quad (3.17a)$$

$$\langle \psi_i(\theta) \psi_u(\theta) \psi_t(\theta) \rangle = \begin{cases} 0 & i+u+t = \text{odd}, \max(i,u,t) > s \\ \frac{i!u!t!}{(s-i)!(s-u)!(s-t)!} & \text{otherwise } (s = \frac{i+u+t}{2}) \end{cases}. \quad (3.17a)$$

Then the unknown coefficients of approximation polynomial, A_u , is derived by the above simultaneous equations.

Now, we can substitute Eq. (3.6), Eq. (3.11) and Eq. (3.12) into Eq. (3.3) as follows.

$$\begin{aligned} & \mathbf{k}^{ne}(\theta) \\ &= \int_{-1}^{+1} \int_{-1}^{+1} \left(\mathbf{B}_0^T \mathbf{D} \mathbf{B}'_0 + \mathbf{B}_0^T \mathbf{D} \mathbf{B}'_1 \theta + \mathbf{B}_1^T \mathbf{D} \mathbf{B}'_0 \theta + \mathbf{B}_1^T \mathbf{D} \mathbf{B}'_1 \theta^2 \right) \left(\sum_{u=0}^6 A_u \psi_u(\theta) \right) d\xi d\eta. \end{aligned} \quad (3.18)$$

By rearranging the above equation, we can obtain a new equation which is represented by θ .

$$\mathbf{k}^{ne}(\theta) = \sum_{i=0}^8 \mathbf{k}_i^{ne} \theta^i, \quad (3.19)$$

where the coefficients, \mathbf{k}_i^{e} , is expressed as follows.

$$\mathbf{k}_0^{e} = \sum_{i=1}^4 \mathbf{B}_0'^T(\xi_i, \eta_i) \mathbf{D}\mathbf{B}'_0(\xi_i, \eta_i) A_0 w(\xi_i, \eta_i), \quad (3.20-1)$$

$$\begin{aligned} \mathbf{k}_1^{e} &= \sum_{i=1}^4 \mathbf{B}_1'^T(\xi_i, \eta_i) \mathbf{D}\mathbf{B}'_0(\xi_i, \eta_i) A_1 w(\xi_i, \eta_i) \\ &+ \sum_{i=1}^4 (\mathbf{B}_1'^T(\xi_i, \eta_i) \mathbf{D}\mathbf{B}'_0(\xi_i, \eta_i) + \mathbf{B}_0'^T(\xi_i, \eta_i) \mathbf{D}\mathbf{B}'_1(\xi_i, \eta_i)) A_0 w(\xi_i, \eta_i), \end{aligned} \quad (3.20-2)$$

$$\begin{aligned} \mathbf{k}_2^{e} &= \sum_{i=1}^4 \mathbf{B}_0'^T(\xi_i, \eta_i) \mathbf{D}\mathbf{B}'_0(\xi_i, \eta_i) A_2 w(\xi_i, \eta_i) \\ &+ \sum_{i=1}^4 (\mathbf{B}_1'^T(\xi_i, \eta_i) \mathbf{D}\mathbf{B}'_0(\xi_i, \eta_i) + \mathbf{B}_0'^T(\xi_i, \eta_i) \mathbf{D}\mathbf{B}'_1(\xi_i, \eta_i)) A_1 w(\xi_i, \eta_i) \\ &+ \sum_{i=1}^4 \mathbf{B}_1'^T(\xi_i, \eta_i) \mathbf{D}\mathbf{B}'_1(\xi_i, \eta_i) A_0 w(\xi_i, \eta_i), \end{aligned} \quad (3.20-3)$$

$$\begin{aligned} \mathbf{k}_3^{e} &= \sum_{i=1}^4 \mathbf{B}_0'^T(\xi_i, \eta_i) \mathbf{D}\mathbf{B}'_0(\xi_i, \eta_i) A_3 w(\xi_i, \eta_i) \\ &+ \sum_{i=1}^4 (\mathbf{B}_1'^T(\xi_i, \eta_i) \mathbf{D}\mathbf{B}'_0(\xi_i, \eta_i) + \mathbf{B}_0'^T(\xi_i, \eta_i) \mathbf{D}\mathbf{B}'_1(\xi_i, \eta_i)) A_2 w(\xi_i, \eta_i) \\ &+ \sum_{i=1}^4 \mathbf{B}_1'^T(\xi_i, \eta_i) \mathbf{D}\mathbf{B}'_1(\xi_i, \eta_i) A_1 w(\xi_i, \eta_i), \end{aligned} \quad (3.20-4)$$

$$\begin{aligned} \mathbf{k}_4^{e} &= \sum_{i=1}^4 \mathbf{B}_0'^T(\xi_i, \eta_i) \mathbf{D}\mathbf{B}'_0(\xi_i, \eta_i) A_4 w(\xi_i, \eta_i) \\ &+ \sum_{i=1}^4 (\mathbf{B}_1'^T(\xi_i, \eta_i) \mathbf{D}\mathbf{B}'_0(\xi_i, \eta_i) + \mathbf{B}_0'^T(\xi_i, \eta_i) \mathbf{D}\mathbf{B}'_1(\xi_i, \eta_i)) A_3 w(\xi_i, \eta_i) \\ &+ \sum_{i=1}^4 \mathbf{B}_1'^T(\xi_i, \eta_i) \mathbf{D}\mathbf{B}'_1(\xi_i, \eta_i) A_2 w(\xi_i, \eta_i), \end{aligned} \quad (3.20-5)$$

$$\begin{aligned} \mathbf{k}_5^{e} &= \sum_{i=1}^4 (\mathbf{B}_1'^T(\xi_i, \eta_i) \mathbf{D}\mathbf{B}'_0(\xi_i, \eta_i) + \mathbf{B}_0'^T(\xi_i, \eta_i) \mathbf{D}\mathbf{B}'_1(\xi_i, \eta_i)) A_4 w(\xi_i, \eta_i) \\ &+ \sum_{i=1}^4 \mathbf{B}_1'^T(\xi_i, \eta_i) \mathbf{D}\mathbf{B}'_1(\xi_i, \eta_i) A_3 w(\xi_i, \eta_i), \end{aligned} \quad (3.20-6)$$

$$\begin{aligned}
\mathbf{k}_6'^e &= \sum_{i=1}^4 \mathbf{B}_1'^T(\xi_i, \eta_i) \mathbf{D}\mathbf{B}_1'(\xi_i, \eta_i) A_4 w(\xi_i, \eta_i) \\
&+ \sum_{i=1}^4 \left(\mathbf{B}_0'^T(\xi_i, \eta_i) \mathbf{D}\mathbf{B}_1'(\xi_i, \eta_i) + \mathbf{B}_1'^T(\xi_i, \eta_i) \mathbf{D}\mathbf{B}_0'(\xi_i, \eta_i) \right) A_5 w(\xi_i, \eta_i),
\end{aligned} \tag{3.20-7}$$

$$\begin{aligned}
\mathbf{k}_7'^e &= \sum_{i=1}^4 \mathbf{B}_1'^T(\xi_i, \eta_i) \mathbf{D}\mathbf{B}_1'(\xi_i, \eta_i) A_5 w(\xi_i, \eta_i) \\
&+ \sum_{i=1}^4 \left(\mathbf{B}_0'^T(\xi_i, \eta_i) \mathbf{D}\mathbf{B}_1'(\xi_i, \eta_i) + \mathbf{B}_1'^T(\xi_i, \eta_i) \mathbf{D}\mathbf{B}_0'(\xi_i, \eta_i) \right) A_6 w(\xi_i, \eta_i),
\end{aligned} \tag{3.20-8}$$

$$\begin{aligned}
\mathbf{k}_8'^e &= \sum_{i=1}^4 \mathbf{B}_1'^T(\xi_i, \eta_i) \mathbf{D}\mathbf{B}_1'(\xi_i, \eta_i) A_6 w(\xi_i, \eta_i) \\
&+ \sum_{i=1}^4 \left(\mathbf{B}_0'^T(\xi_i, \eta_i) \mathbf{D}\mathbf{B}_1'(\xi_i, \eta_i) + \mathbf{B}_1'^T(\xi_i, \eta_i) \mathbf{D}\mathbf{B}_0'(\xi_i, \eta_i) \right) A_7 w(\xi_i, \eta_i).
\end{aligned} \tag{3.20-9}$$

Then we need rewrite equation from the θ form (Eq. 3.19) to $\psi_i(\theta)$ form.

$$\mathbf{k}''^e = \sum_{i=0}^8 \mathbf{k}_i''^e \psi_i(\theta), \tag{3.21}$$

where,

$$\begin{aligned}
\mathbf{k}_0''^e &= \mathbf{k}_0'^e + \mathbf{k}_2'^e + 3\mathbf{k}_4'^e + 15\mathbf{k}_6'^e + 105\mathbf{k}_8'^e, \\
\mathbf{k}_1''^e &= \mathbf{k}_1'^e + 3\mathbf{k}_3'^e + 15\mathbf{k}_5'^e + 105\mathbf{k}_7'^e, \\
\mathbf{k}_2''^e &= \mathbf{k}_2'^e + 6\mathbf{k}_4'^e + 45\mathbf{k}_6'^e + 420\mathbf{k}_8'^e, \\
\mathbf{k}_3''^e &= \mathbf{k}_3'^e + 10\mathbf{k}_5'^e + 105\mathbf{k}_7'^e, \\
\mathbf{k}_4''^e &= \mathbf{k}_4'^e + 15\mathbf{k}_6'^e + 210\mathbf{k}_8'^e, \\
\mathbf{k}_5''^e &= \mathbf{k}_5'^e + 21\mathbf{k}_7'^e, \\
\mathbf{k}_6''^e &= \mathbf{k}_6'^e + 28\mathbf{k}_8'^e, \\
\mathbf{k}_7''^e &= \mathbf{k}_7'^e, \\
\mathbf{k}_8''^e &= \mathbf{k}_8'^e.
\end{aligned} \tag{3.22}$$

As shown above, the element stiffness matrix is derived by the polynomial of order eight based on the basis functions, $\psi_i(\theta)$.

(2) Stochastic Force Vector

The force vector is changed when the shape of the analysis domain is changed and the force is applied to the moved boundary. Here formulation of the force vector is derived where the distributed load, is applied to the changing (moving) element edge (see edge 1-2 in Fig.3.2(a)).

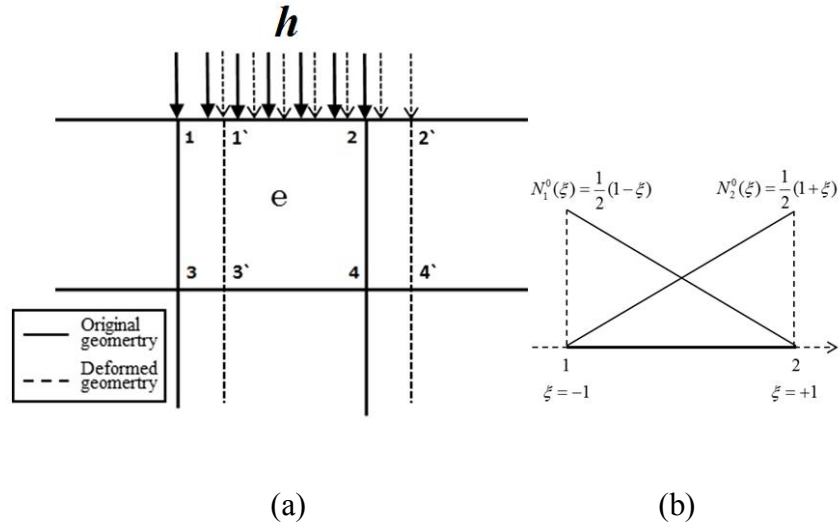


Fig.3.2: The Distributed Load along the Side of Element

When constant surface force vector (\mathbf{h}) in one element edge is considered, the force vector in node A is represented as follows:

$$\mathbf{f}'_A(\theta) = \int_{-1}^{+1} N_A \left(N_1^0 \mathbf{h} + N_2^0 \mathbf{h} \right) j'_e(\xi; \theta) d\xi, \quad (3.23)$$

where N_1^0, N_2^0 are the shape functions for the surface force applied to the edge(1-2)(see Fig.3(b)), and j'_e is the line Jacobian. And it is shown as follows.

$$j'_e = \sqrt{\left(\frac{dx'}{d\xi} \right)^2 + \left(\frac{dy'}{d\xi} \right)^2}. \quad (3.24)$$

The global coordinate (x', y') is expressed as follows by using shape functions (N_i^0) .

$$\begin{aligned} x' &= \sum_{i=1}^2 N_i^0 x'_i, \\ y' &= \sum_{i=1}^2 N_i^0 y'_i. \end{aligned} \quad (3.25)$$

We can substitute Eq. (3.25) into Eq. (3.24) as follows.

$$j'_e = \frac{1}{2}(x_1 - x_2 + (\alpha_1 - \alpha_2)l_0 + (\alpha_1 - \alpha_2)l_1\theta). \quad (3.26)$$

The force vector can be obtained by substitute Eq. (3.26) into Eq. (3.23)

$$\begin{aligned} \mathbf{f}'^e &= \int_{-1}^{+1} \frac{1}{2} N_A (N_1^0 \mathbf{h}_1 + N_2^0 \mathbf{h}_2) \times (x_1 - x_2 + (\alpha_1 - \alpha_2)l_0 + (\alpha_1 - \alpha_2)l_1\theta) d\xi. \end{aligned} \quad (3.27)$$

So, the force vector can be written as follows.

$$\mathbf{f}'^e = \mathbf{f}'_0{}^e + \mathbf{f}'_1{}^e \theta, \quad (3.28)$$

where,

$$\mathbf{f}'_0{}^e = \int_{-1}^{+1} \frac{1}{2} N_A (N_1^0 \mathbf{h}_1 + N_2^0 \mathbf{h}_2) \times (x_1 - x_2 + (a_1 - a_2)l_0) d\xi, \quad (3.29-1)$$

$$\mathbf{f}'_1{}^e = \int_{-1}^{+1} \frac{1}{2} N_A (N_1^0 \mathbf{h}_1 + N_2^0 \mathbf{h}_2) \times (a_1 - a_2)l_1 d\xi. \quad (3.29-2)$$

Eq. (2.28) can be rewritten as Hermite polynomials form as is the case of the stiffness matrix.

$$\mathbf{f}'^e = \sum_{i=0}^1 \mathbf{f}_i''^e \psi_i(\theta), \quad (3.30)$$

where $\mathbf{f}_i''^e = \mathbf{f}_i'^e$.

(3) The Stiffness Equation of SFEM

Formulation of SFEM is performed by using the element stiffness matrix, the force vector and the approximate response surface of the displacement.

The element stiffness equation involving random variable (θ) is written as follows:

$$\mathbf{k}^e \mathbf{u}^e = \mathbf{f}^e, \quad (3.31)$$

where the element stiffness matrix, \mathbf{k}^e (Eq. (3.21)), and the force vector, \mathbf{f}^e (Eq. (3.30)), are represented by basis functions, $\psi_i(\theta)$. The unknown displacement response \mathbf{u}^e of Eq. (3.31) is also approximated by using Hermite polynomial.

$$\mathbf{u}^e = \sum_{i=0}^q \mathbf{u}_i^e \psi_i(\theta). \quad (3.32)$$

Substituting Eq. (3.21), Eq. (3.30) and Eq. (3.32) into Eq. (3.31) the stiffness equation becomes as follows:

$$\sum_{i=0}^8 \mathbf{k}_i''^e \psi_i(\theta) \left(\sum_{i=0}^8 \mathbf{u}_i^e \psi_i(\theta) \right) = \sum_{i=0}^1 \mathbf{f}_i''^e \psi_i(\theta), \quad (3.33)$$

where the element stiffness matrix \mathbf{k}^e is approximated by 8th order polynomial as shown in Eq. (3.21). Thus, in this study, the order (q) of PCE approximation of Eq. (3.33) is assumed as eight.

Multiplying both sides of Eq. (3.33) by $\psi_i(\theta)w(\theta)$, integrating the equation, we have:

$$\sum_{i=0}^8 \mathbf{k}_i''^e \sum_{j=0}^8 \mathbf{u}_j^e \langle \psi_i(\theta) \psi_j(\theta) \psi_i(\theta) \rangle = \sum_{i=0}^1 \mathbf{f}_i''^e \langle \psi_i(\theta) \psi_i(\theta) \rangle. \quad (3.34)$$

Thus the element stiffness equation can be derived as follows:

$$\begin{bmatrix} \mathbf{K}_{00}^{''e} & \mathbf{K}_{01}^{''e} & \cdots & \mathbf{K}_{08}^{''e} \\ \mathbf{K}_{10}^{''e} & \mathbf{K}_{11}^{''e} & \cdots & \mathbf{K}_{18}^{''e} \\ \vdots & \vdots & \ddots & \vdots \\ \mathbf{K}_{80}^{''e} & \mathbf{K}_{81}^{''e} & \cdots & \mathbf{K}_{88}^{''e} \end{bmatrix} \begin{bmatrix} \mathbf{u}_0^{'e} \\ \mathbf{u}_1^{'e} \\ \vdots \\ \mathbf{u}_8^{'e} \end{bmatrix} = \begin{bmatrix} \mathbf{F}_0^{''e} \\ \mathbf{F}_1^{''e} \\ \vdots \\ \mathbf{F}_8^{''e} \end{bmatrix}, \quad (3.35)$$

where, $\mathbf{K}_{ij}^{''e} = \sum_{i=0}^8 \mathbf{k}_i^{''e} \langle \psi_i(\theta) \psi_j(\theta) \psi_t(\theta) \rangle$, $\mathbf{F}_t^{''e} = \sum_{i=0}^1 \mathbf{f}_i^{'e} \langle \psi_i(\theta) \psi_t(\theta) \rangle$.

Compared with the usual deterministic element stiffness equation, it involves not only the unknown displacement of deterministic part ($\mathbf{u}_0^{'e}$) but also involves the unknown displacement of stochastic part (the stochastic part of order 1 ($\mathbf{u}_1^{'e}$), the stochastic part of order 2 ($\mathbf{u}_2^{'e}$), \cdots). The unknown displacement of the all node ($\mathbf{u}_0', \mathbf{u}_1', \cdots$) is derived by solving the global equation system which can be obtained by assembly of element stiffness matrices. The uncertainty of stress can be assessed by Eq. (3.36) with Eq. (3.11), Eq. (3.12) and Eq. (3.32) after the displacement is obtained.

$$\boldsymbol{\sigma}' = \mathbf{DB}'\mathbf{u}' = \sum_{i=0}^{15} \boldsymbol{\sigma}'_i \psi_i(\theta). \quad (3.36)$$

It is noted that the uncertainty of response of displacement can be estimated by the proposed method that solves the main stiffness equation only once.

3.1.3 Numerical Example

In this study, we developed SFEM program by using C language which can deal with a two-dimensional problem considering uncertainty in shape following normal distribution. The validity and feasibility of the proposed method of structural analysis is discussed by two cases, (1) a plate with a circular hole at the center with uncertainty in the size of a circular hole, (2) a cruciform weld joint with uncertainty in the magnitude of misalignment.

(1) A Plate with a Circular Hole with Uncertainty

A plate with a circular hole (Fig. 3.3(a)) is considered and mesh is shown in Fig. 3.3(b). It is assumed that the radius of a circular hole follows Gaussian distribution with mean $\mu = 3\text{mm}$, the standard deviation $\sigma = 0.1\sim 1\text{mm}$. It is also assumed that the distributed load $\sigma_p = 78.4\text{ N/mm}^2$, and symmetry boundary condition is applied to the boundaries, Γ_1 and Γ_2 . The coefficient (α_i, β_i) of each node is defined based on the method shown in the previous section when the radius of the hole changes with length l . The validity of the proposed method (SFEM) is discussed by comparing the result of the method with the MCS solution of the deterministic problems (FEM) for a same mesh size.

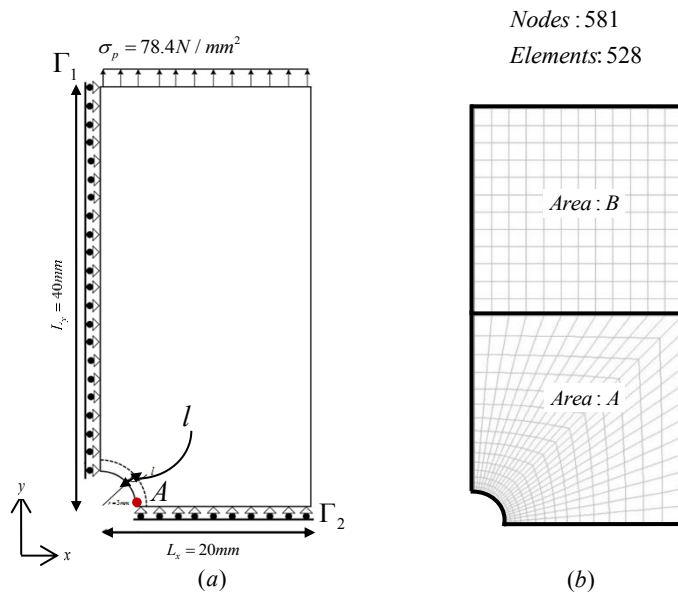


Fig. 3.3: The Geometrical Deformation of the Hole

1) The Mean $\mu = 3\text{mm}$ and the Standard Deviation $\sigma = 0.5\text{mm}$ of the Radius of A Circular Hole

In order to discuss the validity of the proposed SFEM, the method is applied to the problem with the mean $\mu = 3\text{mm}$ and the standard deviation $\sigma = 0.5\text{mm}$. Fig.3.4 shows the stochastic response surface of the stress (Eq. (3.36)) at a particular node (point A in Fig.3.3(a)) in y-direction. In this figure the stress value when the radius of the hole (l_R) is 3mm is shown at

$\theta=0(l=0)$. The black line is response surface by formula of approximating response surface when θ is value from -5 to 5, and the square in Fig.3.4 is reference value which obtained by used FEM. We can find that a good agreement is observed between the results from the stochastic response surface and the reference values. The approximate expression of the response surface is 15th order PCE. However, the 6th order approximate expression of the response surface is shown in Fig.3.4, because the influence is small after 7th order.

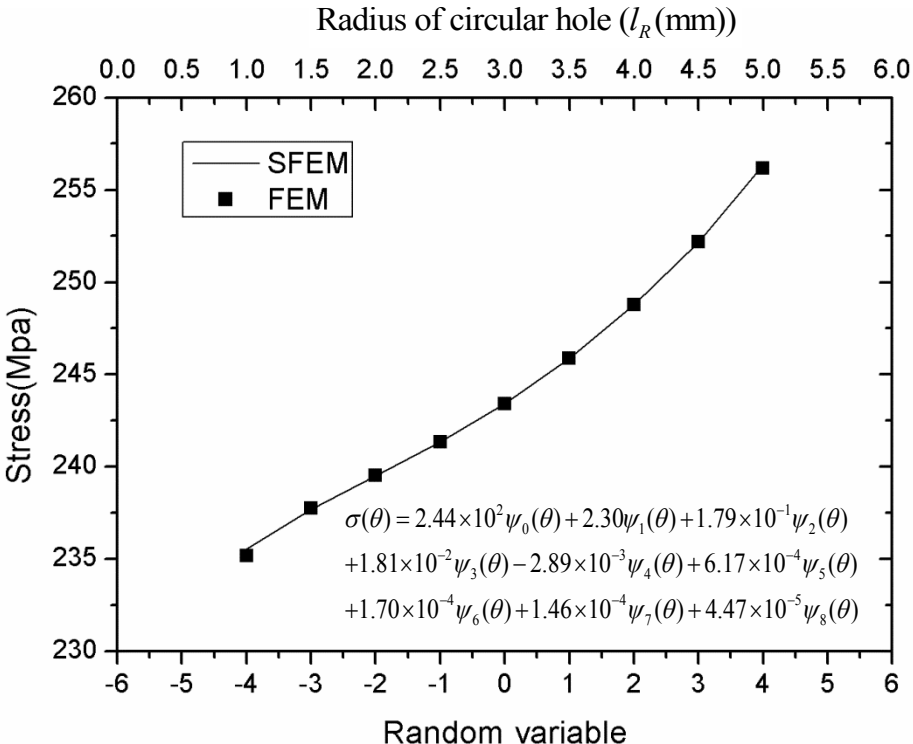


Fig. 3.4: The Response Surface of Stress
(Standard Deviation is 0.5mm)

Fig.3.5 shows the probability density distributions of the stress concentration factor obtained through the SFEM and FEM with Monte Carlo Simulation (FEM(MCS)). This has been obtained by using 10000 realization of the standard random variable θ in the obtained response surface ($k(\theta)$) of the stress concentration factor by the proposed SFEM. It is observed that the probability distribution obtained by the SFEM has good agreement with

the result of MCS with the conventional FEM(MCS). Also, as shown in the table in Fig.3.5, we find that the statistics are reasonably well estimated by the proposed SFEM when compared with those obtained from FEM(MCS). Note that the mean and the standard deviation of “SFEM-PCE” in the Table 3.1 are calculated by Eq. (2.7) and Eq. (2.8), which also takes almost same value.

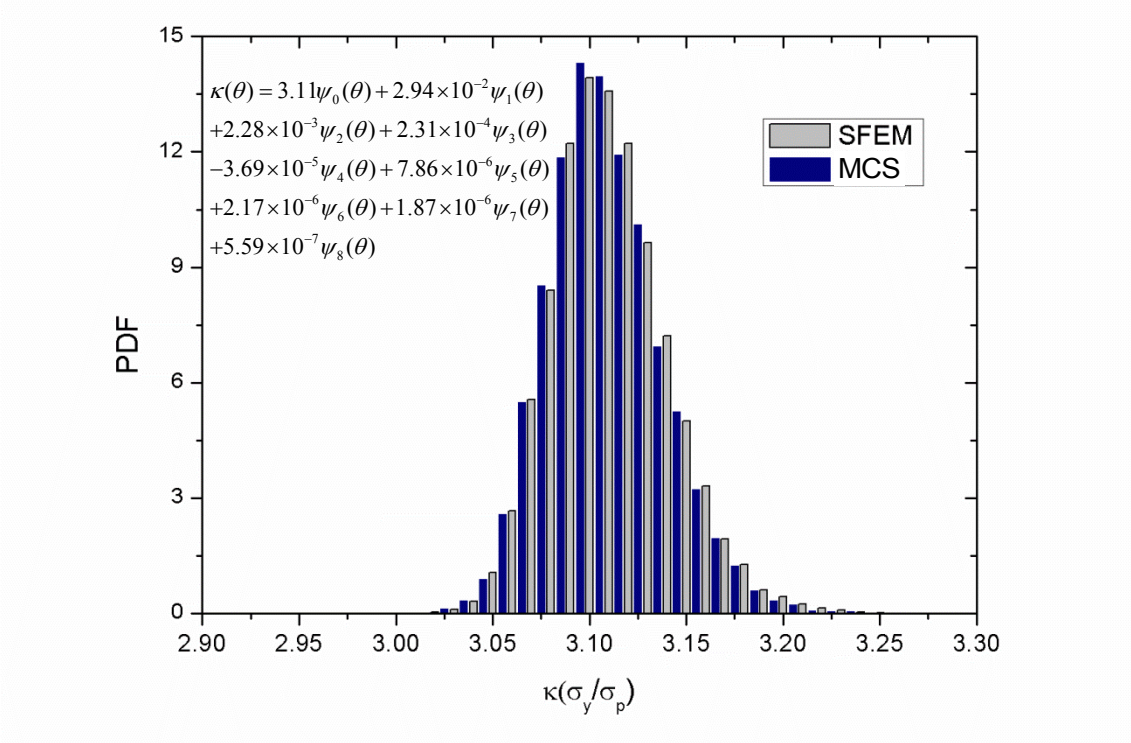


Fig.3.5: Stochastic Responses to Shape Uncertainty

Table 3.1 Statistics of the Stress Concentration Factor

	SFEM	FEM(MCS)	SFEM_PCE
Mean	3.10660	3.10611	3.10703
Std.dev.	0.02982	0.03032	0.02953

2) The Mean $\mu=3\text{mm}$ and the Standard Deviation $\sigma=0.1\text{mm} \sim 1\text{mm}$ of the Radius of A Circular Hole

In this section, we will assess the accuracy of stress concentration factor through different values of the standard deviation ($\sigma=0.1\text{mm} \sim 1\text{mm}$) with the mean $\mu = 3\text{mm}$.

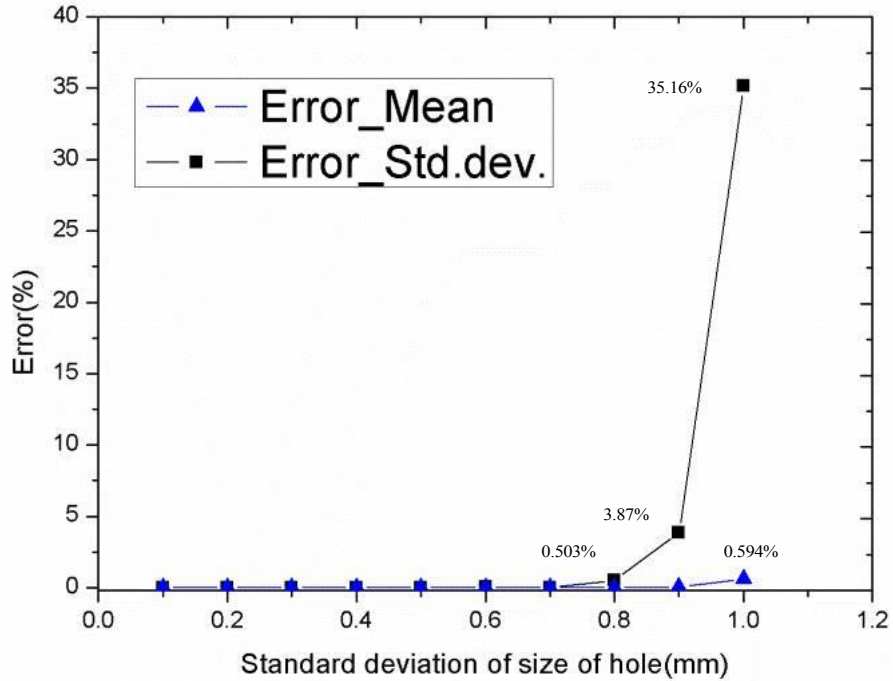


Fig.3.6: Error of the Stress Concentration Factor

Fig.3.6 shows the errors of the mean and the standard deviation of the stress concentration factor obtained from SFEM and FEM when the standard deviation of the size of the hole is changed. This clearly shows the error of mean of stress concentration factor does not change a lot, but the error of standard deviation becomes larger as the standard deviation of the size of the hole becomes larger. The error becomes 35.16% when the standard deviation of size of hole is 1mm.

In order to investigate the cause of the error, we show the response surface of $1/|J'(\xi, \eta; \theta)|$

when the standard deviation is 1mm in Fig.3.7. As shown in the figure, $1/|J'(\xi, \eta; \theta)|$ becomes less than 0 when the deviation length is less than $-3(l < -3)$. This is because the mean minus 3 times of the standard deviation (3σ) in this case means that the radius of the hole becomes negative value. This negative radius is not appropriate for problem definition. It is concluded that proper problem definition is necessary when we use the proposed SFEM. It is noted that a good agreement is observed between the results from the response surface of $1/|J'(\xi, \eta; \theta)|$ and $1/|J'(\xi, \eta; \theta)|$ within -5σ to $+5\sigma$ range when the standard deviation is 0.1 to 0.8.

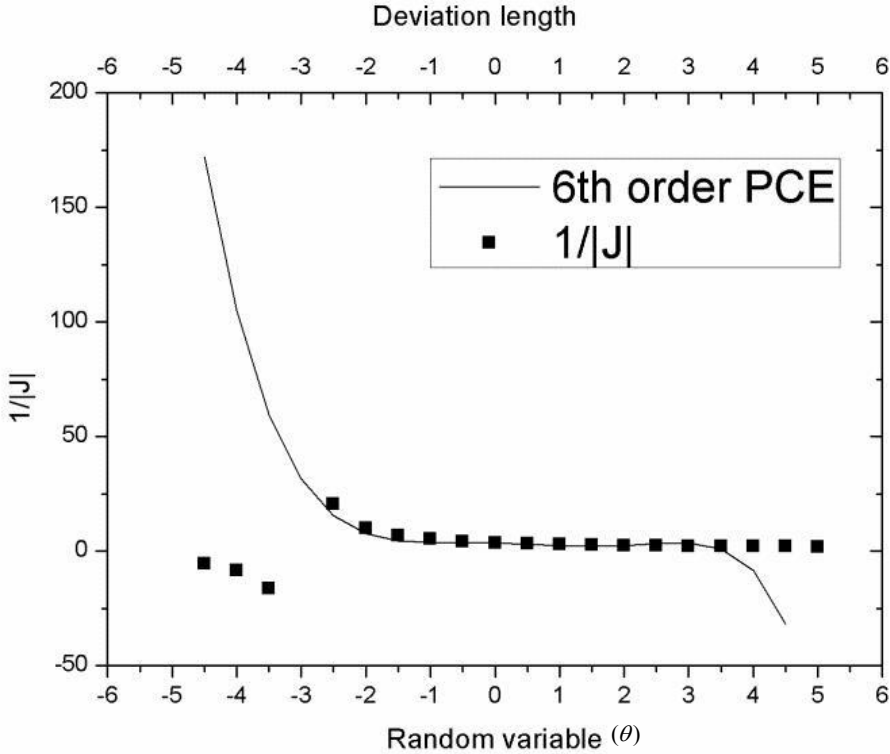


Fig.3.7: Response Surface of $1/|J'(\xi, \eta; \theta)|$
(Standard Deviation is 1mm)

Thus we can understand that in the example of the uncertainty in the size of circular hole, when the standard deviation of the size of circular hole is large, it becomes unsuitable

problem because the size of circular hole can become negative with relatively high probability. It is concluded that proper problem definition is important when we use the proposed SFEM. Based on the above, in section 3.2, we will develop an SFEM which can define inherent uncertainty of non-normal distribution, such as the log-normal distribution, by which negative size of the shape can be avoided in the problem definition.

(2) A Cruciform Weld Joint with Uncertainty in the Magnitude of Misalignment

In this section, we assess a cruciform weld joint with uncertainty in the magnitude of misalignment by the developed SFEM. The cruciform weld joint shown in Fig. 3.8(a) is considered with the mesh shown in Fig. 3.8(b).

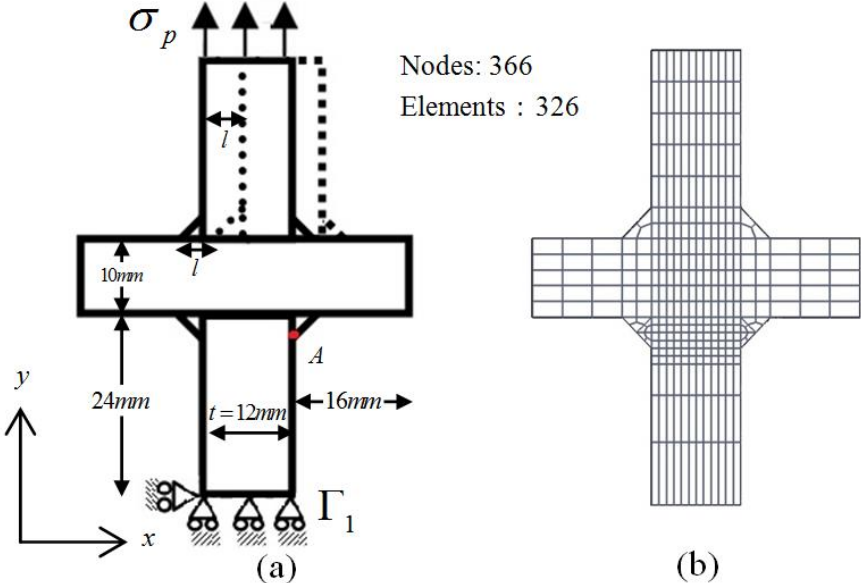


Fig.3.8: The Cruciform Weld Joint

In the rule of IACS(1999) for tolerance of misalignment, the magnitude of the misalignment is restricted within $t/3$ where t is the thickness of the plate. In this problem, we define the mean of misalignment as 0mm and the standard deviation as 1.333mm, so

that 3 times of the standard deviation (3σ) becomes equal to $t/3$ where the plate thickness $t=12\text{mm}$. It is also assumed that the distributed load $\sigma_p=78.4\text{N/mm}^2$, symmetry boundary condition is applied to the boundary Γ_1 as shown in Fig.3.8(a). The validity of the proposed method is discussed by comparing the result of the method with the MCS solution using the deterministic FEM for the same mesh size.

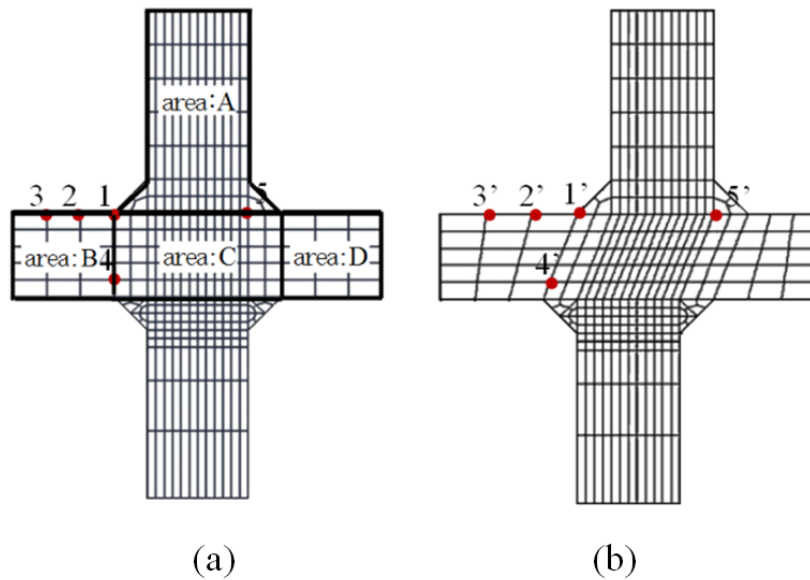


Fig.3.9: Model of Linear Deformation

1) Setting of the Uncertainty of Misalignment

First, we will describe about the deviation length of mesh (the deviation length (l) and coefficient of the degree of shape change for each node (α_i, β_i)) with change in the magnitude of misalignment. As shown in Fig.3.8 and 3.9, we assume that “area: A” moves with the distance l to the x -direction, and each node in “area: C” moves in parallel to the x -direction with the movement of “area: A”, and each node in “area: B” and “area: D” moves to the x -direction in a linear relationship with the movement of “area: A”. For example,

when the deviation length of the node 1 (representative node) is set as l , the deviation length of the node 2 is $2l/3$, the node 3 is $l/3$, the node 4 is $l/5$, the node 5 is l , and so on. By this concept, the coefficient of each node (α_i, β_i) is obtained.

2) Analysis Results by SFEM

Fig.3.10 shows the response surface of the stress in y-direction at a particular node (point A in Fig.3.8(a)) obtained by SFEM. A good agreement is observed between the results from the stochastic response surface and the reference values by usual deterministic FEM.

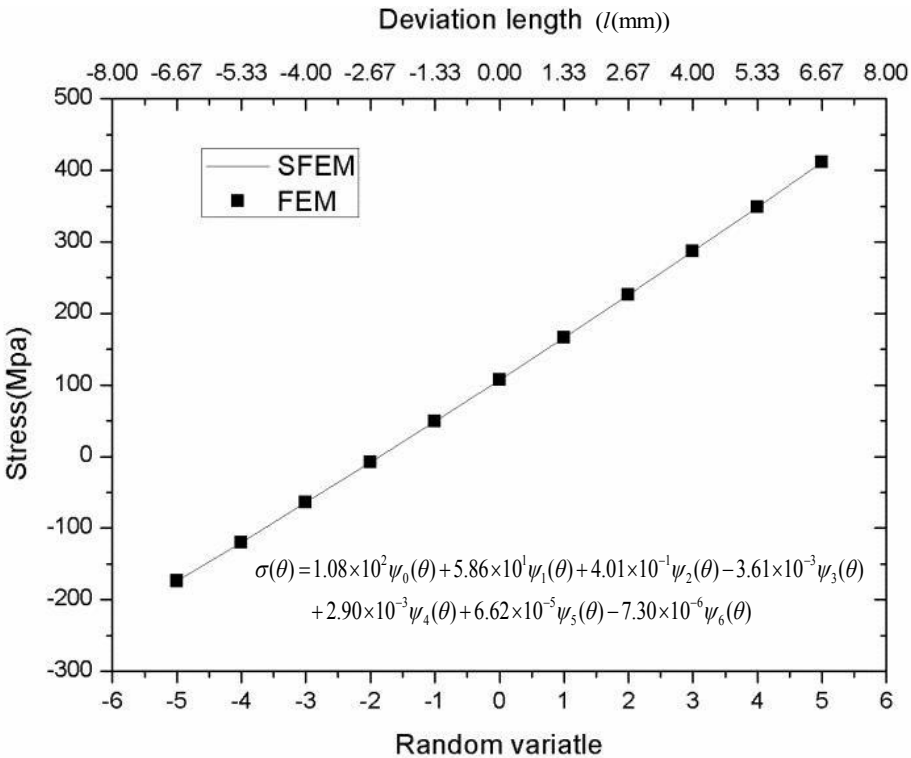


Fig.3.10: The Response Surface of Stress

Table 3.2 Statistics of the Stress Concentration Factor

	SFEM	FEM(MCS)	SFEM_PCE
Mean	2.85505	2.85505	2.85634
Std.dev.	0.10543	0.10544	0.10509

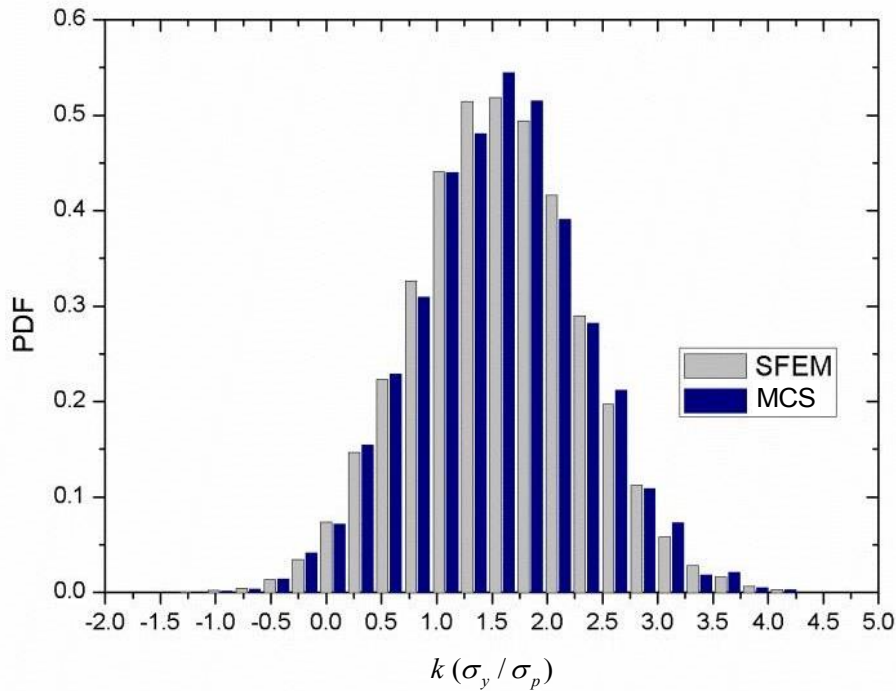


Fig.3.11: Stochastic Responses to Shape Uncertainty

Fig.3.11 show the probability density distributions of the stress concentration factor obtained from the SFEM and the FEM of 3000 samples. A similar distribution is obtained and the mean and standard deviation of the FEM(MCS), SFEM and SFEM_PCE is also almost same as indicated in the table in Fig.3.11.

Form the results in this section, it can be concluded that the proposed methodology is valid and effective for probabilistic estimation of the misalignment of cruciform weld joint.

And we can find that the stress in point A is increased 2.1 times when the deviation length is 2.67 mm, and the stress is increased 2.7 times when the deviation length is 4mm compared with that at the mean value (the deviation length is 0mm). we can consider that it only is a small variability compared with size of structure, but the stress at this point has been greatly changed. We consider that it cannot be ignored in practice from a security perspective.

3.1.4 Conclusions

In this section, the stochastic finite element method (SFEM) based on response surface methodology considering uncertainty in shape is formulated by an Hermite PCE.

1. The validity and feasibility of the proposed method is demonstrated by two cases in which the uncertainty in shape exists in the size of circular hole, and in the misalignment of weld joint. The probabilistic characteristics (the response surface of stress, and the probability distribution of the response) can be accurately estimated by the proposed method that solves the main stiffness equation only once.
2. In the example of the uncertainty in the size of circular hole, when the standard deviation of the size of circular hole is large, it becomes unsuitable problem because the size of circular hole can become negative with relatively high probability. It is concluded that proper problem definition is important when we use the proposed SFEM.
3. In the proposed SFEM, the degree of freedom is increased 9 times compared to the deterministic finite element method. So it is considered that the computational cost becomes higher by increase of random variables or increase of order of approximate expression. However, by using the proposed method, it is possible to obtain

approximate response surface is theoretically reasonable from the viewpoint of response surface approximation concept, which is different from the Monte Carlo method with conventional FEM.

4. In the proposed SFEM, only the normal distribution can be used to represent the inherent randomness of the shape. However, it is considered that the random parameter for the shape does not necessarily following a normal distribution, and may also cause unrealistic problems when negative size of the shape. Thus, in next section, we develop an SFEM which can define inherent uncertainty of non-normal distribution.

3.2 The Formularization of Stochastic Finite Element Method for Uncertainty in Shape Following Non-normal Distribution

In this study, the Stochastic Finite Element Method (SFEM) based on response surface methodology is formulated for the 2D problem with uncertainty in shape following non-normal distribution. And we develop a new algorithm which can deal with arbitrary order of PCE approximation.

3.2.1 An Approximate Method for Non-normal Distribution

In this section, we assume that the input random parameter (about uncertainty in shape) follow non-normal distribution, such as the log-normal distribution, arbitrary distribution. However, we can find a non-normal distribution cannot be expressed as a polynomial form (for example, an arbitrary normal distribution (x) can be expressed as a relation to the normal random variable of a standard normal distribution (θ) ($x = \mu + \sigma\theta$)), so the SFEM which deal with arbitrary distribution cannot be formulated. Thus, we need do to approximate for a random parameter (l) following non-normal distribution. This approximated method is proposed by Xiu and Karniadakis[32]. Here, the random parameter (l) following non-normal distribution is assumed to be approximated by Hermite PCE as follows.

$$l(\theta) = \sum_{i=0}^n l_i \psi_i(\theta), \quad (3.37)$$

where, n is the order of expansion terms. l_i are the unknown coefficients that need to be determined to define the approximating response surface. The determination method and approximation process of l_i are expounded as follows when the random parameter is defined as no-normal distribution.

Firstly, multiplying $\psi_i(\theta)w(\theta)$ to both sides of Eq. (3.37), and integrating the equation,

the unknown coefficients l_i is obtained as follows.

$$l_i = \frac{\int_D l \psi_i(\theta) w(\theta) d\theta}{\int_D \psi_i(\theta) \psi_i(\theta) w(\theta) d\theta}. \quad (3.38)$$

We need to transform the fully correlated random variables l and θ to the same probability space because the two random variables might be defined on different probability space. Here, let us assume that the random variable u is uniformly distributed in $(0, 1)$. A transformation of variables in probability space is shown as follow.

$$\begin{aligned} du &= f(l)dl = g(\theta)d\theta, \\ u &= F(l) = G(\theta), \end{aligned} \quad (3.39)$$

where $f(l), F(l)$ is the probability density functions and the cumulative distribution function for l , respectively. It is shown as follows.

$$f(l) = \frac{1}{\sqrt{2\pi}\sigma l} e^{-\frac{(\ln l - \mu)^2}{2\sigma^2}}, \quad (3.40)$$

$$F(l) = \frac{1}{2} \operatorname{erfc} \left[-\frac{\ln l - \mu}{\sqrt{2}\sigma} \right], \quad (3.41)$$

‘erfc’ is complementary error function which is defined by the error function ‘erf’ as

$\operatorname{erfc}(x) = 1 - \operatorname{erf}(x) = \frac{2}{\sqrt{\pi}} \int_x^\infty e^{-t^2} dt$. And $g(\theta), G(\theta)$ is the probability density functions

and the cumulative distribution function for θ , respectively. It is shown as follows.

$$g(\theta) = \frac{1}{\sqrt{2\pi}} e^{-\theta^2/2}, \quad (3.42)$$

$$G(\theta) = \frac{1}{2} \left(1 + \operatorname{erf} \frac{\theta}{\sqrt{2}} \right), \quad (3.43)$$

The Inverse function $F^{-1}(u), G^{-1}(u)$ is obtained by an approximation formula[34].

$$\begin{aligned}
l &= F^{-1}(u) = e^{\left(\mu - \sigma \times \left(\text{sign}\left(u - \frac{1}{2}\right) \left(t - \frac{c_0 + c_1 t + c_2 t^2}{1 + d_1 t + d_2 t^2 + d_3 t^3} \right) \right) \right)}, \\
\theta &= G^{-1}(u) = \text{sign}\left(u - \frac{1}{2}\right) \left(t - \frac{c_0 + c_1 t + c_2 t^2}{1 + d_1 t + d_2 t^2 + d_3 t^3} \right), \\
t &= \sqrt{-\ln[\min(u, 1-u)]^2}, \\
c_0 &= 2.515517, c_1 = 0.802853, c_2 = 0.010328, \\
d_1 &= 1.432788, d_2 = 0.189269, d_3 = 0.001308.
\end{aligned} \tag{3.44}$$

Here, we have effectively transformed the two different random variables l and θ to the same probability space defined by $u \in U(0,1)$, and substituting Eq. (3.44) into Eq. (3.38), the coefficients equation can be performed as follows:

$$l_i = \frac{\int_D l \psi_i(\theta) w(\theta) d\theta}{\int_D \psi_i(\theta) \psi_i(\theta) w(\theta) d\theta} = \frac{\int_0^1 F^{-1}(u) \psi_i(G^{-1}(u)) du}{\langle \psi_i(\theta) \rangle^2}, \tag{3.45}$$

The coefficients can be evaluated by using a numerical integration method to evaluate the above integral. When the coefficients are evaluated, and substituting l_i into Eq. (3.37), the random parameter (l) following non-normal distribution can be represented by Hermite PCE.

3.2.2 Example for Approximation of Non-normal Distribution

In section 3.2.1, it is expound that the random parameter (l) following non-normal distribution can be represented by random variable (θ) following standard normal distribution. In this section, the example for approximation of non-normal distribution is shown. As an example, we consider that the non-normal distribution is log-normal distribution with the mean $\mu = 1$ and the standard deviation $\sigma = 0.5$. Fig.3.12 shows the

probability density distributions of the random parameter (l) following log-normal distribution obtained from the exact results and the approximate method in section 3.2.1. This has been obtained by using 10000 realization of the standard random variable θ in the obtained response surface $l(\theta)$. Here, we assume that the approximate expression of the response surface is 6th order PCE. It is noted that a good agreement is observed between the results. Thus it is understood that lognormal distribution l is fully expressed by response surface of 6th order.

However, in order to obtain a good approximation precision for different problems (different distribution of input parameter), we need to adjust (to increase or to reduce) the order (n) of PCE approximation accordingly. In the following sections, it is developed that an algorithm which can deal with arbitrary order (n) of PCE approximation.

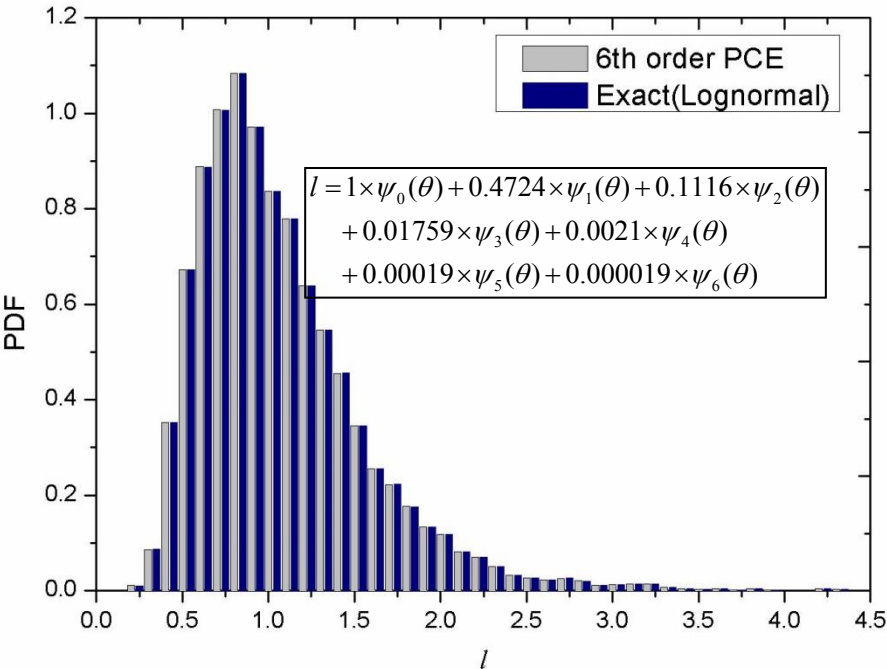


Fig.3.12: Probability Density Estimate of l

3.2.3 Stochastic Finite Element Formulation

In this section, we derive SFEM formulation involving random variable by using the assumption of uncertainty in shape shown in section 3.1.1 (mesh change). The SFEM formulation is different with the SFEM formulation in section 3.1.2. In this section, this method can deal with uncertainty in shape following non-normal distribution and it can also deal with arbitrary order of PCE approximation. The algorithm of SFEM with uncertainty in shape is developed in the following section.

(1) Stochastic Element Stiffness Matrix

The element stiffness matrix considering the uncertainty in shape is considered, and the following integration in terms of element coordinates (ξ, η) should be evaluated.

$$\mathbf{k}^{e}(\theta) = \int_{-1}^{+1} \int_{-1}^{+1} \mathbf{B}'^T(\xi, \eta; \theta) \mathbf{D} \mathbf{B}'(\xi, \eta; \theta) |\mathbf{J}'(\xi, \eta; \theta)| d\xi d\eta, \quad (3.46)$$

where the definition of notations can be found in section 3.1.2. $|\mathbf{J}'|$ and \mathbf{B}' involving uncertainty in shape (θ) is treated as follows.

1) Representation of $|\mathbf{J}'(\xi, \eta; \theta)|$

The Jacobian matrix $\mathbf{J}'(\xi, \eta; \theta)$ with the uncertainty variable (θ) is derived from Eq. (3.37),

Eq. (3.46) and the mapping relationship $\left(x' = \sum_{i=1}^4 N_i(\xi, \eta) x'_i, y' = \sum_{i=1}^4 N_i(\xi, \eta) y'_i \right)$ as follows.

$$\begin{aligned}
\mathbf{J}'(\xi, \eta; \theta) &= \begin{bmatrix} \frac{\partial x'}{\partial \xi} & \frac{\partial y'}{\partial \xi} \\ \frac{\partial x'}{\partial \eta} & \frac{\partial y'}{\partial \eta} \end{bmatrix} \\
&= \begin{bmatrix} \sum_{i=1}^4 \frac{\partial N_i}{\partial \xi} \left(x_i + \alpha_i \sum_{i=0}^n l_i \psi_i(\theta) \right) & \sum_{i=1}^4 \frac{\partial N_i}{\partial \xi} \left(y_i + \beta_i \sum_{i=0}^n l_i \psi_i(\theta) \right) \\ \sum_{i=1}^4 \frac{\partial N_i}{\partial \eta} \left(x_i + \alpha_i \sum_{i=0}^n l_i \psi_i(\theta) \right) & \sum_{i=1}^4 \frac{\partial N_i}{\partial \eta} \left(y_i + \beta_i \sum_{i=0}^n l_i \psi_i(\theta) \right) \end{bmatrix}.
\end{aligned} \tag{3.47}$$

The determinant of the Jacobian matrix is derived by Eq. (3.47), and can be written in the form of the polynomial of random variable (θ) as follows.

$$|\mathbf{J}'(\xi, \eta; \theta)| = |\mathbf{J}'_0(\xi, \eta)| + |\mathbf{J}'_1(\xi, \eta)|\theta + \dots + |\mathbf{J}'_{2n}(\xi, \eta)|\theta^{2n}, \tag{3.48}$$

where l is n^{th} order PCE approximation, which is different from section 3.1.2 where l is 1st order PCE approximation. Thus, $|\mathbf{J}'(\xi, \eta; \theta)|$ is $2n$ order PCE approximation in Eq. (3.48). In the following formulation, the form of the polynomial of random variable (θ) needs to be written as the form of Hermite polynomial $\psi(\theta)$ because we will use orthogonality of the polynomial.

$$|\mathbf{J}'(\xi, \eta; \theta)| = \sum_{i=0}^{2n} |\mathbf{J}'_i(\xi, \eta)| \theta^i = \sum_{i=0}^{2n} |\mathbf{J}'_i(\xi, \eta)| \psi_i(\theta), \tag{3.49}$$

where, n is order of PCE approximation for the uncertainty of shape following an arbitrary non-normal distribution. We can see that $2n$ order of PCE approximation is obtained from the arbitrary order of PCE approximation. It is noted that $|\mathbf{J}'_i(\xi, \eta)|$ can be calculated based on the author developed automatic transformation algorithm which is introduced in section 3.2.4.

2) Representation of \mathbf{B}'

Generally in the finite element formulation, the component, $\partial N_A / \partial x'$ and $\partial N_A / \partial y'$, in the \mathbf{B}' matrix is depicted as follows.

$$\begin{bmatrix} \frac{\partial N_A}{\partial x'} \\ \frac{\partial N_A}{\partial y'} \end{bmatrix} = [\mathbf{J}'(\xi, \eta; \theta)]^{-1} \begin{bmatrix} \frac{\partial N_A}{\partial \xi} \\ \frac{\partial N_A}{\partial \eta} \end{bmatrix}. \quad (3.50)$$

Using Eq. (3.49), we can arrange Eq. (3.50) as follows.

$$\begin{aligned} \frac{\partial N_A}{\partial x'} &= \frac{1}{|\mathbf{J}'_0| + |\mathbf{J}'_1|\theta + \dots + |\mathbf{J}'_{2n}|\theta^{2n}} \times \left(H_{AX0} + \sum_{u=1}^n H_{AXu}\theta^u \right), \\ \frac{\partial N_A}{\partial y'} &= \frac{1}{|\mathbf{J}'_0| + |\mathbf{J}'_1|\theta + \dots + |\mathbf{J}'_{2n}|\theta^{2n}} \times \left(H_{AY0} + \sum_{u=1}^n H_{AYu}\theta^u \right). \end{aligned} \quad (3.51)$$

Therefore, when we arrange Eq.(3.51), $\mathbf{B}'(\xi, \eta; \theta)$ can be written as shown below.

$$\mathbf{B}'(\xi, \eta; \theta) = \frac{1}{|\mathbf{J}'(\xi, \eta; \theta)|} \times \sum_{u=0}^n \mathbf{B}'_u(\xi, \eta)\theta^u. \quad (3.52)$$

3) Approximation of $\frac{1}{|\mathbf{J}'(\xi, \eta; \theta)|}$

In this section, it is assumed that $1/|\mathbf{J}'(\xi, \eta; \theta)|$ can be approximated by an arbitrary order (p order) of Hermite PCE as follows.

$$\frac{1}{|\mathbf{J}'(\xi, \eta; \theta)|} = \sum_{u=0}^p A_u \psi_u(\theta), \quad (3.53)$$

where, A_u are unknown coefficients of approximated polynomial, $\psi_u(\theta)$ are the basis functions, represented by Hermite polynomial, and $p+1$ is the number of expansion terms.

The unknown coefficients, A_u , can be decided as follows.

Firstly, Eq. (3.53) is rewritten as follows by using Eq. (3.49) and Hermite polynomial.

$$\sum_{i=0}^{2n} |\mathbf{J}''_i(\xi, \eta)| \psi_i(\theta) \times \sum_{u=0}^p A_u \psi_u(\theta) = 1. \quad (3.54)$$

Multiplying $\psi_t(\theta)w(\theta)$ to both sides of Eq. (3.54), and integrating the equation, we have following equation.

$$\int_{-\infty}^{\infty} \sum_{i=0}^{2n} |J_i^n| \psi_i(\theta) \times \sum_{u=0}^p A_u \psi_u(\theta) \psi_t(\theta) w(\theta) d\theta = \int_{-\infty}^{\infty} 1 \times \psi_t(\theta) w(\theta) d\theta . \quad (3.55)$$

This equation can be depicted as follows when consider $\int_D (\text{Eq.}(3.56)) \psi_t(\theta) w(\theta) d\theta = \langle (\text{Eq.}(3.56)) \psi_t(\theta) \rangle$

$$\sum_{i=0}^{2n} |J_i^n| \sum_{u=0}^p A_u \langle \psi_i(\theta) \psi_u(\theta) \psi_t(\theta) \rangle = \langle \psi_t(\theta) \rangle . \quad (3.56)$$

This means that the following simultaneous equations about the coefficients, A_i , are obtained.

$$\begin{bmatrix} J_{00}'''e & J_{01}'''e & \cdots & J_{0p}'''e \\ J_{10}'''e & J_{11}'''e & \cdots & J_{1p}'''e \\ \vdots & \vdots & \vdots & \vdots \\ J_{p0}'''e & J_{p1}'''e & \cdots & J_{pp}'''e \end{bmatrix} \begin{bmatrix} A_0 \\ A_1 \\ \vdots \\ A_p \end{bmatrix} = \begin{bmatrix} 1 \\ 0 \\ \vdots \\ 0 \end{bmatrix} , \quad (3.57)$$

where $J_{ut}'''e$ is $\sum_{i=0}^{2n} |J_i^n| \langle \psi_i(\theta) \psi_u(\theta) \psi_t(\theta) \rangle$.

Then the unknown coefficients of approximation polynomial, A_u , is derived by solving the above simultaneous equations.

When we substitute Eq. (3.53) into Eq. (3.52), it is found that Eq. (3.52) contains both $\psi_u(\theta)$ and θ^u . Thus a polynomial transformation will be implemented for Eq. (3.53) as follows.

$$\frac{1}{|J'(\xi, \eta; \theta)|} = \sum_{u=0}^p A_u \psi_u(\theta) = \sum_{u=0}^p A'_u \theta^u . \quad (3.58)$$

Finally, the element stiffness matrix is obtained by rearranging Eq. (3.46) using Eq. (3.52) and Eq. (3.58) which is represented by the Hermite polynomial of order $2n+p$ based on the basis functions, $\psi_i(\theta)$.

$$\mathbf{k}^{e} = \sum_{i=0}^{2n+p} \mathbf{k}_i^{n_e} \psi_i(\theta) . \quad (3.59)$$

It is noted that “Transformation from Hermite polynomial to general polynomial” in Eq. (3.58) and “Transformation from general polynomial to Hermite polynomial” in Eq. (3.49) is done automatically by the author developed transformation algorithm in this study.

(2) Force Vector

The force vector is changed when the shape of the analysis domain is changed and the force is applied to the moved boundary. Here the force vector will be derived through the same consideration in the element stiffness matrix and it can be represented by the Hermite polynomial of order n .

$$\mathbf{f}^{e} = \sum_{i=0}^n \mathbf{f}_i^{f_e} \psi_i(\theta) . \quad (3.60)$$

(3) Assembly of Global Stiffness Matrix

In this study, it is very difficult to assemble a global stiffness matrix for each element like the usual finite element method because order of PCE approximation is introduced into the equation as a parameter. Thus, we assemble a global stiffness matrix separately for the element stiffness matrix ($\mathbf{k}_i^{n_e} (i=0, \dots, 2n+p)$) of each order (i) in Eq. (3.59). Finally, we can obtain the global stiffness matrix and the force vector which contains both order of PCE approximation (p) and that of random variable (n).

$$\mathbf{k}' = \sum_{i=0}^{2n+p} \mathbf{k}_i^{k'} \psi_i(\theta), \quad (3.61)$$

$$\mathbf{f}' = \sum_{i=0}^n \mathbf{f}'_i \psi_i(\theta). \quad (3.62)$$

(4) The Stiffness Equation of SFEM

Formulation of SFEM is performed by using the stiffness matrix, the force vector and the approximate response surface of the displacement.

The global stiffness equation involving random variable (θ) is written as follows:

$$\mathbf{k}'\mathbf{u}' = \mathbf{f}' , \quad (3.63)$$

where the global stiffness matrix, \mathbf{k}' (Eq. (3.61)), and the force vector, \mathbf{f}' (Eq. (3.62)), are represented by basis functions, $\psi_i(\theta)$. The unknown displacement response \mathbf{u}' of Eq. (3.63) is also approximated by using Hermite polynomial of q order.

$$\mathbf{u}' = \sum_{i=0}^q \mathbf{u}'_i \psi_i(\theta). \quad (3.64)$$

Substituting Eq. (3.61), Eq. (3.62) and Eq. (3.64) into Eq. (3.63) the stiffness equation becomes as follows:

$$\sum_{i=0}^{2n+p} \mathbf{k}'_i \psi_i(\theta) \left(\sum_{i=0}^{2n+p} \mathbf{u}'_i \psi_i(\theta) \right) = \sum_{i=0}^n \mathbf{f}'_i \psi_i(\theta) , \quad (3.65)$$

where the global stiffness matrix \mathbf{k}' is approximated by $2n+p$ order polynomial. Thus, the order (q) of PCE approximation of Eq. (3.65) is assumed as $2n+p$.

Multiplying both sides of Eq. (3.65) by $\psi_i(\theta)w(\theta)$, integrating the equation, we have:

$$\sum_{i=0}^{2n+p} \mathbf{k}''_i \sum_{j=0}^{2n+p} \mathbf{u}'_j \langle \psi_i(\theta) \psi_j(\theta) \psi_t(\theta) \rangle = \sum_{i=0}^n \mathbf{f}'_i \langle \psi_i(\theta) \psi_t(\theta) \rangle. \quad (3.66)$$

Thus the global stiffness equation can be derived as follows:

$$\begin{bmatrix} \mathbf{K}''_{00} & \mathbf{K}''_{01} & \cdots & \mathbf{K}''_{0(2n+p)} \\ \mathbf{K}''_{10} & \mathbf{K}''_{11} & \cdots & \mathbf{K}''_{1(2n+p)} \\ \vdots & \vdots & \vdots & \vdots \\ \mathbf{K}''_{(2n+p)0} & \mathbf{K}''_{(2n+p)1} & \cdots & \mathbf{K}''_{(2n+p)(2n+p)} \end{bmatrix} \begin{bmatrix} \mathbf{u}'_0 \\ \mathbf{u}'_1 \\ \vdots \\ \mathbf{u}'_{2n+p} \end{bmatrix} = \begin{bmatrix} \mathbf{F}''_0 \\ \mathbf{F}''_1 \\ \vdots \\ \mathbf{F}''_{2n+p} \end{bmatrix}, \quad (3.67)$$

where, $\mathbf{K}''_{ij} = \sum_{i=0}^{2n+p} \mathbf{k}''_i \langle \psi_i(\theta) \psi_j(\theta) \psi_t(\theta) \rangle$, $\mathbf{F}''_t = \sum_{i=0}^n \mathbf{f}''_i \langle \psi_i(\theta) \psi_t(\theta) \rangle$.

Compared with the usual deterministic global stiffness equation, it involves not only the unknown displacement of deterministic part (\mathbf{u}'_0) but also involves the unknown displacement of stochastic part (the stochastic part of order 1 (\mathbf{u}'_1), the stochastic part of order 2 (\mathbf{u}'_2), ..., the stochastic part of order $2n+p$ (\mathbf{u}'_{2n+p})). And the uncertainty of stress can be assessed by Eq. (3.52) with Eq. (3.53), Eq. (3.64) after the displacement is obtained.

$$\boldsymbol{\sigma}' = \mathbf{DB}'\mathbf{u}' = \sum_{i=0}^{3n+2p} \boldsymbol{\sigma}'_i \psi_i(\theta). \quad (3.68)$$

3.2.4 Algorithm of SFEM with Uncertainty in Shape

In this section, we will expound algorithm of proposed SFEM. This section falls into two parts: Overview of analysis procedure and Algorithm of SFEM.

(1) Overview of Analysis Procedure

In the above formulation of SFEM, we find that we need to develop a new algorithm which can deal with an approximate polynomial of arbitrary order (n) when input parameter of uncertainty in shape following non-normal distribution and an approximate polynomial of

arbitrary order (p) of $1/|J|$. In this section, it is proposed that an algorithms applicable to arbitrary approximate order n and p . And the algorithm is shown in Fig.3.13.

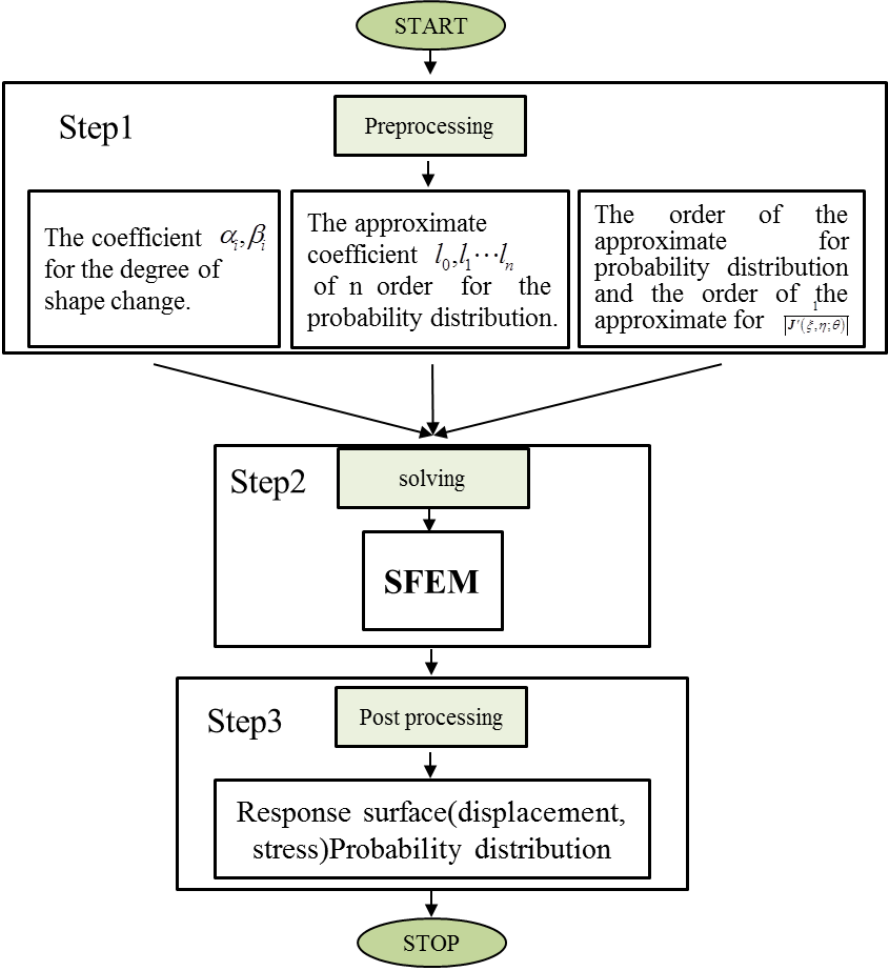


Fig.3.13: An Overall Flowchart

Step 1: Pre processing

In the pre-processing, we need to determine the input parameters such as $\alpha_i, \beta_i (i=1,2\dots nodes), n, l_j (j=1,2\dots n), p$, for use in the next step solver, where, the α_i, β_i are the coefficients of the degree of shape change and it is given in section 3.1.1. The n is

the order of PCE approximation about input parameter (uncertainty of shape), and the l_0, l_1, \dots, l_n are the unknown coefficients that can be determined by refer to section 3.2.1.

The p is the order of PCE approximation of $1/|\mathbf{J}'(\xi, \eta; \theta)|$.

Step 2: Solving

In this step we will use the above input parameter as input data to the stochastic finite element method (SFEM).

Step 3: Post processing

In the post processing, the response surface of the displacement response/the stress response of each node is evaluated by using the proposed SFEM, and the statistics of response (mean value, standard deviation) and probability distribution can be obtained by the obtained response surface.

It is noted that the SFEM in step2, we need to develop an algorithm which can deal with arbitrary approximate order n and p automatically. In the next section, the algorithm of SFEM will be explained.

(2) Algorithm of SFEM

Fig.3.14 shows the Flowchart of the SFEM.

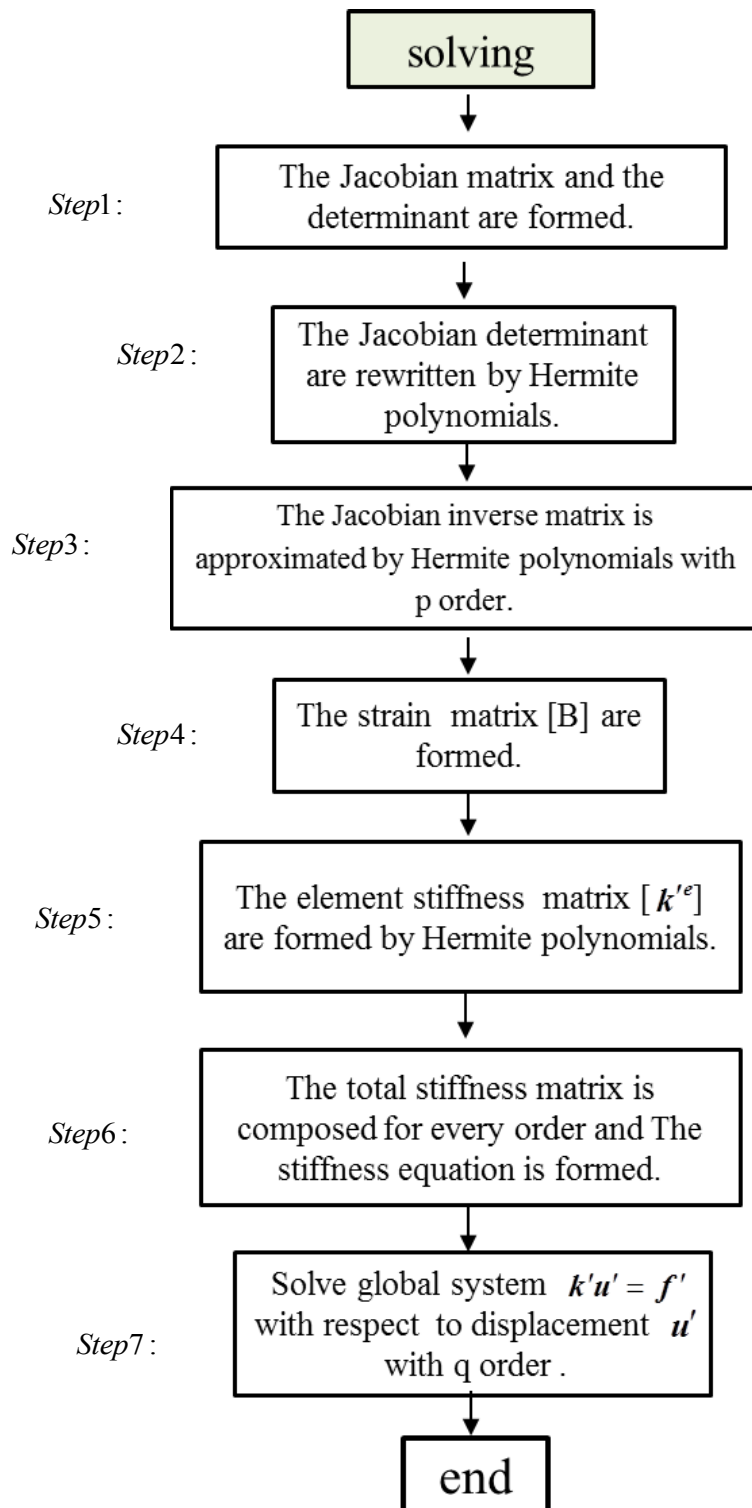


Fig.3.14: Flowchart of the SFEM

Step1:

The Jacobian matrix is computed using Eq. (3.47). And the determinant for the zeroth order $|J'_0(\xi, \eta)|$, the first order $|J'_1(\xi, \eta)|$, the second order $|J'_2(\xi, \eta)|$, ..., and the 2nth order $|J'_{2n}(\xi, \eta)|$ (see Eq.(3.48)) is also computed, respectively.

Step2:

We can find that it is necessary to transform the general polynomial form $\sum_{i=0}^{2n} |J'_i(\xi, \eta)| \theta^i$ to the Hermite polynomial form $\sum_{i=0}^{2n} |J''_i(\xi, \eta)| \psi_i(\theta)$ as shown in Eq.(3.49). In this study, we developed an algorithm to realize automatic transformation from the general polynomial form to the Hermite polynomial form. Here, as an example, we will explain the polynomial transforms of the m order such as the following equation.

$$\sum_{i=0}^m a_i \theta^i \rightarrow \sum_{i=0}^m b_i \psi_i(\theta). \quad (3.69)$$

Table 3.3 The Coefficients t_{ij} of θ of Hermite Polynomial $\psi_i(\theta)$

$i \backslash j$	θ^0	θ^1	θ^2	θ^3	...
0	1	0	0	0	...
1	0	1	0	0	...
2	-1	0	1	0	...
3	0	-3	0	1	...
...

Here, we assume that the coefficients $a_i (i=1, 2, \dots, m)$ of Eq.(3.69) is given. And a table is also shown in which i is order of polynomial, j is the j^{th} power of θ , and the values t_{ij} is

coefficients of θ^j in each order, it is corresponding to the basis function of Table 2.1. The coefficient b_i of the Eq.(3.69) can be computed by the following procedure.

(i)

Firstly, let me consider the coefficient a_m of the highest order term (θ^m). When the Table 3.3 is used, the $a_m\theta^m$ can be expressed as follows.

$$a_m\theta^m = a_m\psi_m(\theta) - a_m \sum_{j=0}^{m-1} t_{mj} \theta^j, \quad (3.70)$$

where, $b_m = a_m$. However, we can see that Eq.(3.70) has a remainder term $a_m \sum_{j=0}^{m-1} t_{mj} \theta^j$. This coefficient need be added to a_j ($j=0,1,\dots,m-1$) that is, the coefficient a_j can be given as follows.

$$a_j = a_j - a_m t_{mj} \quad (j=0,1,\dots,m-1). \quad (3.71)$$

For example: when $m=3$ is considered, the $a_3\theta^3$ can be rewrite as $a_3\theta^3 = a_3(\theta^3 - 3\theta) + 3a_3\theta$ in which $\psi_3(\theta) = \theta^3 - 3\theta$, $t_{30} = 0$, $t_{31} = -3$, $t_{32} = 0$. By adding the remainder term $3a_3\theta$ to the coefficient a_1 of θ^1 on the left side of equation (3.69), we can obtained a new coefficient $a_1 = a_1 + 3a_3$, and execute the following steps.

(ii)

Secondly, we consider the coefficient a_{m-1} of second highest order term θ^{m-1} . By using the same method as (i), $b_{m-1} = a_{m-1}$ can be obtained. Thus, the coefficient a_j on the left side of equation (3.69) can be expressed as $a_j = a_j - a_{m-1} t_{m-1,j}$, ($j=0,1,2,\dots,m-2$) because terms less than $m-2$ is remained.

(iii)

Finally, the coefficients of θ^{m-j} ($j=2,3,\dots,m$) can be obtained in order by reducing the order.

Thus, by the above concept, the polynomial of $2n$ order can be automatically transformed into Hermite polynomial.

Step3:

In step3, the reciprocal of the Jacobian determinant $(1/|J'(\xi, \eta; \theta)|)$ can be approximated by Hermite PCE of p order. Here, based on the same concept as step2, an algorithm which can deal with an arbitrary approximate order (p) is developed to achieve the automatic transformation of Eq. (3.58), and another algorithm is also developed to achieve the approximation of Eq. (3.53) for an arbitrary approximate order (p).

Step4:

A strain matrix $\mathbf{B}'(\xi, \eta; \theta)$ involving random variable (θ) is generated.

Step5:

The element stiffness matrix is generated in step5.

Step6:

The global stiffness matrix is assembled for each order.

Step7:

The global stiffness equation is made (Eq.3.67), and by solving the equation, the unknown response of displacement can be evaluated. Finally, we can obtain the response surface of the displacement at each node (Eq. (3.64)) and the response surface of stress (Eq. (3.68)).

As described above, in this study, we developed an algorithm that can deal with arbitrary order for uncertainty of shape following non-normal distribution.

3.2.5 Numerical Example

In this study, the validity and feasibility of the proposed method of structural analysis is discussed by two examples, (1) A plate with a circular hole at the center with uncertainty in the size of a circular hole, (2) A cruciform weld joint with uncertainty in the weld toe radius.

(1) A Plate with a Circular Hole with Uncertainty

In this example, the problem of a plate with a circular hole with uncertainty problem is discussed again. However, the case is different with section 3.1.3(1) because a negative size of the shape will be avoided by assuming the uncertainty of shape following log-normal distribution.

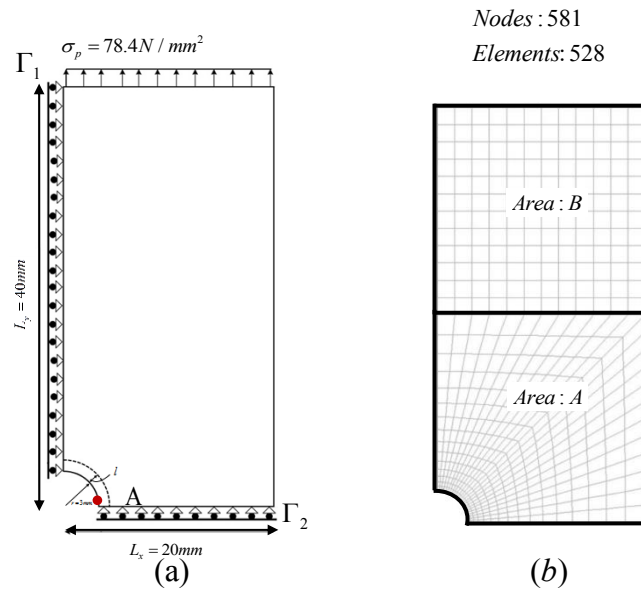


Fig.3.15: The Geometrical Deformation of the Hole

A plate with a circular hole (Fig. 3.15(a)) is considered and mesh is shown in Fig. 3.15(b). It is assumed that the distributed load $\sigma_p = 78.4 \text{ N/mm}^2$, and symmetry boundary condition is applied to the boundaries, Γ_1 and Γ_2 . The validity of the proposed method (SFEM) is discussed by comparing the result of the method with the MCS solution of the deterministic

problems (FEM) for a same mesh size.

In this case, the coefficient (α_i, β_i) of each node is defined based on the considering method shown in the previous section 3.1.1 when the radius of the hole changes with length l . However, in order to maintain a low aspect ratio (close to a square) for the elements near the circular hole, we need adjust coefficient (α_i, β_i) of each node appropriately, to prevent lower analysis accuracy due to the distortion of the element. The effect of defining of the coefficient (α_i, β_i) of each node on accuracy will be discussed in later section.

Here, a circular hole following log-normal distribution will be considered. It is assumed that minimum value of the radius of a circular (l_r) is 2mm, and the deviation length is assumed following log-normal distribution with mean $\mu = 1$ mm, and the standard deviation $\sigma = 0.5$ mm. And the deviation length (Eq. (3.37)) is approximated by Hermite PCE of 6th order ($n=6$), and $1/|\mathbf{J}'(\xi, \eta; \theta)|$ is also approximated by Hermite PCE of 6th order ($p=6$). Thus, we deduce that the response surface of stress should be an approximate polynomial of 30th order ($3n+2p$) based on the approximate order of input ($n=6$) and the approximate order of $1/|\mathbf{J}'(\xi, \eta; \theta)|$ ($p=6$).

Fig.3.16 shows the stochastic response surface of the stress at a particular node (point A) in y-direction. The equation in Fig.3.16 is approximate expression of the response surface by SFEM, where, the 8th order approximate expression of the response surface is shown because the influence is small after 9th order. We can find that good agreement is observed between the results from the stochastic response surface and the reference values obtained by used FEM within the wide limits. Note that the approximation accuracy of the response surface is worse near the minimum value of radius of the circular ($l_r = 2$ mm) and maximum of radius of the circular ($l_r = 11.49$ mm). In order to investigate the effect of them on analysis results, we also show the probability density distributions and statistics in the following.

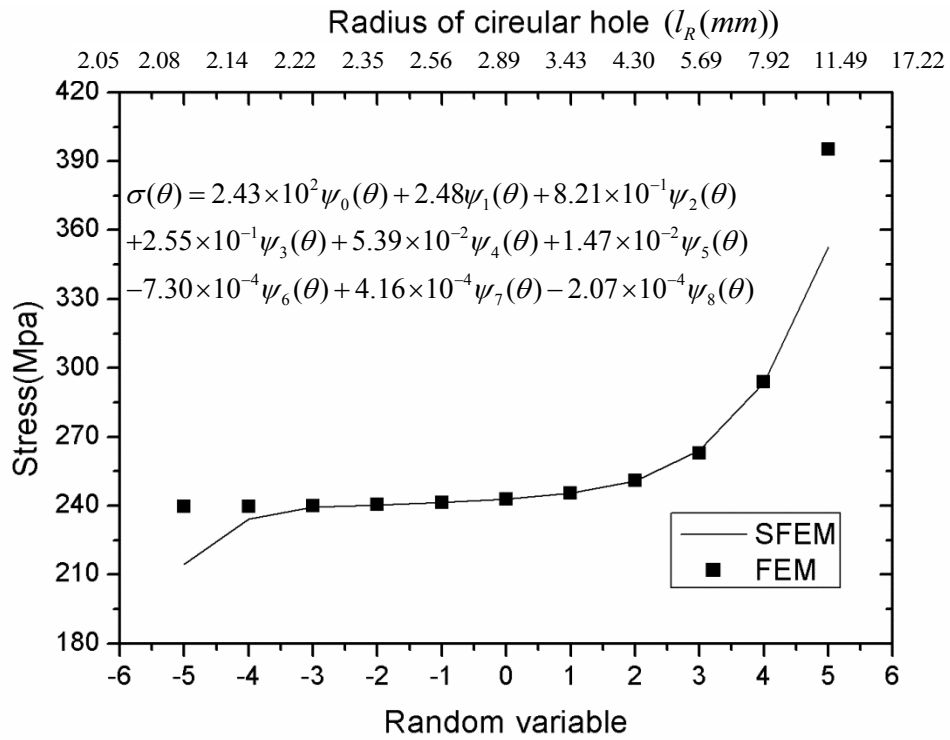


Fig.3.16: The Response Surface of Stress (Logarithmic Distribution)

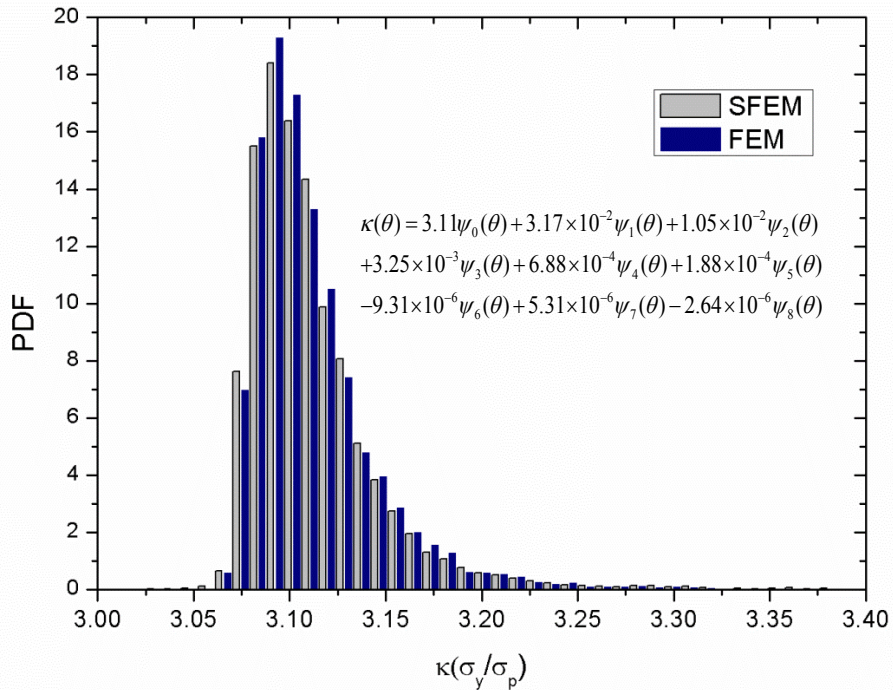


Fig. 3.17: Stochastic Responses to Shape Uncertainty

Table 3.4 Statistics of the Stress Concentration Factor

	SFEM	FEM(MCS)	SFEM_PCE
Mean	3.10553	3.10518	3.10574
Std.dev.	0.03650	0.03580	0.03605

Fig.3.17 shows the probability density distributions of the stress concentration factor obtained through the SFEM and FEM through the deterministic FEM with MCS (FEM(MCS)) with 10000 samples. The distribution by SFEM has been obtained by using 10000 realization of the standard random variable θ in the obtained response surface ($k(\theta)$) of the stress concentration factor by the proposed SFEM. It is observed that the probability distribution obtained by the SFEM has good agreement with the result of MCS with the conventional FEM. Also, as shown in the Table3.4, we find that the statistics are reasonably well estimated by the proposed SFEM and “SFEM-PCE” when compared with those obtained from FEM(MCS). Thus, we can consider that the probability of occurrence of θ is very small near $l_r = 2\text{mm}$ and $l_r = 11.49\text{mm}$, so that the bad accuracy of the response surface shown in Fig3.16 do not affect to the probability distribution of the response in Fig.3.17 and the statistics in Table 3.4.

Here, we also investigated the computational time of the proposed SFEM of this section compared with that of MCS. And two cases are considered, i.e., case1: the deviation length (l) following normal distribution and case2: the deviation length (l) following non-normal distribution uncertainty. In the case 1, n and p in Eq. (3.67) are 1 and 6, we can know that the degree of freedom is $D \times 9$ in which D is the degree of freedom for deterministic problem, and it takes 1.5 hours for solving Eq. (3.67). In the case 2, we can know that it has degree of freedom of $D \times 30$ when n and p in Eq. (3.67) are 6 and 6, and to solve the Eq.(3.67) takes 7.65 hours. On the other hand, the computational time of MCS is shown which is taking 13.9 hours by FEM of 10000 samples. We can find that compute time for case 1 is reduced evidently. However in the case 2 the computational time is only reduced

by half compared with the MCS. In this study, the obtained stiffness matrix of the degree of freedom $D \times (2n+p+1)$ is not a band matrix. This is because the order of PCE approximation is introduced into the equation as a parameter, so it is very difficult to assemble a global stiffness matrix for each element like the usual finite element method. In this study, we use the simple Gaussian elimination to solve the equation which is not good solution for this matrix. As a future work, an efficient numerical analyzing technique will be discussed for to realize quick solving of this matrix.

In conclusion, we can understand that the uncertainty of shape following non-normal distribution can be evaluated by using the program of SFEM which can deal with an arbitrary approximate order. And we can also find that a good agreement can be observed even when there is bigger deviation length as shown in Fig3.16 ($l_R = 7.92\text{mm}$).

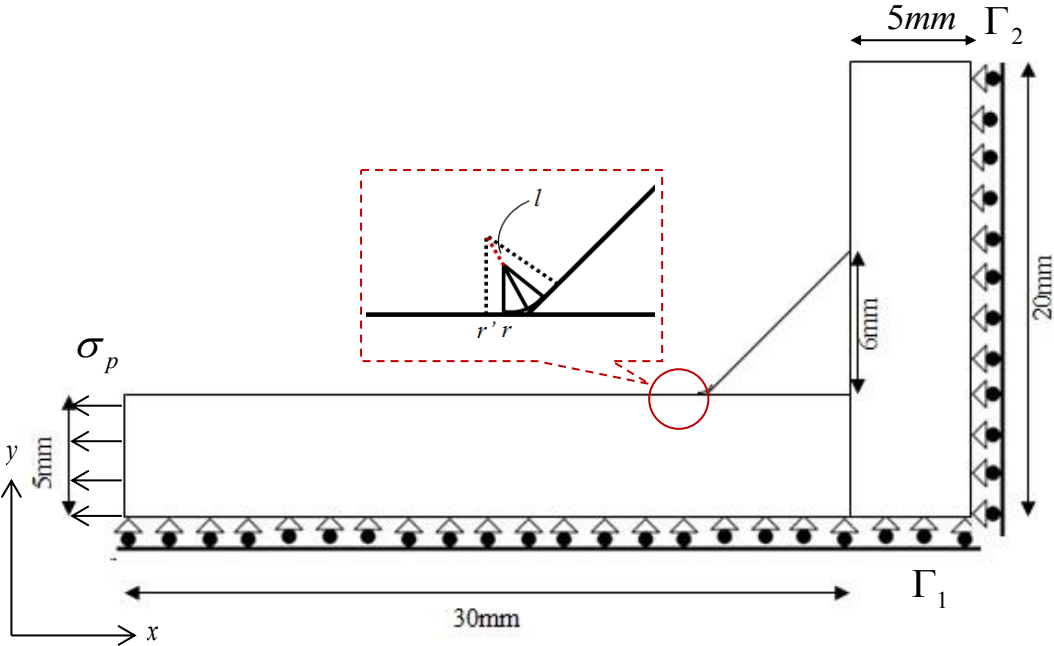
(2) A Cruciform Weld Joint with Uncertainty in the Weld Toe Radius

In this example, we assess a cruciform weld joint with uncertainty in radius of weld toe by the developed SFEM. The cruciform weld joint in Fig. 3.18(a) is considered and the mesh is shown in Fig. 3.18(b).

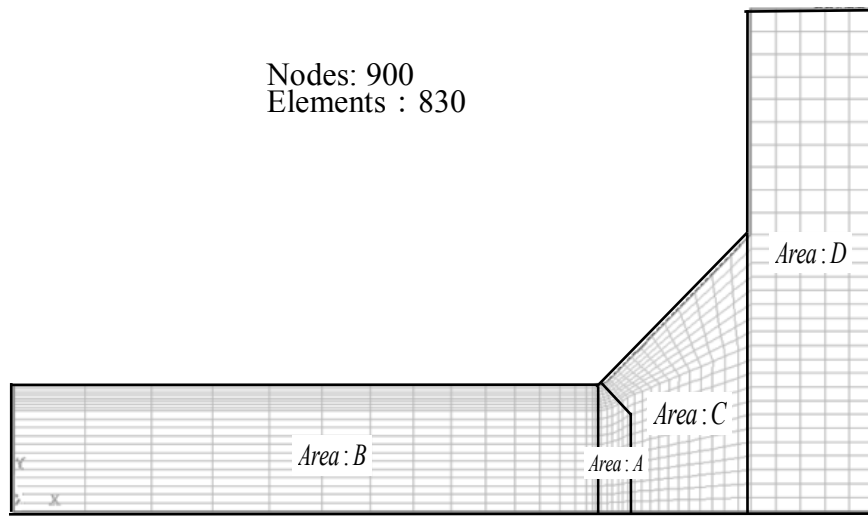
In this problem, we define the radius of weld toe following a lognormal distribution with the mean as 0.9667mm and the standard deviation as 0.474mm and minimum value of radius of weld toe is defined as 0.3mm based on the measurement result data of shape of welding toe in References [40].

Here the minimum value of radius of weld toe (0.3mm) and mean (0.6667mm) and the standard deviation (0.474mm) for the deviation length of radius is used as input data. It is also assumed that the distributed load $\sigma_p = 78.4 \text{ N/mm}^2$, symmetry boundary condition is applied to the boundary Γ_1, Γ_1 as shown in Fig.3.18(a). The validity of the proposed method is discussed by comparing the result of the method with the MCS solution using the deterministic FEM for the same mesh size.

In this case, the coefficient (α_i, β_i) of each node in area A of Fig.3.18(b) is defined based on changing mesh automatically when the radius of weld toe changes with length l in Fig.3.18(a). And in area B and area C, the coefficient (α_i, β_i) of each node can be defined based on an idea in which the each node in area B or area C can move automatically when the each node in area A is moved. In area D, we define the coefficient (α_i, β_i) of each node as $(0, 0)$ because it is considered that the each node in area D is not moved.



(a) Model



(b) Mesh

Fig.3.18: The Cruciform Weld Joint

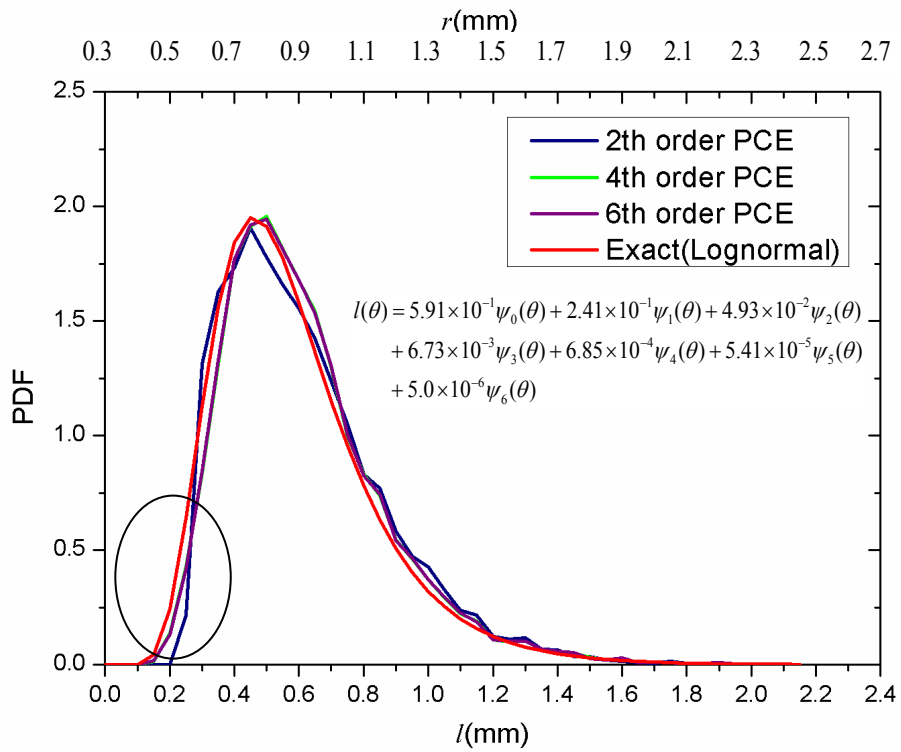


Fig.3.19: Approximation of Probability Distribution

Fig.3.19 shows the probability density distribution (Exact) of the deviation length (l) and the probability density distribution obtained through polynomial approximation

$$(l(\theta) = \sum_{i=0}^n l_i \psi_i(\theta)) \text{ when the } n \text{ are } 2, 4, 6 \text{ respectively.}$$

As shown in the Fig.3.19, we can find that the result by the approximation of PCE of low order ($n = 2$) has a large deviation from the exact distribution and the distribution in the vicinity of the lower limit of the left end. Thus, we will use the approximation of PCE of 6th order for analysis.

Fig.3.20 shows the stochastic response surface of the stress at point A and the reference values obtained by used FEM. Here, the order (p) of the approximation of PCE of $1/|\mathbf{J}'(\xi, \eta; \theta)|$ is assumed as 2, 4, 6, and we can find that a good agreement is observed between the results from the reference values and the stochastic response surface when the order (p) of the approximation of PCE is 6. And Fig.3.20 also shows the stochastic response surface which is obtained through the approximation of input parameter (the deviation length (l)) of low order ($n=2$) and the approximation of $1/|\mathbf{J}'(\xi, \eta; \theta)|$ of 6th order ($p=6$). We can understand that the response surface has bad estimation accuracy when the order of approximation of $1/|\mathbf{J}'(\xi, \eta; \theta)|$ is 6th but the order of approximation of the deviation length (l) is 2nd.

From the above, it is very important that appropriately define the order (p) of approximation of $1/|\mathbf{J}'(\xi, \eta; \theta)|$ and the order (n) of approximation of the input random parameter (l) should be decided appropriately when considering uncertainty in shape following non-normal distribution.

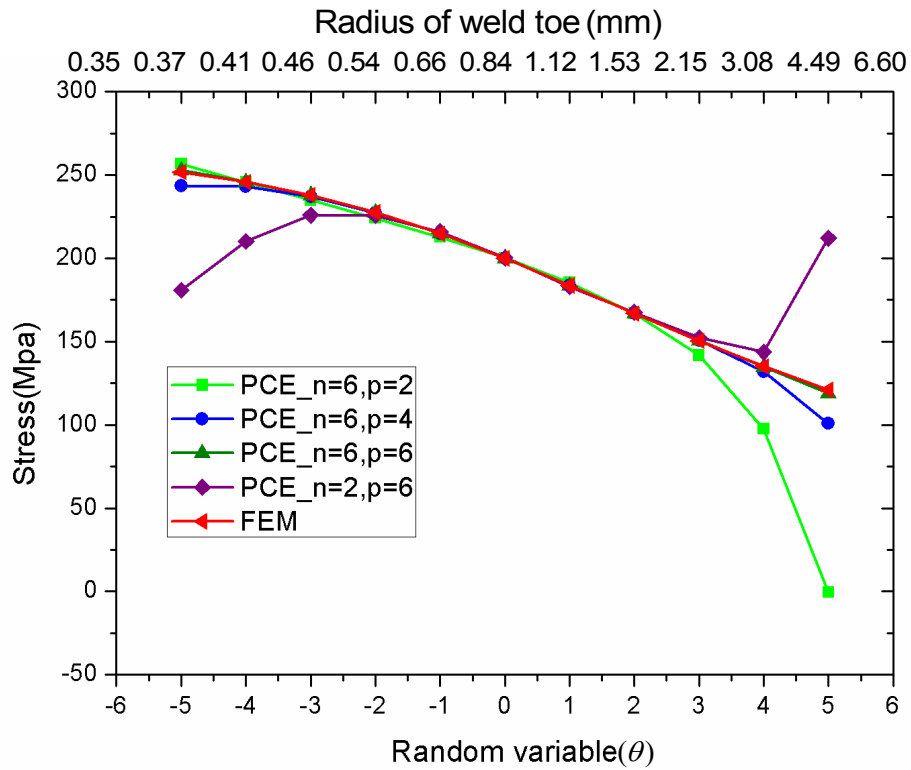


Fig. 3.20: The Response Surface of Stress for Different Degree

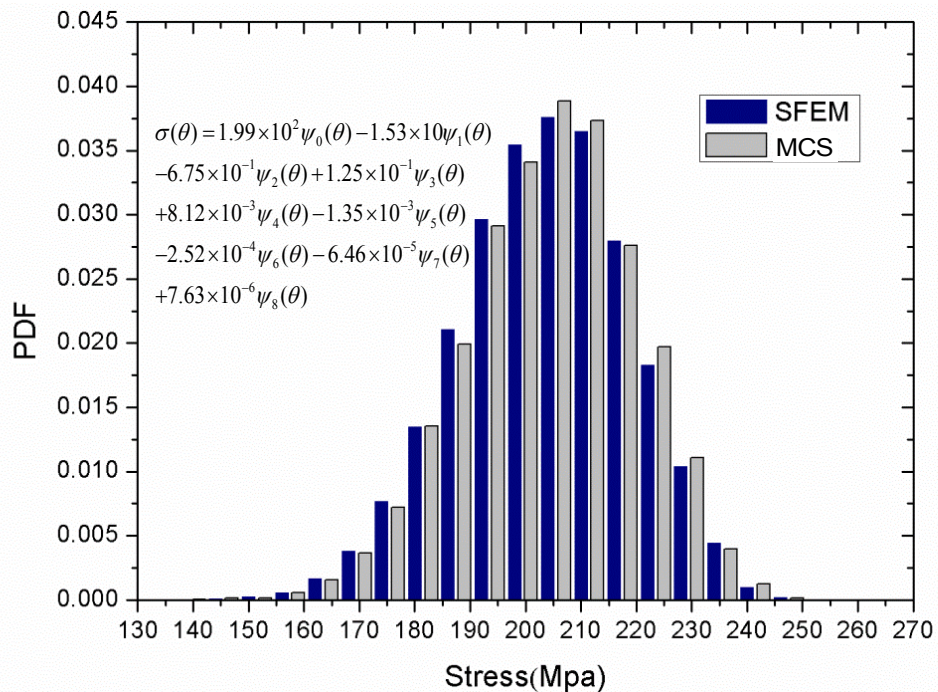


Fig.3.21: Stochastic Responses to Shape Uncertainty

Table 3.5 Statistics of the Stress

	SFEM	FEM(MCS)	SFEM_PCE
Mean	199.1278	198.9900	199.3325
Std.dev.	15.3262	15.2963	15.3235

Fig.3.21 shows the probability density distributions of the stress concentration factor obtained through the SFEM which has been obtained by using 10000 realization of the standard random variable θ in the obtained response surface of the stress concentration factor by the proposed SFEM and FEM(MCS).

Also, it is observed that the probability distribution obtained by the SFEM has good agreement with the result of MCS with the conventional FEM in which the MCS obtained by using 5000 realization. As shown in the Table 3.5, we find that the mean and standard deviation of stress are reasonably well estimated by the proposed SFEM when compared with those obtained from FEM.

The results in this section provide a possibility for uncertainty estimation of the response using the proposed methodology when the input parameter is considered as non-normal distribution. And we also can find that the stress can be reduced when the radius of weld toe becomes larger, such that when the radius of weld toe is increased from 0.54mm to 1.85mm, the stress is reduced from 186.71Mpa to 140.81Mpa.

3.2.6 Conclusions

In this section, the stochastic finite element method (SFEM) based on response surface methodology considering uncertainty in shape is formulated by an Hermite PCE, in which the uncertainty in shape is following normal distribution. And by the proposed method, the probabilistic characteristics (the response surface of stress and the probability distribution of the response) can be accurately estimated.

In the proposed algorithm, it is possible that the order of approximate of uncertainty of shape is given as an input parameter. And highly accurate analysis result can be obtained by defining appropriate the order of approximate.

We developed SFEM program by using C language which can deal with a two-dimensional problem considering uncertainty in shape with a higher order of approximate (non-normal distribution). And the validity and feasibility of the proposed method is demonstrated by two cases in which the uncertainty in shape exists in the size of circular hole, and in the radius of weld joint.

In the example of the uncertainty in the size of circular hole, the section 3.1.3(i) discussed a case for the uncertainty in the size following normal distribution. The negative size of the radius is occurred because the lower limit value does not exist in the normal distribution. Thus correct analysis results cannot be obtained when the standard deviation becomes larger. In this study, we can see that negative size of the shape can be avoided because the non-normal distribution has a lower limit value. So, it is considered that the developed method can be applied to more practical problem.

In the proposed SFEM, the degree of freedom is increased $D \times (2n+p+1)$ times compared to the deterministic finite element method. So it is considered that the computational cost becomes higher by increase of random variables or increase of order of approximate expression.

In this study, we can find that computational time is reduced by using proposed SFEM compared with MCS. However, we also find that the computational time is increased significantly when the degree of freedom is increased. In formulation, we can understand that the obtained stiffness matrix for the degree of freedom $D \times (2n+p+1)$ is not a band matrix. Thus solving Eq.(3.67) takes a lot of time by using Gaussian elimination. It is considered that Gaussian elimination is not good solution for this matrix. As a future work, an efficient numerical analyzing technique will be discussed to realize quick solving this matrix (reduction of computational time).

3.3 Evaluation of Accuracy of the Analysis Method

In this section, we will discuss the accuracy of the proposed analysis method by an example for the uncertainty in the size of circular hole which is same as the problem in section 3.1.3(1).

First, we investigate the effect of nodal point movement method of mesh on accuracy of the analysis method because the mesh is moved when the shape is changed. Here the nodal movement methods of two cases are discussed in the following.

Case(1):

As show in Fig.3.22, it is assumed that when the nodal point 1(representative node) and the points on the circle of the hole moves length l in the direction of the radius, the all nodal points from the nodal point 2 will be moved by a linear relationship. For example, the nodal point 2 is moved with length $5l/6$, the nodal point 3 is moved with length $4l/6$. Thus, the coefficient (α_i, β_i) of all nodes can be defined in this way.

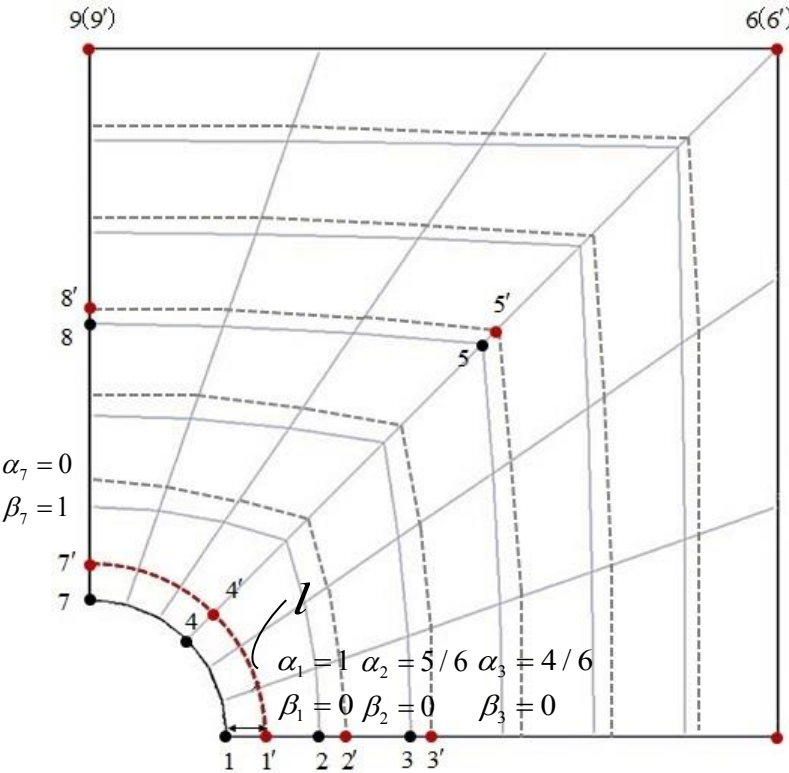


Fig.3.22 Mesh for Case1

Case(2):

As show in Fig.3.23, it is assumed that the nodal point 1(representative node), the points on the circle of the hole moves length l and adjacent nodal points (including the point 2) have a same movement length l in the direction of the radius, and the all nodal points around these nodes will be moved by a linear relationship. For example, the nodal point 2 is moved with length l , the nodal point 3 is moved with length $4l/5$. The coefficient (α_i, β_i) of all nodes can be defined by this way.

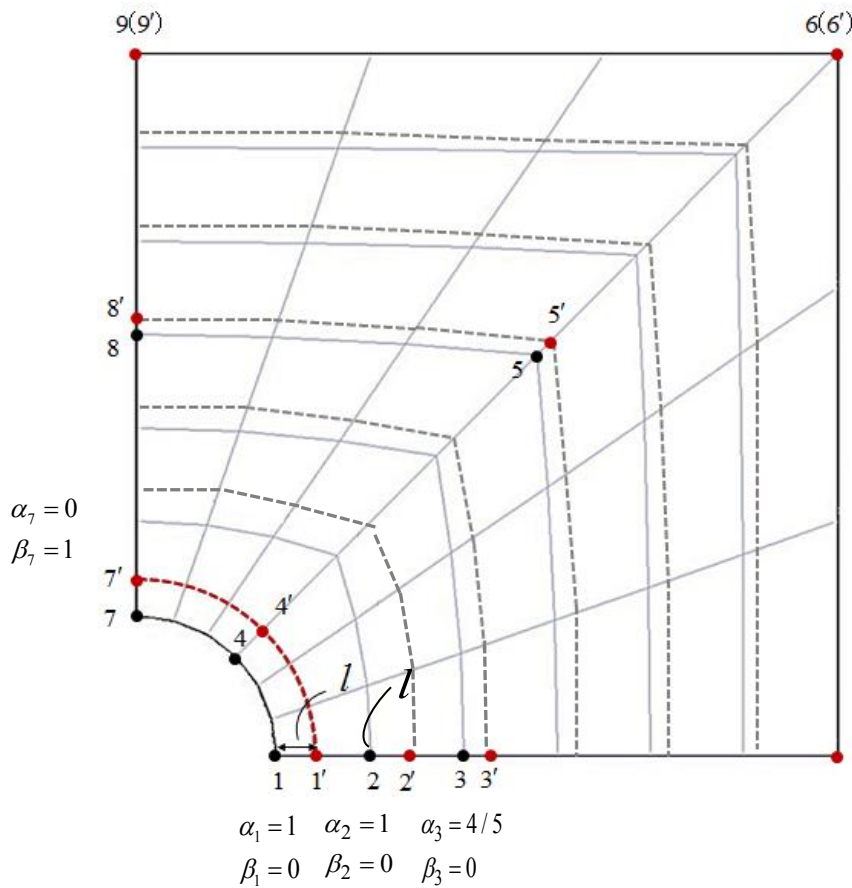


Fig.3.23 Mesh for Case2

Table3.6 shows the analysis results of stress concentration factor of the two cases at a particular node (point A in Fig.3.3(a)) when the radius of circular hole is considered as $\mu-2\sigma$, μ , $\mu+2\sigma$ ($\mu=3\text{mm}$, $\sigma=0.5\text{mm}$ by referencing section 3.1.3(1)). And we also show results of stress variability which is the difference between the analysis result when the radius is μ

and that when the radius is $\mu-2\sigma$ or radius is $\mu+2\sigma$ in Table3.7. Here, we consider these results as indices representing the variation of responses when the radius varies from the mean.

Table 3.6 Analysis Result for Three Radiuses (in Point A [MPa])

	Radius	Theoretical value	Case 1	Error (%)	Case 2	Error (%)
$\mu-2\sigma$	2mm	239.51	240.40	0.37	239.51	0
μ	3mm	243.36	243.54	0.07	243.41	0.02
$\mu+2\sigma$	4mm	249	248.03	0.39	248.77	0.09

Table 3.7 Result for stress variability [MPa]

Variability	Theoretical value	Case 1	Case 2
-2σ	3.85	3.14	3.9
2σ	5.64	5.25	5.36

As show in Table 3.6, when this radius is μ (3mm), the error is 0.07% compared to theoretical value. And when the radius is $\mu-2\sigma$ (2mm) or $\mu+2\sigma$ (4mm), the errors is 0.37% and 0.39% respectively. We can consider that the case 1 has an appropriate result by these small error values. However, we can see that the errors for the radius of 2mm or 4mm become large compared to the error for radius of 3mm.

And by the results for stress variability in Table 3.7, we can find that result for stress variability has a difference from the theoretical value especially in case 1 especially when the radius of circular hole is smaller than the mean value.

However, the case 2 has a small error by Table 3.6 in which error are 0%, 0.02% and 0.09% respectively when the radiuses are $\mu-2\sigma$, μ , $\mu+2\sigma$. And Table 3.7 also shows the case 2 has a small variability compared to case 1.

In order to investigate the cause of this error, the meshes near circular hole of case 1 and case 2 are compared when the radius is $\mu-2\sigma$ (2mm); that is, the meshes near the stress concentration part is compared for the two different nodal point movement method, and the meshes are shown in Fig.3.24 and Fig.3.25.

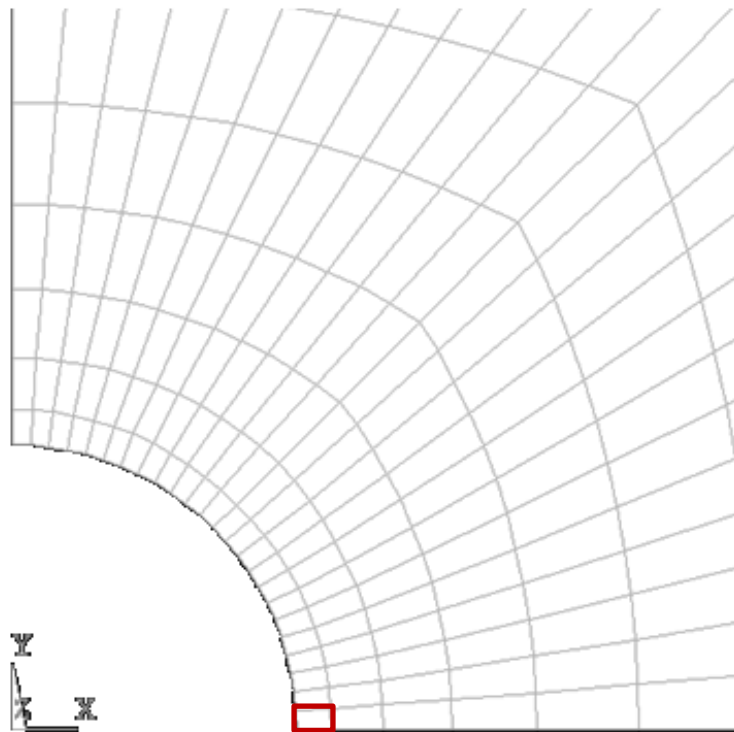


Fig.3.24: Mesh near Circular Hole for Case1

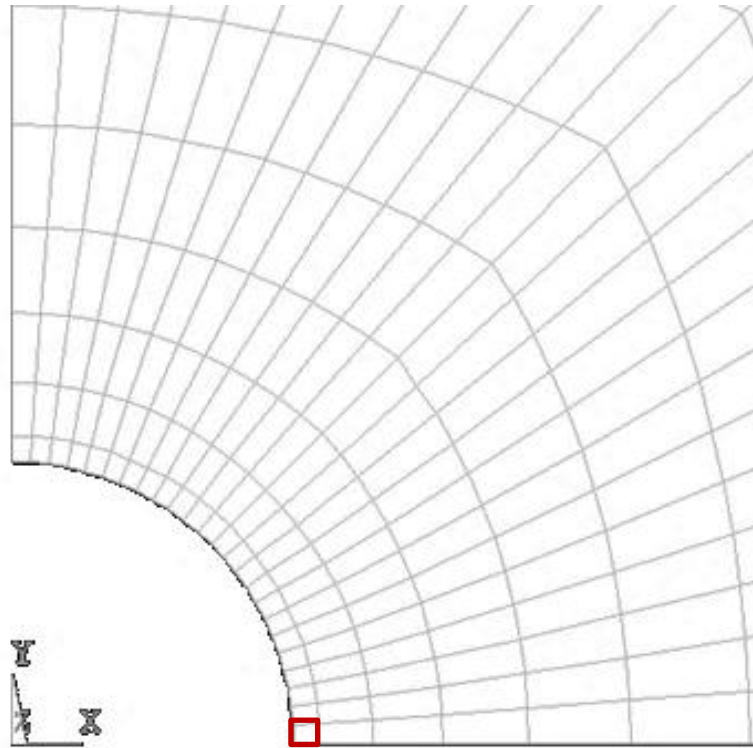


Fig.3.25: Mesh near Circular Hole for Case2

In Fig.3.24, it is understood that the mesh near the circular hole is distorted as the radius becomes small because node 1 and node 2 have different movement length. Especially, the elements with high aspect ratio is observed (red box in Fig.3.24) around the circular hole. That is, it is considered that the calculation accuracy will be influenced to some extent if the mesh for the elements around the circular hole produces distortion when the shape is changed. However, by the nodal point movement methods of case 2, we can see the mesh for the elements around the circular hole (Fig.3.25) has a good shape compared to case 1 when the radius is $\mu-2\sigma$.

As described above, by using the nodal point movement method of case 2, the elements of the stress concentration part (elements of the red box) can maintain a lower aspect ratio (close a square) compared to case 1. That is, in the case 2, the mesh of a good shape is kept in the large stress gradient direction. Thus, we can understand that the error is reduced due to the influence of the mesh movement when the nodal point movement method is proper

defined. It is concluded that we can obtain accurate results by the proposed methods.

4. Stochastic eigenvalue Problem

Eigenvalue analysis is an important problem in a variety of fields. In structural mechanics in the field of naval architecture and ocean engineering, eigenvalue problems commonly appear in the context of, e.g. vibrations and buckling. In eigenvalue analysis, the physical characteristics are not deterministic, such as mass, geometries, stiffness in the structures. Such uncertainties may cause serious problems because the influence of the uncertainties is in general unknown. The proposed method makes use of an Hermite polynomial chaos expansion (PCE) (response surface method) to represent the inherent uncertainty and the response (eigenvalues and eigenvectors) uncertainty, and involves a mathematical formulation which is a natural extension of the deterministic eigenvalue problem to the space of random variables. In order to solve the stochastic eigenvalue problem, some researchers have tried to propose some methods (see chapter 1.1.3(2))[28-29]. However, we found that these methods sometimes cannot give good results. Thus, in this chapter we have proposed two methods. Firstly, the improved stochastic inverse power method (I-SIPM) is proposed. The method is different with previous stochastic inverse power method. The minimum eigenvalue and eigenvector of stochastic eigenvalue problems can be evaluated by using the proposed method. Secondly, the stochastic Wielandt deflation method (SWDM) is proposed which can realize to evaluate $i^{\text{th}}(i>1)$ eigenvalues and eigenvectors of stochastic eigenvalue problems. This is very important for solving natural mode and buckling mode analysis problem. Next, three example problems are investigated to show the validity of two new methods compared with a Monte-Carlo simulation, i.e. the vibration problem of a discrete 2-DOF system, the buckling problem of a continuous beam with uncertainty in section dimension and the buckling problem with uncertainty in Young's Modulus. Finally, the uncertainty estimation for the dynamic damper problem is discussed by using proposed method. The probability of resonance occurrence is shown when the dynamic damper has a stochastic mass and stiffness.

4.1 Statement of the Stochastic Eigenvalue Problem

The generalized eigenvalue problem can be written as follows.

$$\mathbf{K}\mathbf{u} = \lambda\mathbf{R}\mathbf{u}, \quad (4.1)$$

where \mathbf{K} is a stiffness matrix with dimension N . \mathbf{R} is mass matrix in vibrations analysis or it is initial stress matrix in buckling analysis with dimension N . The generalized eigenvalue problem may be converted to a standard eigenvalue problem.

$$\mathbf{A}\mathbf{u} = \lambda\mathbf{u}, \quad (4.2)$$

where \mathbf{A} is $\mathbf{R}^{-1}\mathbf{K}$, Note that \mathbf{R} is regular (nonsingular) matrix in general vibration and buckling problems. The objective of solving the deterministic eigenvalue problem is to find a scalar eigenvalue (λ) and the corresponding eigenvector (\mathbf{u}) by using the deterministic eigenvalue equation (Eq. (4.2)).

For systems with uncertain parameters, the equation switches to the stochastic standard eigenvalue problem given as follows.

$$\mathbf{A}'(\boldsymbol{\theta})\mathbf{u}'(\boldsymbol{\theta}) = \lambda'(\boldsymbol{\theta})\mathbf{u}'(\boldsymbol{\theta}), \quad (4.3)$$

where ' is used to indicate involving random variables ($\boldsymbol{\theta}$). $\mathbf{A}'(\boldsymbol{\theta}) = \mathbf{R}'^{-1}(\boldsymbol{\theta})\mathbf{K}'(\boldsymbol{\theta})$, $\mathbf{K}'(\boldsymbol{\theta})$ is a stiffness matrix involving random variables ($\boldsymbol{\theta}$), and $\mathbf{R}'(\boldsymbol{\theta})$ is a mass matrix involving random variables ($\boldsymbol{\theta}$) in vibrations analysis or it is initial stress matrix involving random variables ($\boldsymbol{\theta}$) in buckling analysis. Thus the stiffness matrix $\mathbf{K}'(\boldsymbol{\theta})$ and matrix $\mathbf{R}'(\boldsymbol{\theta})$ are considered as a stochastic matrix. The stochastic stiffness matrix $\mathbf{K}'(\boldsymbol{\theta})$ can be represented by using limited PCE with $n_1 + 1$ terms of basis functions.

$$\mathbf{K}'(\boldsymbol{\theta}) = \sum_{i=0}^{n_1} \mathbf{K}'_i \Psi_i(\boldsymbol{\theta}). \quad (4.4)$$

When the uncertain physical characteristics are considered in mass or initial stress matrix, the stochastic matrix $\mathbf{R}'(\boldsymbol{\theta})$ also can be represented by using PCE with $n_2 + 1$ terms of basis functions.

$$\mathbf{R}'(\boldsymbol{\theta}) = \sum_{i=0}^{n_2} \mathbf{R}'_i \Psi_i(\boldsymbol{\theta}). \quad (4.5)$$

Thus, $\mathbf{A}'(\boldsymbol{\theta})$ can be represented as follows.

$$\mathbf{A}'(\boldsymbol{\theta}) = \sum_{i=0}^{n_3} \mathbf{A}'_i \Psi_i(\boldsymbol{\theta}), \quad (4.6)$$

where n_3 is the order of expansion terms by the sum of the approximate order of $\mathbf{R}'^{-1}(\boldsymbol{\theta})$ and $n_1 + n_2$. See Appendix 1 and Appendix 2 for derivation of the coefficients (\mathbf{A}'_i). The coefficient matrix $\mathbf{A}'(\boldsymbol{\theta})$ is considered as stochastic by Eq.(4.6), thus the eigenvalues λ and eigenvectors \mathbf{u} also become functions of the random variables such as $\lambda'(\boldsymbol{\theta})$ and $\mathbf{u}'(\boldsymbol{\theta})$. Accordingly, the stochastic eigenvalues response and eigenvectors response can be approximated by using PCE with n terms of basis functions.

$$\lambda'(\boldsymbol{\theta}) = \sum_{i=0}^n \lambda'_i \Psi_i(\boldsymbol{\theta}), \quad (4.7)$$

$$\mathbf{u}'(\boldsymbol{\theta}) = \sum_{i=0}^n \mathbf{u}'_i \Psi_i(\boldsymbol{\theta}). \quad (4.8)$$

The purpose of the stochastic eigenvalue problem is to derive unknown PCE coefficients ($\lambda'_i, \mathbf{u}'_i$) of eigenvalues and eigenvectors. Substituting Eq. (4.6), Eq. (4.7) and Eq. (4.8) into Eq. (4.3), the stochastic generalized eigenvalue equation becomes as follows.

$$\sum_{i=0}^{n_3} \mathbf{A}'_i \Psi_i(\boldsymbol{\theta}) \left(\sum_{i=0}^n \mathbf{u}'_i \Psi_i(\boldsymbol{\theta}) \right) = \sum_{i=0}^n \lambda'_i \Psi_i(\boldsymbol{\theta}) \left(\sum_{i=0}^n \mathbf{u}'_i \Psi_i(\boldsymbol{\theta}) \right), \quad (4.9)$$

where the coefficient matrix $\mathbf{A}'(\boldsymbol{\theta})$ is approximated by n_3^{th} order polynomial as shown in

Eq. (4.9) . Thus, in this study, the order (n) of PCE approximation of Eq. (4.7)(4.8) is assumed as n_3 .

Multiplying both sides of Eq. (4.9) by $\Psi_t(\boldsymbol{\theta})W(\boldsymbol{\theta})$, integrating the equation over the stochastic domain ($\int_D (\text{Eq.}(4.9))\Psi_t(\boldsymbol{\theta})W(\boldsymbol{\theta})d\boldsymbol{\theta} = \langle (\text{Eq.}(4.9))\Psi_t(\boldsymbol{\theta}) \rangle$), we have following equation.

$$\sum_{i=0}^{n_3} \sum_{j=0}^{n_3} \mathbf{A}'_i \mathbf{u}'_j \langle \Psi_i(\boldsymbol{\theta}) \Psi_j(\boldsymbol{\theta}) \Psi_t(\boldsymbol{\theta}) \rangle = \sum_{i=0}^{n_3} \sum_{j=0}^{n_3} \lambda'_i \mathbf{u}'_j \langle \Psi_i(\boldsymbol{\theta}) \Psi_j(\boldsymbol{\theta}) \Psi_t(\boldsymbol{\theta}) \rangle. \quad (4.10)$$

Thus the stochastic generalized eigenvalue equation when the $t=0, \dots, n_3$ can be derived as follows.

$$\begin{bmatrix} \mathbf{A}''_{00} & \cdots & \mathbf{A}''_{0n_3} \\ \vdots & \ddots & \vdots \\ \mathbf{A}''_{n_3 0} & \cdots & \mathbf{A}''_{n_3 n_3} \end{bmatrix} \begin{bmatrix} \mathbf{u}'_0 \\ \vdots \\ \mathbf{u}'_{n_3} \end{bmatrix} = \sum_{i=0}^{n_3} \lambda'_i \begin{bmatrix} c_{i00} \mathbf{I} & \cdots & c_{i0n_3} \mathbf{I} \\ \vdots & \ddots & \vdots \\ c_{in_3 0} \mathbf{I} & \cdots & c_{in_3 n_3} \mathbf{I} \end{bmatrix} \begin{bmatrix} \mathbf{u}'_0 \\ \vdots \\ \mathbf{u}'_{n_3} \end{bmatrix}, \quad (4.11)$$

where, $\mathbf{A}''_{ij} = \sum_{i=0}^{n_3} \mathbf{A}'_i \langle \Psi_i(\boldsymbol{\theta}) \Psi_j(\boldsymbol{\theta}) \Psi_t(\boldsymbol{\theta}) \rangle$, $c_{ij} = \langle \Psi_i(\boldsymbol{\theta}) \Psi_j(\boldsymbol{\theta}) \Psi_t(\boldsymbol{\theta}) \rangle$.

By Eq.(4.11), we can find that it is difficult to be solved by the conventional method of eigenvalue analysis.

In order to solve the stochastic eigenvalue problem, the Monte Carlo simulation (MCS) is usually used. The stochastic results are obtained by the solution of Eq.(4.1) (deterministic eigenvalue problem) again and again for many times. However, MCS needs heavy and a large number of calculations, and the application of MCS to practical problems is sometimes very difficult to get reasonable results. So, it is desirable to solve stochastic eigenvalues (λ'_i) and eigenvectors (\mathbf{u}'_i) directly from Eq.(4.10) or (4.11). However, at present, there is no algorithm available to solve Eq.(4.10) or (4.11) directly. As a numerical algorithm to solve deterministic eigenvalue problems, the inverse power method is developed to compute minimum eigenvalue and eigenvector [37]. The algorithm is early

used for evaluating stochastic eigenvalue problems in Verhoosel et al. [28] by which satisfactory results sometimes cannot be obtained in the authors' experience.

In the following section, we improve the algorithm and develop the improved stochastic inverse power method formularization.

4.2 The Formularization of I-SIPM for Solution of the Stochastic Eigenvalue Problem

In study by Verhoosel et al. [28], the stochastic inverse power method (SIPM) algorithm is proposed. However the correct eigenvalue and eigenvector cannot be obtained when we use the algorithm to solve a simple stochastic eigenvalue problem. Here, we improved *step3* of the method in reference 28, and the improved stochastic inverse power method (I-SIPM) is proposed to obtain a correct eigenvalue and eigenvector. In this section, I-SIPM algorithm is elaborated and the formularization is provided.

(i). The formularization for Step1

As shown in Algorithm, the Rayleigh quotient is used to update the stochastic eigenvalue based on the normalized stochastic eigenvector $\mathbf{u}^{(q)}$ of the previous iteration.

$$\lambda^{(q+1)} = \left(\mathbf{u}^{(q)}\right)^T \mathbf{A}' \mathbf{u}^{(q)}. \quad (4.12)$$

Substituting Eq. (4.7), Eq. (4.8) into Eq. (4.12) the equation becomes as follows.

$$\begin{aligned} & \sum_{i=0}^n \lambda_i^{(q+1)} \Psi_i(\boldsymbol{\theta}) \\ &= \left(\sum_{i=0}^n \mathbf{u}_i^{(q)} \Psi_i(\boldsymbol{\theta}) \right)^T \left(\sum_{i=0}^n \mathbf{A}'_i \Psi_i(\boldsymbol{\theta}) \right) \left(\sum_{i=0}^n \mathbf{u}_i^{(q)} \Psi_i(\boldsymbol{\theta}) \right). \end{aligned} \quad (4.13)$$

Multiplying both sides of Eq. (4.13) by $\Psi_t(\boldsymbol{\theta}) \mathcal{W}(\boldsymbol{\theta})$, integrating the equation, we have following equation.

$$\begin{aligned} & \sum_{i=0}^n \lambda_i^{(q+1)} \langle \Psi_i(\boldsymbol{\theta}) \Psi_t(\boldsymbol{\theta}) \rangle \\ &= \sum_{i=0}^n \sum_{j=0}^n \sum_{k=0}^n \mathbf{u}_i^{T(q)} \mathbf{A}'_k \mathbf{u}_j^{(q)} \langle \Psi_i(\boldsymbol{\theta}) \Psi_j(\boldsymbol{\theta}) \Psi_k(\boldsymbol{\theta}) \Psi_t(\boldsymbol{\theta}) \rangle. \end{aligned} \quad (4.14)$$

Then the update equation of the eigenvalue can be shown as follows.

$$\begin{aligned} & \lambda_t^{(q+1)} \\ &= \frac{1}{\langle \Psi_t^2(\boldsymbol{\theta}) \rangle} \sum_{i=0}^n \sum_{j=0}^n \sum_{k=0}^n \mathbf{u}_i^{\prime T(q)} \mathbf{A}_k^{\prime(q+1)} \mathbf{u}_j^{\prime(q)} \langle \Psi_i(\boldsymbol{\theta}) \Psi_j(\boldsymbol{\theta}) \Psi_k(\boldsymbol{\theta}) \Psi_t(\boldsymbol{\theta}) \rangle. \end{aligned} \quad (4.15)$$

The deterministic part ($\lambda_0^{(q+1)}$) of the eigenvalue is calculated when $t=0$, and the stochastic parts ($\lambda_t^{(q+1)}$) of the eigenvalue can be calculated when $t=1, \dots, n$.

(ii). The formularization for Step2

The stochastic eigenvector is updated by solving the below equation.

$$\mathbf{A}' \mathbf{u}^{\prime(q+1)} = \lambda^{\prime(q+1)} \mathbf{u}^{\prime(q)}. \quad (4.16)$$

Substituting Eq. (4.7), Eq. (4.8) into Eq. (4.16) the equation becomes as follows.

$$\left(\sum_{i=0}^n \mathbf{A}'_i \Psi_i(\boldsymbol{\theta}) \right) \left(\sum_{i=0}^n \mathbf{u}_i^{\prime(q+1)} \Psi_i(\boldsymbol{\theta}) \right) = \left(\sum_{i=0}^n \lambda_i^{\prime(q+1)} \Psi_i(\boldsymbol{\theta}) \right) \left(\sum_{i=0}^n \mathbf{u}_i^{\prime(q)} \Psi_i(\boldsymbol{\theta}) \right). \quad (4.17)$$

Multiplying both sides of Eq. (4.17) by $\Psi_t(\boldsymbol{\theta}) W(\boldsymbol{\theta})$, integrating the equation, we can obtain the following equation.

$$\begin{aligned} & \sum_{i=0}^n \sum_{j=0}^n \mathbf{A}'_i \mathbf{u}_j^{\prime(q+1)} \langle \Psi_i(\boldsymbol{\theta}) \Psi_j(\boldsymbol{\theta}) \Psi_t(\boldsymbol{\theta}) \rangle \\ &= \sum_{i=0}^n \sum_{j=0}^n \lambda_i^{\prime(q+1)} \mathbf{u}_i^{\prime(q)} \langle \Psi_i(\boldsymbol{\theta}) \Psi_j(\boldsymbol{\theta}) \Psi_t(\boldsymbol{\theta}) \rangle. \end{aligned} \quad (4.18)$$

Thus when the $t=0, \dots, n$, the update stochastic eigenvector equation can be derived as follows.

$$\begin{bmatrix} \boldsymbol{\Omega}_{00} & \cdots & \boldsymbol{\Omega}_{0n} \\ \vdots & \ddots & \vdots \\ \boldsymbol{\Omega}_{n0} & \cdots & \boldsymbol{\Omega}_{nn} \end{bmatrix} \begin{bmatrix} \mathbf{u}_0^{\prime(q+1)} \\ \vdots \\ \mathbf{u}_n^{\prime(q+1)} \end{bmatrix} = \begin{bmatrix} \zeta_0 \\ \vdots \\ \zeta_n \end{bmatrix}, \quad (4.19)$$

where $\mathbf{\Omega}_{ii}$ and ζ_t can be shown as follow.

$$\mathbf{\Omega}_{ii} = \sum_{j=0}^n \mathbf{A}'_j \langle \Psi_i(\boldsymbol{\theta}) \Psi_j(\boldsymbol{\theta}) \Psi_t(\boldsymbol{\theta}) \rangle, \quad (4.20)$$

$$\zeta_t = \sum_{i=0}^n \sum_{j=0}^n \lambda_i^{r(q+1)} \mathbf{u}'_i^{(q)} \langle \Psi_i(\boldsymbol{\theta}) \Psi_j(\boldsymbol{\theta}) \Psi_t(\boldsymbol{\theta}) \rangle. \quad (4.21)$$

The stochastic eigenvector can be updated by solving the derived Eq. (4.19). We can update stochastic eigenvector $\mathbf{u}'^{(q)}(\boldsymbol{\theta})$ using Eq.(4.8) when the coefficients $(\mathbf{u}'_0^{(q)}, \dots, \mathbf{u}'_n^{(q)})$ of stochastic eigenvector is calculated. But derived stochastic eigenvector $\mathbf{u}'^{(q)}$ is not normalized and the length of eigenvector could change when the value of random variables $\boldsymbol{\theta}$ are changed.

(iii). The formularization for Step3

In this section, the improved normalization method is formularized in *step3*, which is different with the previous stochastic inverse power method [28] and is indispensable to achieve solving stochastic eigenvalue problems. The stochastic eigenvector is normalized by using the below equation.

$$\mathbf{u}'^{(q+1)} \rightarrow \frac{\mathbf{u}'^{(q+1)}}{\|\mathbf{u}'^{(q+1)}\|_{L^2_s}}. \quad (4.22)$$

Substituting Eq. (4.8) into Eq. (4.22) the equation becomes as follows.

$$\begin{aligned} \mathbf{u}'^{(q+1)} &\rightarrow \frac{\mathbf{u}'^{(q+1)}}{\|\mathbf{u}'^{(q+1)}\|_{L^2_s}} \\ &= \frac{\sum_{i=0}^n \mathbf{u}'_i^{(q+1)} \Psi_i(\boldsymbol{\theta})}{\sqrt{\sum_{i=0}^n \sum_{j=0}^n (\mathbf{u}'_i^{(q+1)})^T \mathbf{u}'_j^{(q+1)} \Psi_i(\boldsymbol{\theta}) \Psi_j(\boldsymbol{\theta})}}, \end{aligned} \quad (4.23)$$

It can be seen that the denominator of Eq. (4.23) involves random variables $\boldsymbol{\theta}$. Though the coefficient vector, $\mathbf{u}_i^{(q)}$, should be decided for the next iteration based on the normalization equation, it is not possible to solve the above equation directly. Thus, to overcome this problem, the solution is elaborated as follows.

Firstly, we arrange Eq. (4.24) as follows.

$$\mathbf{u}^{(q+1)} \rightarrow \frac{\mathbf{u}^{(q+1)}}{\|\mathbf{u}^{(q+1)}\|_{L_3^2}} = \frac{\sum_{i=0}^n \mathbf{u}_i^{(q+1)} \Psi_i(\boldsymbol{\theta})}{\sqrt{\sum_{i=0}^{2n} U_i^{(q+1)} \Psi_i(\boldsymbol{\theta})}}, \quad (4.24)$$

where $U_i^{(q+1)} = (\mathbf{u}_i^{(q+1)})^T \mathbf{u}_j^{(q+1)}$ and the order of expansion becomes $2n$ because two basis functions ($\Psi_i(\boldsymbol{\theta})$ and $\Psi_j(\boldsymbol{\theta})$) are multiplied (see Appendix 2).

Next, in order to overcome the problem of the denominator which involves random variables $\boldsymbol{\theta}$, it is assumed that $1/\sqrt{\sum_{i=0}^{2n} U_i^{(q+1)} \Psi_i(\boldsymbol{\theta})}$ can be approximated by Hermite PCE as follows.

$$\frac{1}{\sqrt{\sum_{i=0}^{2n} U_i^{(q+1)} \Psi_i(\boldsymbol{\theta})}} = \sum_{i=0}^{p_1} Z_i^{(q+1)} \Psi_i(\boldsymbol{\theta}), \quad (4.25)$$

where, $Z_i^{(q+1)}$ are unknown coefficients of approximated polynomial, $\Psi_i(\boldsymbol{\theta})$ are the basis functions, represented by Hermite polynomial, and p_1 is the order of approximated expansion terms. It can be seen that the unknown coefficients $Z_i^{(q+1)}$ need to be determined. Eq. (4.26) is rewritten as follows.

$$\left(\sum_{i=0}^{p_1} Z_i^{(q+1)} \Psi_i(\boldsymbol{\theta}) \right)^2 \left(\sum_{i=0}^{2n} U_i^{(q+1)} \Psi_i(\boldsymbol{\theta}) \right) = 1. \quad (4.26)$$

Multiplying $\Psi_i(\boldsymbol{\theta})W(\boldsymbol{\theta})$ to both sides of Eq. (4.26), and integrating the equation, we

have.

$$\begin{aligned} & \int_D \sum_{i=0}^{p_1} \sum_{j=0}^{p_1} \sum_{k=0}^{2n} Z_i^{(q+1)} Z_j^{(q+1)} Z_k^{(q+1)} \Psi_i(\boldsymbol{\theta}) \Psi_j(\boldsymbol{\theta}) \Psi_k(\boldsymbol{\theta}) \Psi_t(\boldsymbol{\theta}) W(\boldsymbol{\theta}) d\boldsymbol{\theta} \\ & = \int_D \Psi_t(\boldsymbol{\theta}) W(\boldsymbol{\theta}) d\boldsymbol{\theta}. \end{aligned} \quad (4.27)$$

This equation can be depicted as follows:

$$\sum_{i=0}^{p_1} \sum_{j=0}^{p_1} \sum_{k=0}^{2n} Z_i^{(q+1)} Z_j^{(q+1)} U_k^{(q+1)} \langle \Psi_i(\boldsymbol{\theta}) \Psi_j(\boldsymbol{\theta}) \Psi_k(\boldsymbol{\theta}) \Psi_t(\boldsymbol{\theta}) \rangle = \langle \Psi_t(\boldsymbol{\theta}) \rangle. \quad (4.28)$$

This means that the following nonlinear simultaneous equations about the coefficients, $Z_i^{(q+1)}$ and $Z_j^{(q+1)}$, are obtained when $t = 0, \dots, p_1$.

$$\begin{aligned} & \sum_{i=0}^{p_1} \sum_{j=0}^{p_1} \sum_{k=0}^{2n} Z_i Z_j U_k^{(q+1)} \langle \Psi_i(\boldsymbol{\theta}) \Psi_j(\boldsymbol{\theta}) \Psi_k(\boldsymbol{\theta}) \Psi_0(\boldsymbol{\theta}) \rangle = \langle \Psi_0(\boldsymbol{\theta}) \rangle, \\ & \sum_{i=0}^{p_1} \sum_{j=0}^{p_1} \sum_{k=0}^{2n} Z_i Z_j U_k^{(q+1)} \langle \Psi_i(\boldsymbol{\theta}) \Psi_j(\boldsymbol{\theta}) \Psi_k(\boldsymbol{\theta}) \Psi_1(\boldsymbol{\theta}) \rangle = \langle \Psi_1(\boldsymbol{\theta}) \rangle, \\ & \quad \vdots \\ & \sum_{i=0}^{p_1} \sum_{j=0}^{p_1} \sum_{k=0}^{2n} Z_i Z_j U_k^{(q+1)} \langle \Psi_i(\boldsymbol{\theta}) \Psi_j(\boldsymbol{\theta}) \Psi_k(\boldsymbol{\theta}) \Psi_{p_1}(\boldsymbol{\theta}) \rangle = \langle \Psi_{p_1}(\boldsymbol{\theta}) \rangle. \end{aligned} \quad (4.28)$$

Eq. (4.28) is solved by using Newton's method, and the detailed process is indicated in follows.

Firstly, the Eq. (4.28) with $\langle \Psi_0(\boldsymbol{\theta}) \rangle = 1, \langle \Psi_{i \geq 1}(\boldsymbol{\theta}) \rangle = 0$ is rewritten as follows in the form

$\mathbf{F}(\mathbf{Z}) = 0$ where \mathbf{Z} is a vector containing the set $\{Z_0, Z_1, \dots, Z_{p_1}\}$.

$$\begin{aligned}
f_1(Z_0, Z_1 \dots Z_{p_1}) &= \sum_{i=0}^{p_1} \sum_{j=0}^{p_1} \sum_{k=0}^{2n} Z_i Z_j U_k^{(q+1)} \langle \Psi_i(\boldsymbol{\theta}) \Psi_j(\boldsymbol{\theta}) \Psi_k(\boldsymbol{\theta}) \Psi_0(\boldsymbol{\theta}) \rangle - 1, \\
f_2(Z_0, Z_1 \dots Z_{p_1}) &= \sum_{i=0}^{p_1} \sum_{j=0}^{p_1} \sum_{k=0}^{2n} Z_i Z_j U_k^{(q+1)} \langle \Psi_i(\boldsymbol{\theta}) \Psi_j(\boldsymbol{\theta}) \Psi_k(\boldsymbol{\theta}) \Psi_1(\boldsymbol{\theta}) \rangle, \\
&\vdots \\
f_{p_1+1}(Z_0, Z_1 \dots Z_{p_1}) &= \sum_{i=0}^{p_1} \sum_{j=0}^{p_1} \sum_{k=0}^{2n} Z_i Z_j U_k^{(q+1)} \langle \Psi_i(\boldsymbol{\theta}) \Psi_j(\boldsymbol{\theta}) \Psi_k(\boldsymbol{\theta}) \Psi_{p_1}(\boldsymbol{\theta}) \rangle.
\end{aligned} \tag{4.29}$$

$\mathbf{Z} = \{Z_0, Z_1 \dots Z_{p_1}\}$ are obtained by using following the iterative equation.

$$\mathbf{Z}^{(q_1+1)} = \mathbf{Z}^{(q_1)} + \delta(\mathbf{Z}^{(q_1)}), \tag{4.30}$$

where q_1 is iteration number and $\delta(\mathbf{Z}^{(q_1)}) = -\mathbf{J}(\mathbf{Z}^{(q_1)})^{-1} \mathbf{F}(\mathbf{Z}^{(q_1)})$, $\mathbf{J}(\mathbf{Z}^{(q_1)})$ is depicted as follows.

$$\mathbf{J}(\mathbf{Z}^{(q_1)}) = \begin{pmatrix} \frac{\partial f_1(\mathbf{Z}^{(q_1)})}{\partial Z_0} & \dots & \frac{\partial f_1(\mathbf{Z}^{(q_1)})}{\partial Z_0} \\ \vdots & \vdots & \vdots \\ \frac{\partial f_{p_1+1}(\mathbf{Z}^{(q_1)})}{\partial Z_p} & \dots & \frac{\partial f_{p_1+1}(\mathbf{Z}^{(q_1)})}{\partial Z_p} \end{pmatrix}. \tag{4.31}$$

On the above method, the unknown coefficients of approximation polynomial, $Z_i^{(q+1)}$, can be derived. Thus Eq.(4.25) can be represented by Hermite polynomial. More details about the Newton's method can be found in reference [41].

Now, we can substitute Eq. (4.25) into Eq. (4.23) as follows.

$$\mathbf{u}^{(q+1)} \rightarrow \sum_{i=0}^n \sum_{j=0}^{p_1} \mathbf{u}_i^{(q+1)} Z_j^{(q+1)} \Psi_i(\boldsymbol{\theta}) \Psi_j(\boldsymbol{\theta}). \tag{4.32}$$

After the right hand side of Eq. (4.32) is expanded and simplified by the method in Appendix 2, the Eq. (4.32) can be represented by the basis functions, $\Psi_i(\boldsymbol{\theta})$ as shown

below.

$$\mathbf{u}^{(q+1)} \rightarrow \sum_{i=0}^{n+p_1} \mathbf{u}_i^{(q+1)} \Psi_i(\boldsymbol{\theta}). \quad (4.33)$$

As shown above, the stochastic normalized equation is derived by the polynomial of order $n + p_1$. Because the stochastic normalization equation includes the random variables $\boldsymbol{\theta}$, it is considered that the length of eigenvector should become 1 for the different value of the variables $\boldsymbol{\theta}$. This condition can be satisfied by the above proposed method which is very important to get appropriate results. In references [28] and [29], the correct eigenvalue and eigenvector sometimes cannot be obtained because the stochastic eigenvector is averagely normalized in *step3*.

(iv). The formularization for Step4

The convergence of the stochastic method is evaluated by the relative change, and the equation is shown as follows:

$$\varepsilon^{(q+1)} = \frac{|V_{\lambda}^{(q+1)} - V_{\lambda}^{(q)}|}{|V_{\lambda}^{(q+1)}|}, \quad (4.33)$$

where, the $V_{\lambda}^{(q)}$ is the coefficient of variation of the eigenvalue, $V_{\lambda}^{(q)} = \sqrt{\text{Var}[\lambda]} / E[\lambda]$, where $\sqrt{\text{Var}[\lambda]}$, $E[\lambda]$ is obtained by Eq.(2.7) and Eq.(2.8), respectively. The convergence condition definition can be used as a stopping criterion because it will go to zero when the case tends to be convergent. In this improved stochastic inverse power method (I-SIPM), good convergence performance can be obtained using only this convergence criterion.

The above formularized improved stochastic inverse power method is summarized as follows (Algorithm 4.1):

Algorithm 4.1 The Improved Stochastic Inverse Power Method (I-SIPM)

Initialize: $\mathbf{u}'^{(0)}$

While $\varepsilon > \varepsilon^*$

$$\text{Step 1: } \lambda_i'^{(q+1)} = \frac{1}{\langle \Psi_t(\boldsymbol{\theta}) \Psi_t(\boldsymbol{\theta}) \rangle} \sum_{i=0}^n \sum_{j=0}^n \sum_{k=0}^n \mathbf{u}_i'^{T(q)} \mathbf{A}_k'^{(q+1)} \mathbf{u}_j'^{(q)} \langle \Psi_i(\boldsymbol{\theta}) \Psi_j(\boldsymbol{\theta}) \Psi_k(\boldsymbol{\theta}) \Psi_t(\boldsymbol{\theta}) \rangle$$

$$\text{Step 2: } \begin{bmatrix} \boldsymbol{\Omega}_{00} & \cdots & \boldsymbol{\Omega}_{0n} \\ \vdots & \ddots & \vdots \\ \boldsymbol{\Omega}_{n0} & \cdots & \boldsymbol{\Omega}_{nn} \end{bmatrix} \begin{bmatrix} \mathbf{u}_0'^{(q+1)} \\ \vdots \\ \mathbf{u}_n'^{(q+1)} \end{bmatrix} = \begin{bmatrix} \zeta_0 \\ \vdots \\ \zeta_n \end{bmatrix}$$

$$\text{Step 3: } \mathbf{u}'^{(q+1)} \rightarrow \sum_{i=0}^{n+p_1} \mathbf{u}_i'^{(q+1)} \Psi_i(\boldsymbol{\theta})$$

$$\text{Step 4: } \varepsilon^{(q+1)} = \frac{|V_{\lambda}^{(q+1)} - V_{\lambda}^{(q)}|}{|V_{\lambda}^{(q)}|}$$

End While

Result: λ'^* , \mathbf{u}'^*

The minimum eigenvalue can be calculated by using the proposed improved stochastic inverse power method (I-SIPM). Compared with the usual inverse power method, it involves not only the deterministic part ($\lambda_0'^{(q+1)}$) of eigenvalue but also involves the stochastic parts (the stochastic part of order 1 ($\lambda_1'^{(q+1)}$), the stochastic part of order 2 ($\lambda_2'^{(q+1)}$), ...). And the unknown coefficients ($\mathbf{u}_0'^{(p+1)}$, $\mathbf{u}_1'^{(p+1)}$, ...) of the stochastic eigenvector are derived by solving the updated stochastic eigenvector equation (Eq. (4.19)).

4.3 The Formularization of the Stochastic Wielandt Deflation Method

In section 4.2, the I-SIPM is proposed to evaluate minimum eigenvalue and eigenvector, which we call mode-1 eigenvalue and eigenvector as $\lambda_{(1)}$, $\mathbf{u}_{(1)}$. However, mode-2, mode-3 and other modes are often important, while these modes cannot be evaluated by the proposed I-SIPM. Thus, as the other purpose of this study, the stochastic Wielandt deflation method (SWDM) is proposed to achieve evaluating the i^{th} ($i > 1$) eigenvalues and eigenvectors of a general stochastic eigenvalue problem. In this section, we derive the SWDM formularization. The deterministic WDM is expounded in section 2.3.3(2).

(i). The formularization for Step1

In *step1*, a new stochastic matrix $\mathbf{B}'(\boldsymbol{\theta})$ can be made from the stochastic matrix $\mathbf{A}'(\boldsymbol{\theta})$ as follows.

$$\mathbf{B}'(\boldsymbol{\theta}) = \mathbf{A}'(\boldsymbol{\theta}) - \frac{1}{u'_{(1),1}(\boldsymbol{\theta})} \mathbf{u}'_{(1)}(\boldsymbol{\theta}) \mathbf{A}'_1(\boldsymbol{\theta}), \quad (4.34)$$

where the \mathbf{B}' is a matrix involving random variables ($\boldsymbol{\theta}$) because the matrix \mathbf{A}' and eigenvector $\mathbf{u}'_{(1)}$ involve random variables ($\boldsymbol{\theta}$). $\mathbf{A}'(\boldsymbol{\theta})$ and $\mathbf{u}'_{(1)}(\boldsymbol{\theta})$ is represented by matrix form (See Eq. (4.6)(4.8)).

$$\mathbf{A}'(\boldsymbol{\theta}) = \sum_{i=0}^n \begin{bmatrix} A_{11i} & \cdots & A_{1Ni} \\ \vdots & \ddots & \vdots \\ A_{N1i} & \cdots & A_{NNi} \end{bmatrix} \Psi_i(\boldsymbol{\theta}), \quad (4.35)$$

$$\mathbf{u}'_{(1)}(\boldsymbol{\theta}) = \sum_{i=0}^{n+p_1} \begin{bmatrix} u_{(1),1i} \\ \vdots \\ u_{(1),Ni} \end{bmatrix} \Psi_i(\boldsymbol{\theta}). \quad (4.36)$$

Then, $u'_{(1),1}(\boldsymbol{\theta})$ is defined as value in the first row of eigenvector $\mathbf{u}'_{(1)}(\boldsymbol{\theta})$, $\mathbf{A}'_1(\boldsymbol{\theta})$ is defined as the first row (row vector) of matrix $\mathbf{A}'(\boldsymbol{\theta})$. They are shown as follows.

$$u'_{(1),1}(\boldsymbol{\theta}) = \sum_{i=0}^{n+p_1} u_{(1),1i} \Psi_i(\boldsymbol{\theta}), \quad (4.37)$$

$$\mathbf{A}'_1(\boldsymbol{\theta}) = \left[\sum_{i=0}^n A_{11i} \Psi_i(\boldsymbol{\theta}) \quad \cdots \quad \sum_{i=0}^n A_{1Ni} \Psi_i(\boldsymbol{\theta}) \right]. \quad (4.38)$$

Substituting Eq. (4.35), Eq. (4.36), Eq. (4.37) and Eq. (4.38) into Eq. (4.34) the Eq. (4.34) becomes as follows:

$$\begin{aligned} & \mathbf{B}'(\boldsymbol{\theta}) \\ &= \sum_{i=0}^n \begin{bmatrix} A_{11i} & \cdots & A_{1Ni} \\ \vdots & \ddots & \vdots \\ A_{N1i} & \cdots & A_{NNi} \end{bmatrix} \Psi_i(\boldsymbol{\theta}) \\ & - \frac{1}{\sum_{i=0}^{n+p_1} u_{(1),li} \Psi_i(\boldsymbol{\theta})} \begin{bmatrix} \sum_{i=0}^{n+p_1} u_{(1),li} \Psi_i(\boldsymbol{\theta}) \\ \vdots \\ \sum_{i=0}^{n+p_1} u_{(1),Ni} \Psi_i(\boldsymbol{\theta}) \end{bmatrix} \left[\sum_{i=0}^n A_{11i} \Psi_i(\boldsymbol{\theta}) \quad \cdots \quad \sum_{i=0}^n A_{1Ni} \Psi_i(\boldsymbol{\theta}) \right]. \end{aligned} \quad (4.39)$$

We can find that the denominator of Eq.(4.39) involves random variables (θ). In order to solve this problem, it is assumed that $1/\sum_{i=0}^n u_{(1),li} \Psi_i(\boldsymbol{\theta})$ can be approximated by Hermite PCE as follows.

$$\frac{1}{\sum_{i=0}^n u_{(1),li} \Psi_i(\boldsymbol{\theta})} = \sum_{u=0}^{p_2} R_u \Psi_u(\boldsymbol{\theta}). \quad (4.40)$$

Again details about approximation method can be found in Appendix 1.

Now, we can substitute Eq. (4.40) into Eq. (4.39) as follows.

$$\mathbf{B}'(\boldsymbol{\theta}) = \begin{bmatrix} 0 & \cdots & 0 \\ B_{21} & \cdots & B_{2N} \\ \vdots & \ddots & \vdots \\ B_{N1} & \cdots & B_{NN} \end{bmatrix}, \quad (4.40)$$

where $B_{ts} = \sum_{i=0}^n A_{tsi} \Psi_i(\boldsymbol{\theta}) - \sum_{i=0}^{p_2} \sum_{j=0}^{n+p_1} \sum_{k=0}^n R_i u_{(1),ij} A_{tsk} \Psi_i(\boldsymbol{\theta}) \Psi_k(\boldsymbol{\theta}) \Psi_j(\boldsymbol{\theta})$. After the right hand side of Eq. (4.40) is expanded and simplified by the method of Appendix 2, the Eq. (4.41) can be derived based on the basis functions, $\Psi_i(\boldsymbol{\theta})$.

$$\mathbf{B}'(\boldsymbol{\theta}) = \sum_{i=0}^{2n+p_1+p_2} \begin{bmatrix} 0 & \cdots & 0 \\ B'_{21} & \cdots & B'_{2N} \\ \vdots & \ddots & \vdots \\ B'_{N1} & \cdots & B'_{NN} \end{bmatrix} \Psi_i(\boldsymbol{\theta}). \quad (4.41)$$

(ii). The formularization for Step2

In *step2*, we can obtain the matrix $\mathbf{B}'_{(1)}(\boldsymbol{\theta})$ with dimension $N-1$ by deleting 0 in the first row and deleting the first column. Then $\mathbf{B}'_{(1)}(\boldsymbol{\theta})$ has eigenvalues $\lambda'_{(2)}, \lambda'_{(3)}, \dots, \lambda'_{(N)}$.

$$\mathbf{B}'_{(1)}(\boldsymbol{\theta}) = \sum_{i=0}^{2n+p_1+p_2} \begin{bmatrix} B'_{22} & \cdots & B'_{2N} \\ \vdots & \ddots & \vdots \\ B'_{N2} & \cdots & B'_{NN} \end{bmatrix} \Psi_i(\boldsymbol{\theta}). \quad (4.42)$$

(iii). The formularization for Step3

The minimum eigenvalue $\lambda'_{(2)}(\boldsymbol{\theta})$ (this is, the 2nd eigenvalue in $\mathbf{A}'(\boldsymbol{\theta})$) and corresponding eigenvector $\mathbf{v}'_{(2)}(\boldsymbol{\theta})$ in the matrix $\mathbf{B}'_{(1)}(\boldsymbol{\theta})$ can be evaluated by using the improved

stochastic inverse power method (I-SIPM) in the *step3*.

$$\lambda'_{(2)}(\boldsymbol{\theta}) = \sum_{i=0}^{2n+p_1+p_2} \lambda'_{(2)i} \Psi_i(\boldsymbol{\theta}), \quad (4.43)$$

$$\mathbf{v}'_{(2)}(\boldsymbol{\theta}) = \sum_{i=0}^{2n+2p_1+p_2} \mathbf{v}'_{(2)i} \Psi_i(\boldsymbol{\theta}). \quad (4.44)$$

However we can find that the eigenvector, $\mathbf{v}'_{(2)}(\boldsymbol{\theta})$, is a vector with dimension $N-1$. In next step, the vector with dimension $N-1$ will be transformed as a vector with dimension N which is the 2nd eigenvector in the matrix $\mathbf{A}'(\boldsymbol{\theta})$.

(iv). The formularization for Step4

In *step4*, Eq. (4.45) is used to obtain the eigenvector $\mathbf{u}'_{(2)}(\boldsymbol{\theta})$ of the matrix $\mathbf{A}'(\boldsymbol{\theta})$ as follows.

$$\mathbf{u}'_{(2)}(\boldsymbol{\theta}) = \frac{1}{u'_{(1),1}(\boldsymbol{\theta})} \mathbf{u}'_{(1)}(\boldsymbol{\theta}) - \frac{\lambda'_{(1)}(\boldsymbol{\theta}) - \lambda'_{(2)}(\boldsymbol{\theta})}{\mathbf{A}_{1,1} \overline{\mathbf{v}'_{(2)}(\boldsymbol{\theta})}} \overline{\mathbf{v}'_{(2)}(\boldsymbol{\theta})}, \quad (4.45)$$

where $\lambda'_{(1)}(\boldsymbol{\theta})$ is minimum eigenvalue and $\mathbf{u}'_{(1)}(\boldsymbol{\theta})$ is corresponding eigenvector in the matrix $\mathbf{A}'(\boldsymbol{\theta})$ obtained by the I-SIPM shown section 4.1. $\overline{\mathbf{v}'_{(2)}(\boldsymbol{\theta})}$ is defined as follows.

$$\overline{\mathbf{v}'_{(2)}(\boldsymbol{\theta})} = \frac{1}{v'_{(2),1}(\boldsymbol{\theta})} \begin{pmatrix} 0 \\ \mathbf{v}'_{(2)}(\boldsymbol{\theta}) \end{pmatrix}, \quad (4.46)$$

where $v'_{(2),1}(\boldsymbol{\theta})$ is value in the first row of eigenvector $\mathbf{v}'_{(2)}(\boldsymbol{\theta})$. In this equation, it can be seen that the denominator involves random variables $\boldsymbol{\theta}$ when substituting Eq. (4.44) into Eq. (4.46). Thus it will be again approximated by Hermite PCE as follows by the method in Appendix 1.

$$\frac{1}{\sum_{i=0}^{2n+p_1+p_2} v_{(2),li} \Psi_i(\boldsymbol{\theta})} = \sum_{i=0}^{p_3} G_i \Psi_i(\boldsymbol{\theta}). \quad (4.47)$$

Substituting Eq. (4.7), Eq. (4.8), Eq. (4.37), Eq. (4.38), Eq. (4.43), Eq. (4.44), Eq. (4.46) and Eq. (4.47) into Eq. (4.45), the Eq. (4.45) becomes as follows.

$$\mathbf{u}'_{(2)}(\boldsymbol{\theta}) = \begin{bmatrix} u'_{(2),1} \\ u'_{(2),2} \\ \vdots \\ u'_{(2),N} \end{bmatrix}, \quad (4.48)$$

where

$$u'_{(2),1} = \sum_{i=0}^{p_2} \sum_{j=0}^{n+p_1} R_i u_{(1),1j} \Psi_i(\boldsymbol{\theta}) \Psi_j(\boldsymbol{\theta}) \times \left(\begin{array}{l} \sum_{i=0}^n A_{12i} \Psi_i(\boldsymbol{\theta}) \\ + \sum_{i=0}^{p_3} \sum_{j=0}^{2n+2p_1+p_2} \sum_{k=0}^n G_i v_{(2),N-1j} A_{1Nk} \Psi_i(\boldsymbol{\theta}) \Psi_j(\boldsymbol{\theta}) \Psi_k(\boldsymbol{\theta}) \end{array} \right), \quad (4.49-1)$$

$$u'_{(2),2} = \sum_{i=0}^{p_2} \sum_{j=0}^{n+p_1} R_i u_{(1),2j} \Psi_i(\boldsymbol{\theta}) \Psi_j(\boldsymbol{\theta}) \times \left(\begin{array}{l} \sum_{i=0}^n A_{12i} \Psi_i(\boldsymbol{\theta}) \\ + \sum_{i=0}^{p_3} \sum_{j=0}^{2n+2p_1+p_2} \sum_{k=0}^n G_i v_{(2),N-1j} A_{1Nk} \Psi_i(\boldsymbol{\theta}) \Psi_j(\boldsymbol{\theta}) \Psi_k(\boldsymbol{\theta}) \end{array} \right) - \left(\sum_{i=0}^n \lambda_{(1)i}(\boldsymbol{\theta}) \Psi_i(\boldsymbol{\theta}) - \sum_{i=0}^{2n+p_1+p_2} \lambda_{(2)i}(\boldsymbol{\theta}) \Psi_i(\boldsymbol{\theta}) \right), \quad (4.49-2)$$

$$u'_{(2),s} = \sum_{i=0}^{p_2} \sum_{j=0}^{n+p_1} R_i u_{(1),sj} \Psi_i(\boldsymbol{\theta}) \Psi_j(\boldsymbol{\theta}) \times \left(\begin{array}{l} \sum_{i=0}^n A_{12i} \Psi_i(\boldsymbol{\theta}) \\ + \sum_{i=0}^{p_3} \sum_{j=0}^{2n+2p_1+p_2} \sum_{k=0}^n G_i v_{(2),N-1j} A_{1Nk} \Psi_i(\boldsymbol{\theta}) \Psi_j(\boldsymbol{\theta}) \Psi_k(\boldsymbol{\theta}) \end{array} \right) - \sum_{i=0}^{p_3} \sum_{j=0}^{2n+2p_1+p_2} \sum_{k=0}^n G_i v_{(2),s-1j} \lambda_{(1)k}(\boldsymbol{\theta}) \Psi_i(\boldsymbol{\theta}) \Psi_j(\boldsymbol{\theta}) \Psi_k(\boldsymbol{\theta}) - \sum_{i=0}^{p_3} \sum_{j=0}^{2n+2p_1+p_2} \sum_{k=0}^{2n+p_1+p_2} G_i v_{(2),s-1j} \lambda_{(2)k}(\boldsymbol{\theta}) \Psi_i(\boldsymbol{\theta}) \Psi_j(\boldsymbol{\theta}) \Psi_k(\boldsymbol{\theta}). \quad (4.49-3)$$

where, $s = 3, \dots, N$. And they can be simplified to the following equation.

$$\mathbf{u}'_{(2)}(\boldsymbol{\theta}) = \sum_{i=0}^{4n+3p_1+2p_2+p_3} \mathbf{u}'_{(2)i} \Psi_i(\boldsymbol{\theta}) . \quad (4.50)$$

Consequently, the 2nd eigenvalue and eigenvector in $\mathbf{A}'(\boldsymbol{\theta})$ can be obtained by the above proposed method. Also we can understand that the 2nd eigenvalue is approximated by the polynomial of order $2n+p_1+p_2$ in Eq.(4.43), and the 2nd eigenvector is by the polynomial of order $4n+3p_1+2p_2+p_3$ in Eq.(4.50).

It is noted that by using the procedure to reduce dimensionality of the matrix ($\mathbf{A}'(\boldsymbol{\theta}) \rightarrow \mathbf{B}'_{(1)}(\boldsymbol{\theta})$, $\mathbf{B}'_{(1)}(\boldsymbol{\theta}) \rightarrow \mathbf{B}'_{(2)}(\boldsymbol{\theta})$, \dots ($\mathbf{B}'_{(2)}(\boldsymbol{\theta})$ is the matrix with dimension $N-2$)), it is possible to achieve solving m^{th} eigenvalue, $\lambda'_{(m)}(\boldsymbol{\theta})$, and corresponding eigenvector, $\mathbf{u}'_{(m)}(\boldsymbol{\theta})$, of the matrix $\mathbf{A}'(\boldsymbol{\theta})$.

The above formularized improved stochastic inverse power method is summarized as follows (Algorithm 4.2).

Algorithm 4.2 The Stochastic Wielandt Deflation Method (SWDM)

Input : $\mathbf{u}'_{(1)}(\boldsymbol{\theta}), \lambda'_{(1)}(\boldsymbol{\theta})$

Step 1 : $\mathbf{B}'(\boldsymbol{\theta})$

$$\begin{aligned}
 &= \sum_{i=0}^n \begin{bmatrix} A_{11i} & \cdots & A_{1Ni} \\ \vdots & \ddots & \vdots \\ A_{N1i} & \cdots & A_{NNi} \end{bmatrix} \Psi_i(\boldsymbol{\theta}) - \frac{1}{\sum_{i=0}^{n+p_1} u_{(1),li} \Psi_i(\boldsymbol{\theta})} \begin{bmatrix} \sum_{i=0}^{n+p_1} u_{(1),li} \Psi_i(\boldsymbol{\theta}) \\ \vdots \\ \sum_{i=0}^{n+p_1} u_{(1),Ni} \Psi_i(\boldsymbol{\theta}) \end{bmatrix} \begin{bmatrix} \sum_{i=0}^n A_{11i} \Psi_i(\boldsymbol{\theta}) & \cdots & \sum_{i=0}^n A_{1Ni} \Psi_i(\boldsymbol{\theta}) \end{bmatrix} \\
 &= \sum_{i=0}^{2n+p_1+p_2} \begin{bmatrix} 0 & \cdots & 0 \\ B'_{21} & \cdots & B'_{2N} \\ \vdots & \ddots & \vdots \\ B'_{N1} & \cdots & B'_{NN} \end{bmatrix} \Psi_i(\boldsymbol{\theta})
 \end{aligned}$$

$$\text{Step 2 : } \mathbf{B}'_{(1)}(\boldsymbol{\theta}) = \sum_{i=0}^{2n+p_1+p_2} \begin{bmatrix} B'_{22} & \cdots & B'_{2N} \\ \vdots & \ddots & \vdots \\ B'_{N2} & \cdots & B'_{NN} \end{bmatrix} \Psi_i(\boldsymbol{\theta})$$

$$\begin{aligned}
 \text{Step 3 : I-SIPMにより } \lambda'_{(2)}(\boldsymbol{\theta}) &= \sum_{i=0}^{2n+p_1+p_2} \lambda'_{(2)i} \Psi_i(\boldsymbol{\theta}) \\
 \mathbf{v}'_{(2)}(\boldsymbol{\theta}) &= \sum_{i=0}^{2n+2p_1+p_2} \mathbf{v}'_{(2)i} \Psi_i(\boldsymbol{\theta})
 \end{aligned}$$

$$\begin{aligned}
 \text{Step 4 : } \mathbf{u}'_{(2)}(\boldsymbol{\theta}) &= \frac{1}{\mathbf{u}'_{(1),1}(\boldsymbol{\theta})} \mathbf{u}'_{(1)}(\boldsymbol{\theta}) - \frac{\lambda'_{(1)}(\boldsymbol{\theta}) - \lambda'_{(2)}(\boldsymbol{\theta})}{\mathbf{A}_{1,1} \mathbf{v}'_{(2)}(\boldsymbol{\theta})} \mathbf{v}'_{(2)}(\boldsymbol{\theta}) \\
 &= \sum_{i=0}^{4n+3p_1+2p_2+p_3} \mathbf{u}'_{(2)i} \Psi_i(\boldsymbol{\theta})
 \end{aligned}$$

Result : $\lambda'_2(\boldsymbol{\theta}), \mathbf{u}'_2(\boldsymbol{\theta})$

4.4 Numerical Examples

In this study, we developed I-SIPM program and SWDM program by using C language which can deal with discrete and continuous model considering uncertainty. The validity and feasibility of the proposed methods is discussed by four cases, (1) eigen frequency problem - a simple discrete 2-DOF undamped system with uncertainty in stiffness, (2) buckling eigenvalue problem - a continuous beam model with uncertainty in size, and (3) buckling eigenvalue problem - a continuous beam model with uncertainty in Young's Modulus. Finally, (4) the dynamic damper problem is discussed by using proposed method as a more practical example.

4.4.1 Two Degrees of Freedom Undamped System

A discrete 2-DOF undamped system is considered. In this example, in order to prove validity of the proposed two methods, the two cases are discussed. Case(1): three springs stiffness is assumed to be following Gaussian distribution and obeying same random variable θ_1 . Case(2): two of springs stiffness is assumed to be following Gaussian distribution and obeying same random variable θ_1 , the other springs stiffness is assumed to be obeying random variable θ_2 .

(1) Case (1): The Three Springs Stiffness is Considered as Obeying Some Variable θ_1

The statistical properties of uncertain parameters are given in Table 4.1. The three springs stiffness $k_1(\theta_1)$, $k_2(\theta_1)$, $k_3(\theta_1)$ obeying same random variable θ_1 , where, $\theta = \{\theta_1\}$. The masses are deterministic with $m_1 = 1kg$, $m_2 = 2kg$. The validity of the proposed methods (I-SIPM and SWDM) is discussed by comparing the results of the method with the MCS of

the deterministic problems for the same condition.

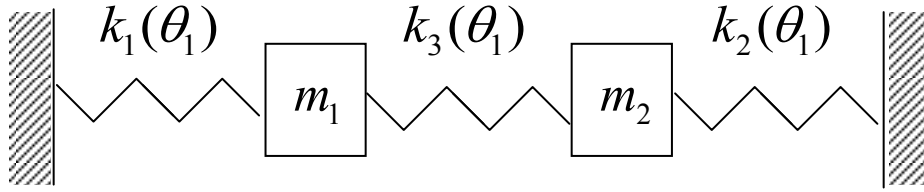


Fig.4.1: A Discrete 2-DOF Undamped System

Table 4.1 The Statistical Parameters of the Undamped System (N/m)

Uncertain variable	Mean	Standard deviation
$k_1(\theta_1)$	2.5	0.4
$k_2(\theta_1)$	7	1
$k_3(\theta_1)$	1	0.15

The system stiffness matrix involving random variables $\boldsymbol{\theta}$ can be obtained as follows.

$$\begin{aligned}
 \mathbf{K}'(\boldsymbol{\theta}) &= \begin{bmatrix} k_1(\theta_1) + k_3(\theta_1) & -k_3(\theta_1) \\ -k_3(\theta_1) & k_2(\theta_1) + k_3(\theta_1) \end{bmatrix} \\
 &= \begin{bmatrix} 3.5 & -1 \\ -1 & 8 \end{bmatrix} \Psi_0(\boldsymbol{\theta}) + \begin{bmatrix} 0.55 & -0.15 \\ -0.15 & 1.15 \end{bmatrix} \Psi_1(\boldsymbol{\theta}).
 \end{aligned} \tag{4.51}$$

And the system mass matrix is as follows.

$$\mathbf{M} = \begin{bmatrix} m_1 & 0 \\ 0 & m_2 \end{bmatrix} = \begin{bmatrix} 1 & 0 \\ 0 & 2 \end{bmatrix} \Psi_0(\boldsymbol{\theta}) \quad (\Psi_0(\boldsymbol{\theta}) = 1). \tag{4.52}$$

The stochastic eigenvalue problem is represented by Eq.(4.3), where $\mathbf{R}'(\boldsymbol{\theta})$ is the system mass matrix and is deterministic form as shown Eq.(4.52). The 1st stochastic eigenvalue $\lambda'_{(1)}(\boldsymbol{\theta})$ and corresponding eigenvector $\mathbf{u}'_{(1)}(\boldsymbol{\theta})$ can be evaluated by using proposed I-SIPM. Also, the 2nd stochastic eigenvalue $\lambda'_{(2)}(\boldsymbol{\theta})$ and corresponding eigenvector $\mathbf{u}'_{(2)}(\boldsymbol{\theta})$ can be evaluated by using proposed SWDM.

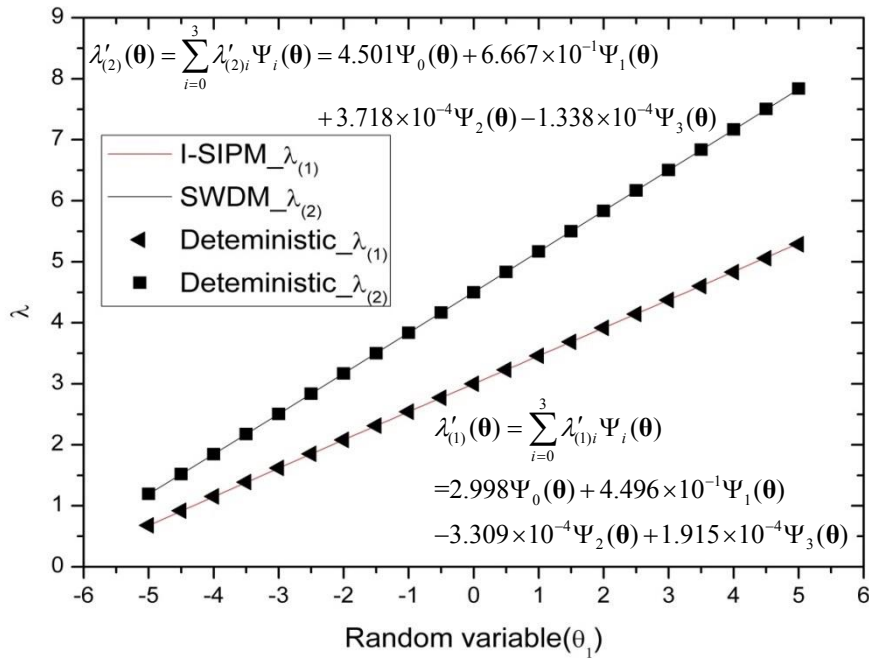


Fig. 4.2: The Response Surface of Eigenvalues

In Fig.4.2, the response surfaces of stochastic eigenvalues ($\lambda'_{(1)}(\boldsymbol{\theta})$ and $\lambda'_{(2)}(\boldsymbol{\theta})$) and determinate results are described. As can be seen, a good agreement is observed between the results from the stochastic response surfaces and the reference values (deterministic cases).

Fig. 4.3 and Fig. 4.4 show probability density distributions of stochastic eigenvalues obtained through the proposed methods (The 1st stochastic eigenvalue obtained through I-SIPM, and the 2nd stochastic eigenvalue obtained through SWDM) which has been obtained by using 10000 realization of the standard random variable θ_1 in the obtained response

surface of the eigenvalue and the reference distribution obtained by MCS by solving many deterministic eigenvalue problems. As can be seen, the results of the proposed methods agree well with the results from the Monte Carlo simulation (MCS) of 10000 samples. Also, as shown in the Table in Fig.4.3, we find that statistical properties are reasonably well estimated by the proposed I-SIPM when compared with those obtained from determinate (MCS) result. And we can also find from Fig.4.4 that statistical properties of the second eigenvalue by the proposed SWDM have a good agreement with the MCS result. Note that the mean and the standard deviation of “I-SIPM_PCE/SWDM_PCE” in the Table4.2 and Table4.3 are calculated by Eq. (2.7) and Eq. (2.8), which also takes almost the same value.

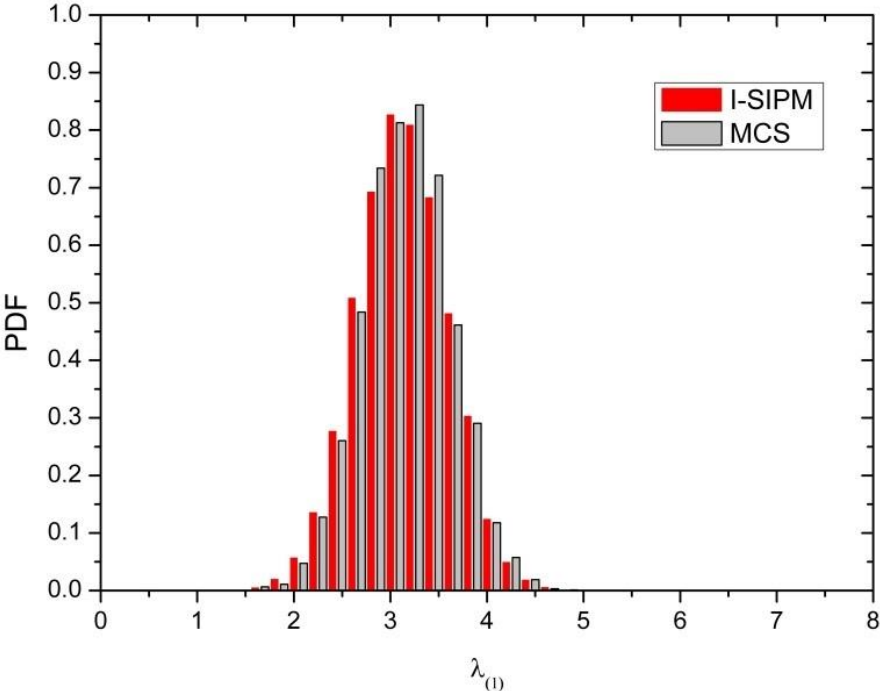


Fig.4.3: The Probability Density Distributions of Eigenvalue $\lambda'_{(1)}(\theta)$

Table 4.2 Statistics of Eigenvalue $\lambda'_{(1)}(\boldsymbol{\theta})$

	I-SIPM	MCS	I-SIPM_PCE
Mean	2.996	3.003	2.999
Std.dev.	0.465	0.456	0.459

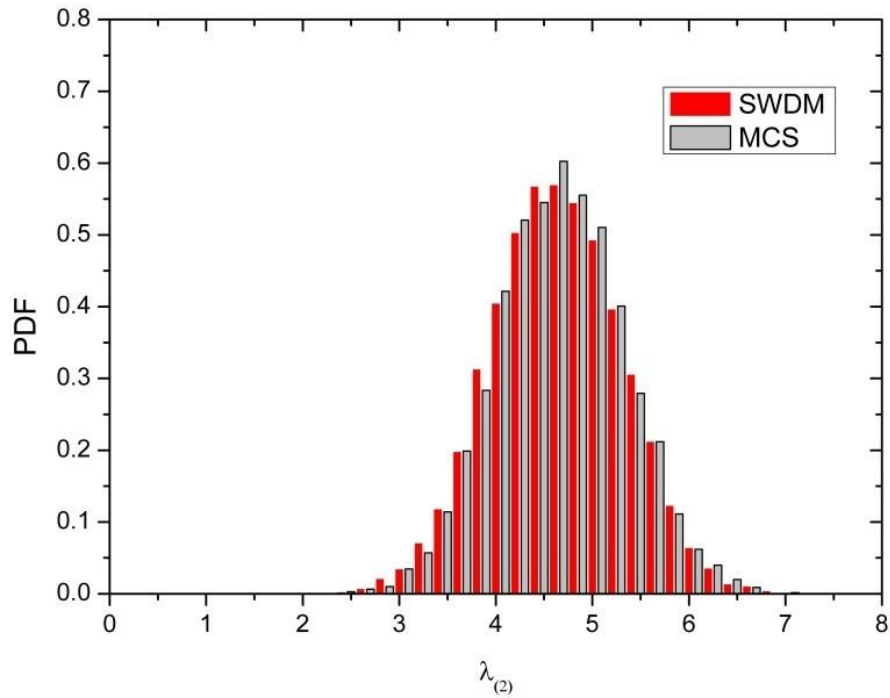


Fig.4.4: The Probability Density Distributions of Eigenvalue $\lambda'_{(2)}(\boldsymbol{\theta})$

Table 4.3 Statistics of Eigenvalue $\lambda'_{(2)}(\boldsymbol{\theta})$

	SWDM	MCS	SWDM_PCE
Mean	4.498	4.506	4.500
Std.dev.	0.674	0.663	0.667

Fig. 4.5 and Fig. 4.6 show the response surfaces for the components $\{u'_{(1),1}, u'_{(1),2}\}^T$ and $\{u'_{(2),1}, u'_{(2),2}\}^T$ of eigenvectors $\mathbf{u}'_{(1)}(\boldsymbol{\theta})$ and $\mathbf{u}'_{(2)}(\boldsymbol{\theta})$ respectively. They showed good agreement between proposed two methods and reference values obtained by deterministic eigenvalue analysis. And the probability density distributions are also shown in the Fig.4.7 and Fig.4.8. As can be seen, the reasonable results are shown for solving eigenvectors problem. Thus, from the results in this section we can conclude the proposed I-SIPM is valid for evaluating 1st eigenvalue and eigenvector. And the validity of the proposed SWDM is also demonstrated for evaluating 2nd eigenvalue and eigenvector. Also, as shown in the Table4.4 and Table4.5, we find that the statistics are reasonably well estimated by the proposed I-SIPM when compared with those obtained from MCS with deterministic eigenvalue analysis. Note that the mean and the standard deviation of “I-SIPM_PCE/SWDM_PCE” in the Table4.4 and Table4.5 are calculated by Eq. (2.7) and Eq. (2.8), which also takes almost same value. We can understand the statistics can be easy evaluated using by using Eq. (2.7) and Eq. (2.8) based on obtained response surface.

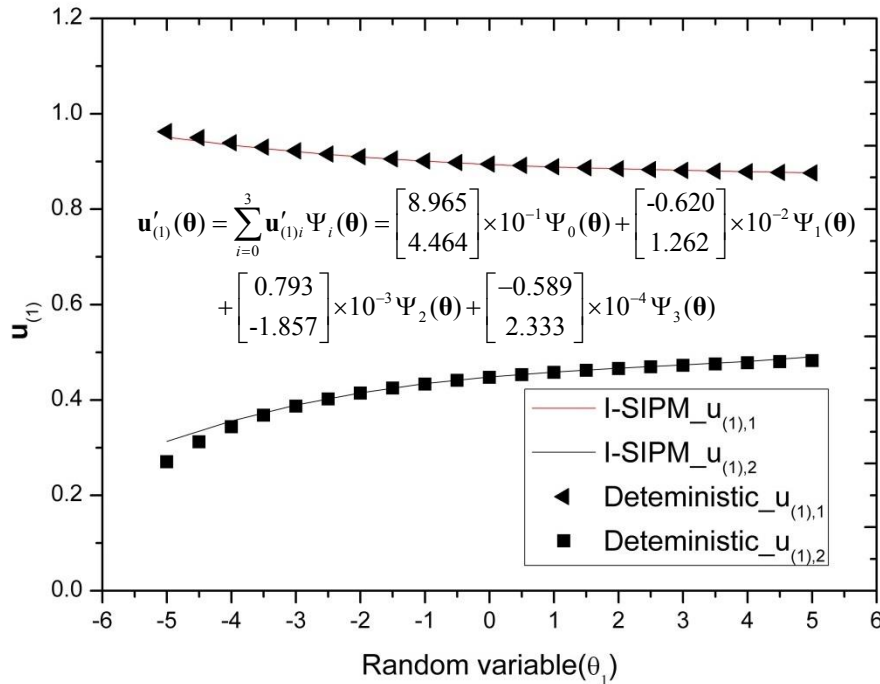


Fig.4.5: The Response Surface of Eigenvector Components: $\mathbf{u}'_{(1)}(\theta)$

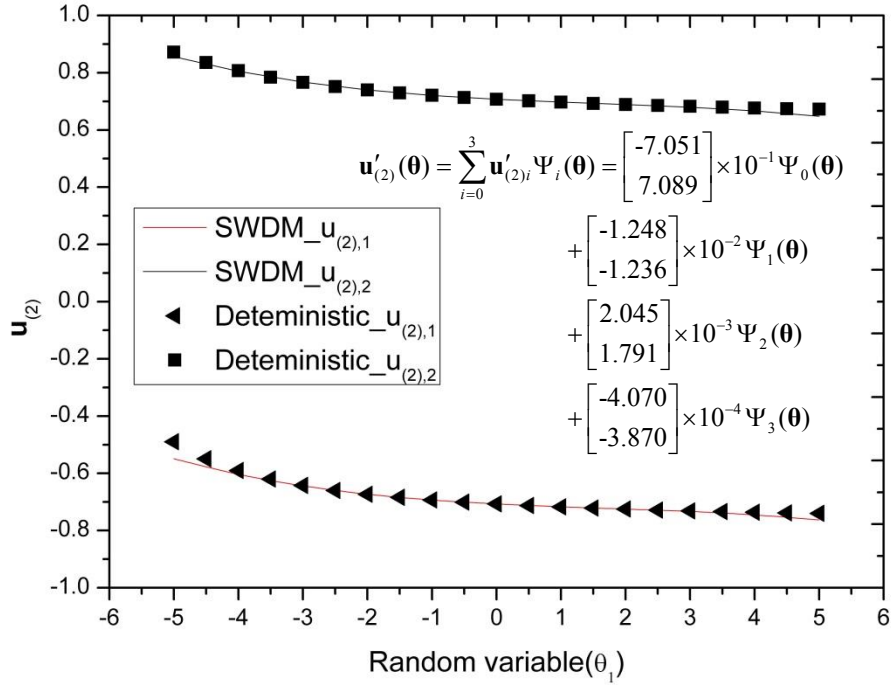


Fig.4.6: The Response Surface of Eigenvector Components: $\mathbf{u}'_{(2)}(\theta)$

It is noted that the approximate expressions of the stochastic minimum eigenvalue response surface and the stochastic eigenvector components response surface are 5th ($n=5$) and 10th ($n=5$ and $p_1=5$) order PCE, respectively. The approximate expressions of the stochastic 2nd eigenvalue response surface and the stochastic eigenvector components response surface are 20th ($n=5$, $p_1=5$ and $p_2=5$) and 50th ($n=5$, $p_1=5$, $p_2=5$ and $p_3=5$) order PCE, respectively. However, only the 3rd order approximate expressions of the response surfaces are shown in Fig.4.2, Fig.4.5 and Fig.4.6, because the influence is small after the 4th order.

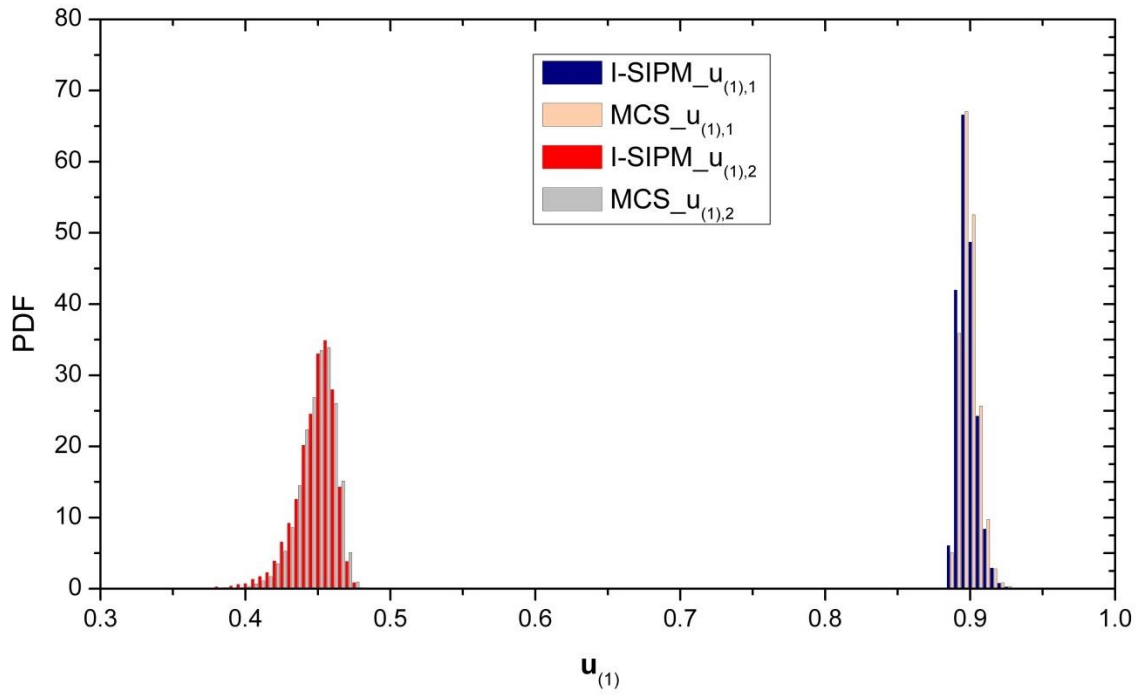


Fig.4.7: The Probability Density Distributions of Eigenvector $u'_{(1)}(\theta)$

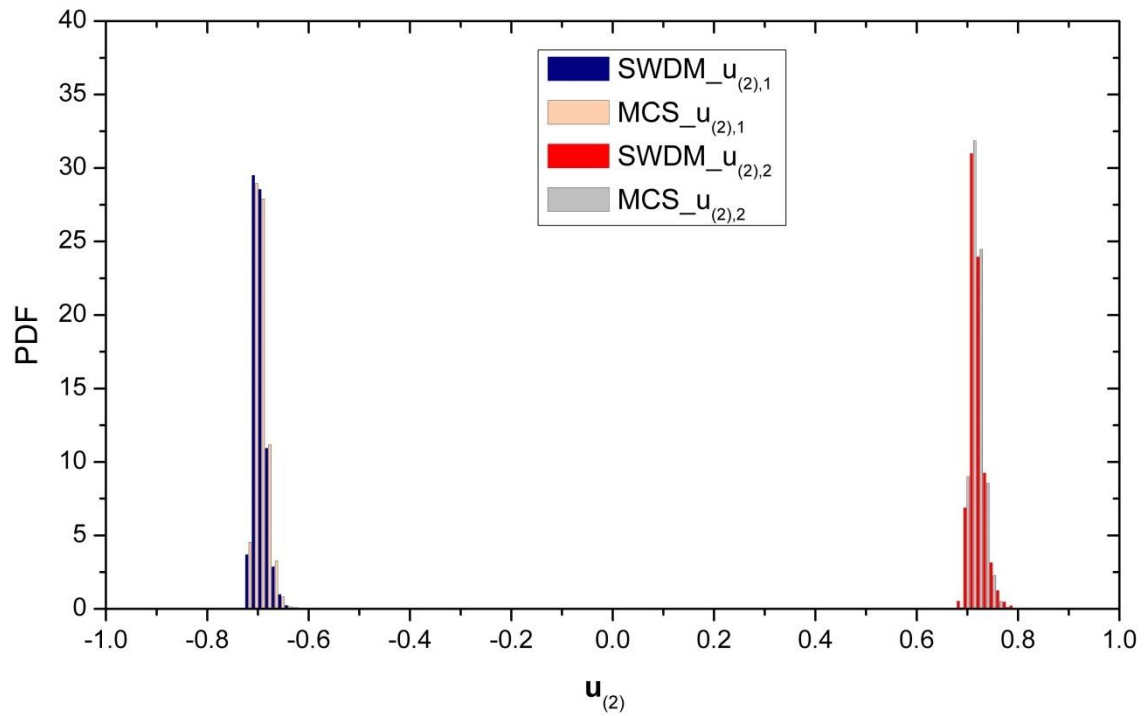


Fig.4.8: The Probability Density Distributions of Eigenvector $u'_{(2)}(\theta)$

Table 4.4 Statistics of Eigenvector $\mathbf{u}'_{(1)}(\boldsymbol{\theta})$

		I-SIPM	MCS	I-SIPM_PCE
$u'_{(1),1}(\boldsymbol{\theta})$	Mean	0.8946	0.8951	0.8947
	Std.dev.	0.0063	0.0062	0.0063
$u'_{(1),2}(\boldsymbol{\theta})$	Mean	0.4447	0.4456	0.4464
	Std.dev.	0.0145	0.0127	0.0129

Table 4.5 Statistics of Eigenvector $\mathbf{u}'_{(2)}(\boldsymbol{\theta})$

		SWDM	MCS	SWDM_PCE
$u'_{(2),1}(\boldsymbol{\theta})$	Mean	-0.7052	-0.7053	-0.7051
	Std.dev.	0.0128	0.0128	0.0128
$u'_{(2),2}(\boldsymbol{\theta})$	Mean	0.7106	0.7087	0.7089
	Std.dev.	0.0152	0.0125	0.0127

(2) Case (2): The Three Springs Stiffness is Considered as Obeying Different Variables θ_1, θ_2

The statistical properties of uncertain parameters are given in Table 4.6. The two springs stiffness $k_1(\theta_1), k_2(\theta_1)$, obeying same random variable θ_1 , the other spring stiffness $k_3(\theta_2)$ obeying random variable θ_2 , where, $\theta = \{\theta_1, \theta_2\}$. The masses are deterministic with $m_1 = 1kg$, $m_2 = 2kg$. The validity of the proposed methods (I-SIPM and SWDM) is discussed for the two variables problem by comparing the results of the method with the MCS of the deterministic problems for the same condition.

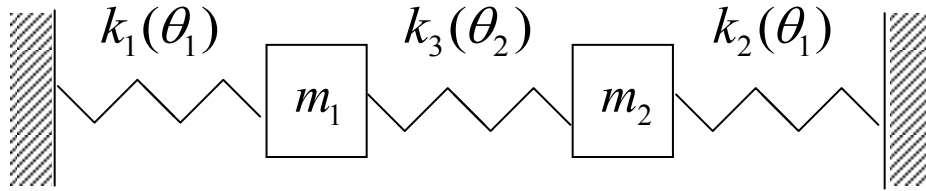


Fig.4.9: A Discrete 2-DOF Undamped System

Table 4.6 The Statistical Parameters of the Undamped System (N/m)

Uncertain variable	Mean	Standard deviation
$k_1(\theta_1)$	2.5	0.4
$k_2(\theta_1)$	7	1
$k_3(\theta_2)$	1	0.15

Here, we firstly show the system stiffness matrix when it has the two variables problem.

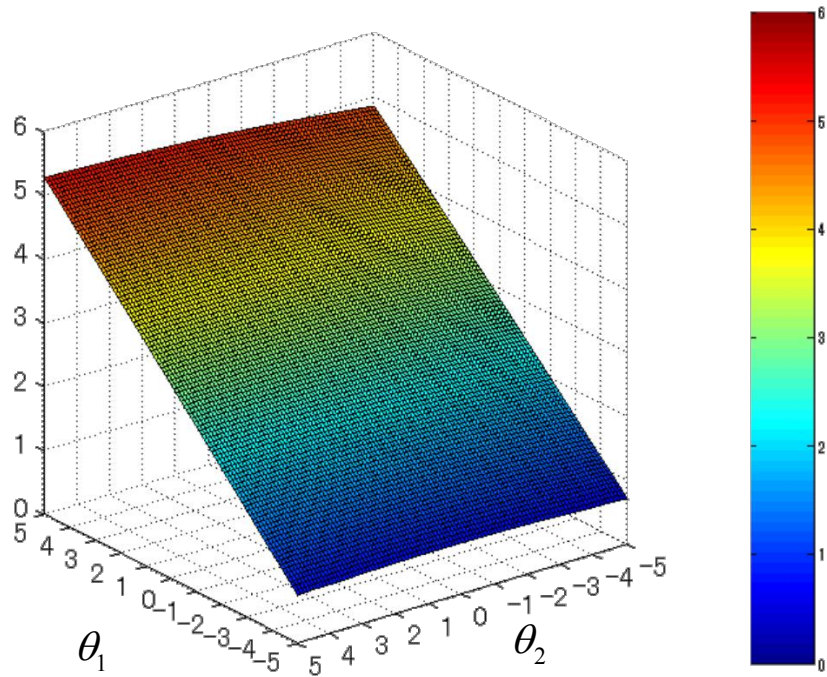
The system stiffness matrix involving random variables $\boldsymbol{\theta}$ can be obtained as follows.

$$\begin{aligned}\mathbf{K}'(\boldsymbol{\theta}) &= \begin{bmatrix} k_1(\theta_1) + k_3(\theta_2) & -k_3(\theta_2) \\ -k_3(\theta_2) & k_2(\theta_1) + k_3(\theta_2) \end{bmatrix} \\ &= \begin{bmatrix} 3.5 & -1 \\ -1 & 8 \end{bmatrix} \Psi_0(\boldsymbol{\theta}) + \begin{bmatrix} 0.4 & 0 \\ 0 & 1 \end{bmatrix} \Psi_1(\boldsymbol{\theta}) + \begin{bmatrix} 0.15 & -0.15 \\ -0.15 & 0.15 \end{bmatrix} \Psi_2(\boldsymbol{\theta}).\end{aligned}\quad (4.53)$$

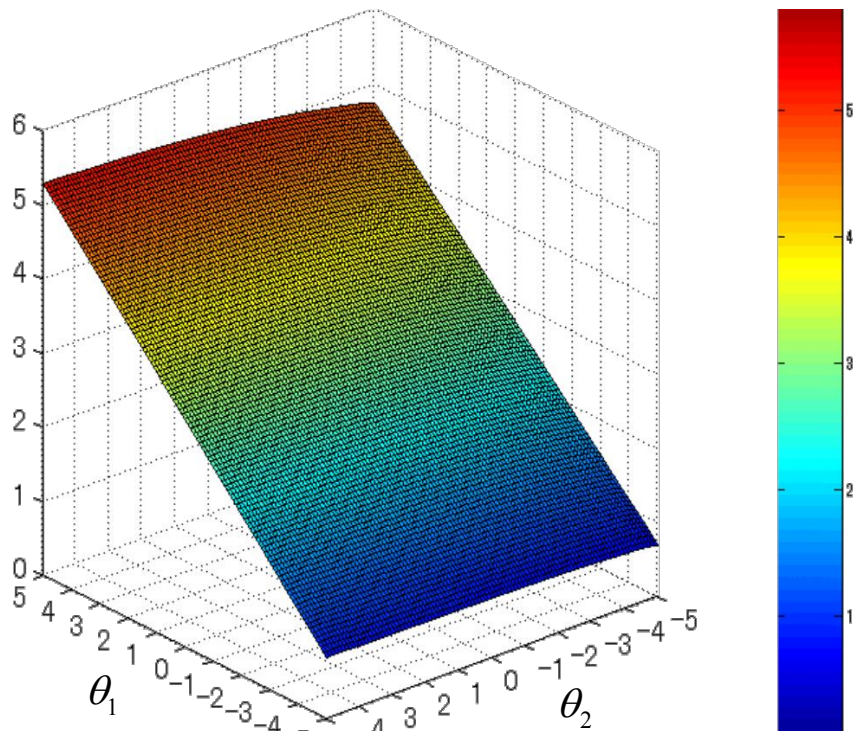
And the system mass matrix is as follows.

$$\mathbf{M} = \begin{bmatrix} m_1 & 0 \\ 0 & m_2 \end{bmatrix} = \begin{bmatrix} 1 & 0 \\ 0 & 2 \end{bmatrix} \Psi_0(\boldsymbol{\theta}) \quad (\Psi_0(\boldsymbol{\theta}) = 1). \quad (4.54)$$

The stochastic eigenvalue problem is represented by Eq.(4.3), where $\mathbf{R}'(\boldsymbol{\theta})$ is the system mass matrix and is deterministic form as shown Eq.(4.54). The 1st stochastic eigenvalue $\lambda'_{(1)}(\boldsymbol{\theta})$ and corresponding eigenvector $\mathbf{u}'_{(1)}(\boldsymbol{\theta})$ can be evaluated by using proposed I-SIPM. Also, the 2nd stochastic eigenvalue $\lambda'_{(2)}(\boldsymbol{\theta})$ and corresponding eigenvector $\mathbf{u}'_{(2)}(\boldsymbol{\theta})$ can be evaluated by using proposed SWDM.



(a) I-SIPM



(b) The reference values (deterministic cases)

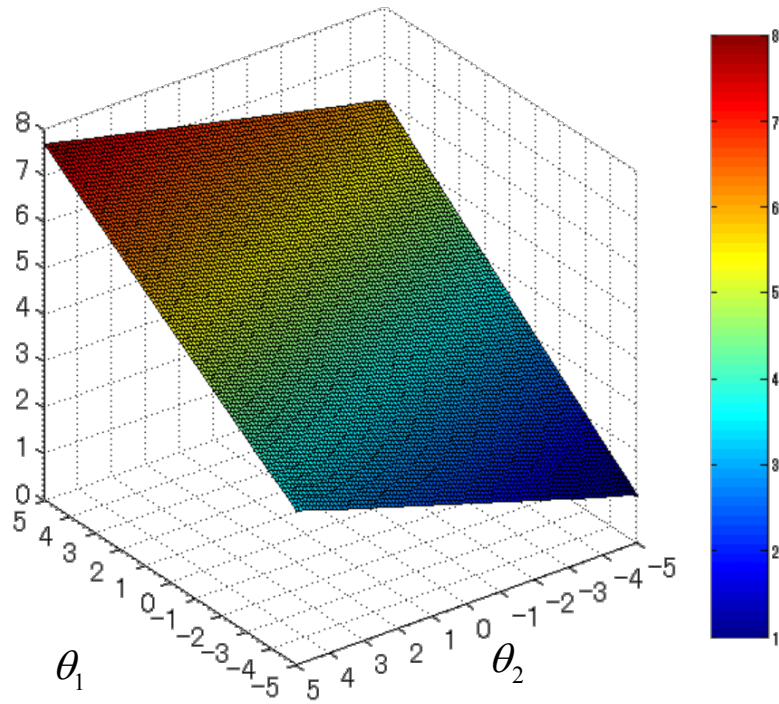
Fig. 4.10: The Response Surface of Eigenvalues $\lambda'_{(1)}(\boldsymbol{\theta})$

$$\begin{aligned}
& \lambda'_{(1)}(\boldsymbol{\theta}) \\
& = 3.00\Psi_0(\boldsymbol{\theta}) + 4.34 \times 10^{-1}\Psi_1(\boldsymbol{\theta}) + 2.32 \times 10^{-2}\Psi_2(\boldsymbol{\theta}) + 3.90 \times 10^{-3}\Psi_3(\boldsymbol{\theta}) \\
& \quad - 1.43 \times 10^{-2}\Psi_4(\boldsymbol{\theta}) - 3.10 \times 10^{-3}\Psi_5(\boldsymbol{\theta}) - 1.23 \times 10^{-4}\Psi_6(\boldsymbol{\theta}).
\end{aligned} \tag{4.55}$$

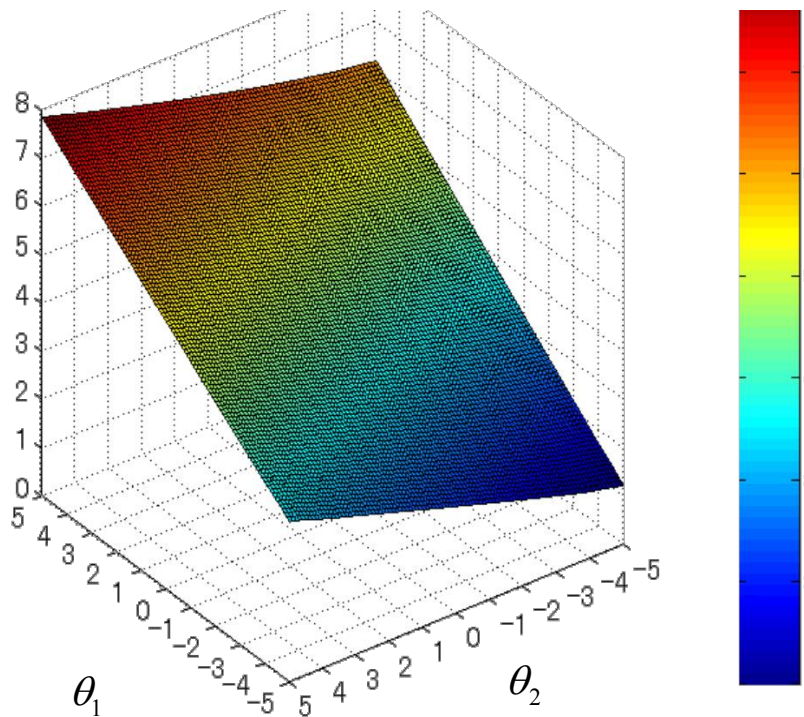
In Fig.4.10, the response surfaces of stochastic eigenvalues ($\lambda'_{(1)}(\boldsymbol{\theta})$) and determinate results are described. Where I-SIPM is described by Eq.4.55 in which the two variables θ_1, θ_2 are values from -5 to 5, respectively. It is noted that the approximate expressions of the stochastic minimum eigenvalue response surface is 6th ($n=6$). As can be seen, a good agreement is observed between the results from the stochastic response surfaces and the reference values (deterministic cases).

$$\begin{aligned}
& \lambda'_{(2)}(\boldsymbol{\theta}) \\
& = 4.50\Psi_0(\boldsymbol{\theta}) + 4.67 \times 10^{-1}\Psi_1(\boldsymbol{\theta}) + 2.00 \times 10^{-1}\Psi_2(\boldsymbol{\theta}) - 4.47 \times 10^{-3}\Psi_3(\boldsymbol{\theta}).
\end{aligned} \tag{4.56}$$

In Fig.4.11, the response surfaces of stochastic eigenvalues ($\lambda'_{(2)}(\boldsymbol{\theta})$) and the determinate results are described. The I-SIPM is described by Eq.4.56. It is noted that the stochastic 2nd eigenvalue response surface should be 20th because of $n=5, p_1=5$ and $p_2=5$, but by Eq.4.56, we can see only the 3rd order approximate expressions of the response surfaces is shown because the coefficients of approximation polynomial are approaching zero after the 3rd order. As can be seen, a good agreement is observed between the results from the stochastic response surfaces and the reference values (deterministic cases) by SWDM, and 2nd eigenvalue response surface is approaching plane compared to 1st eigenvalue response surface. So the response has hardly any the quadratic term.



(a)SWDM



(b) The reference values (deterministic cases)

Fig. 4.11: The Response Surface of Eigenvalues $\lambda'_{(2)}(\boldsymbol{\theta})$

Fig. 4.12 and Fig. 4.13 show probability density distributions of stochastic eigenvalues which obtained through the proposed methods (The 1st stochastic eigenvalue obtained through I-SIPM, and the 2nd stochastic eigenvalue obtained through SWDM) which has been obtained by using 10000 realization of the standard random variables θ_1 and θ_2 in the obtained response surface of the eigenvalue and the reference distribution obtained by MCS respectively. As can be seen, the results of proposed methods agree well with the results from the Monte Carlo simulation (MCS) of 10000 samples. And we can also find from Fig.4.13 that statistical properties of the second eigenvalue by the proposed SWDM have a good agreement with the MCS result. And we show statistics of eigenvalue in Table 4.7 and Table 4.8.

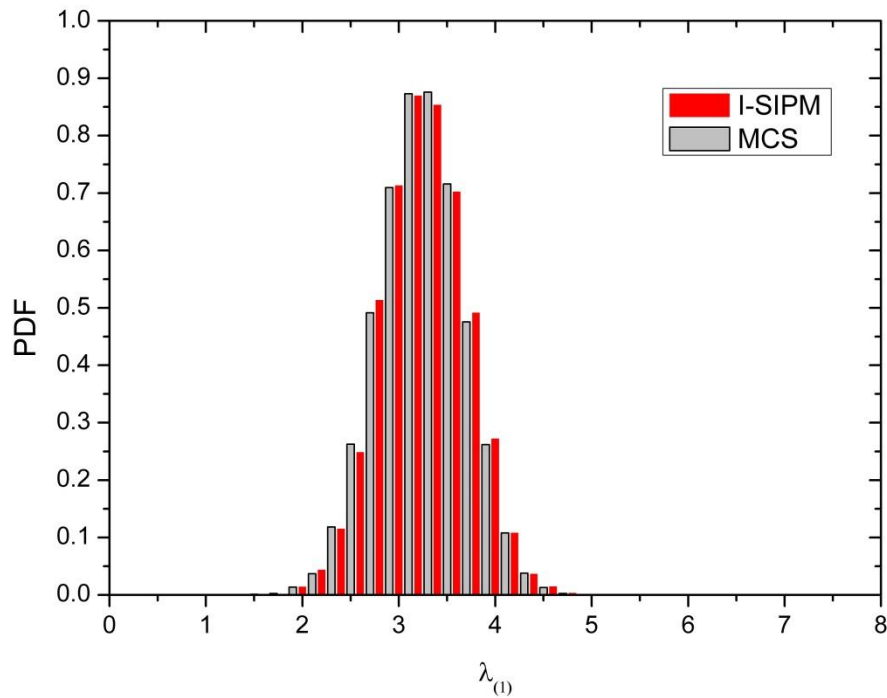


Fig.4.12: The Probability Density Distributions of Eigenvalue $\lambda'_{(1)}(\theta)$

In Table 4.7, we can see that mean values are almost same value by the proposed I-SIPM when compared with those obtained from determinate (MCS) result. But the standard deviation is almost same value for the I-SIPM and MCS, the SIPM_PCE has error which 0.9%. We can consider that is a small error.

Table 4.7 Statistics of Eigenvalue $\lambda'_{(1)}(\theta)$

	I-SIPM	MCS	I-SIPM_PCE
Mean	2.993	2.996	2.995
Std.dev.	0.439	0.438	0.434

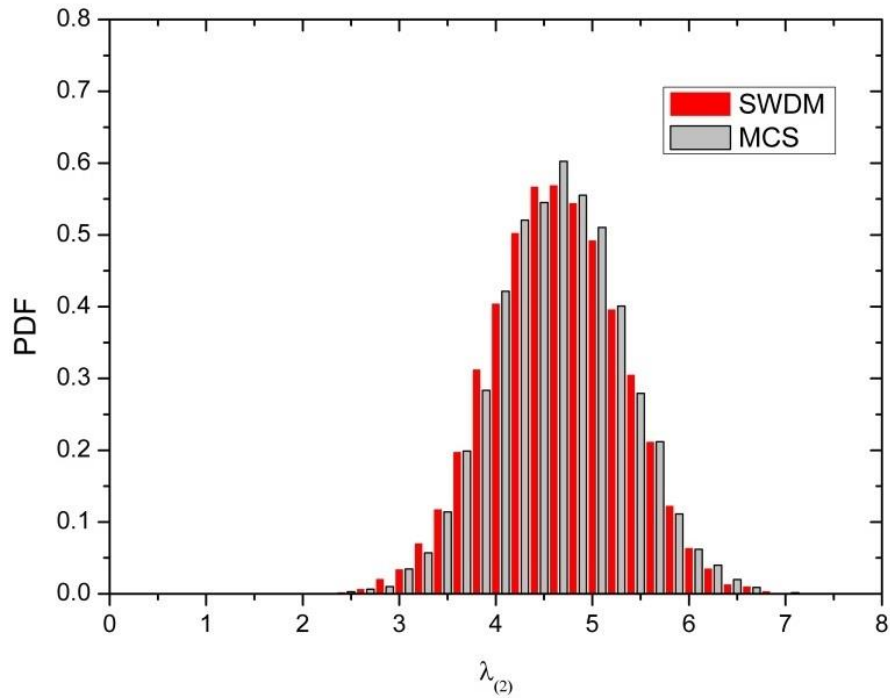


Fig.4.13: The Probability Density Distributions of Eigenvalue $\lambda'_{(2)}(\theta)$

In Table 4.8, we can see that the error of mean values and the standard deviation are 0.25% and 0.04% for the SWDM and MCS, the error of mean values and the standard deviation are 0.17% and 0.78% for the SWDM_PCE and MCS. We can consider that is a small error. It is concluded that the proposed two methods are very efficient methods to estimate statistics response.

Table 4.8 Statistics of Eigenvalue $\lambda'_{(2)}(\boldsymbol{\theta})$

	SWDM	MCS	SWDM_PCE
Mean	4.498	4.509	4.501
Std.dev.	0.514	0.512	0.508

$$\begin{aligned}
\mathbf{u}'_{(1)}(\boldsymbol{\theta}) &= \sum_{i=0}^5 \mathbf{u}'_{(1)i} \Psi_i(\boldsymbol{\theta}) \\
&= \sum_{i=0}^5 \begin{bmatrix} \mathbf{u}'_{(1),1i} \\ \mathbf{u}'_{(1),2i} \end{bmatrix} \Psi_i(\boldsymbol{\theta}) \begin{bmatrix} 8.949 \\ 4.437 \end{bmatrix} \times 10^{-1} \Psi_0(\boldsymbol{\theta}) + \begin{bmatrix} 1.192 \\ -2.364 \end{bmatrix} \times 10^{-2} \Psi_1(\boldsymbol{\theta}) \quad (4.57) \\
&\quad + \begin{bmatrix} -1.819 \\ 3.638 \end{bmatrix} \times 10^{-2} \Psi_2(\boldsymbol{\theta}) + \begin{bmatrix} 0.307 \\ 1.791 \end{bmatrix} \times 10^{-4} \Psi_3(\boldsymbol{\theta}) \\
&\quad + \begin{bmatrix} -6.864 \\ 5.920 \end{bmatrix} \times 10^{-4} \Psi_4(\boldsymbol{\theta}) + \begin{bmatrix} 1.099 \\ -4.048 \end{bmatrix} \times 10^{-3} \Psi_5(\boldsymbol{\theta}).
\end{aligned}$$

Fig. 4.14 and Fig. 4.15 show the response surfaces for the components $\{\mathbf{u}'_{(1),1}, \mathbf{u}'_{(1),2}\}^T$ of eigenvectors $\mathbf{u}'_{(1)}(\boldsymbol{\theta})$ respectively, in which the response surfaces are obtained by Eq.(4.57). In Fig.4.14, they show good agreement between the proposed I-SIPM and the reference values in the most of the areas. Though they have some inconsistent results in edges (for example: θ_1 is around 5 and θ_2 is around -5, θ_1 is around -5 and θ_2 is around 5.), and the results in edges have more big values by I-SIPM, if we see Table 4.9, it does not affect the statistical properties because the probabilities of occurrence are very low in the edges. In Fig.4.15, we also can find that they show good agreement between the proposed I-SIPM and the reference values in the most of the areas. Although they have some inconsistent results in the edges, they again do but did not affect the results of statistical properties if we see Table 4.9.

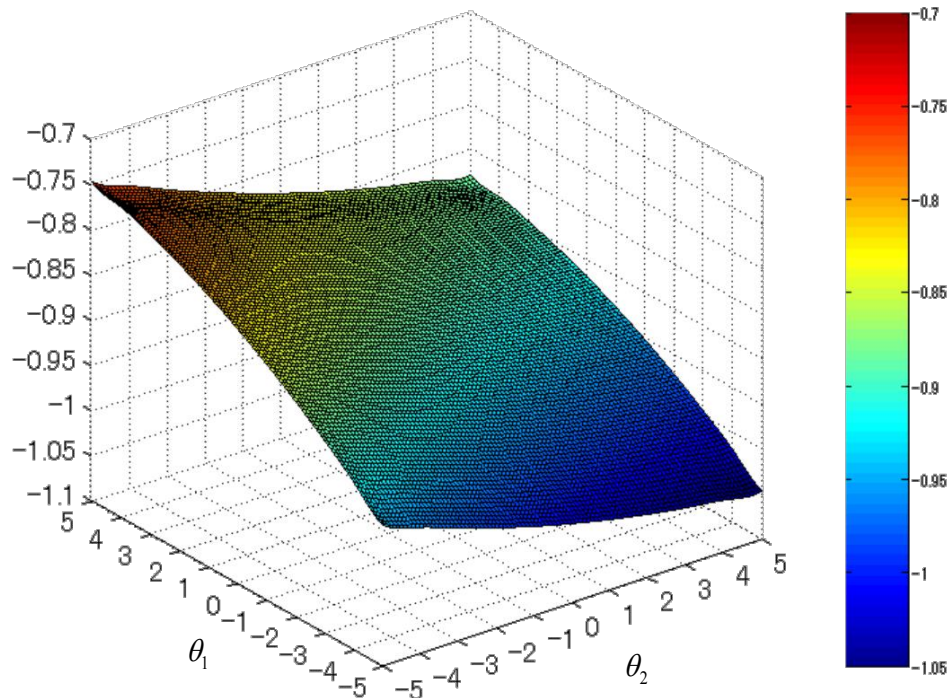
$$\begin{aligned}
\mathbf{u}'_{(2)}(\boldsymbol{\theta}) &= \sum_{i=0}^5 \mathbf{u}'_{(2)i} \Psi_i(\boldsymbol{\theta}) \\
&= \sum_{i=0}^5 \begin{bmatrix} \mathbf{u}'_{(2),1i} \\ \mathbf{u}'_{(2),2i} \end{bmatrix} \Psi_i(\boldsymbol{\theta}) \begin{bmatrix} -7.003 \\ 7.112 \end{bmatrix} \times 10^{-1} \Psi_0(\boldsymbol{\theta}) + \begin{bmatrix} 2.403 \\ 2.227 \end{bmatrix} \times 10^{-2} \Psi_1(\boldsymbol{\theta}) \quad (4.58) \\
&\quad + \begin{bmatrix} -3.338 \\ -3.595 \end{bmatrix} \times 10^{-2} \Psi_2(\boldsymbol{\theta}) + \begin{bmatrix} -2.482 \\ -0.294 \end{bmatrix} \times 10^{-3} \Psi_3(\boldsymbol{\theta}) \\
&\quad + \begin{bmatrix} 8.320 \\ 0.230 \end{bmatrix} \times 10^{-4} \Psi_4(\boldsymbol{\theta}) + \begin{bmatrix} 4.427 \\ 2.404 \end{bmatrix} \times 10^{-3} \Psi_5(\boldsymbol{\theta}).
\end{aligned}$$

Fig. 4.16 and Fig. 4.17 show the response surfaces for the components $\{u'_{(2),1}, u'_{(2),2}\}^T$ of eigenvectors $\mathbf{u}'_{(2)}(\boldsymbol{\theta})$ respectively, in which the response surfaces are obtained by Eq.(4.58). In Fig.4.16, they show good agreement between the proposed SWDM and the reference values in almost all of the areas by using SWDM. In Fig.4.17, we also can find that they show good agreement between the proposed SWDM and the reference values in the most of the areas. Though they have some inconsistent results in edges (for example: θ_1 is around 5 and θ_2 is around -5, θ_1 is around -5 and θ_2 is around 5.), and the results in edges have more big values by SWDM, if we see Table 4.10, it does not affect the statistical properties because the probabilities of occurrence are very low in the edges.

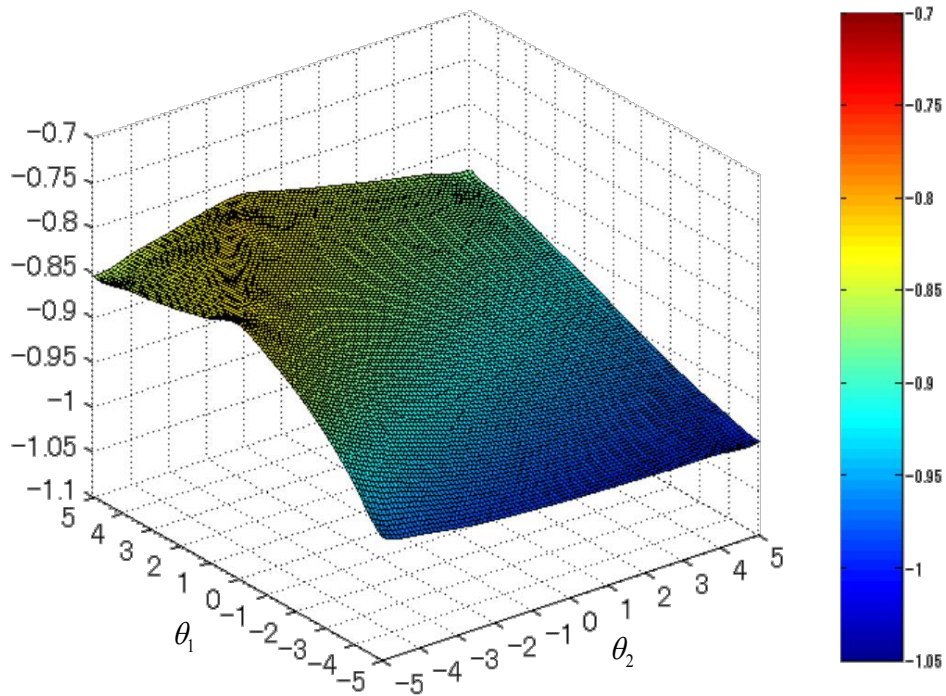
It is noted that the approximate expressions of the stochastic minimum eigenvector components response surface is 10th ($n=5$ and $p_1=5$) order PCE. And the approximate expressions of the stochastic 2nd eigenvector components response surface is 50th ($n=5$, $p_1=5$, $p_2=5$ and $p_3=5$) order PCE. However, only the 5rd order approximate expressions of the response surfaces are shown, because the influence is small after 6th order.

And the probability density distributions are also shown in the Fig.4.18 and Fig.4.19. The Fig.4.18 shows the probability density distributions of the 1st eigenvector components $u'_{(1),1}(\boldsymbol{\theta})$ and $u'_{(1),2}(\boldsymbol{\theta})$, respectively. As can be seen, the reasonable results are shown by contrasting MCS results for solving eigenvectors problem.

The Fig.4.19 shows the probability density distributions of 2st eigenvector components $u'_{(2),1}(\boldsymbol{\theta})$ and $u'_{(2),2}(\boldsymbol{\theta})$, respectively. As can be seen, the reasonable results are also shown for solving eigenvectors problem by using the proposed SWDM.

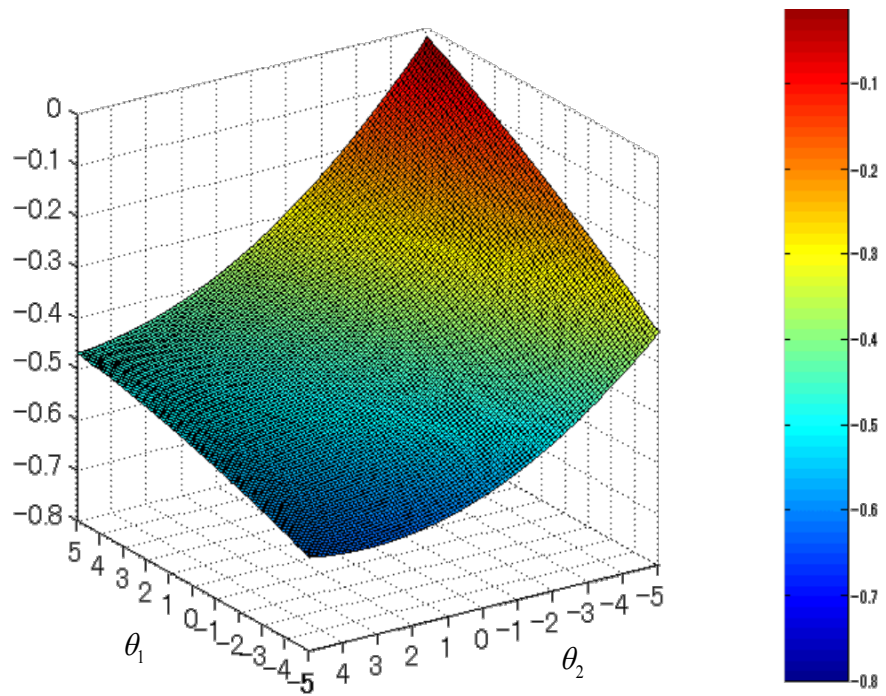


(a)I-SIPM

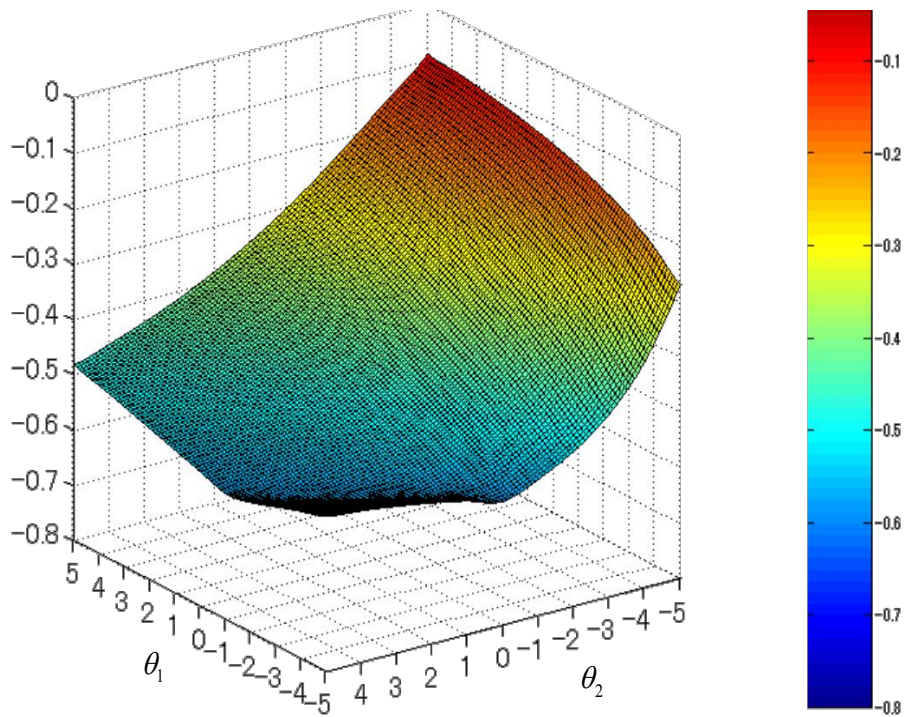


(b) The reference values (deterministic cases)

Fig. 4.14: The Response Surface of Eigenvector Components: $u'_{(1),1}(\theta)$

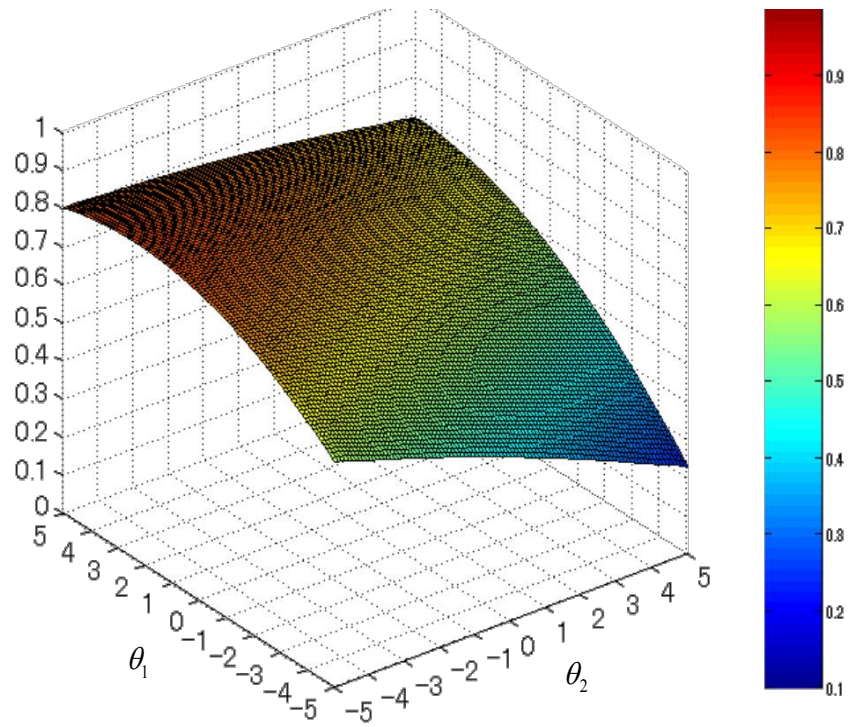


(a) I-SIPM

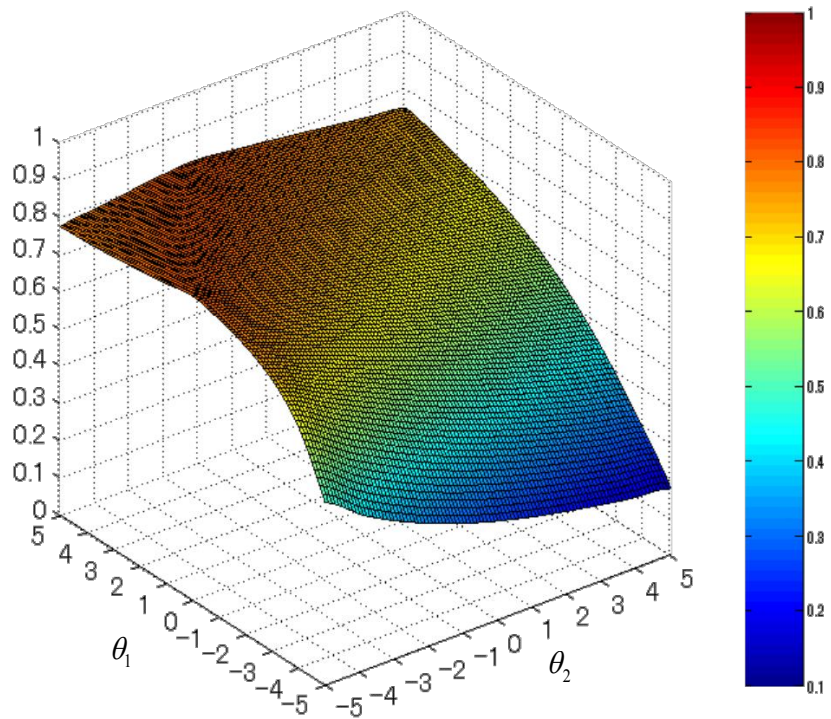


(b) The reference values (deterministic cases)

Fig. 4.15: The Response Surface of Eigenvector Components: $u'_{(1),2}(\theta)$

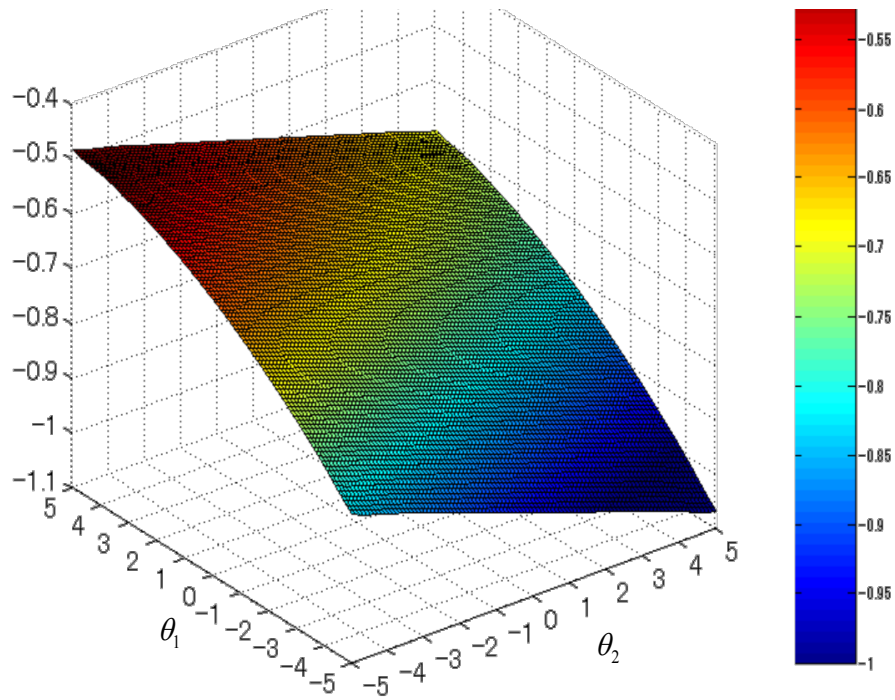


(a)SWDM

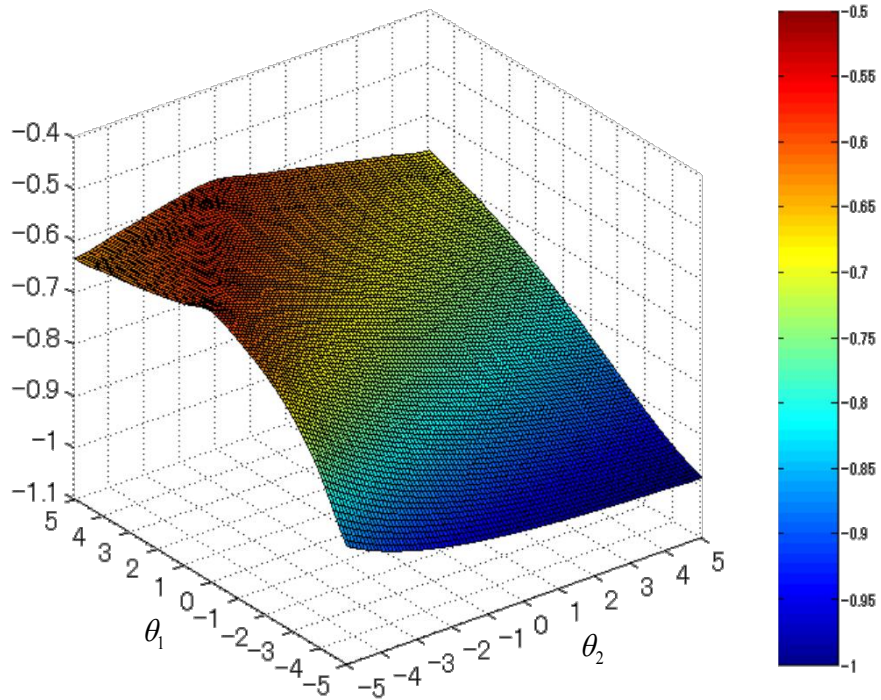


(b) The reference values (deterministic cases)

Fig. 4.16: The Response Surface of Eigenvector Components: $u'_{(2),1}(\theta)$

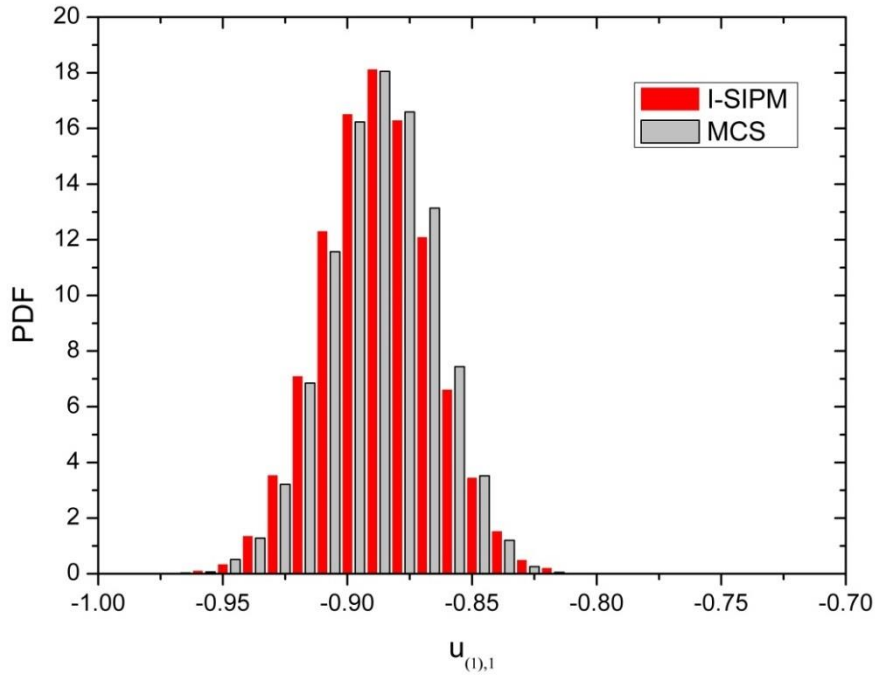


(a)SWDM

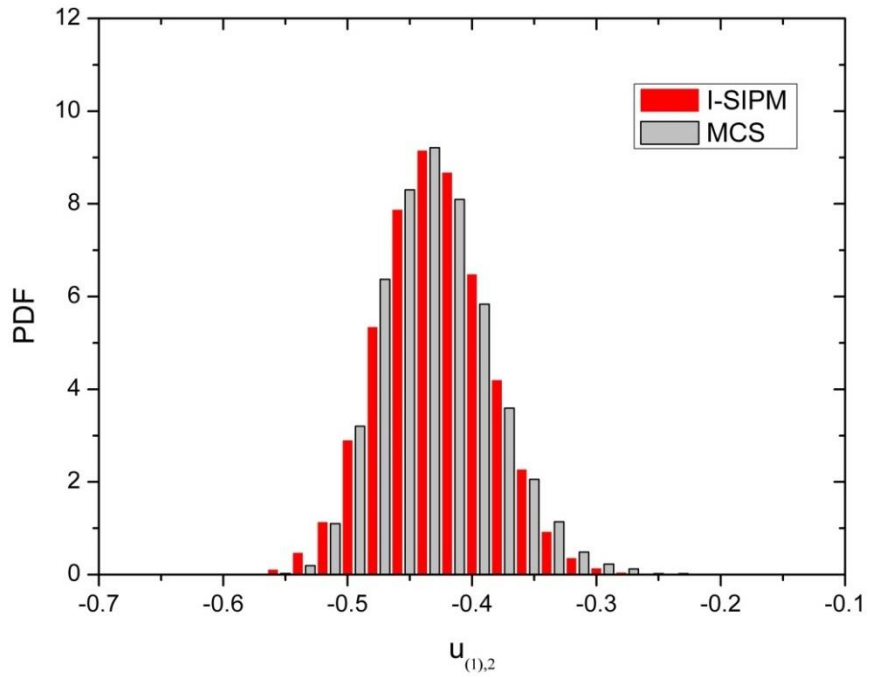


(b) The reference values (deterministic cases)

Fig. 4.17: The Response Surface of Eigenvector Components: $u'_{(2),2}(\theta)$



(a) $u'_{(1),1}(\theta)$



(b) $u'_{(1),2}(\theta)$

Fig.4.18: The Probability Density Distributions of Eigenvector $\mathbf{u}'_{(1)}(\theta)$

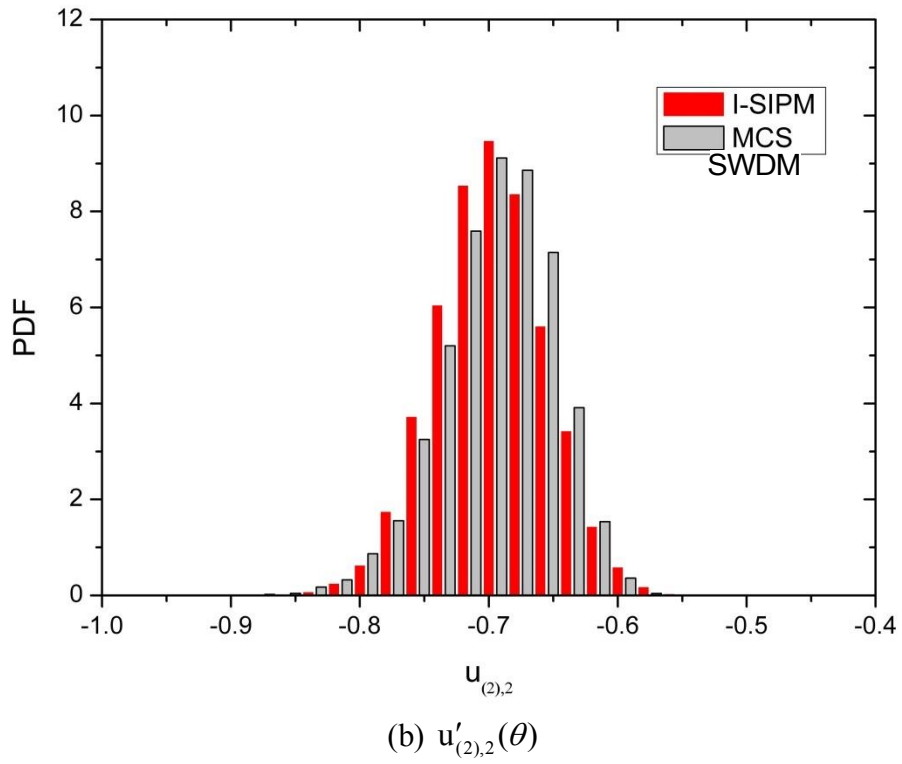
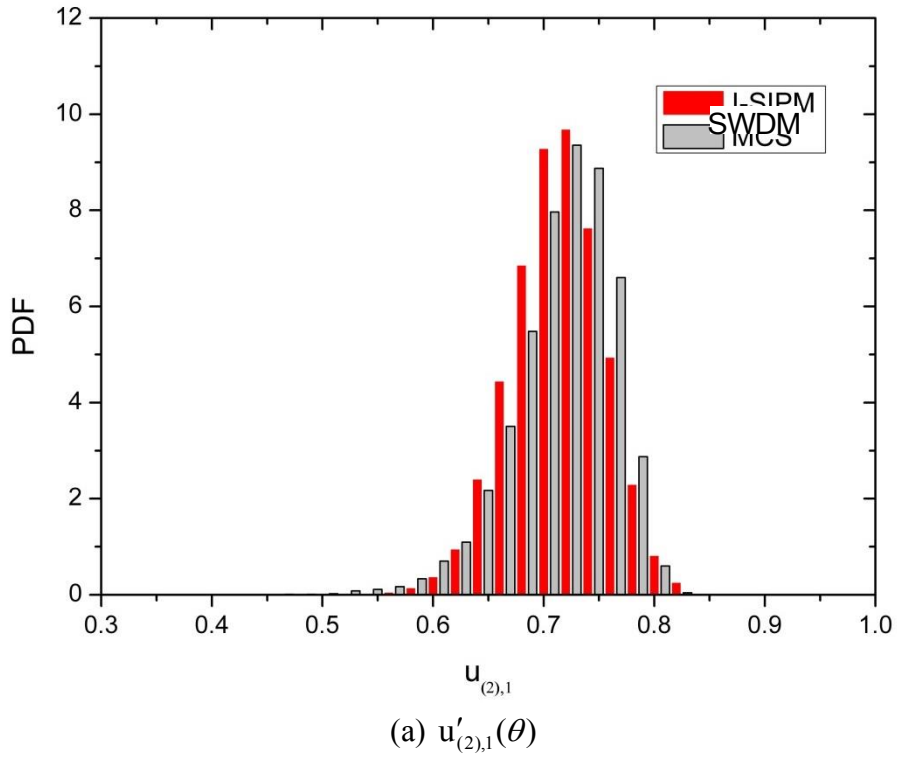


Fig.4.19: The Probability Density Distributions of Eigenvector $\mathbf{u}'_{(2)}(\theta)$

Table 4.9 Statistics of Eigenvector $\mathbf{u}'_{(1)}(\boldsymbol{\theta})$

		I-SIPM	MCS	I-SIPM_PCE
$u'_{(1),1}(\boldsymbol{\theta})$	Mean	-0.8950	-0.8945	-0.8949
	Std.dev.	0.0218	0.0214	0.0218
$u'_{(1),2}(\boldsymbol{\theta})$	Mean	-0.4437	-0.4443	0.4437
	Std.dev.	0.0432	0.0441	0.0438

Table 4.10 Statistics of Eigenvector $\mathbf{u}'_{(2)}(\boldsymbol{\theta})$

		SWDM	MCS	SWDM_PCE
$u'_{(2),1}(\boldsymbol{\theta})$	Mean	0.7000	0.7018	0.7003
	Std.dev.	0.0410	0.0454	0.0417
$u'_{(2),2}(\boldsymbol{\theta})$	Mean	-0.7116	-0.7096	-0.7112
	Std.dev.	0.0423	0.0432	0.0426

Thus, from the results in this section we can conclude that the proposed I-SIPM is valid for evaluating 1st eigenvalue and eigenvector. And the validity of the proposed SWDM is also demonstrated for evaluating 2nd eigenvalue and eigenvector.

4.4.2 A Continuous Beam with Uncertainty in Section Dimension

In this section, a continuous free-standing beam problem (buckling problem shown in Fig.4.20 (a)) is considered to prove that (i) the proposed method can deal with continuous problem, (ii) the method can solve buckling problem, and (iii) the method is valid for solving multi degree of freedom problem.

The buckling problem of a beam is discussed considering beam section dimension H with uncertainty, which is solved by the developed I-SIPM. The mesh is shown in Fig. 4.20(b) and the beam section dimension is shown in Fig. 4.20(c), and the depth H is assumed to be following Gaussian distribution and obeying random variable θ_1 , where $\theta = \{\theta_1\}$. It will be discussed through two cases with the different standard deviation. It is also assumed that the concentrated load $P = 1 \text{ N/mm}^2$, Young's modulus $E = 206000 \text{ N/mm}^2$, the length of beam $l = 5000 \text{ mm}$, and fixed boundary condition is applied to the boundary Γ_1 . The moment of inertia of area about the stronger axis is considered, assuming that the column deflection is supported to its weaker direction. The validity of the proposed method (I-SIPM) is discussed by comparing the results of the deterministic problem for the same condition.

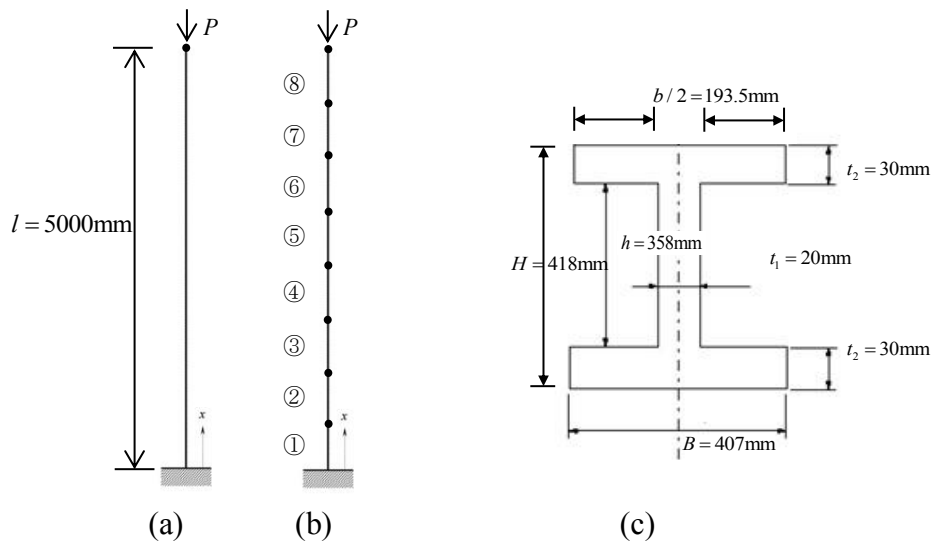


Fig.4.20: Free-Standing Beam

(1) Case (1): The Depth H is Assumed as Including A Small Deviation

In the rule of JIS G3192[42] for tolerance of H-sections, the tolerance of depth (H) is $\pm 3\text{mm}$ when over 400mm in width (B). In this problem, we define the mean of depth as 418mm and the standard deviation as 1mm, so that 3 times of the standard deviation (3σ) becomes equal to 3mm. The statistical properties of uncertain parameter H are given in Table 4.11.

Table 4.11 The Statistical Parameters of Free-Standing Beam

Uncertain parameter	Mean(H_0)	Std.dev.(H_1)
$H(\theta_1)$	418mm	1mm

The parameter depth, H , is represented using a standard normal random variable θ_1 as follows by the above condition.

$$H(\theta_1) = H_0 + H_1\theta_1, \quad (4.59)$$

where H_0 is mean with 418mm, and H_1 is standard deviation with 1mm. The cross section A and the moment of inertia of area I are related to the depth H . In order to construct the element stiffness matrix and the element initial stress matrix considering the uncertainty in depth H , A and I involving uncertainty in depth H is treated as follows.

For H-shaped steel, the equation of cross section A is given as follows.

$$A = BH - bh. \quad (4.60)$$

The cross section $A'(\boldsymbol{\theta})$ with the uncertain parameter is derived by substituting Eq. (4.59) into Eq. (4.60).

$$A'(\boldsymbol{\theta}) = A_0\Psi_0(\boldsymbol{\theta}) + A_1\Psi_1(\boldsymbol{\theta}), \quad (4.61)$$

where $A_0 = BH_0 - bh$, $A_1 = BH_1$.

The moment of inertia of area I is given as follows.

$$I = \frac{BH^3 - bh^3}{12}. \quad (4.62)$$

Substituting Eq. (4.59) into Eq. (4.62), we can derive the moment of inertia of area $I'(\boldsymbol{\theta})$ with uncertain parameter.

$$I'(\boldsymbol{\theta}) = I_0\Psi_0(\boldsymbol{\theta}) + I_1\Psi_1(\boldsymbol{\theta}) + I_2\Psi_2(\boldsymbol{\theta}) + I_3\Psi_3(\boldsymbol{\theta}), \quad (4.63)$$

where, $I_0 = (BH_0^3 - bh + 3BH_0H_1^2)/12$, $I_1 = (BH_0^2H_1 + BH_1^3)/4$, $I_2 = BH_0H_1^2/4$, $I_3 = BH_1^3/12$.

Thus, the element stiffness matrix involving random variables $\boldsymbol{\theta}$ can be derived as follows by the polynomial of 3rd order (See [43] for the formulation of the deterministic problem).

$$\mathbf{k}^{te}(\boldsymbol{\theta}) = \sum_{i=0}^3 \begin{bmatrix} EA_i/l & 0 & 0 & -EA_i/l & 0 & 0 \\ 0 & 12EI_i/l^3 & 6EI_i/l^2 & 0 & -12EI_i/l^3 & 6EI_i/l^2 \\ 0 & 6EI_i/l^2 & 4EI_i/l & 0 & -6EI_i/l^2 & 2EI_i/l \\ -EA_i/l & 0 & 0 & EA_i/l & 0 & 0 \\ 0 & -12EI_i/l^3 & -6EI_i/l^2 & 0 & 12EI_i/l^3 & -6EI_i/l^2 \\ 0 & 6EI_i/l^2 & 2EI_i/l & 0 & -6EI_i/l^2 & 4EI_i/l \end{bmatrix} \Psi_i(\boldsymbol{\theta}). \quad (4.64)$$

And the element initial stress matrix is as follows. ($\Psi_0(\boldsymbol{\theta}) = 1$)

$$\mathbf{k}_G^e = P \begin{bmatrix} 1/l & 0 & 0 & -1/l & 0 & 0 \\ 0 & 6/5l & 1/10 & 0 & -6/5l & 1/10 \\ 0 & 1/10 & 2l/15 & 0 & -1/10 & -l/30 \\ -1/l & 0 & 0 & 1/l & 0 & 0 \\ 0 & -6/5l & -1/10 & 0 & 6/5l & -1/10 \\ 0 & 1/10 & -l/30 & 0 & -1/10 & 2l/15 \end{bmatrix} \Psi_0(\boldsymbol{\theta}). \quad (4.65)$$

By assembly of element system, we can derive a global equation system which has 24 degrees of freedom. The eigenvalue is derived by solving Eq.(4.3) in which $\mathbf{R}'(\boldsymbol{\theta})$ is initial stress matrix with deterministic (Eq.(4.65)) and $\mathbf{K}'(\boldsymbol{\theta})$ is stiffness matrix with uncertainty (Eq.(4.64)).

In Fig.4.21, we show the obtained response surface of the buckling load (1st eigenvalue) which is represented by Eq.(4.66) . The approximate expression of the response surface is 5th order PCE. However, only the 1st order approximate expression of the response surface is shown because the influence is small after the 2nd order. And we can see that a good agreement is observed between the results from the stochastic response surface and the reference values by usual theoretical formula.

$$P(\boldsymbol{\theta}) = 2.028 \times 10^7 \Psi_0(\boldsymbol{\theta}) + 3.615 \times 10^5 \Psi_1(\boldsymbol{\theta}). \quad (4.66)$$

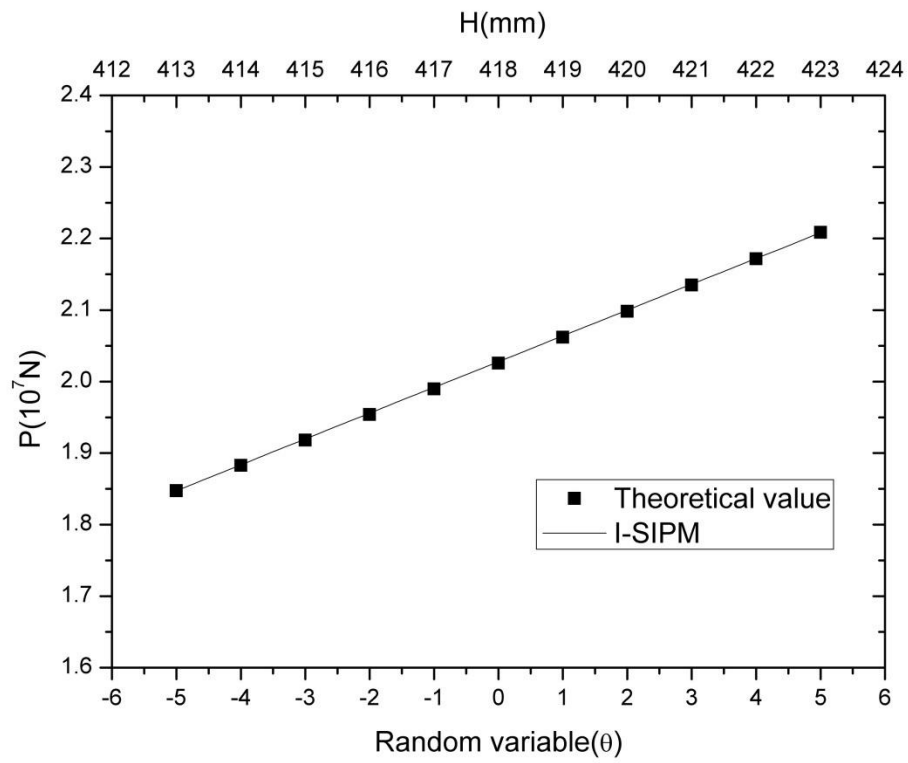


Fig. 4.21: The Response Surface of the Buckling Load

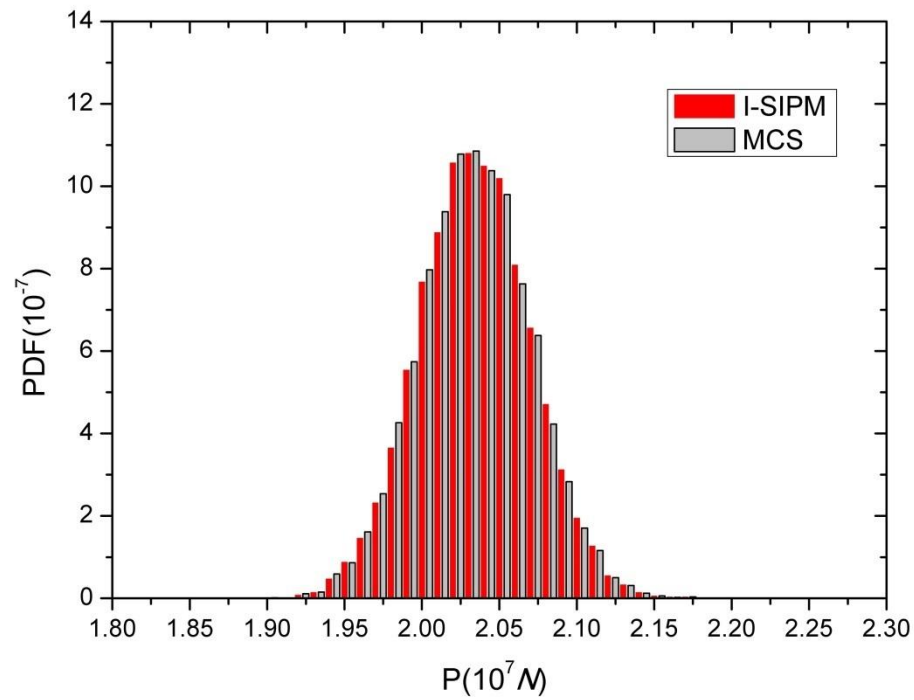


Fig. 4.22: The Probability Density Distributions of the Buckling Load

In Fig.4.22, the probability density distributions are also shown to prove that the results are well consistent with MCS results. Also, as shown in Table 4.12, we find that the statistics are reasonably well estimated by the proposed I-SIPM when compared with those obtained from MCS. Note that the mean and the standard deviation of “I-SIPM-PCE” in the Table 4.12 are calculated by Eq. (2.7) and Eq. (2.8), which also takes almost same value.

Table 4.12 Statistics of the Buckling Load ($\times 10^7$ N)

	I-SIPM	MCS	I-SIPM_PCE
Mean	2.028	2.026	2.028
Std.dev.	0.036	0.036	0.036

From the results in this section, it can be concluded that the proposed methodology can effectively evaluate (i) the continuous problem, (ii) the buckling problem, and (iii) the multi degree of freedom problem.

It is observed that the linear responses of buckling load (see Fig.4.21) is obtained even though the input parameter \mathbf{K} is PCE of 3th order because the variability of the depth H is very small(the standard deviation is 1mm) then the input parameter \mathbf{K} is considered as liner ($I_2 = I_3 \approx 0$ in Eq.(4.63)). In following case, we will discuss that the depth H has a relatively large deformation to validate the reason.

(2) Case (2): The Depth H is Assumed as Including A Large Deviation

In this case, we define the mean of depth as 418mm and the standard deviation as 12mm, and the statistical properties of uncertain parameter H are given in Table 4.13.

Table 4.13 The Statistical Parameters of Free-Standing Beam

Uncertain parameter	Mean(H_0)	Std.dev.(H_1)
$H(\theta_1)$	418mm	12mm

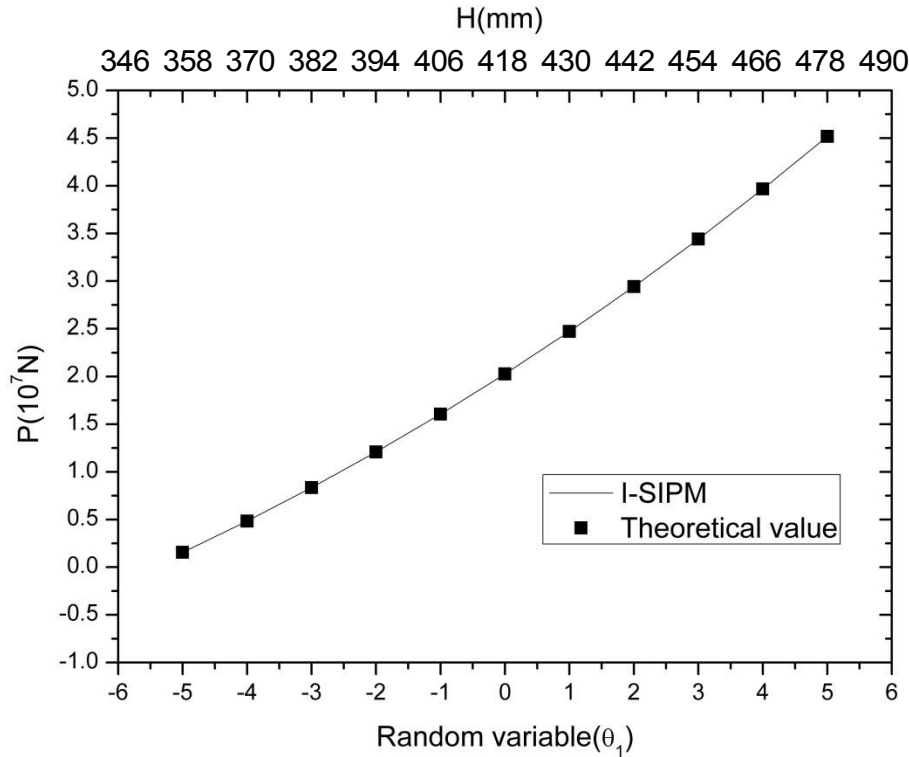


Fig. 4.23: The Response Surface of the Buckling Load

In Fig.4.23 and Eq.4.67, we show the response surface of the buckling load which is obtained by the proposed method Eq.(4.67) . The approximate expression of the response surface is 5th order PCE. However, the 3st order approximate expression of the response surface is shown because the influence is small after the 4th order. And we can see that a good agreement is observed even if the standard deviation become as a large value. As shown Fig4.23 we also find that a nonlinear result (response surface) is obtained compared with linear response Fig.4.21 when the large standard deviation is considered.

$$P(\boldsymbol{\theta}) = 2.040 \times 10^7 \Psi_0(\boldsymbol{\theta}) + 4.341 \times 10^6 \Psi_1(\boldsymbol{\theta}) + 1.245 \times 10^5 \Psi_2(\boldsymbol{\theta}) + 1.191 \times 10^3 \Psi_3(\boldsymbol{\theta}). \quad (4.67)$$

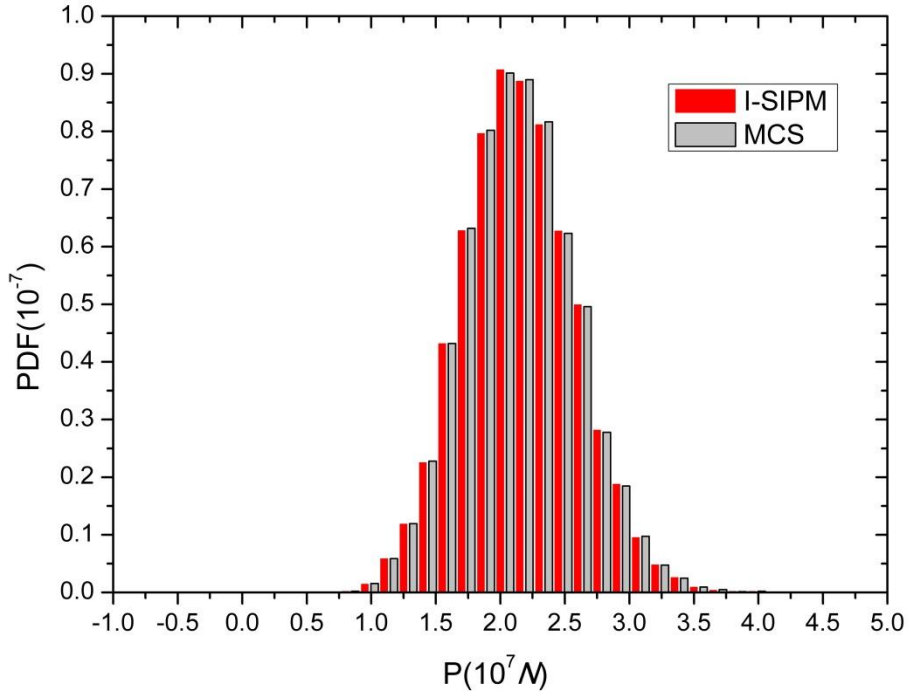


Fig. 4.24: The Probability Density Distributions of the Buckling Load

In Fig.4.24, the probability density distributions are also shown to prove that the results are well consistent with MCS results. Also, as shown in Table 4.14, we find that the statistics are reasonably well estimated by the proposed I-SIPM and I-SIPM-PCE when compared with those obtained from MCS.

Table 4.14 Statistics of the Buckling Load ($\times 10^7 N$)

	I-SIPM	MCS	I-SIPM_PCE
Mean	2.040	2.038	2.040
Std.dev.	0.434	0.434	0.434

And we can find that the buckling load when the depth H is ‘Meam-1 Std.dev.’ (406mm) is 1.6×10^7 , then the buckling load is reduced 25% compared with that at the mean value (418mm). Also, the buckling load when the depth H is ‘Meam-3 Std.dev.’ (382mm) is 8.4×10^6 , then the buckling load is reduced 49% compared with that at the mean value (418mm). That is, even if the depth H has a small variability, the buckling load also will greatly change. This is very dangerous from the viewpoint of structural safety.

4.4.3 A Beam with Uncertainty in Young’s Modulus

In this section, the buckling problem of a beam is discussed considering Young’s modulus with uncertainty, which is solved by the developed I-SIPM. The mesh is shown in Fig. 4.25(b) and the beam section dimension is shown in Fig. 4.25(c). It is assumed that the concentrated load $P=1 \text{ N/mm}^2$, the length of beam $l=5000\text{mm}$, and fixed and supported boundary condition are applied to the boundary Γ_1 and Γ_2 respectively. As uncertainty parameter, the Young’s modulus E in some elements is assumed to be following Gaussian distribution and obeying random variable θ_1 , where $\boldsymbol{\theta} = \{\theta_1\}$. The assumptions of Young’s modulus for each element are given in Table 4.15. The moment of inertia of area about the stronger axis is considered, assuming that the column deflection is supported to its weaker direction. The validity of the proposed method (I-SIPM) is discussed by comparing the results of the deterministic problem for the same condition.

Table 4.15 The Statistical Parameters of Young's Modulus (N/mm^2)

Element number		parameter	Mean(E_0)	Std.dev.(E_1)
1,2,6,7,8	Deterministic	E	206000	0
3,4,5	Uncertainty	E	400000	80000

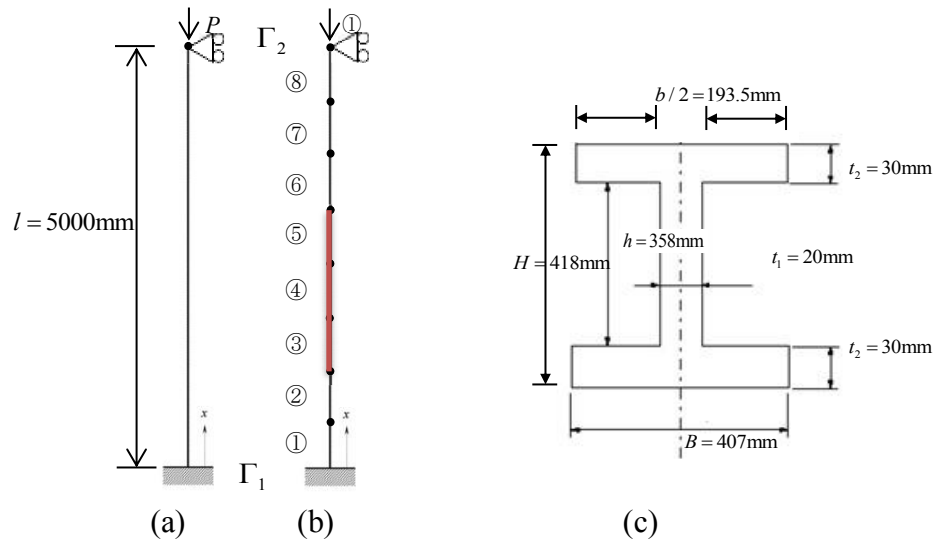


Fig.4.25: Free-Standing Beam

In Fig.4.26, we show the response surface of the buckling load which is obtained by the proposed method and represented by Eq.(4.68) . The approximate expression of the response surface is 4th order PCE. And we can see that a good agreement is observed between the results from the stochastic response surface and the reference values by usual theoretical formula.

$$\begin{aligned}
 P(\boldsymbol{\theta}) = & 3.38 \times 10^8 \Psi_0(\boldsymbol{\theta}) + 1.33 \times 10^7 \Psi_1(\boldsymbol{\theta}) - 2.58 \times 10^6 \Psi_2(\boldsymbol{\theta}) \\
 & + 4.92 \times 10^5 \Psi_3(\boldsymbol{\theta}) - 8.32 \times 10^4 \Psi_4(\boldsymbol{\theta}) .
 \end{aligned}
 \tag{4.68}$$

In Fig.4.27, the probability density distributions are also shown to prove that the results are well consistent with MCS results. Also, as shown in Table 4.16, we find that the statistics are reasonably well estimated by the proposed I-SIPM when compared with those obtained from MCS. Note that the mean and the standard deviation of “I-SIPM-PCE” in the Table 4.16 are calculated by Eq. (2.7) and Eq. (2.8), which also takes almost same value.

Table 4.16 Statistics of the Buckling Load ($\times 10^8$ N)

	I-SIPM	MCS	I-SIPM_PCE
Mean	3.382	3.382	3.382
Std.dev.	0.137	0.139	0.138

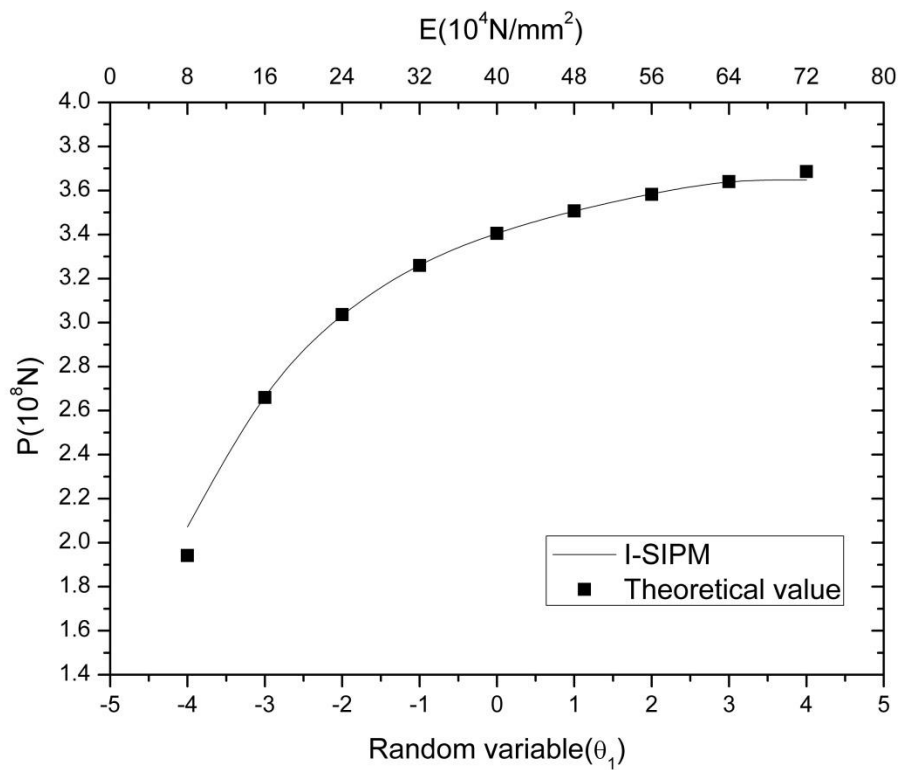


Fig. 4.26: The Response Surface of the Buckling Load

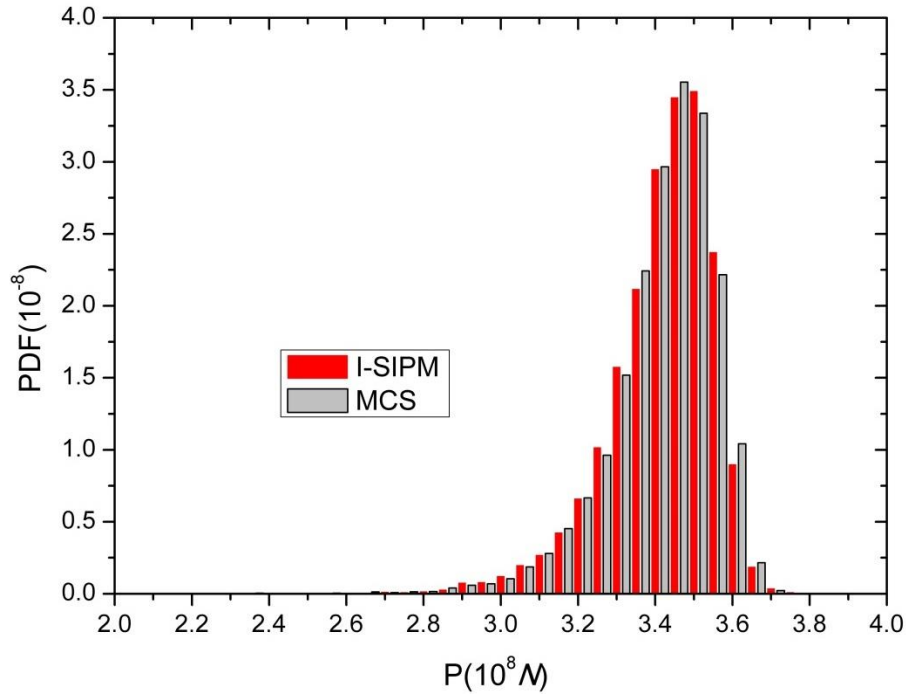


Fig. 4.27: The Probability Density Distributions of the Buckling Load

In Fig.4.28, we show the buckling mode with $n=1$ which is obtained by using I-SIPM, and Fig.4.29 shows the buckling mode with $n=1$ which is obtained by usual theoretical formula when the θ is value form -4 to 4. We can see that a good agreement is observed between the buckling mode from I-SIPM and the reference values. And we also find that the buckling mode dose not change greatly when consider the Young's modulus of element 3,4,5 with uncertainty. However, we can find that when the Young's modulus of element 3,4,5 is large (for example $\theta=4$), the shape of the element 3,4,5 approach line compare with small Young's modulus(for example $\theta=-4$).

Form the results in this section, we can conclude that the proposed method is valid for the beam problem with uncertainty in Young's modulus (middle element with uncertainty). And it is understood that the buckling load has large changes, whereas the buckling mode dose not change greatly, when the Young's modulus of the elements 3,4,5 is changes between 8×10^4 to 72×10^4 .

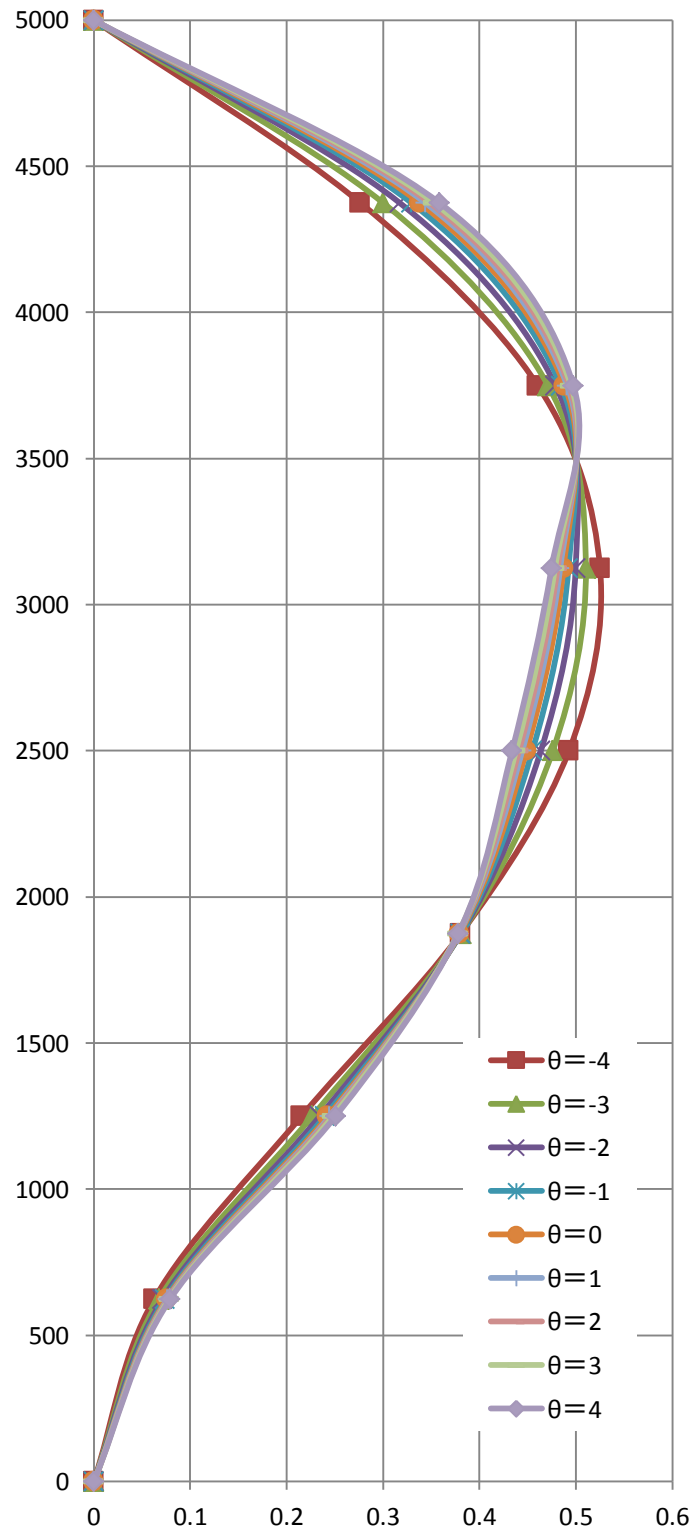


Fig.4.28: The Buckling Mode 1 by using I-SIPM

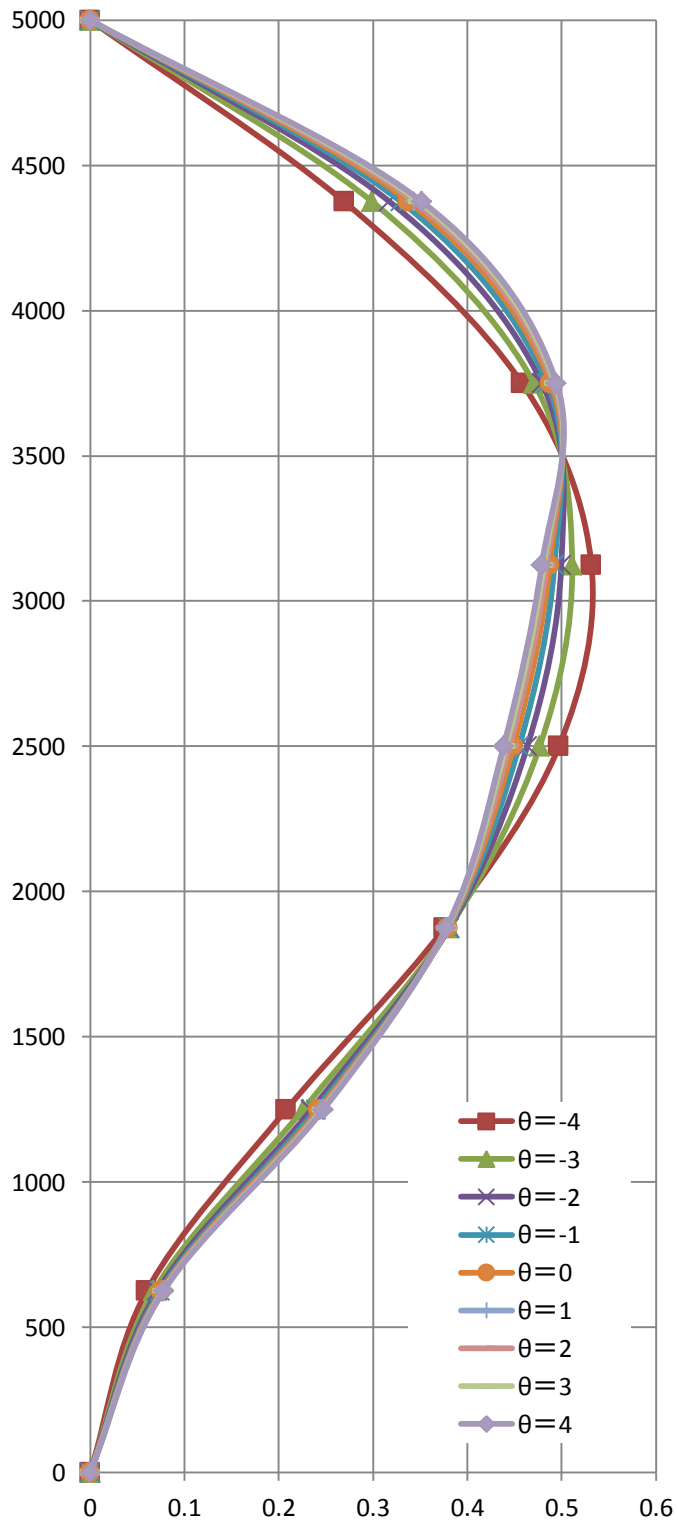


Fig.4.29: The Buckling Mode 1 by usual theoretical formula

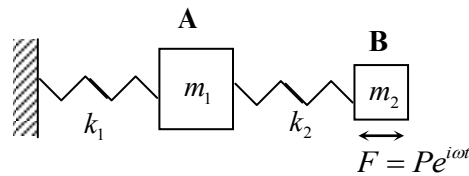
4.4.4 The Dynamic Damper

The validity and feasibility of the proposed methods is concluded by the previous two examples for vibrations problems and buckling problems. In this section, we will discuss a dynamic damper problem as a more practical example in which stiffness and mass are considered as uncertain parameters. The probability of resonance occurrence of ship structure is studied by using the developed I-SIPM.

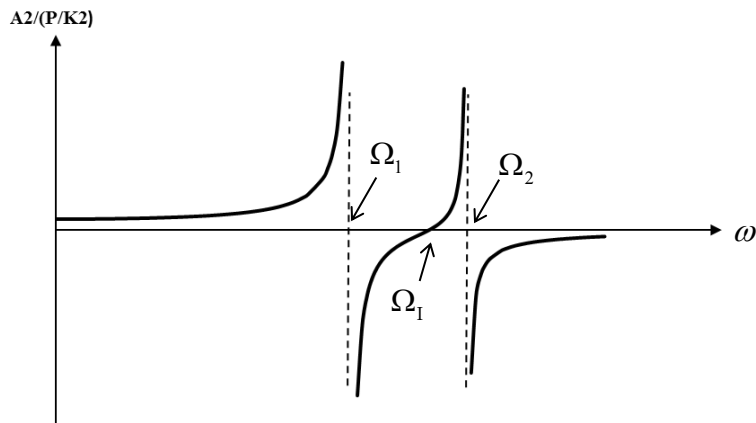
(1) Concepts of Dynamic Damper

A dynamic damper is a tuned spring-mass system which can reduce or eliminates the resonance of a system when the exciting frequently is close to the natural frequencies of the system.

Here, in order to illustrate basic theory of dynamic damper, we consider the 2DOF system (without the dynamic damper attached) in Fig. 4.30(a), and resonance curve for the main mass B of the 2DOF system is shown in Fig.4.30 (b). We can see that the system will be causing resonance when the exciting frequency (ω) equals the first order natural frequency (Ω_1) of the system, and it can cause severe problems for the vibrating systems.



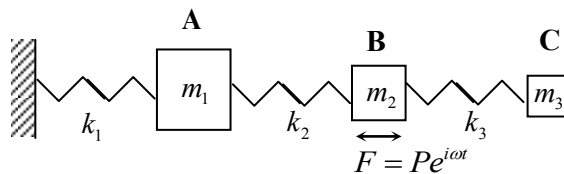
(a) 2DOF system



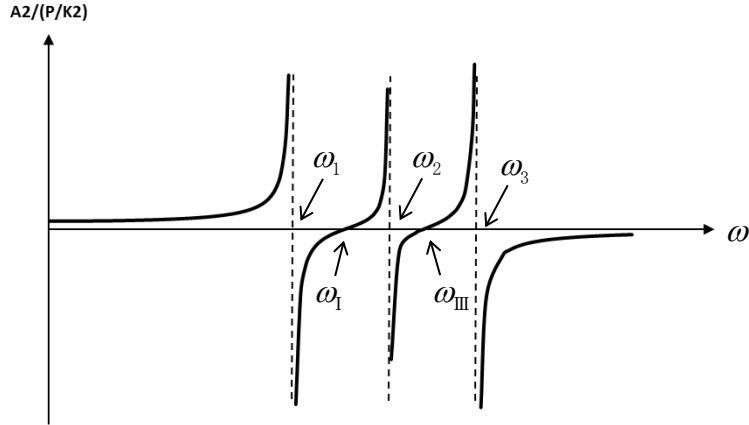
(b) Resonance curve for DOF system

Fig. 4.30: The 2DOF System (Without the Dynamic Damper Attached)

However, when a dynamic damper is considered, it can be considered as the 3DOF system as shown in Fig.4.31 (a). And we also show the resonance curve for the main mass **B** of the 3DOF system in Fig.4.31 (b). It can be seen that when a mass-spring system (dynamic damper **C**) is attached to the main mass **B** so that the ω_1 in Fig.4.31(b) matches to the first natural frequency (Ω_1) of the system with the main mass **A** and **B**(Fig.4.30(b)), the motion of the main mass **B** is reduced to zero at its resonance frequency. This is because the system has changed from the 2-DOF system to the 3-DOF system and now has three natural frequencies. That is, the first and the second order natural frequencies of the 3-DOF system avoid the exciting frequency (the first order natural frequency (Ω_1) of the 2DOF system). Thus attaching a dynamic damper with appropriate mass and stiffness can achieve to avoid resonance. In following section, selection methods for the mass and stiffness of a dynamic damper will be introduced.



(a) 3DOF system



(b) Resonance curve for 3DOF system

Fig. 4.31: 3DOF System (The Dynamic Damper Attached)

(2) Selection Methods for the Mass and Stiffness of A Dynamic Damper [44]

First, we calculate the natural frequencies the 2-DOF undamped system in Fig.4.30 (a).

We can get the equations of motion as follows.

$$\begin{aligned} m_1 \ddot{x}_1 + (k_1 + k_2)x_1 - k_2 x_2 &= 0, \\ m_2 \ddot{x}_2 - k_2 x_1 + k_2 x_2 &= P e^{i\omega t}, \end{aligned} \quad (4.69)$$

where, x_1 and x_2 are variables describing the motion, and the m_1 and m_2 are mass of **A** and **B**, the k_1 and k_2 are stiffness of **A** and **B**. Eq. (4.69) can be rewritten as a matrix form.

$$\begin{bmatrix} m_1 & 0 \\ 0 & m_2 \end{bmatrix} \begin{bmatrix} \ddot{x}_1 \\ \ddot{x}_2 \end{bmatrix} + \begin{bmatrix} k_1 + k_2 & -k_2 \\ -k_2 & k_2 \end{bmatrix} \begin{bmatrix} x_1 \\ x_2 \end{bmatrix} = \begin{bmatrix} 0 \\ P e^{i\omega t} \end{bmatrix}. \quad (4.70)$$

The displacement and the second derivative of the displacement can be described by the following equations.

$$\begin{aligned}
\begin{bmatrix} x_1 \\ x_2 \end{bmatrix} &= \begin{bmatrix} A_1 \\ A_2 \end{bmatrix} e^{i\omega t}, \\
\begin{bmatrix} \dot{x}_1 \\ \dot{x}_2 \end{bmatrix} &= i\omega \begin{bmatrix} A_1 \\ A_2 \end{bmatrix} e^{i\omega t}, \\
\begin{bmatrix} \ddot{x}_1 \\ \ddot{x}_2 \end{bmatrix} &= -\omega^2 \begin{bmatrix} A_1 \\ A_2 \end{bmatrix} e^{i\omega t},
\end{aligned} \tag{4.71}$$

where A_1 and A_2 are constants that denote the maximum amplitudes of x_1 and x_2 . Substituting Eq. (4.71) into Eq. (4.70), we have following equation.

$$-\omega^2 \begin{bmatrix} A_1 \\ A_2 \end{bmatrix} + \begin{bmatrix} \frac{k_1+k_2}{m_1} & -\frac{k_2}{m_1} \\ -\frac{k_2}{m_2} & \frac{k_2}{m_2} \end{bmatrix} \begin{bmatrix} A_1 \\ A_2 \end{bmatrix} = \begin{bmatrix} 0 \\ \frac{P}{m_2} \end{bmatrix}. \tag{4.72}$$

Rearranging Eq.(4.72), we can obtain the maximum amplitudes of x_1 and x_2 .

$$\begin{bmatrix} A_1 \\ A_2 \end{bmatrix} = \frac{P/m_2}{(\Omega_1^2 - \omega^2)(\Omega_2^2 - \omega^2)} \begin{bmatrix} \frac{k_2}{m_1} \\ \Omega_1^2 - \omega^2 \end{bmatrix}. \tag{4.73}$$

By Eq.(4.73), we can see that the amplitudes of the main mass \mathbf{B} can be shown as follows.

$$A_2 = \frac{P/m_2}{(\Omega_1^2 - \omega^2)(\Omega_2^2 - \omega^2)} (\Omega_1^2 - \omega^2). \tag{4.74}$$

The resonance will cause when the $\omega = \Omega_1, \omega = \Omega_2$.

Next, we calculate the natural frequencies the 3-DOF undamped system in which the mass and the stiffness of the dynamic damper are m_3 and k_3 in Fig.4.31 (a).

We can get the equations of motion as follows.

$$\begin{aligned}
m_1 \ddot{x}_1 + (k_1 + k_2)x_1 - k_2 x_2 &= 0, \\
m_2 \ddot{x}_2 - k_2 x_1 + (k_2 + k_3)x_2 - k_3 x_3 &= P e^{i\omega t}, \\
m_3 \ddot{x}_3 - k_3 x_2 + k_3 x_3 &= 0,
\end{aligned} \tag{4.75}$$

where, x_1, x_2, x_3 is variables describing the motion. Eq. (4.75) can be rewritten as a matrix form.

$$\begin{bmatrix} m_1 & 0 & 0 \\ 0 & m_2 & 0 \\ 0 & 0 & m_3 \end{bmatrix} \begin{bmatrix} \ddot{x}_1 \\ \ddot{x}_2 \\ \ddot{x}_3 \end{bmatrix} + \begin{bmatrix} k_1 + k_2 & -k_2 & 0 \\ -k_2 & k_2 + k_3 & -k_3 \\ 0 & -k_3 & k_3 \end{bmatrix} \begin{bmatrix} x_1 \\ x_2 \\ x_3 \end{bmatrix} = \begin{bmatrix} 0 \\ P e^{i\omega t} \\ 0 \end{bmatrix}. \tag{4.76}$$

The displacement and the second derivative of the displacement can be described by following equation.

$$\begin{aligned}
\begin{bmatrix} x_1 \\ x_2 \\ x_3 \end{bmatrix} &= \begin{bmatrix} A_1 \\ A_2 \\ A_3 \end{bmatrix} e^{i\omega t}, \\
\begin{bmatrix} \dot{x}_1 \\ \dot{x}_2 \\ \dot{x}_3 \end{bmatrix} &= i\omega \begin{bmatrix} A_1 \\ A_2 \\ A_3 \end{bmatrix} e^{i\omega t}, \\
\begin{bmatrix} \ddot{x}_1 \\ \ddot{x}_2 \\ \ddot{x}_3 \end{bmatrix} &= -\omega^2 \begin{bmatrix} A_1 \\ A_2 \\ A_3 \end{bmatrix} e^{i\omega t},
\end{aligned} \tag{4.77}$$

where A_1, A_2 and A_3 are constants that denote the maximum amplitudes of x_1, x_2 and x_3 , respectively. Substituting Eq. (4.77) into Eq. (4.76), and rearranging we have following equation.

$$\begin{bmatrix} \frac{k_1+k_2}{m_1}-\omega^2 & -\frac{k_2}{m_1} & 0 \\ -\frac{k_2}{m_2} & \frac{k_2+k_3}{m_2}-\omega^2 & -\frac{k_3}{m_2} \\ 0 & -\frac{k_3}{m_3} & \frac{k_3}{m_3}-\omega^2 \end{bmatrix} \begin{bmatrix} A_1 \\ A_2 \\ A_3 \end{bmatrix} = \begin{bmatrix} 0 \\ \frac{P}{m_2} \\ 0 \end{bmatrix}. \quad (4.78)$$

We can obtain the maximum amplitudes of x_1 , x_2 and x_3 as follows.

$$\begin{bmatrix} A_1 \\ A_2 \\ A_3 \end{bmatrix} = \begin{bmatrix} \frac{k_1+k_2}{m_1}-\omega^2 & -\frac{k_2}{m_1} & 0 \\ -\frac{k_2}{m_2} & \frac{k_2+k_3}{m_2}-\omega^2 & -\frac{k_3}{m_2} \\ 0 & -\frac{k_3}{m_3} & \frac{k_3}{m_3}-\omega^2 \end{bmatrix}^{-1} \begin{bmatrix} 0 \\ \frac{P}{m_2} \\ 0 \end{bmatrix} \quad (4.79)$$

$$= \frac{P/m_2}{(\omega_1^2 - \omega^2)(\omega_{II}^2 - \omega^2)(\omega_{III}^2 - \omega^2) - (\omega_1^2 - \omega^2)\left(\frac{k_3^2}{m_2 m_3}\right) - (\omega_{III}^2 - \omega^2)\left(\frac{k_2^2}{m_1 m_2}\right)} \begin{bmatrix} (\omega_{III}^2 - \omega^2)\frac{k_2}{m_1} \\ (\omega_1^2 - \omega^2)(\omega_{III}^2 - \omega^2) \\ (\omega_1^2 - \omega^2)\frac{k_3}{m_3} \end{bmatrix},$$

where, $\omega_1^2 = \frac{k_1+k_2}{m_1}$, $\omega_{II}^2 = \frac{k_2+k_3}{m_2}$, $\omega_{III}^2 = \frac{k_3}{m_3}$ (see Fig.4.31(b)), By Eq.(4.79), we can see that

the amplitudes of the main mass **B** can be equal to 0 when

$\omega^2 = \omega_1^2 = \frac{k_1+k_2}{m_1}$, $\omega^2 = \omega_{III}^2 = \frac{k_3}{m_3}$ as shown in Fig.4.31(b). By using the condition, the

mass and stiffness of the dynamic damper is satisfying the following conditions to avoid resonance of the first order natural frequency (Ω_1) of the 2DOF system.

$$\omega_{III}^2 = \frac{k_3}{m_3} = \Omega_1^2. \quad (4.80)$$

Thus, the relationship between mass (m_3) and stiffness (k_3) can be shown by Eq.(4.80) when the mass (m_3) is considered as a fixed value, the stiffness (k_3) can be calculated by using the mass of dynamic damper (m_3) and the first order natural frequency (Ω_1) of the 2DOF system.

Based on the above, in the following section, we will discuss the resonance of the superstructure of a ship.

(3) Modelling and Condition

In large ship structures, the resonance of the superstructure of a ship to engine or propeller exciting force is an important problem. In order to reduce the resonance response of the superstructure, the dynamic damper is attracted as a counterplan of avoiding resonance [45]. The main structure **A** and the dodger **B** are shown in Fig.4.32. A simple model of two degrees of freedom (Fig.4.33 (a)) is proposed to model the superstructure of the ship and the dodger in Fig.4.32. And when the dynamic damper attached on the dodger **B** is considered, we can use a simple model of the three degrees of freedom to model the system where k_3 and m_3 represent the dynamic damper system (Fig.4.33 (b)).

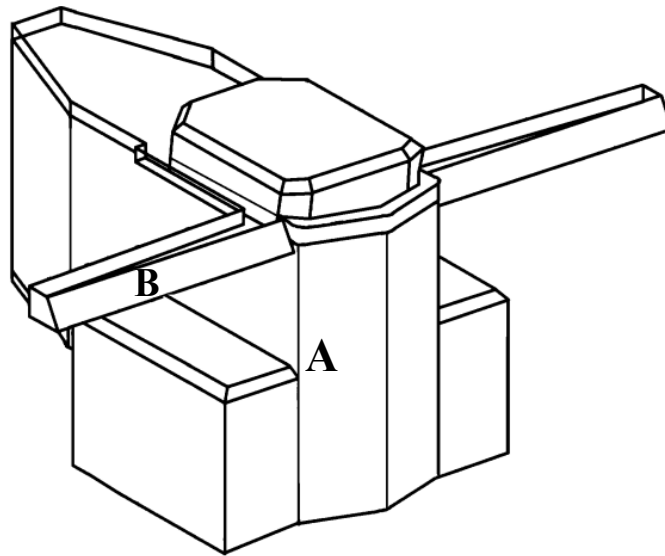


Fig.4.32: Superstructure

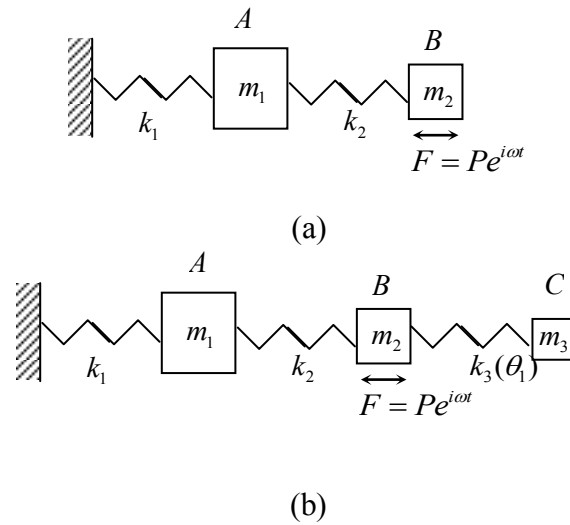


Fig.4.33: Superstructure (Simple Model)

In this example, it is considered that first order natural frequency of two degrees of freedom (Fig.4.33 (a)) is close to the fourth order exciting frequency component of the main engine. So the system will produce serious vibration with large amplitude. And we can understand that when the dynamic damper is attached (three degrees of freedom (Fig.4.33 (b)), the first order natural frequency will be decreased so that the fourth order exciting frequency can be avoided. However, there is a possibility that the first order natural frequency of the three degrees of freedom becomes close to the third order exciting frequency component of the main engine (That is, the first order natural frequency is probably entering the range between third order and fourth order exciting frequency component of the main engine.). Thus, we will discuss the problem to avoid the third and the fourth order exciting frequencies of the main engine in the following.

As problem conditions, it is assumed that the third order exciting frequency component of the main engine is 4Hz ($3^{\text{rd}}\text{order} \times 80\text{rpm}/60$), and the fourth order exciting frequency component of the main engine is 5.33Hz ($4^{\text{th}}\text{order} \times 80\text{rpm}/60$) with main engine with normal revolution of 80rpm[46]. In order to avoid resonance, it is necessary to avoid ranges of the third order and fourth order exciting frequency of the main engine which are assumed as 3.8Hz ~ 4.2Hz ($\pm 5\%$ of 4Hz), 5.07Hz ~ 5.60Hz ($\pm 5\%$ of 5.33Hz), respectively. The image is shown in Fig.4.34.

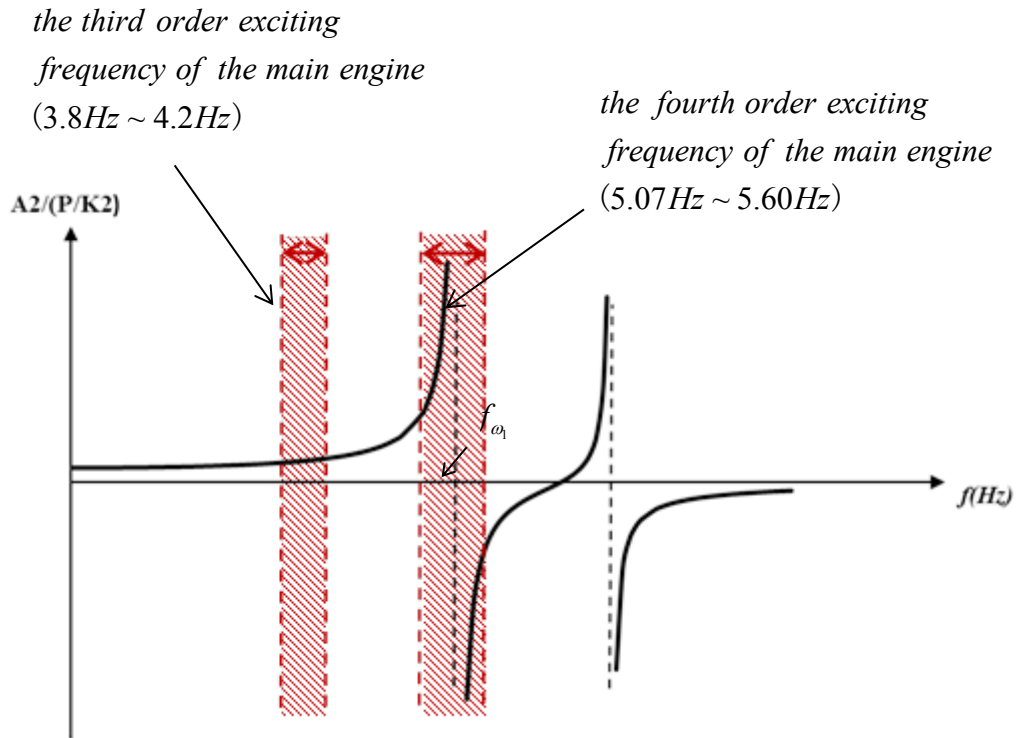


Fig.4.34: The Image for Ranges of the Third Order and the Fourth Order Exciting Frequency of the Main Engine

Table 4.17 The Parameters of Model (Deterministic Parameters)

Structure	The spring stiffness(N/m)	The mass (kg)
The main structure A	$k_1 = 7.27 \times 10^8$	$m_1 = 1.8 \times 10^5$
The dodger B	$k_2 = 2.31 \times 10^7$	$m_2 = 2.0 \times 10^4$

The parameters of model are assumed as shown in Table 4.17 which is a practical assumption by the references [47][48]. As a result of the coupled vibration of the main structure and the dodger, the first and the second order natural frequencies are calculated to be 5.30Hz and 10.33Hz, respectively. The first order natural frequency is completely within the range of fourth order exciting frequency of the main engine, very possibly causing excessive vibration of the superstructure. To avoid this resonance, the two cases are discussed in the following:

- 1) The spring stiffness of the dynamic damper is assumed as including random variable θ_1 and the mass is deterministic value (see section (4)).
- 2) The spring stiffness of the dynamic damper is assumed as including a random variable θ_1 , and the mass of dynamic damper is assumed as including another random variable, θ_2 (see section (5)).

(4) The Spring Stiffness of Dynamic Damper with Uncertainty

In this case, the spring stiffness with uncertainty is discussed through different values of the mass of the dynamic damper. In Table 4.18, the statistical properties of the two cases are given. In both cases, the spring stiffness of the dynamic damper is assumed to be following Gaussian distribution and obeying random variable θ_1 . Also in case (1), the mass is deterministic value with $\mu = 1/110$, and in case (2), the mass is deterministic value with $\mu = 1/40$. Note that μ is defined as $\mu = m_3/m_2$. The general relationship between the spring stiffness and the mass of the dynamic damper can be found from the dynamic damper theory in section (2)(Eq.4.80).

Table 4.18 The Statistical Parameters of the Dynamic Damper

Case	The spring stiffness (N/m) (Uncertain parameters)		The mass (m_3) (kg) ($\mu = m_3/m_2$)
	Mean ($k_{3\mu}$)	Standard deviation ($k_{3\sigma}$)(C.V. is 8%)	(deterministic value)
(1)	1.995×10^5	1.596×10^4	180($\mu = 1/110$)
(2)	5.542×10^5	4.434×10^4	500($\mu = 1/40$)

Here, the system stiffness matrix involving random variables θ can be derived as follows.

$$\begin{aligned}
 \mathbf{K}'(\theta) &= \begin{bmatrix} k_1 + k_2 & -k_2 & 0 \\ -k_2 & k_2 + k_3(\theta_1) & -k_3(\theta_1) \\ 0 & -k_3(\theta_1) & k_3(\theta_1) \end{bmatrix} \\
 &= \begin{bmatrix} k_1 + k_2 & -k_2 & 0 \\ -k_2 & k_2 + k_{3\mu} & -k_{3\mu} \\ 0 & -k_{3\mu} & k_{3\mu} \end{bmatrix} \Psi_0(\theta) \\
 &+ \begin{bmatrix} k_1 + k_2 & -k_2 & 0 \\ -k_2 & k_2 + k_{3\sigma} & -k_{3\sigma} \\ 0 & -k_{3\sigma} & k_{3\sigma} \end{bmatrix} \Psi_1(\theta),
 \end{aligned} \tag{4.81}$$

where, $k_{3\mu}$ is mean of the spring stiffness of the dynamic damper and $k_{3\sigma}$ is standard deviation. And the system mass matrix is represented as follows.

$$\mathbf{M} = \begin{bmatrix} m_1 & 0 & 0 \\ 0 & m_2 & 0 \\ 0 & 0 & m_3 \end{bmatrix} \Psi_0(\theta) \quad (\Psi_0(\theta) = 1). \tag{4.82}$$

The matrix $\mathbf{A}'(\boldsymbol{\theta})$ in Eq.(4.3) can be obtained by using Eq.(4.81) and Eq.(4.82), and we solve Eq.(4.3) by using the proposed I-SIPM. When the spring stiffness k_3 is considered as uncertain parameter, the first order natural frequency is considered as uncertain response which will be described as probability distribution. So the stochastic eigenvalue can be evaluated to observe the probability of resonance occurrence.

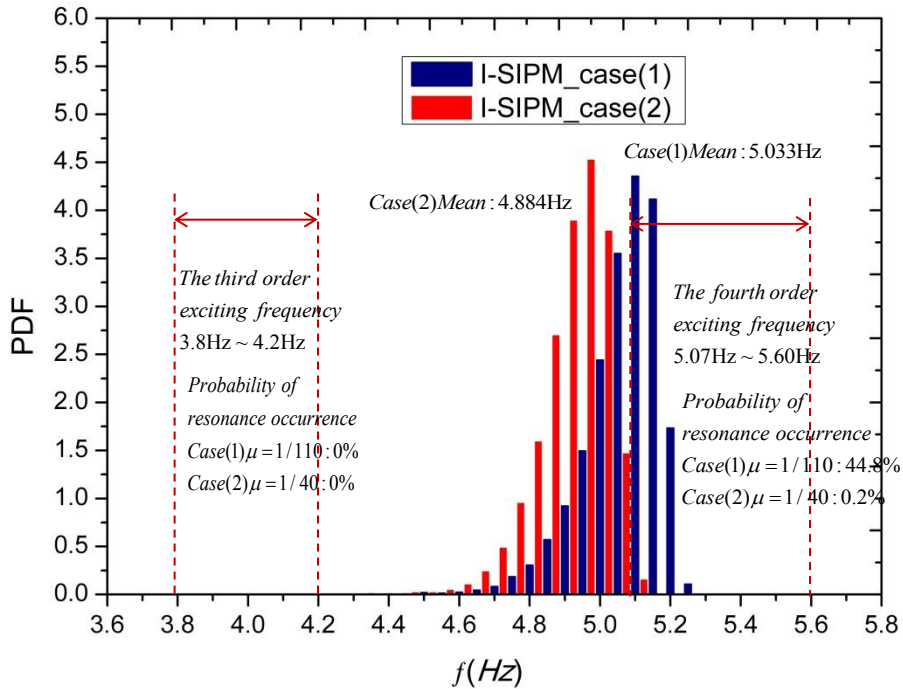


Fig.4.35: The Probability Density Distributions of First Order Frequency.
(The Spring Stiffness with Uncertainty)

In Fig.4.35, the probability density distributions of first order natural frequency are shown for the case (1) and the case (2). As can be seen, in both cases, the mean values of the first order natural frequency are moving toward the range of third order exciting frequency of the main engine and are out of the range of the fourth order exciting frequency of the main engine. However, they are more closer to the range of fourth order exciting frequency of the main engine, while the resonance due to the third order exciting frequency of the main

engine is completely avoided.

In case (1), when the mass is 180kg, observing the blue histogram in Fig.4.33, we can see that the resonance due to the fourth order exciting frequency cannot be avoided because the first order natural frequency has a probabilistic nature and the most of the right of the distribution overlaps with the fourth order exciting frequency range. The probability of resonance occurrence reaches up to 44.8%. This is very dangerous because of a large probability of resonance occurrence for this practical problem.

In case (2), we attempt to increase the mass of the dynamic damper to 500kg to discuss the probability of resonance occurrence. Here the probability density distribution is shown in Fig.4.35. Observing the red histogram, we can see that the probability density distribution of the first order natural frequency moves to more left when the mass ratio μ becomes larger compared with case(1). And the probability becomes smaller for entering the range of the fourth order exciting frequency of the main engine. It should be clear that the probability of resonance occurrence becomes a small value, 0.2%.

So we can understand that when the mass ratio μ becomes larger, the probability density distribution of the first order natural frequency moves closer to the range of the third order exciting frequency of the main engine compared with a small mass ratio, and the probability of resonance occurrence becomes smaller. From the synthetically viewpoint considering the probability of resonance occurrence and the economic cost, the appropriate selection of the mass is necessary.

Regarding the second order natural frequency, the probability of resonance occurrence can be evaluated in the same manner using SWDM. Here, we have confirmed that the natural frequency is sufficiently above the range of fourth order exciting frequency of the main engine, and the probability of resonance occurrence is very small, both in case (1) and in case (2).

(5) Both the Spring Stiffness and Mass of Dynamic Damper with Uncertainty

In this case, both the spring stiffness and the mass with uncertainty are discussed through different mean values of the mass of the dynamic damper. The statistical properties of two cases are given in Table 4.19. In both cases, the spring stiffness of the dynamic damper is assumed to be following Gaussian distribution and obeying random variable θ_1 , and the mass is also assumed to be following Gaussian distribution represented by another random variable, θ_2 . Also in case(1), the mean of the mass is considered as 180kg ($\mu=1/110$). In case (2), the mean of the mass is considered as 500kg ($\mu=1/40$). It is noted that in these two cases, the two random variables $\theta=\{\theta_1, \theta_2\}$ is used to solve the stochastic eigenvalue problem. It is noted that this two random variables problem is different from the two random variables problem in case (2) of section 4.4.1 because the uncertainty parameter is assumed to exists in the mass and stiffness respectively.

Table 4.19 The Statistical Parameters of the Dynamic Damper

Case	The spring stiffness (N/m)		The mass (kg)	
	(Uncertain parameters)		(Uncertain parameters)	
	Mean	Standard deviation	Mean	Standard deviation
	$(k_{3\mu})$	$(k_{3\mu})(C.V. \text{ is } 8\%)$	$(m_{3\mu})$	$(m_{3\mu})(C.V. \text{ is } 5\%)$
(1)	1.995×10^5	1.596×10^4	$180(\mu=1/110)$	9
(2)	5.542×10^5	4.434×10^4	$500(\mu=1/40)$	25

Here, the system stiffness matrix involving random variables θ is same as Eq.(4.80) except that two dimensional basis functions are used ($\Psi_0(\theta)=1, \Psi_1(\theta)=\theta_1, \Psi_2(\theta)=\theta_2, \dots$, by Table 2.2). The system mass matrix involving random variable θ is derived as follows

because the mass is also uncertain parameter.

$$\begin{aligned}
 \mathbf{M}'(\boldsymbol{\theta}) &= \begin{bmatrix} m_1 & 0 & 0 \\ 0 & m_2 & 0 \\ 0 & 0 & m_3(\theta_2) \end{bmatrix} \\
 &= \begin{bmatrix} m_1 & 0 & 0 \\ 0 & m_2 & 0 \\ 0 & 0 & m_{3\mu} \end{bmatrix} \Psi_0(\boldsymbol{\theta}) + \begin{bmatrix} 0 & 0 & 0 \\ 0 & 0 & 0 \\ 0 & 0 & m_{3\sigma} \end{bmatrix} \Psi_2(\boldsymbol{\theta}),
 \end{aligned} \tag{4.83}$$

where $m_{3\mu}$ is mean of the mass of the dynamic damper and $m_{3\sigma}$ is standard deviation. The $\mathbf{R}'(\boldsymbol{\theta})$ in Eq.(4.3) is mass matrix, $\mathbf{M}'(\boldsymbol{\theta})$. The matrix $\mathbf{A}'(\boldsymbol{\theta})$ can be derived by solving $\mathbf{A}'(\boldsymbol{\theta}) = \mathbf{R}'^{-1}(\boldsymbol{\theta})\mathbf{K}'(\boldsymbol{\theta})$, where, $\mathbf{R}'^{-1}(\boldsymbol{\theta})$ is derived by Appendix 1 and the simplification of $\mathbf{R}'^{-1}(\boldsymbol{\theta})\mathbf{K}'(\boldsymbol{\theta})$ is done by the method in Appendix 2. The stochastic eigenvalue can be evaluated using the proposed I-SIPM to solve Eq.(4.3).

Firstly, we will discuss validity of the proposed I-SIPM for the system with two random variables, $\boldsymbol{\theta} = \{\theta_1, \theta_2\}$. In Fig.4.36, the response surface by I-SIPM is shown for case(2), while that obtained by many deterministic analyses is shown in Fig.4.37. As can be seen, a good agreement is observed between the results from the stochastic response surface and deterministic results in the most of the areas. Though they have some inconsistent results in edges (for example: θ_1 is around 5 and θ_2 is around -5, θ_1 is around -5 and θ_2 is around 5.), if we see Table 4.20, it does not affect to the statistical properties because the probabilities of occurrence are very low in the edges.

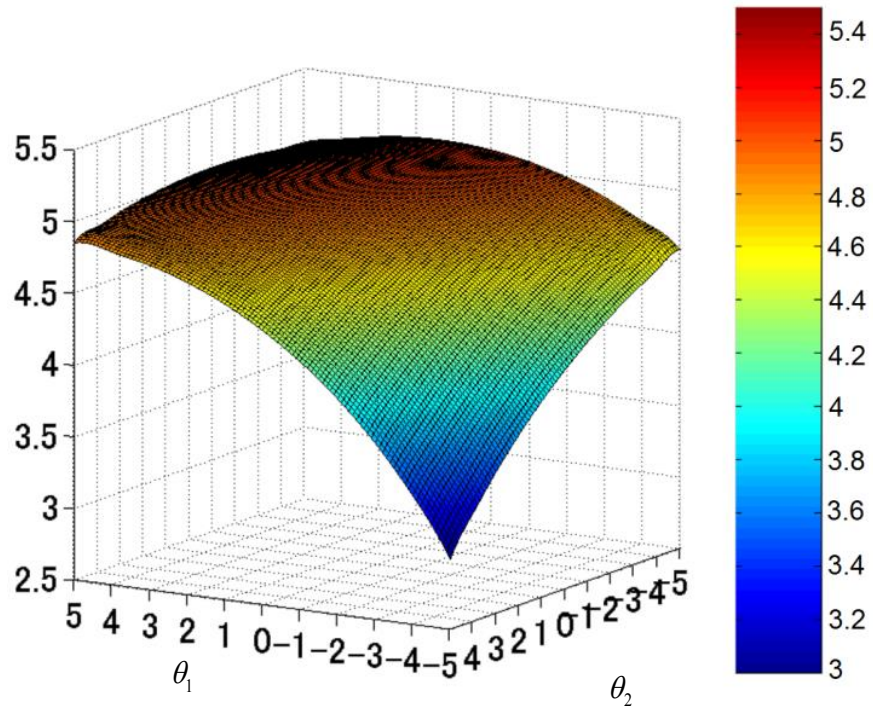


Fig. 4.36: The Response Surface by I-SIPM (Case(2))

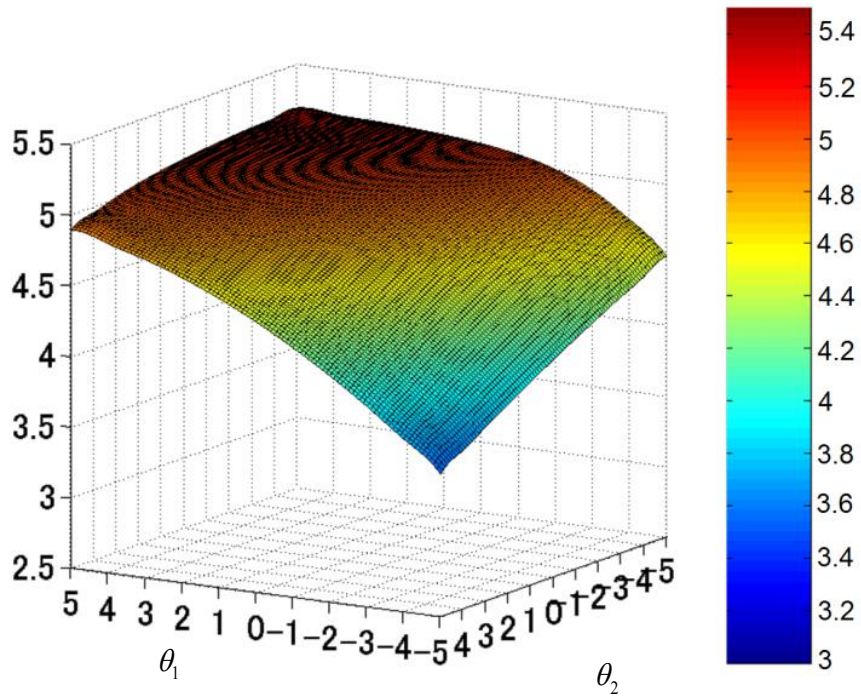


Fig. 4.37: The Response Surface by Deterministic Values (Case(2))

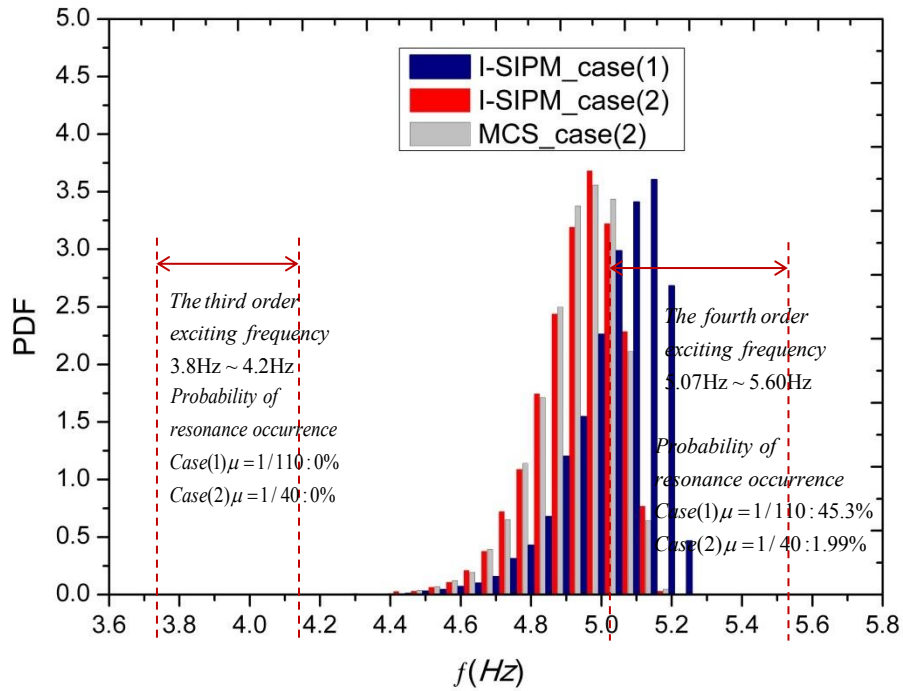


Fig.4.38: The Probability Density Distributions of First Order Frequency
(Both the Spring Stiffness and the Mass with Uncertainty)

Table 4.20 Statistical Properties of Case (2) (Hz)

	I-SIPM	MCS
Mean	4.883	4.882
Std.dev.	0.118	0.116

Fig.4.38 also showed the probability density distributions of first order natural frequency obtained from the I-SIPM (red graph) and MCS (gray graph) of 10000 samples in case(2). They have good agreement from the two results for the two random variables problem. In Fig.4.38, we can also find the probability density distribution of the first order natural frequency in case(1) by using I-SIPM.

In case(1), The probability of resonance occurrence is 45.3%. As can be seen, the probability becomes larger for entering the range of the fourth order exciting frequency of the main engine compared with case(1) in section (4) because both the spring stiffness k_3 and the mass m_3 are considered as uncertain parameters.

In case(2), from the observation of the red histogram in Fig.4.38, we can see that the probability density distribution of the first order natural frequency moves toward the range of the third order exciting frequency of the main engine when the mass ratio μ becomes larger. The probability of resonance occurrence becomes 1.99%, which is significantly reduced compared with case(1). And we can also see the probability is larger compared with case(2) in section (4).

From the results in this section, it can be concluded that the proposed I-SIPM is valid for the system with two random variables $\boldsymbol{\theta} = \{\theta_1, \theta_2\}$. And by applying the proposed method to the dynamic damper problem, it is possible to evaluate the probability of resonance occurrence, and to propose an effective countermeasure to reduce the probability of resonance by appropriate selection of the mass and the spring of the dynamic damper.

4.5 Conclusions

In this section, we present summarize about stochastic eigenvalue analysis as follows.

1. In this study, the stochastic eigenvalue problem is formulated. And in order to solve a stochastic eigenvalue problem, as a numerical analysis algorithm, the improved stochastic inverse power method (I-SIPM) based on response surface methodology is formulated by an Hermite PCE. The method is different with the previous stochastic inverse power method. The minimum eigenvalue and eigenvector of stochastic eigenvalue problems can be validly evaluated by using the proposed method.
2. As another purpose of this study, the stochastic Wielandt deflation method (SWDM) is proposed and formulated to evaluate $i^{\text{th}}(i>1)$ eigenvalues and eigenvectors of stochastic eigenvalue problems. Bases on the I-SIPM, the proposed SWDM can successfully evaluate i^{th} eigenvalues and eigenvectors.
3. In discrete 2-DOF example, the 1st and 2nd eigenvalues and eigenvectors are computed by the proposed I-SIPM and SWDM. The validity and feasibility of the proposed I-SIPM and SWDM are demonstrated by solving the one variable problem $\theta = \{\theta_1\}$ and the two variables problem $\theta = \{\theta_1, \theta_2\}$ of the eigen frequency problem in which the uncertainty exists in spring stiffness. The probabilistic characteristics (the response surface and the probability distribution of the response) can be accurately estimated by the proposed methods.
4. As an example of buckling eigenvalue problem, a continuous free-standing beam is considered with uncertainty of beam section dimension, H . The validity and feasibility of the proposed I-SIPM are demonstrated in that (i) the proposed method can deal with continuous problem, (ii) the method can solve buckling problem, and (iii) the method is valid to solve multi degree of freedom problem. And the validity of a beam problem with uncertainty of Young's modulus is also demonstrated.
5. In the final example, the practicability of the proposed method is proved by the problem

of resonance avoidance by the application of the dynamic damper. When the spring stiffness is considered as uncertain parameter, the probability of resonance occurrence is obtained. It is understood that the probability of resonance occurrence could be significantly reduced by appropriate selection of the mass of the dynamic damper. And also it is understood that the probability of resonance occurrence becomes larger when the mass is also considered as uncertain parameter. By the dynamic damper example, the validity and feasibility of the proposed I-SIPM is demonstrated by solving the two variables problem $\theta = \{\theta_1, \theta_2\}$ in which the uncertainty exists in both the spring stiffness and the mass.

6. In the proposed I-SIPM, the degree of freedom is increased compared to the deterministic Inverse power method(IPM). However the overall results including response surface and probability distribution of the response can be obtained by solving the proposed method only once. It is considered that the computational cost becomes higher by increase of random variables or increase of order of approximate expression. However, by using the proposed method, it is possible to obtain approximate response surface which is theoretically reasonable from the viewpoint of response surface approximation concept, which is different from the Monte Carlo simulation (MCS) with conventional eigenvalue analysis.
7. The proposed methods are very important for solving stochastic vibrations and buckling problem for safety assessment of ships and offshore structures. As a future work, the proposed methods can be used to deal with multi degrees of freedom problem which consider uncertainty in the practical large structures such as ships and offshore structures.

5. Conclusions and Future Recommendations

5.1 Conclusions

In this chapter, we will present the conclusions which including two parts, i.e., linear static analysis and eigenvalue analysis.

5.1.1 Conclusions: Linear Static Analysis

1. In this study, the stochastic finite element method (SFEM) based on response surface methodology considering uncertainty in shape following normal distribution and non-normal distribution is formulated by an Hermite PCE.
2. The validity and feasibility of the proposed method is demonstrated by some example cases. The probabilistic characteristics (the response surface of stress and the probability distribution of the response) can be accurately estimated by the proposed method that solves the main stiffness equation only once.
3. In this study, an algorithm is developed in which the order of approximate of the random parameter of uncertainty of shape is given as an input. And highly accurate analysis result can obtain by defining appropriate order of approximation.
4. In the example of the uncertainty in the size of circular hole following normal distribution. The negative size of the radius is caused because the lower limit value does not exist in the normal distribution, thus correct analysis results may occurs be obtained when the standard deviation becomes larger. However, we can see that negative size of the shape can be avoided when the uncertainty in shape following non-normal distribution because the non-normal distribution has a lower limit value. So, it is considered that the proposed method which can deal with non-normal distribution can be applied to more practical problems.
5. In the proposed SFEM, the degree of freedom is increased n times compared to the deterministic finite element method, where the n is related to the order of approximate of

input parameter and the order of approximate of $1/|\mathbf{J}|$. So it is considered that the computational cost becomes higher by increase of random variables or increase of order of approximate expression. However, by using the proposed method, it is possible to obtain approximate response surface which is theoretically reasonable from the viewpoint of response surface approximation concept, which is different from the Monte Carlo method with conventional FEM.

5.1.2 Eigenvalue Analysis

1. In this study, the stochastic eigenvalue problem is formulated. And in order to solve a stochastic eigenvalue problem, as a numerical analysis algorithm, the improved stochastic inverse power method (I-SIPM) based on response surface methodology is formulated by an Hermite PCE. The method is different with the previous stochastic inverse power method. The minimum eigenvalue and eigenvector of stochastic eigenvalue problems can be validly evaluated by using the proposed method.
2. As another purpose of this study, the stochastic Wielandt deflation method (SWDM) is proposed and formulated to evaluate $i^{\text{th}}(i>1)$ eigenvalues and eigenvectors of stochastic eigenvalue problems. Bases on the I-SIPM, the proposed SWDM can successfully evaluate i^{th} eigenvalues and eigenvectors.
3. The validity and feasibility of the proposed I-SIPM are demonstrated in that (i) the proposed method can deal with discrete problem, (ii) the proposed method can deal with vibration problem, (iii) the proposed method can deal with continuous problem, (iv) the method can solve buckling problem, (v) the method is valid to solve multi degree of freedom problem, and (vi) the method is valid to solve the two variables problem.
4. The practicability of the proposed method is proved by the problem of resonance

avoidance by the application of the dynamic damper. When the spring stiffness is considered as uncertain parameter, the probability of resonance occurrence is obtained by using proposed method.

5. In the proposed I-SIPM, the degree of freedom is increased compared to the deterministic Inverse Power Method (IPM). However the overall results including response surface and probability distribution of the response can be obtained by solving the proposed method only once. It is considered that the computational cost becomes higher by increase of random variables or increase of order of approximate expression. However, by using the proposed method, it is possible to obtain approximate response surface which is theoretically reasonable from the viewpoint of response surface approximation concept, which is different from the Monte Carlo simulation (MCS) with conventional eigenvalue analysis.

5.2 Future Work

In this chapter, we will present future recommendations as follows.

1. The proposed methods are very important for solving stochastic vibrations and buckling problem for safety assessment of ships and offshore structures. As a future work, the proposed methods can be used to deal with multi degrees of freedom problem which consider uncertainty in the practical large structures such as ships and offshore structures.
2. It is well known that the buckling strength of shell structures such as spherical shell, cylindrical shell and stiffened plate is reduced by initial shape imperfections (uncertainty in shape). As a future work, we will develop a structural analysis method with uncertainty in shape which can deal with 3D shell structures. Then by combining the above concept and the concept of stochastic eigenvalue solution, it may become possible to evaluate the stochastic buckling strength of shell structures considering uncertainty in shape (initial imperfections).

BIBLIOGRAPHY

1. Point of management for steel frame construction, Japan Federation of Construction Contractors, 2015. (InJapanese)
2. Htun M. M., Kawamura Y., Ajiki M., A Study on Random Field Model for Representation of Geometry of Corroded Plates and Estimation of Stochastic Properties of Their Strength, Journal of the Japan Society of Naval Architects and Ocean Engineers Vol. 18, pp91-99, 2013.
3. Stefanou G., The stochastic finite element method: past, present and future, Computer Methods in Applied Mechanics and Engineering, Volume 198, pp1031-1051, 2009.
4. Arregui-Mena J. D., Margetts L., Mummery Paul M. Practical Application of the Stochastic Finite Element Method, Archives of Computational Methods in Engineering, Volume 23, pp171–190, 2016.
5. Astill C. J., Imosseir S. B. and Shinozuka M., Impact Loading on Structures with Random Properties, Journal of Structural Mechanics , pp63-77,1972.
6. Argyris J., Papadrakakis M., Stefanou G., Stochastic finite element analysis of shells, Comput. Methods Appl. Mech. Engrg, 191, pp4781–4804, 2002.
7. Van den Nieuwenhof B., Coyette J.P., Modal approaches for the stochastic finite element analysis of structures with material and geometric uncertainties, Comput. Methods Appl. Mech. Engrg. 192, pp3705–3729, 2003.
8. Stefanou G., Papadrakakis M., Stochastic finite element analysis of shells with combined random material geometric properties, Comput. Methods Appl. Mech. Engrg. pp139–160, 2004.
9. Schenk C.A., Schuëller G.I., Buckling analysis of cylindrical shells with cutouts including random boundary and geometric imperfections, Comput.Methods Appl. Mech. Engrg. pp3424–3434, 2007.
10. Schoebsa F., Chevreuil M., Pasqualinia O., Cazuguelb M., Partial safety factor calibration from stochastic finite element computation of welded joint with random geometries. Reliability Engineering and System Safety, p44–54, 2016.
11. Liu W.K., Belytschko, T. Mani A., Probabilistic finite elements for nonlinear structural dynamics, Comput. Methods Appl. Mech. Engrg. pp61–86, 1986.

12. Çavdar Ö., Bayraktar A., Çavdar A., Adanur S., Perturbation based stochastic finite element analysis of the structural systems with composite sections under earthquake forces, *Steel Compos. Struct.* pp129–1448, 2008.
13. Stefanou G., Savvas D., Papadrakakis M.. Stochastic finite element analysis of composite structures based on material microstructure. *Composite Structures*, pp384–392, 2015.
14. Kamiński M., Świta P.. Structural stability and reliability of the underground steel tanks with the Stochastic Finite Element Method. *ARCHIVES OF CIVIL AND MECHANICAL ENGINEERING*, pp593-602, 2015.
15. Wu F., Gao Q., Xu X. M., Zhong W. X., A modified computational scheme of the stochastic perturbation finite element method, *Latin American Journal of Solids and Structures*, Volume 12, pp2480–2505, 2015.
16. Xu Y. L., Qian Y., Song G. B., Stochastic finite element method for free vibration characteristics of random FGM beams. *Applied Mathematical Modelling*, Volume 40, December, pp10238–10253, 2016.
17. Da Silva G.A., Cardoso E.L., Stress-based topology optimization of continuum structures under uncertainties. *Computer Methods in Applied Mechanics and Engineering*, pp647–672, 2017.
18. Kleiber M., Hien T.D., *The stochastic finite element method*. Wiley: Chichester, 1992.
19. Ghanem R., Spsnos P., *Stochastic finite elements: a spectral approach*. Springer-Verlag: New York, 1991.
20. Ghanem R.G., Kruger R.M., Numerical solution of spectral stochastic finite element systems. *Comput Method Appl Mech Eng* 129(3), pp289-303, 1996.
21. Nouy A., Recent developments in spectral stochastic methods for the numerical solution of stochastic partial differential equations. *Arch Comput Methods Eng* 16(3), pp251–285, 2009.
22. Ghanem R., Ingredients for a general purpose stochastic finite elements implementation. *Comput Methods Appl Mech Eng* 168, pp19-34, 1999.
23. Choi S.K., Grandhi R.V., Canfield R.A., *Reliability-based structural design*. Springer, 2007.
24. Sepahvanda K.. Stochastic collocation-based finite element of structural nonlinear

dynamics with application in composite structures. MATEC Web of Conferences-International Conference on Structural Nonlinear Dynamics and Diagnosis (CSNDD2016), 16 November, 2016, (5 pages).

25. Do D.M., Gao W., Song C., Stochastic finite element analysis of structures in the presence of multiple imprecise random field parameters, *Computer Methods in Applied Mechanics and Engineering*, Volume 300, pp657–688, 2016.

26. Nakagiri S., Hisada T., and Itotani Y., Analysis of structure with uncertainty in shape by stochastic finite element method (In Japanese). *Transactions of the Japan Society of Mechanical Engineers Series A*, pp339-348, 1982.

27. Honda R., Spectral stochastic boundary element method for elastic problems with geometrical uncertainty (In Japanese). *Japan Society of Civil Engineers*, pp111-120, 2004.

28. Verhoosel C.V., Gutiérrez M.A., Hulshoff S.J., Iterative solution of the random eigenvalue problem with application to spectral stochastic finite element systems. *Int J Numer Meth Engng*, pp401–424, 2006.

29. Sepahvand K., Marburg S., Hardtke HJ, Stochastic structural modal analysis involving uncertain parameters using generalized polynomial chaos expansion. *International Journal of Applied Mechanics* 3(3), pp587-606, 2011.

30. Wiener N., "The Homogeneous Chaos". *American Journal of Mathematics* (American Journal of Mathematics, Vol. 60 (4), pp897–936, 1938.

31. Panayirci H. M., Schuëller G. I., On the Capabilities of the Polynomial Chaos Expansion Method within SFE Analysis—An Overview, *Archives of Computational Methods in Engineering*, Vol. 18(1), pp43-55, 2011.

32. Xiu D., Karniadakis G., The Wiener–Askey polynomial chaos for stochastic differential equations. *Journal of Scientific Computing* 24(2), pp619–644, 2002.

33. Seung-Kyum Choi, Grandhi R.V. and Canfield R.A., *Reliability-based Structural Design*, Springer, 2007.

34. Fishman G., *Monte Carlo: Concepts, Algorithms, and Applications*, Springer-Verlag New York, Inc., 1996.

35. Thoma J.R.Hughes, *The Finite Element Method LINEAR: Linear Static and Dynamic Finite Element Analysis*, Dover Civil and Mechanical Engineering, 2000.

36. Meirovitch L., *Analytical methods in vibrations*, The Macmillan Co, 1967.

37. Pohlhausen E., Berechnung der Eigenschwingungen statisch-bestimmter Fachwerke. Zeitschrift für Angewandte Mathematik und Mechanik 1, pp28-42,1921.
38. Meirovitch L., Computational methods in structural dynamics. The Netherlands: Sijthoff and Noordhoff, 1980.
39. Szego G., Orthogonal Polynomials, fourth ed., American Mathematical Society, Providence, 1975.
40. Lee C. H., Chang K. H., Jang G. C., Lee C. Y., Effect of weld geometry on the fatigue life of non-load-carrying fillet welded cruciform joints. Engineering Failure Analysis 16, pp849-855, 2009.
41. Tjalling J.Y., Historical development of the Newton–Raphson method. Society for Industrial and Applied Mathematics 37, pp531–551,1995.
42. Japanese Industrial Standard (JIS) G3192, Hot Rolled Sections Section properties of all JIS hot rolled sections, 2008.
43. Holand, I. and Bell, K., Finite element methods in stress analysis, Tapir-Trykk Trondheim-Norway, 1969.
44. Korenev B.G., Reznikov L.M., Dynamic vibration absorbers: theory and technical applications. Chichester [England] New York : Wiley, 1993.
45. Matsuura Y., Matsumoto K., Mizuuchi M., Arima K., Jouichi H., A study of mechanical dynamic dampers to reduce ship vibration (In Japanese). Kansai Soc N A Jnl 197, pp117-126,1985.
46. Miyashita K., Kobayashi K., Takaoka Y., Ebira K., Toma Y., Kubo M., The larger LNG carrier (145,000 m³ type) aiming at low operation cost. The 14th International Conference & Exhibition on Liquefied Natural Gas, Doha, Qatar, 2004.
47. Kondo K., Ohta T., Satoh H., On the vibration control of superstructures of ships by means of a dynamic vibration absorber with an adjustable mass (in Japanese). J Soc Nav Archit Jpn 162, pp356–363,1987.
48. Tamai S., Itoh M, Kanayama T., Development of tuned mass damper (In Japanese), IHI Engineering Review 41(1), pp27-31, 2001.

APPENDICES

Appendix 1: Approximation method of $1/\sum_{i=0}^n Q_i \Psi_i(\boldsymbol{\theta})$

Here we show the approximation method. When denominator of $1/\sum_{i=0}^n Q_i \Psi_i(\boldsymbol{\theta})$ involves random variables $(\boldsymbol{\theta})$, the orthogonality of basis functions cannot be used in the formulation. In this study, to overcome this problem, it is assumed that $1/\sum_{i=0}^n Q_i \Psi_i(\boldsymbol{\theta})$ can be approximated by Hermite PCE as follows.

$$\frac{1}{\sum_{i=0}^n Q_i \Psi_i(\boldsymbol{\theta})} = \sum_{u=0}^m H_u \Psi_u(\boldsymbol{\theta}) \quad (\text{A1})$$

where H_u are unknown coefficients of approximated polynomial, $\Psi_u(\boldsymbol{\theta})$ are the basis functions, represented by Hermite polynomial, and m is the order of expansion terms.

The unknown coefficients, H_u , can be decided as follows:

Firstly, Eq. (A1) is rewritten as follows:

$$\sum_{i=0}^n Q_i \Psi_i(\boldsymbol{\theta}) \times \sum_{u=0}^m H_u \Psi_u(\boldsymbol{\theta}) = 1 \quad (\text{A2})$$

Multiplying $\Psi_t(\boldsymbol{\theta})W(\boldsymbol{\theta})$ to both sides of Eq. (A2), and integrating the equation, we have:

$$\begin{aligned} \int_{-\infty}^{\infty} \sum_{i=0}^n Q_i \Psi_i(\boldsymbol{\theta}) \times \sum_{u=0}^m H_u \Psi_u(\boldsymbol{\theta}) \Psi_t(\boldsymbol{\theta}) W(\boldsymbol{\theta}) d\boldsymbol{\theta} \\ = \int_{-\infty}^{\infty} 1 \times \Psi_t(\boldsymbol{\theta}) W(\boldsymbol{\theta}) d\boldsymbol{\theta} \end{aligned} \quad (\text{A3})$$

This equation can be depicted as follows:

$$\sum_{i=0}^n \sum_{u=0}^m Q_i H_u \langle \Psi_i(\boldsymbol{\theta}) \Psi_u(\boldsymbol{\theta}) \Psi_t(\boldsymbol{\theta}) \rangle = \langle \Psi_t(\boldsymbol{\theta}) \rangle \quad (\text{A4})$$

This means that the following simultaneous equations about the coefficients, $A p_u$, are obtained.

$$\begin{bmatrix} \hat{Q}_{00} & \hat{Q}_{01} & \cdots & \hat{Q}_{0m} \\ \hat{Q}_{10} & \hat{Q}_{11} & \cdots & \hat{Q}_{1m} \\ \vdots & \vdots & \vdots & \vdots \\ \hat{Q}_{1m} & \hat{Q}_{2m} & \cdots & \hat{Q}_{mm} \end{bmatrix} \begin{bmatrix} H_0 \\ H_1 \\ \vdots \\ H_m \end{bmatrix} = \begin{bmatrix} 1 \\ 0 \\ \vdots \\ 0 \end{bmatrix} \quad (\text{A5})$$

where $\hat{Q}_{iu} = \sum_{i=0}^n Q_i \langle \Psi_i(\boldsymbol{\theta}) \Psi_u(\boldsymbol{\theta}) \overline{\Psi_t(\boldsymbol{\theta})} \rangle$. It is noted that $\langle \Psi_i(\boldsymbol{\theta}) \Psi_u(\boldsymbol{\theta}) \Psi_t(\boldsymbol{\theta}) \rangle$ can be evaluated by the following equation.

$$\langle \Psi_i(\boldsymbol{\theta}) \Psi_u(\boldsymbol{\theta}) \Psi_t(\boldsymbol{\theta}) \rangle = \int_D \Psi_i(\boldsymbol{\theta}) \Psi_u(\boldsymbol{\theta}) \Psi_t(\boldsymbol{\theta}) W(\boldsymbol{\theta}) d\boldsymbol{\theta} \quad (\text{A6})$$

Then the unknown coefficients of approximation polynomial, H_u , is derived by the above simultaneous equations.

Appendix 2: Derivation of coefficients, C_k , for $\sum_{i=0}^n \sum_{j=0}^n A_i B_j \Psi_i(\boldsymbol{\theta}) \Psi_j(\boldsymbol{\theta}) = \sum_{k=0}^m C_k \Psi_k(\boldsymbol{\theta})$

For easy understanding, here the order n of expansion terms is defined as 2 and $\boldsymbol{\theta} = \{\theta_1\}$ is considered to explain the derivation process. The expansion equation can be shown as follows.

$$\begin{aligned} \sum_{i=0}^2 \sum_{j=0}^2 A_i B_j \Psi_i(\boldsymbol{\theta}) \Psi_j(\boldsymbol{\theta}) = \\ (A_0 \Psi_0(\theta_1) + A_1 \Psi_1(\theta_1) + A_2 \Psi_2(\theta_1))(B_0 \Psi_0(\theta_1) + B_1 \Psi_1(\theta_1) + B_2 \Psi_2(\theta_1)) \end{aligned} \quad (\text{A7})$$

Expand right of Eq.(A7),we have:

$$\begin{aligned} \sum_{i=0}^2 \sum_{j=0}^2 A_i B_j \Psi_i(\boldsymbol{\theta}) \Psi_j(\boldsymbol{\theta}) = \\ = A_0 B_0 \Psi_0(\theta_1) \Psi_0(\theta_1) + A_0 B_1 \Psi_0(\theta_1) \Psi_1(\theta_1) + A_0 B_2 \Psi_0(\theta_1) \Psi_2(\theta_1) \\ + A_1 B_0 \Psi_1(\theta_1) \Psi_0(\theta_1) + A_1 B_1 \Psi_1(\theta_1) \Psi_1(\theta_1) + A_1 B_2 \Psi_1(\theta_1) \Psi_2(\theta_1) \\ + A_2 B_0 \Psi_2(\theta_1) \Psi_0(\theta_1) + A_2 B_1 \Psi_2(\theta_1) \Psi_1(\theta_1) + A_2 B_2 \Psi_2(\theta_1) \Psi_2(\theta_1) \end{aligned} \quad (\text{A8})$$

and referring to Table 2.1, we can understand $\Psi_0(\theta_1) = 1, \Psi_1(\theta_1) = \theta_1, \Psi_2(\theta_1) = \theta_1^2 - 1, \dots$

Substituting basis functions into Eq.(A8), it can show as follows:

$$\begin{aligned} \sum_{i=0}^2 \sum_{j=0}^2 A_i B_j \Psi_i(\boldsymbol{\theta}) \Psi_j(\boldsymbol{\theta}) \\ = A_0 B_0 + A_0 B_1 \theta_1 + A_0 B_2 (\theta_1^2 - 1) \\ + A_1 B_0 \theta_1 + A_1 B_1 \theta_1 \theta_1 + A_1 B_2 \theta_1 (\theta_1^2 - 1) \\ + A_2 B_0 (\theta_1^2 - 1) + A_2 B_1 (\theta_1^2 - 1) \theta_1 + A_2 B_2 (\theta_1^2 - 1) (\theta_1^2 - 1) \end{aligned} \quad (\text{A9})$$

By simplifying Eq.(A9), we can obtain Eq.(A10).

$$\begin{aligned}
& \sum_{i=0}^2 \sum_{j=0}^2 A_i B_j \Psi_i(\boldsymbol{\theta}) \Psi_j(\boldsymbol{\theta}) \\
&= A_0 B_0 - A_0 B_2 - A_2 B_0 + A_2 B_2 \\
&\quad + (A_0 B_1 + A_1 B_0 - A_1 B_2 - A_2 B_1) \theta_1 \\
&\quad + (A_0 B_2 + A_1 B_1 + A_2 B_0 - 2A_2 B_2) \theta_1^2 \\
&\quad + (A_1 B_2 + A_2 B_1) \theta_1^3 \\
&\quad + A_2 B_2 \theta_1^4
\end{aligned} \tag{A10}$$

By rewriting Eq.(A10), the $\sum_{i=0}^n \sum_{j=0}^n A_i B_j \Psi_i(\boldsymbol{\theta}) \Psi_j(\boldsymbol{\theta})$ can be represented by basis functions, $\Psi_i(\theta_1)$ as follows.

$$\begin{aligned}
& \sum_{i=0}^2 \sum_{j=0}^2 A_i B_j \Psi_i(\boldsymbol{\theta}) \Psi_j(\boldsymbol{\theta}) \\
&= (A_0 B_0 + A_1 B_1 - A_2 B_2 + 3A_2 B_2) \Psi_0(\theta_1) \\
&\quad + (A_0 B_1 + A_1 B_0 + 2A_1 B_2 + 2A_2 B_1) \Psi_1(\theta_1) \\
&\quad + (A_0 B_2 + A_1 B_1 + A_2 B_0 + 4A_2 B_2) \Psi_2(\theta_1) \\
&\quad + (A_1 B_2 + A_2 B_1) \Psi_3(\theta_1) \\
&\quad + A_2 B_2 \Psi_4(\theta_1)
\end{aligned} \tag{A11}$$

Then, C_k is derived as follows, and the order m is 4.

$$C_0 = A_0 B_0 + A_1 B_1 - A_2 B_2 + 3A_2 B_2 \tag{A12-1}$$

$$C_1 = A_0 B_1 + A_1 B_0 + 2A_1 B_2 + 2A_2 B_1 \tag{A12-2}$$

$$C_2 = A_1 B_2 + A_2 B_1 \tag{A12-3}$$

$$C_4 = A_2 B_2 \tag{A12-4}$$

Thus, $\sum_{i=0}^n \sum_{j=0}^n A_i B_j \Psi_i(\boldsymbol{\theta}) \Psi_j(\boldsymbol{\theta}) = \sum_{k=0}^m C_k \Psi_k(\boldsymbol{\theta})$ is derived. This derivation method is implemented in the developed program for arbitrary n .